Scp-20

Microwave Treatment of Minerals and Ores

by

Antonio Jose Cumbane

M.Res., Licentiate, Grad IMMM

Thesis submitted to The University of Nottingham for the degree of Doctor of Philosophy

October 2003

Abstract

Microwave energy has previously been shown to have a major influence on the comminution behaviour of minerals and ores. Significant reductions in Bond Work Index have been reported for microwave treated samples when compared to non-treated samples. It has been suggested that this is a result of differential expansion/contraction at grain boundaries. Previous test work has been carried out utilizing 'multimode' type microwave cavities. Although flexible, these cavities are known to be inefficient in their operation. This project has investigated the application of high electric field strength microwave energy to minerals and ores and also measurement of dielectric properties of minerals. The application of high electric field strength microwave energy means that the heating rates of the materials are orders of magnitude faster. Therefore, higher sample temperatures can be reached more quickly and develop more, significant, stress fractures.

Various important ore types and minerals have been selected and their textures, dielectric and thermal properties quantified. Ore strength, using UCS and point load index testing; specific comminution energy using a drop weight tester and grindability batch grinding and Bond Work Index using ball mill have all been used to quantify the microwave effect on ores. High electric field strength microwave energy has been found to reduce the required sample cavity residence times to less than 0.2 seconds whilst enabling ore strength reductions of up to 70%.

Mineral liberation assessment of microwave treated ores has also been conducted using QEM.SEM analysis and the research concluded with an analysis that shows that benefits are achieved with less than one kWh/t of the energy added into the process.

LIST OF PUBLICATIONS

1. Recent Developments in Microwave Assisted Comminution (Submitted and accepted to the International Journal of Mineral Processing)

2. An Investigation into the Influence of Microwave Treatment on Mineral Ore (Submitted to the Powder Technology, May 2003)

3. Dielectric Properties of Sulphide Minerals (Submitted to the Journal of Microwave Power Electromagnetic and Energy, August 2003)

LIST OF CONTENTS

ABSTRACT
LIST OF PUBLICATIONS
ACKNOLODGEMENTS
LIST OF CONTENTS
LIST OF FIGURES
LIST OF TABLES
LIST OF SYMBOLS

CHAPTER ONE
INTRODUCTION 1

CHAPTER TWO
THEORETICAL ASPECTS OF MICROWAVE HEATING 4
2.1 Introduction 4
2.2 Volumetric Heating 4
2.2.1. Microwave Interaction with Materials 7
2.2.2. Mechanisms of Microwave Heating 8
2.2.2.1. Ionic Polarisation 9
2.2.2.2. Orientation Polarisation 9
2.2.2.3. Interfacial Polarisation 10
2.3. Microwave Equipment 10
2.4. Dielectric Properties of Materials 11
2.4.1. Loss Factor 12
2.4.2. Measurement Techniques 13
2.4.2.1. Coaxial Line Technique 14
2.4.2.2. Resonant Cylindrical Cavity Technique 17
2.4.2.3. Calculation of Penetration Depth 23
2.4.3. Power Flow and the Power Dissipation Density 24
2.4.4. Calculation of Temperature Change 25
2.4.5. Factors Affecting the Dielectric Properties of a Material 26
2.4.5.1. Frequency Dependence 27
2.4.5.2. Temperature Dependence 27
2.4.5.3. Density Dependence 28
2.4.5.4. Influence of Crystallography 28
2.5. Applicators 28
2.5.1. Travelling Wave Applicator 29

2.5.2. Multimode Cavities 30
2.5.2.1. Field Distribution and Heating Uniformity 32
2.5.3. Single Mode Cavities 33
2.6. Conclusions 36

CHAPTER THREE 37
APPLICATIONS OF MICROWAVE RADIATION IN MINERAL PROCESSING 37
3.1. Introduction 37
3.2. Microwave Application in the Minerals Industry: Early Work 37
3.3. Determination of Dielectric Properties of Minerals 40
3.4. Microwave Assisted Liberation 43
3.5. Effects of Microwave Radiation on Mineral Properties 55
3.5.1. Effect of Microwave Radiation on Mineral Surface Area 55
3.5.2. Effect of Microwave Radiation on the Magnetic Properties of Minerals 56
3.6. Applications of Microwave Radiation in Extractive Metallurgy 57
3.7. Applications of Microwave Radiation in the Processing of Coal 58
3.8. Conclusions and Further Work 61

CHAPTER FOUR 63
DIELECTRIC PROPERTIES OF MINERALS 63
4.1. Introduction 63
4.2. Measurement Technique 63
4.2.1. Experimental Procedure 66
4.2.1.1. Sample Preparation 66
4.2.1.2. Dielectric Properties Measurement 67
4.2.1.3. Thermo-gravimetric analysis 67
4.3. Calibration and Validation of the Technique 68
4.3.1. Procedure 68
4.3.2. Example Calculations 68
4.3.3. Results 69
4.3.4. Discussion 71
4.3.4.1. Effect of Temperature on the Dielectric Properties 71
4.3.4.2. Modelling Density Effect on Dielectric Properties 73
4.4. Dielectric Properties of Sulphides 76
4.4.1. Nature of Sulphides 77

4.4.2. Results 79
4.4.2.1. Dielectric Properties 79
4.4.2.2. Thermo-gravimetric results 81
4.4.3. Discussion 82
4.4.3.1. Modelling Density Effect 82
4.4.3.2. Effect of Frequency 85
4.4.3.3. Effect of Temperature 86
4.5. Dielectric Properties of Oxides 90
4.5.1. Nature of Oxides 90
4.5.2. Results 91
4.5.3. Discussion 93
4.5.3.1. Effect of Frequency 94
4.5.3.2. Modelling Density Effect 94
4.6. Dielectric Properties of Silicates 96
4.6.1. Nature of Silicates 97
4.6.2. Results 97
4.6.3. Discussion 98
4.6.3.1. Effect of Temperature 98
4.6.3.2. Effect of Frequency 99
4.6.3.3. Effect of Density 100
4.7. Conclusions 102

CHAPTER FIVE 104
INVESTIGATION ON MICROWAVE ASSISTED COMMINUTION AND LIBERATION OF PALABORA ORE 104
5.1. Introduction 104
5.1.1. Geology and Reserves 104
5.1.2. Ore Treatment 106
5.1.3. Palabora Comminution: Current Practice 108
5.2. Mineralogy of Palabora Ore 110
5.2.1. Sample Preparation 111
5.2.2. Methods of Investigation 112
5.2.3. Mineralogical Results 112
5.2.3.1. Transparent Gangue 113
5.2.3.2. Micro-gabbro Rock Fragments 127

5.2.3.3. Magnetite 128
5.2.3.4. Sulphide Minerals 129
5.2.3.5. Accessory Minerals 130
5.3. Effect of Microwave Treatment on Ore Mineralogy 130
5.3.1. Previous Work on the Effects of Microwave Treatment on Palabora Ore 130
5.3.2. Sampling and Sample Preparation 134
5.3.3. Microwave Treatment 134
5.3.3.1. Heating Experiments with Multimode Cavity 135
5.3.3.2. Heating Experiments using a Resonant TE_{10} Cavity 136
5.3.4. Results and Discussion 137
5.4. Influence of Microwave Power on Ore Comminution 142
5.4.1. Introduction 144
5.4.2. Research Plan 145
5.4.3. Influence of Microwave on Ore Strength 145
5.4.3.1. Uniaxial Compressive Strength 145
5.4.3.1.1. Sample Preparation 146
5.4.3.1.2. Test Procedure 147
5.4.3.1.3. Results and Discussion 147
5.4.3.2. Point Load Test 149
5.4.3.2.1. Sample Preparation 151
5.4.3.2.2. Test Procedure 151
5.4.3.2.3. Results and Discussion 152
5.4.4. Influence of Microwave Treatment on Crushing 159
5.4.4.1. Single Breakage Techniques 159
5.4.4.2. Drop Weight Test Procedure 164
5.4.4.2.1. Sample Preparation 164
5.4.4.2.2. Procedure for Drop Weight Test 165
5.4.4.2.3. Data Analysis 166
5.4.4.3. Results of Standard Sample Drop Weight Test 168
5.4.4.3.1. AG/SAG Mill Specific Parameters 168
5.4.4.3.2. Crusher Model Appearance Function 169
5.4.4.4. Palabora Ore Sample Preparation 170
5.4.4.5. Results and Discussion 171
5.4.5. Influence of Microwave on Breakage Rate 178

5.4.5.1. Sample Preparation 180
5.4.5.2. Batch Grinding Test Procedure 180
5.4.5.3. Results 181
5.4.5.4. Discussion 182
5.4.6. Effect of Microwave Treatment on Bond Work Index 184
5.4.6.1. Introduction 184
5.4.6.2. Sample Preparation 185
5.4.6.3. Bond Work Index Test Procedure 186
5.4.6.3.1. Sample Preparation 187
5.4.6.3.2. Test Mill and Charge 187
5.4.6.3.3. Test Procedure 187
5.4.6.4. Results 188
5.4.6.5. Discussion 190
5.5. Effect of Microwave Treatment on Mineral Liberation 191
5.5.1. Sample Preparation 192
5.5.2. Mineral Liberation Test Procedure 192
5.5.3. Results and Discussion 193
5.6. Conclusions 196

CHAPTER SIX **199**
INVESTIGATION ON MICROWAVE ASSISTED COMMINUTION AND LIBERATION OF ZINKGRUVAN ORE 199
6.1. Introduction 199
6.1.1. Geology and Reserves 199
6.1.2. Ore Processing 201
6.2. Mineralogy of Zinkgruvan Ore 203
6.2.1. Sample Preparation 203
6.2.2. Procedure 204
6.2.3. Results and Discussion 204
6.3. Effect of Microwave Treatment on Ore Mineralogy 210
6.3.1. Sample Preparation 210
6.3.2. Microwave Treatment 210
6.3.3. Results and Discussions 211
6.4. Influence of Microwave Treatment on Comminution 215
6.4.1. Introduction 215

6.4.1.1. Research Plan 215
6.4.2. Influence of Microwave Treatment on Ore Strength 215
6.4.2.1. Sample Preparation 215
6.4.2.2. Test Procedure 216
6.4.2.3. Results and Discussion 216
6.4.3. Influence of Microwave on Point Load Test 217
6.4.3.1. Sample Preparation 217
6.4.3.2. Test Procedure 217
6.4.3.3. Results and Discussions 218
6.4.4. Influence of Microwave Treatment on Crushing 220
6.4.4.1. Sample Preparation 220
6.4.4.2. Test Procedure 221
6.4.4.3. Results and Discussion 221
6.4.5. Influence of Microwave Treatment on Breakage Rate 224
6.4.5.1. Sample Preparation 225
6.4.5.2. Test Procedure 225
6.4.5.3. Results and Discussion 226
6.4.6. Influence of Microwave Treatment on Bond Work Index 228
6.4.6.1. Sample Preparation 228
6.4.6.2. Bond Work Index Test Procedure 229
6.4.6.3. Results and Discussion 229
6.5. Effect of Microwave on Mineral Liberation 230
6.5.1. Sample Preparation 230
6.5.2. Test Procedure 231
6.5.3. Results and Discussion 231
6.6. Conclusions 233

CHAPTER SEVEN
CONCLUSIONS AND FURTHER WORK 235
7.1. Conclusions 235
7.2. Further Work 240

REFERENCES 241

ACKNOWLEDGEMENTS

The author wishes to thank and appreciate Professor Nicholas Miles and Dr Samuel Kingman for their invaluable support, supervision and encouragement during the course of this research project. Also would like to extend the appreciation to Prof. Steven Bradshaw, Dr T.E. Cross, Dr Ed. Lester, Dr D. Large and Dr K. Jackson in the discussions of parts of the research project. Many thanks are also extended to the members of staff and colleagues of the School of Chemical, Environmental and Mining Engineering, who have helped throughout the years at the University of Nottingham.

For the generous financial support given by the British Council, Rio Tinto Technical Services Ltd., and The University of Nottingham. To the University Eduardo Mondlane in Mozambique for the authorisation to leave to pursue this research project. I am very grateful.

A personal thank you also goes to my family in Mozambique and friends in UK for the continued support and encouragement given throughout my student years.

Finally,

Hallelujah!

LIST OF FIGURES

CHAPTER TWO

Figure 2.1 Electromagnetic wave components (after Whittaker, 1997).

Figure 2.2 The electromagnetic spectrum (after Metaxas and Meredith, 1983).

Figure 2.3 Classification of materials in the presence of microwave radiation (after Chen et al., 1984)

Figure 2.4 Block diagram of microwave heating system (after Meredith and Metaxas, 1983).

Figure 2.5 The Roberts and Von Hippel method for dielectric measurements. (after Meredith and Metaxas, 1983).

Figure 2.6 High temperature coaxial surface probe and surrounding equipment for dielectric properties measurement, control diagram (after Arai et al., 1992).

Figure 2.7 Cross section of coaxial re-entrant resonator used as a heating and testing chamber (after Tinga, 1992).

Figure 2.8 Schematic diagram of the resonant cylindrical cavity (after Arai et al., 1993).

Figure 2.9. Lower order TM_{lmn} mode chart for an empty resonant cylindrical cavity (after Meredith and Metaxas, 1983).

Figure 2.10. Propagation of a plane wave in a lossy medium (after Metaxas and Meredith, 1983).

Figure 2.11 Typical waveguide applicator (after Hulls, 1992)

Figure 2.12 Frequency shift and damping of mode patterns due to the loading effect of the dielectric in the multimode cavity (after Meredith and Metaxas, 1983).

Figure 2.13. Typical voltage standing wave ratios (VSWR), S, verses frequency response for a single mode resonant cavity (after Metaxas and Meredith, 1983).

Figure 2.14. Photograph illustrating single-mode microwave heating system.

CHAPTER THREE

Figure 3.1. Effect of microwave radiation on the work index of selected samples (after Kingman et al., 1998)

Figure 3.2 Typical Intergranular microwave Induced Fracture on a Norwegian Ilmenite (after Kingman et al., 1998)

Figure 3.3. Model of the Pyrite Calcite ore sample (after Whittles et al 2003).

Figure 3.4. Simulated microwave heating process with higher power density 1x 10^{11} W/m^3 (after Whittles et al 2003).

Figure 3.5. Simulated microwave-heating process with low power density between 3×10^9W/m^3 and 9×10^9W/m^3 (after Whittles et al 2003).

Figure 3.6 Microwave Heating Time (2.6 kW 2.45 GHz power density between 3×10^9W/m^3 and 9×10^9w/m^3) versus Point Load Index (after Whittles et al., 2003).

Figure 3.7. Microwave Heating Time (Power Density =1x 10^{11} watt/m^3) versus Point Load Index (after Whittles et al., 2003).

CHAPTER FOUR

Figure 4.1. Diagrammatic representation of the measurement system (after Greenacre, 1996).

Figure 4.2. Typical displays from the vector network analyzer connected to the resonant cylindrical cavity showing the effect of sample insertion on the TM_{030} mode (after Metaxas et al, 1983).

Figure 4.3. Effect of temperature and density on the dielectric constant of quartz.

Figure 4.4. Effect of temperature and density on the dielectric constant and loss factor of quartz.

Figure 4.5. Effect of temperature on the dielectric constant and loss factor of double distilled water.

Figure 4.6. Effect of temperature on the dielectric constant and loss factor of distilled water (after Meredith, 1998).

Figure 4.7. Relationship between density and dielectric constant of quartz for k=2

Figure 4.8. Relationship between density and dielectric constant of quartz for k=3

Figure 4.9. The dependence of dielectric constant of sulphide minerals with temperature measured at the frequency of 2.21 GHz.

Figure 4.10. The dependence of loss factor of sulphide minerals with temperature measured at the frequency of 2.21 GHz.

Figure 4.11. Thermo-gravimetric analysis of sulphides in air.

Figure 4.12. Thermo-gravimetric analysis of sulphides in a nitrogen atmosphere.

Figure 4.13. Effect of density on dielectric properties of sulphides measured at room temperature

Figure 4.14. Effect of frequency on dielectric properties of pyrite measured at room temperature.

Figure 4.15. Differential thermo-gravimetric analysis of sulphides.

Figure 4.16. Effect of temperature on the dielectric constant of oxides.

Figure 4.17. Effect of temperature on the dielectric loss factor of oxides.

Figure 4.18 Effect of frequency on the dielectric properties of Ilmenite measured at room temperature

Figure 4.19. Effect of density on dielectric properties of oxides. Data obtained at room temperature and frequency of 615 MHz.

Figure 4.20. Effect of temperature on the dielectric constant of silicates measured at the frequency of 2.21GHz.

Figure 4.21. Effect of temperature on the loss factor of silicates measured at the frequency of 2.21GHz.

Figure 4.22. Thermo-gravimetric analysis of quartz and orthoclase.

Figure 4.23. The effect of frequency on the dielectric properties of Orthoclase measured at room temperature (25 °C).

Figure 4.24. The effect of density on the dielectric properties of orthoclase and quartz measured at room temperature (25 °C).

CHAPTER FIVE

Figure 5.1 Geology of the Palabora igneous complex (Aird, 1998)

Figure 5.2 Flowsheet for the processing of Palabora copper ore (Aird, 1998).

Figure 5.3 Conventional grinding circuit of Palabora Mining Operations (Aird, 1998)

Figure 5.4. Second conventional grinding circuit of Palabora Mining Operation (Aird, 1998).

Figure 5.5 Core drill samples of palabora ore (Rio Tinto Technical Report, 2001).

Figure 5.6. False colour backscattered computer enhanced images of a head sample of Palabora open pit ore.

Figure 5.7. Head sample, false coloured backscatter image showing apatite and dolomite grains. Also shows chalcopyrite lamellae in bornite grains and fine grains of chalcocite.

Figure 5.8 Head sample, false coloured backscatter image

Figure 5.9 Head sample, false coloured backscatter image

Figure 5.10 Head sample, false coloured backscatter image

Figure 5.11 Head sample, false coloured backscatter image

Figure 5.12 Head sample, false coloured backscatter image.

Figure 5.13 Head sample, false coloured backscatter image

Figure 5.14 Head sample, false coloured backscatter image

Figure 5.15 Head sample, false coloured backscatter image

Figure 5.16 Head sample, false coloured backscatter image.

Figure 5.17 Head sample, false coloured backscatter image.

Figure 5.18 Head sample, false coloured backscatter image.

Figure 5.19. Plot of penetration depth of calcite and pyrite at the frequency of 2.21GHz.

Figure 5.20. 240 Second treated sample, false colour backscattered image (after Kingman 1999).

Figure 5.21. 240 Second treated sample, false colour backscattered image (after Kingman, 1999).

Figure 5.22. 240 Second treated sample, false colour backscattered image (after Kingman, 1999).

Figure 5.23. Multimode cavity used for microwave treatment.

Figure 5.24. Schematic diagram of the arrangement for test in single mode cavity.

Figure 5.25. 1 Second microwave treated in 15kW multimode cavity.

Figure 5.26. 5 seconds, 15kW multimode treated Palabora ore sample.

Figure 5.27. 0.5 Second, 15kW single mode treated sample of Palabora ore. Fractures occur on grain boundaries

Figure 5.28. 0.2 Second, 15kW single mode treated sample of palabora ore.

Figure 5.29. Typical example of a stress versus strain plot for the uniaxial compression of cylindrical rock (after Jaeger and Cook 1979).

Figure 5.30. Core drill sample of Palabora ore.

Figure 5.31. RDP-Howden 1MN stiff universal loading frame for conducting uniaxial compressive strength.

Figure 5.32. Plot of stress versus strain of Palabora type PD core drilled samples.

Figure 5.33. Suggested sample dimensions for point load testing (Hudson, 1993)

Figure 5.34. Principle of Operation of Point Load Apparatus.

Figure 5.35. Effect of Single mode microwave treatment on the Point Load Test index for Palabora ore –37+31mm particle size.

Figure 5.36. Effect of Single Mode microwave treatment on Point Load test for Palabora ore, -53+45mm particle size.

Figure 5.37. Effect of Multimode microwave treatment on Point Load test for Palabora ore, -37.5+31.5mm particle size.

Figure 5.38 Loss factor of Pyrite and Calcite.

Figure 5.39. Schematic of a twin pendulum device (after Napier-Munn, 1996).

Figure 5.40 Schematic set up of Hopkinson Pressure Bar experiment and wave signal plotted as a function of time (after Kuokkala et al., 2003).

Figure 5.41. Schematic diagram of drop weight tester (after Napier-Munn et al., 1996).

Figure 5.42. Appearance function relating t versus t10 (after Nayaranan and Whiten, 1988).

Figure 5.43. Relationship between t10 and Ecs for standard sample used for drop weight calibration and the SAG/AG mill parameters A and b.

Figure 5.44. Comparative crusher power data of the untreated tested at 100% Ecs and microwave treated samples tested at 50%Ecs.

Figure 5.45. Comparative crusher power data for Palabora ore untreated and microwave treated. Drop weight test carried out at 50% of the original energy input (Ecs).

Figure 5.46. Comparative crusher power data for Palabora ore untreated and microwave treated. Drop weight test carried out at the original energy input.

Figure 5.47. Size distribution of Hopkinson Pressure Bar test.

Figure 5.48. Effect of microwave treatment on breakage rate versus mean particle size relationship.

Figure 5.49. Copper sulphides liberation.

Figure 5.50. Iron-oxide liberation

CHAPTER SIX

Figure 6.1 Geology of southern Sweden (after Stephens et al. 1996).

Figure 6.2. Geological map of the Zinkgruvan ore (after Bengtsson, VC 2000).

Figure 6.3. Schematic diagram of Zinkgruvan ore grinding circuit (Johan et al., 2002).

Figure 6.4. Core drill sample of Zinkgruvan

Figure 6.5. A colour reflected light photomicrograph illustrating the presence of graphitic carbon flakes (pale brown), sphalerite (medium grey), galena (white) and gangue (dark grey) are the phases present in the image.

Figure 6.6. A monochrome backscattered scanning electron microscope image illustrating the preferred orientation of film like galena aggregates (white) within a sphalerite band (medium grey). The gangue (dark grey shades) consists predominatly of quartz and K-feldspar.

Figure 6.7. A colour reflected light photomicrograph illustrating the granular and twinned nature of the sphalerite aggregates (light and dark brown shades).

Galena (silver-blue shades) is present along the margins of the sphalerite grains. Gangue is present (dark grey shades).

Figure 6.8. A monochrome backscattered SEM image illustrating the preferred orientation of film-like galena aggregates (white) within a sphalerite rich band (medium grey). Discrete gangue layers (dark grey shades) also occur on this image.

Figure 6.9. Monochrome backscattered SEM image illustrating galena (white) occurring along fractures in the gangue minerals (dark grey shades)

Figure 6.10. Monochrome SEM image illustrating a transparent gangue rich area (dark grey shades), consisting largely of epidote/clinozoisite.

Figure 6.11. Monochrome backscattered electron images illustrating the rounded and sub-rounded nature of transparent gangue mineral clasts (dark grey shades).

Figure 6.12. Monochrome backscattered electron images illustrating sphalerite and galena occurring between two relatively large transparent gangue mineral clasts.

Figure 6.13. A monochrome backscattered electron image illustrating the typical nature and appearance of transparent gangue minerals

Figure 6.14. Loss tangent of the major constituents of Zinkgruvan ore.

Figure 6.15. Photomicrograph of Zinkgruvan ore microwave treated in a single mode cavity, 10kW, 0.5 s exposure time.

Figure 6.16 Zinkgruvan particle microwave treated on a multimode cavity, exposed for 5 seconds at a) 15kW, b) 10kW and c) 5kW microwave power.

Figure 6.17. Plot of stress versus strain of Zinkgruvan core drilled samples.

Figure 6.18. Effect of microwave exposure time on Point Load test for Zinkgruvan ore.

Figure 6.19. Effect of microwave exposure time on Point Load test of Zinkgruvan ore.

Figure 6.20. Effect of particle size on comparative crusher power data of Zinkgruvan treated and untreated samples and drop weight tested at 60% and standard energy input.

Figure 6.21. Effect of particle size on comparative crusher power data of Zinkgruvan untreated and treated samples and drop weight tested at full Ecs energy input.

Figure 6.22. Effect of particle size on comparative crusher power data of Zinkgruvan treated samples and drop weight tested at full and 60%Ecs energy input.

Figure 6.23. Effect of microwave treatment on breakage rate of Zinkgruvan ore.

Figure 6.24. Galena liberation.

Figure 6.25. Sphalerite liberation.

LIST OF TABLES

CHAPTER TWO

Table 2.1 Loss factors for some common materials (after Hulls 1992)

CHAPTER THREE

Table 3.1 Heating responses of various minerals (after Chen et al 1984)

Table 3.2 Heating responses of various minerals (after Walkiewicz et al 1988)

Table 3.3 Effect of power level on heating rate (after McGill 1988)

Table 3.4 Data for components of complex permittivity at 915 MHz (after Florek et al., 1995)

Table 3.5. Recovery of silica (SiO_2) and phosphorous (P) into magnetite and hematite concentrates (after Andres et al., 1999)

CHAPTER FOUR

Table 4.1 Calculated first-order Bessel function for dielectric measurement

Table 4.2. Readings of frequency shift and Q-factor

Table 4.3. Coefficients of empirical equations relating the dielectric constant (ε') and density (ρ) of quartz

Table 4.4. Standard deviation for experimental and calculated dielectric constant based on equation 4.2 for k=2 and k=3 model.

Table 4.5. Coefficients of empirical equations relating the dielectric constant ($\sqrt{\varepsilon'}$) and density (ρ) of sulphides.

Table 4.6. Dielectric properties of sulphides

Table 4.7. Coefficients of empirical equations relating the dielectric constant ($\sqrt{\varepsilon'}$) and density (ρ) of oxides.

Table 4.8. Dielectric properties of oxides at room temperature

Table 4.9. Coefficients of empirical equations relating the dielectric constant ($\sqrt{\varepsilon'}$) and density (ρ) of silicates.

Table 4.10. Dielectric properties of silicates at room temperature

CHAPTER FIVE

Table 5.1 Production statistics (Rio Tinto annual report, May 2003)

Table 5.2. Sample description for point load test

Table 5.3 Complete drop weight test typical size energy combinations

Table 5.4. Appearance function data, t_n (%)

Table 5.5 Crusher Power data

Table 5.6 Complete drop weight test with 50% of typical size energy combinations

Table 5.7. Drop weight test parameters for Palabora ore SAG/AG mills

Table 5.8. Ball charge used for batch grinding

Table 5.9 Summary of the breakage rate and percentage change results

Table 5.10 Selection of Bond work indices for common materials (Kingman, 1998)

Table 5.11 Sample description for Bond work index test

Table 5.12 Summary of BWI results

Table 5.13. Palabora ore particle types.

CHAPTER SIX

Table 6.1. Zinkgruvan production (after Rio Tinto annual report, May 2003)

Table 6.2. Sample description for point load test

Table 6.3. Sample description for drop weight test

Table 6.4. Zinkgruvan drop weight test results

Table 6.5 Summarized results of the microwave effect on ore breakage rate.

Table 6.6. Particle types.

LIST OF SYMBOLS

A, b ore impact breakage parameters

A_s sample area, mm^2

b_{ij} discrete size breakage function.

c speed of light (m/s)

C specific heat capacity of the material (J/kg°C)

C_o, C_f fringing capacitances associated with the coaxial line,

CSIRO Commonwealth Scientific, Industrial Research Organisation

D internal cavity diameter, cm

dE incremental energy required to produce an incremental change dx in size, kW

D_p penetration depth of the wave (m)

E electric field, Vm^{-1}

e emissivity of the sample,

E_{is} specific input energy, KWh/t

E_{cs} specific comminution energy, KWh/t

F, throughput of new feed (t/h)

f frequency, Hz

f_o resonant frequency of empty cavity (Hz),

f_s Resonant frequency of cavity and sample (Hz),

F_{80}, size at which 80% of the feed passes (μm);

G grindability factor (g/rev)

H magnetic field, T(Tesla)

h_i initial height (cm)

HPB Hopkinson pressure bar

ICP Inductively Coupled Plasma Mass Spectrometry

Is(50) Point load strength corrected to 50mm core, MPa

ISRM International Society for Rock Mechanics

J_1 first order Bessel function

JKMRC Julius Kruschnittch Mineral Research Centre

k, n specific parameters that depend on the ore type.

L internal cavity height, cm

m mass of sample (g)

m_d mass of the particle in air (g)

m_{wet} mass of particle in water (g).

$\overline{m}$ mean particle mass (g),

M_d mass of drop weight (kg).

$m_1(t)$ mass percentage of the feed size at grinding time t (g)

P power draw (kW).

PA Palabora type mineralisation

PB Palabora type mineralisation

PC Palabora type mineralisation

PD Palabora type mineralisation

P_d power density of the material (W/m^3),

P_{80}, size at which 80% of the product passes (μm);

P_1 size of test product (μm)

QEM*SEM Quantitative Evaluation of Materials using Scanning Electron Microscopy

Q_L loaded cavity quality factor

Q_0 unloaded cavity quality factor

Q_s quality factor of cavity and sample,

S_1 specific rate of breakage of the feed size (s^{-1})

T temperature of the material (°C),

t duration of heating (s),

t_{10} percentage passing $1/10^{th}$ of the initial mean size,

TE_{10} Transverse Electric field

UCS Uniaxial compressive strength, MPa

UFLC Ultrafast Load Cell

V_c volume of the cavity (mm^3),

V_s volume of the sample (mm^3),

VSWR voltage standing wave ratios

X initial particle size, m

x_{1m} m^{th} root of the first order Bessel function, $J_1(x)=0$,

x_i upper size of interval i, m

x_o standard size, m.

W, work input (kWh/t);

Wi, work index – a material specific constant (kWh/t);

Z_o, impedance of the coaxial line, Ω (Ohm)

Greek Symbols

α characteristic of the material

ε* complex permitivity, F/m

ε′ permitivity or dielectric constant, F/m

ε″ dielectric loss factor,

ε_r' relative dielectric constant,

ε''_{eff} effective relative loss factor

ε_0 permitivity of free space (8.85×10^{-12} F/m)

γ^* complex input reflection constant,

γ magnitude of the complex input reflection,

φ phase angle, °C

λ wavelength of the radiation (m)

ω angular frequency, s^{-1}

ρ density of the material (kg/m^3)

σ Boltzman Constant, J/deg(K)

CHAPTER ONE

INTRODUCTION

Microwave processing of materials is a developing technology that has proven useful in a number of applications. However, microwave processing has not always been as successful as proponents of the technology had hoped. Due to the complexity of microwave interactions with materials, the successful application of microwave processing demands that the user better understands the technique than is necessary for conventional heating. The blind application of microwave processing is likely to lead to disappointing results; however, wise application may have greater advantages than would be anticipated.

Much of the research carried out in microwave processing of materials has been exploratory in nature, often applying to particular materials, sample sizes and geometries, equipment and processing methods. While providing valuable empirical information, these studies have not advanced the general understanding of microwave processing as much as studies in the fundamental interactions between microwaves and materials that could more readily lead to scalable, repeatable production processes. The present research seeks to develop an understanding of microwave processing, starting with fundamental interactions that include dielectric properties of materials plus microwave power density and its effect on ore mineralogy, strength and liberation.

Objectives of Research

- To develop a greater understanding of the influence of ore mineralogy and texture on the microwave heating characteristics

- Determination of loss factor and penetration depth of pure minerals.

- To investigate the influence of high electric field microwave radiation on mineral breakage and liberation
  - Characterization of breakage function of microwave treated and untreated ore samples
  - Comparison of mineral liberation of microwave treated and untreated ore samples.

Research Methodology

In order to accomplish the objectives of the present investigation, a number of materials and items of equipment were selected. For the better understanding of interaction between microwave radiation and mineralogy, 12 pure mineral specimens found in complex ores worldwide were selected: Magnetite (Fe_3O_4), Galena (PbS), Chalcopyrite ($CuFeS_2$), Wolframite ($(Fe, Mn)WO_2$), Chalcocite (Cu_2S), Hematite (Fe_2O_3), Cassiterite (SnO_2), Sphalerite (ZnS), Quartz (SiO_2), Pyrite (FeS_2), Ilmenite ($FeTiO_3$) and Orthoclase ($KAlSi_3O_8$). Characterization of dielectric and thermal properties has been carried out using the cavity perturbation technique and a Perkin Elmer Pyris 1 Thermo gravimetric Analyser. It also included mineralogical investigations using X-ray diffraction technique.

Hard rock ores of complex mineralogy have also been selected including the Palabora ore from South Africa and Zinkgruvan ore from Sweden. The ores were used for the investigation of the effect of microwave radiation on the comminution and grinding behaviour. A microwave system manufactured by Sairem, consisting of a water-cooled microwave source with a frequency of 2.45 GHz and a magnetron generator up to 15 kW. The microwave system can be coupled to either multimode

and single mode applicators. It is equipped with a control system and an automated tuning system to minimise the reflected power.

For preliminary assessment of the effect of microwave on ore breakage a quick evaluation of breakage energy reduction was conducted using point load test. Thereafter, the drop weight test, developed by JKMRC, University of Queensland, Australia was used for breakage characterization in crushers and autogenous mills. A lab-scale tumbling ball mill was also used for the evaluation of the rate of breakage in ball mills and characterization of Bond Work Index.

The effect of microwave radiation into mineral liberation was also carried out using optical microscopy and QEM*SEM techniques. Detailed information of the nature of mineral and ores, methodology of investigation and techniques in use is given in the following Chapters of this thesis.

CHAPTER TWO
Theoretical Aspects Of Microwave Heating

2.1 Introduction

Heating is widely used in industries such as food, chemical, textiles and ceramics for drying, promoting chemical or physical changes and other purposes. However, it remains a difficult process to control, being slow and imprecise. Conventional heating, i.e. by radiation, conduction and convection or, commonly, a poorly controlled mixture of all three, is limited by the rate of heat flow into the body of the material from the surface. This rate is determined by the physical properties of the material i.e. specific heat capacity, thermal conductivity and density. It is, therefore, not only slow but frequently non-uniform, with the surfaces and, in particular, edges and corners being much hotter than the inside.

Imperfect heating can result in unacceptable levels of product rejection and is also wasteful of energy. In addition, the extended process time often required to ensure even heating rates results in large production areas devoted to ovens. Large ovens are slow to respond to rapid required temperatures changes. Control becomes difficult and expensive. One alternative to the conventional heating is volumetric heating.

2.2 Volumetric Heating

The basis of volumetric heating lies in the ability of an electric field to attract polar or ionic features in the material. When such materials are exposed to a rapidly varying electric field, dipoles are enable to re-align themselves and energy is dissipated volumetrically as the electromagnetic wave propagates (Meredith, 1998). The heat energy induced in the material is transferred through the surface by an

electromagnetic wave (Figure 2.1) and does not flow as a heat flux, as in conventional heating. The rate of heating is no longer limited by thermal diffusivity and surface temperature and the uniformity of heat distribution may be improved. Heating times can be reduced to less than 1% of that required using conventional techniques, with effective energy variation within the material of less than 10% (Whittaker, 1997).

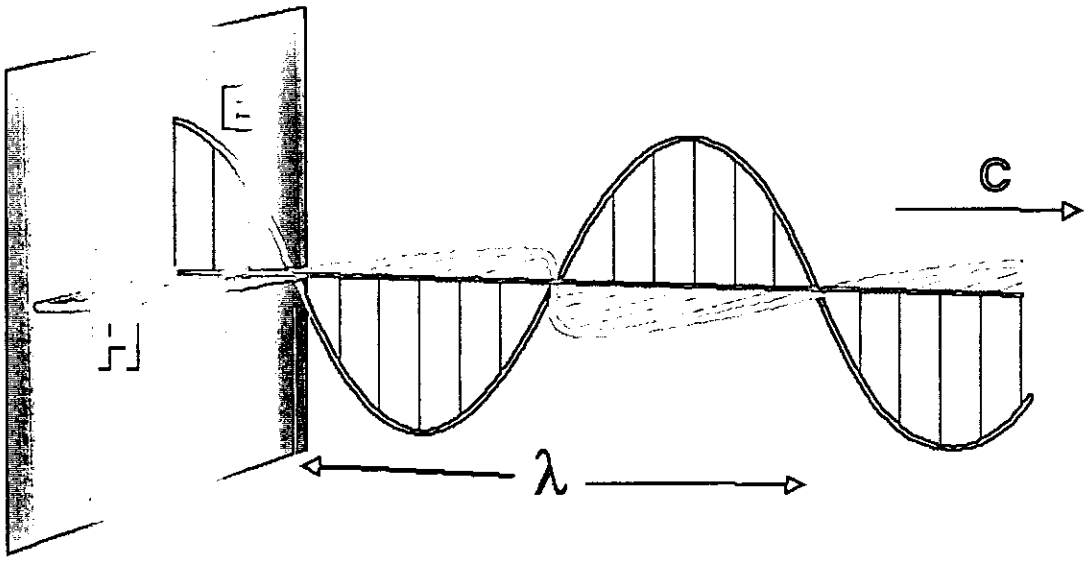

Figure 2.1 Electromagnetic wave components (after Whittaker, 1997). E, electric field, H, magnetic field, λ, wavelength and c, propagation velocity.

The principal characteristics of electromagnetic waves are their wavelength and frequency, which are linked by the equation:

$$c = \lambda . f \qquad (2.1)$$

where:

λ is the wavelength of the radiation (m)

c is the speed of light (m/s)

f is the frequency of the radiation (Hz)

According to Metaxas and Meredith (1983), any material can be heated directly by electromagnetic heating provided that it is neither a perfect electrical conductor nor a perfect insulator. This electromagnetic energy is the same type as that used for broadcasting, television, radar and satellite communications. In communications the purpose is to radiate power into space. In electromagnetic heating the waves are often generated at much higher power levels but must be contained within the equipment. Indeed, the amount of leakage has to be controlled within legal limits for the safety of nearby personnel and to avoid interference to other services.

Such electromagnetic heating techniques have particular operating frequencies that are chosen by international agreement with the principal aim of minimising interference with communications services. Figure 2.2 shows the frequencies allowed for electromagnetic heating techniques relative to those allocated for other uses. The frequencies chosen for RF and microwave heating, often, designated ISM (industrial, scientific and medical) frequencies, are the result of historical evolution and a complexity of international committees, which constantly review the use of the electromagnetic spectrum (Meredith, 1998). In the UK these are 433MHz, 896MHz and 2450MHz. In some countries, 896MHz is replaced by 915MHz.

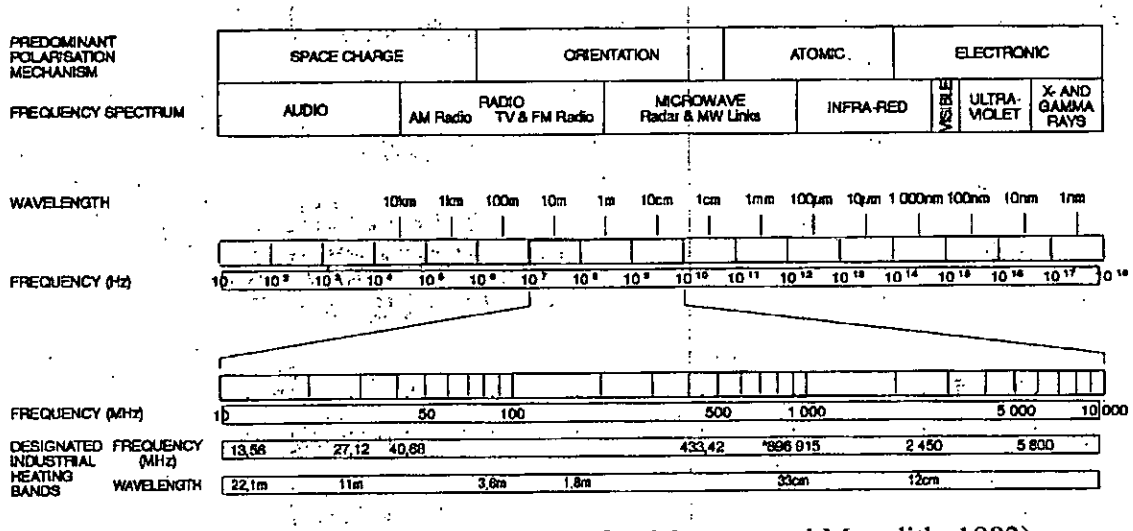

Figure 2.2 The electromagnetic spectrum (after Metaxas and Meredith, 1983).

2.2.1 Microwave Interaction with Materials

The interaction of an electric field with a material has its origin in the response of charged particles to the applied field. The displacement of these charged particles from their equilibrium positions gives rise to induced dipoles. A dipole is essentially two equal and opposite charges separated by a finite distance. An example of this is the stereochemistry of covalent bonds in a water molecule, giving the water molecule a dipole moment. Dipoles may be a natural feature of the material or they may be induced (Meredith, 1998). Distortion of the electron cloud around non-polar molecules or atoms through the presence of an external electric field can induce a temporary dipole moment.

According to Chen et al. (1984), in the presence of microwave radiation materials can be classified into one of three groups: conductors, insulators and absorbers (Figure 2.3). Materials that absorb microwave radiation are called dielectrics and have two important properties (Paoloni, 1989):

- Dielectrics have very few free charge carriers. When the external electric field is applied there is therefore, very little charge carried through the material matrix.
- The molecules or atoms comprising the dielectric exhibit a dipole moment.

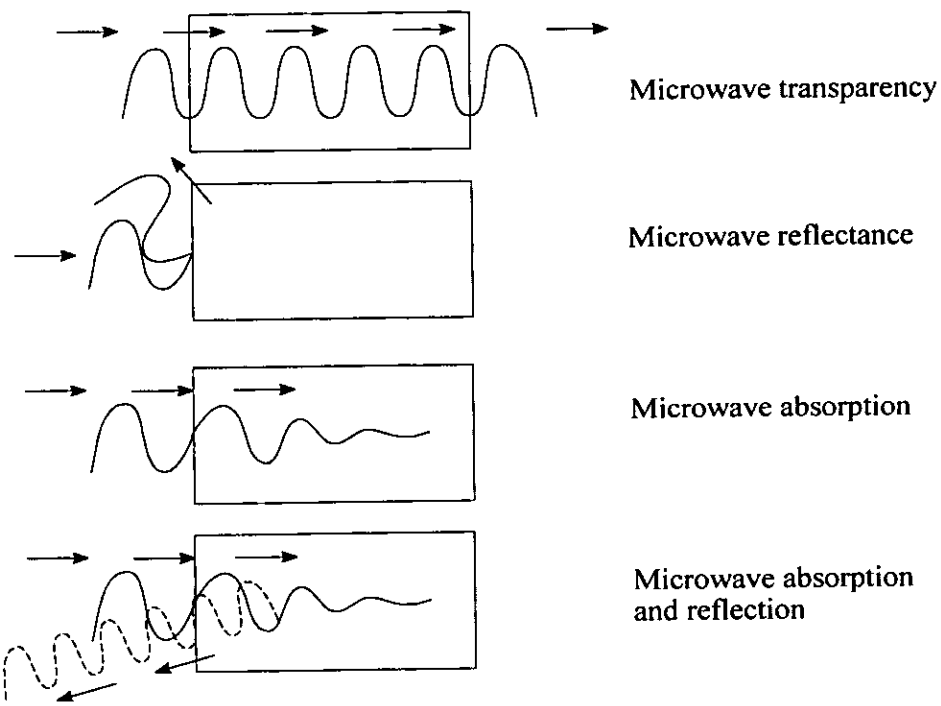

Figure 2.3 Classification of materials in the presence of microwave radiation (after Chen et al., 1984)

2.2.2 Mechanisms of Microwave Heating

When a dielectric material is present in an externally applied electric field the component dipoles align themselves in the direction of the field. This gives the dielectric an increased internal energy. When present in the alternating field associated with microwave radiation, the aligned dipoles flip around at the same frequency as the radiation. Internal energy is lost as friction and the material heats as

a result. Heating may be a result of three basic polarisation mechanisms: ionic polarisation, orientation polarisation and interfacial or Maxwell-Wagner polarisation.

2.2.2.1. Ionic polarisation

Induced dipoles arise mainly from the displacement of electrons around nuclei (electronic polarisation) or from the relative displacement of atomic nuclei as a result of the unequal distribution of charge in molecule formation (atomic polarisation). In the presence of microwave radiation these induced dipoles will cause heating in the sample due to any electrical resistance. If the sample has low electrical resistance, most of the microwave energy will not penetrate the surface of the material, but will be reflected from it. However, high surface voltages may still be induced and, are responsible for the arcing that is observed from metals in microwave fields (Whittaker, 1997).

2.2.2.2. Orientation Polarisation

Liquids such as water, methanol or ethanol contain permanent dipoles due to the asymmetric charge distribution in their molecules. These tend to align under the influence of electric field, thus giving rise to orientation polarisation (Whittaker, 1997 and Meredith and Metaxas, 1983). Under a very high frequency electric field, the polar molecules will attempt to follow the field but intermolecular inertia prevents significant motion before the field has reversed and no net motion results. If the frequency of field oscillation is very low, then the molecules will be polarised uniformly. In the intermediate case, the frequency of the field will be such that the molecules will be almost but not quite able to keep in phase with the field polarity. In this case, the motion resulting as molecules attempt to follow the field gives rise to the heating that is observed in the sample.

2.2.2.3. Interfacial Polarisation

This mechanism has its source of polarisation from charge build-up in interfaces between components in heterogeneous systems. Termed interfacial or Maxwell-Wagner polarisation, it occurs in systems comprised of conducting inclusions in a second, non-conducting material (Meredith and Metaxas, 1983). An example would be a dispersion of metal particles in sulphur. Sulphur is microwave transparent and metals reflect microwaves yet it is found that the combination forms an extremely good microwave absorbing material. Interfacial polarisation is an effect that is very difficult to treat in a simple manner and is viewed as a combination of the conduction and dipolar polarisation effects (Whittaker, 1997).

2.3 Microwave Equipment

Many different electronic components exist that are able to generate significant amounts of microwave energy (Meredith and Metaxas, 1983 and Gallawa, 2000) these include magnetrons, solid-state devices and klystrons. The most popular device for industrial applications, however, is the magnetron. This is because it offers high power output levels and excellent frequency stability in an efficient and cost effective package. A typical microwave system is shown in Figure 2.4. It comprises a microwave power generator unit, the applicator and control unit.

Once generated, microwaves are conducted by an electromagnetic transmission line to an applicator in which they interact with the product to be heated. The transmission line is either a hollow section of metal, known as wave-guide, or a coaxial cable. Wave-guides may be either rectangular or circular and are made either entirely of a conductive material, such as aluminium or copper, or of a non-

conductive material with a thin conductive coating on its inner surface (Meredith and Metaxas, 1983).

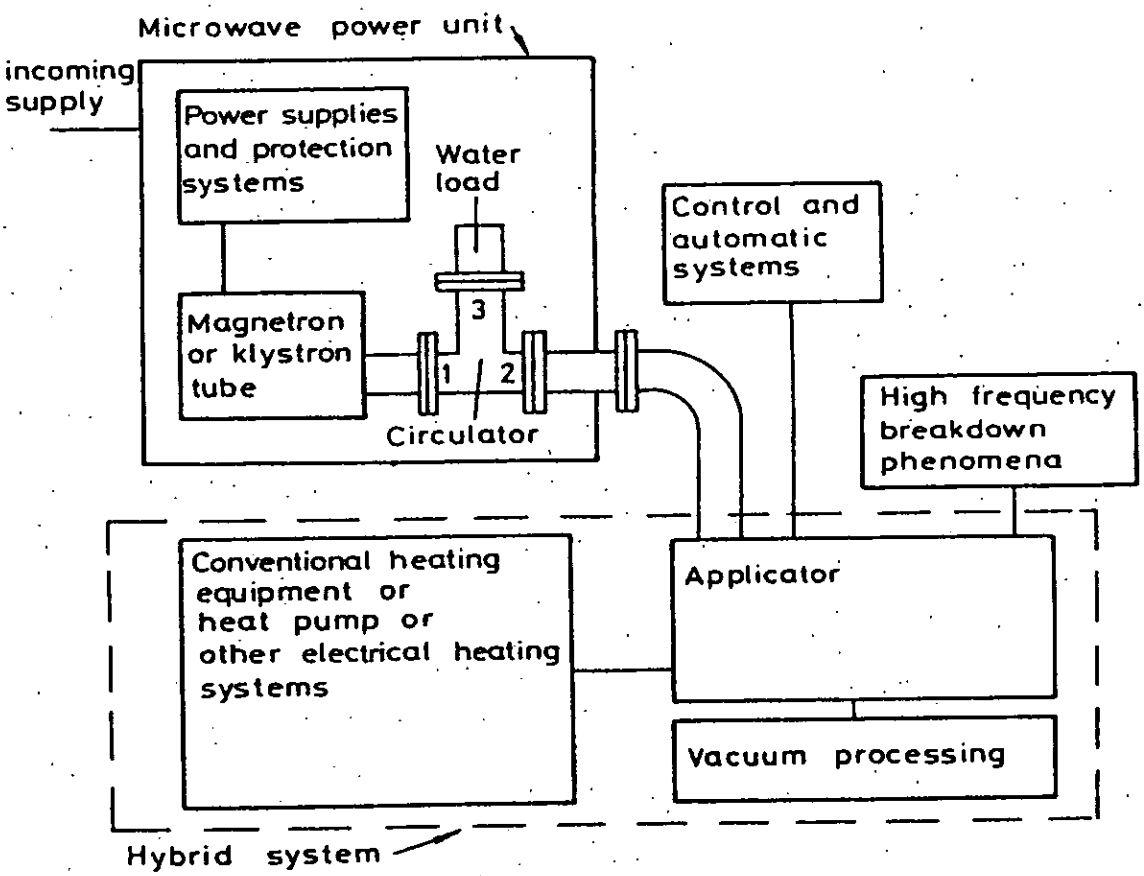

Figure 2.4 Block diagram of microwave heating system (after Meredith and Metaxas, 1983).

The applicator can have different geometries but is usually a metallic box at whose walls the microwaves can be reflected with as little loss as possible and through which they cannot escape. Between the applicator and the magnetron often there is an adjustable tuner and an isolator. The purpose of the tuner is to match the impedance of the generator and transmission line to the impedance of the load. The isolator has the task to redirect excess microwave energy, which is not being absorbed in the load and is being reflected back along the wave-guide, to a water load and thus prevent overheating and consequent damage of the magnetron.

2.4. Dielectric Properties of Materials

Dielectric properties are the physical properties of materials that can be measured and used to predict behaviour in the presence of a microwave field. A good estimate of the dielectric properties of a material is important for cavity design to ensure a realistic prediction of power loss density. In microwave assisted processing, knowledge of material properties is also important for prediction of the best particle size at which to apply the microwave treatment. Specific measurements are required to extract the required parameters. The property that describes the behaviour of a dielectric under the influence of high frequency is known as the complex permittivity, which is defined by equation (2.2):

$$\varepsilon^* = \varepsilon' - j\varepsilon'' = \varepsilon_0(\varepsilon_r' - j\varepsilon_{eff}'') \qquad (2.2)$$

Where ε* is the complex permitivity, ε′ is permitivity or dielectric constant, ε″ is the dielectric loss factor, ε_r' is the relative dielectric constant, ε_{eff}'' is the effective relative loss factor and ε_0 is the permitivity of free space (8.85×10^{-12}F/m). Both ε′ and ε″ are frequency and temperature dependent.

The dielectric constant is a measure of the ability of charges and dipoles in a material to store electromagnetic energy. It also defines the velocity of propagation of an electromagnetic wave through the dielectric and can be related to the refractive index (Meredith and Metaxas, 1983, Fletcher, 1995). The dielectric loss factor is a measure of the ability of the dielectric to dissipate the stored energy as heat in the material. The ratio between the dielectric loss factor and the dielectric constant measures how well a material absorbs the electromagnetic energy and dissipates it as heat in the material. This property, called loss tangent, $tan\delta$, is commonly used to describe the ability of the material to heat in an applied electromagnetic field.

$$\tan\delta = \frac{\varepsilon''}{\varepsilon'} \qquad (2.3)$$

2.4.1. Loss Factor

Not all dielectric materials have the same ability to heat in applied electric fields. Water has a high loss factor and therefore is an excellent dielectric heater (Ghandi, 1981). In general materials with loss factors greater than 0.02 can be regarded as likely dielectric heaters (Meredith and Metaxas, 1983). Where the material is highly absorptive to microwave radiation, most of the incident energy is absorbed within the first few millimetres, leaving the internal parts little affected. This causes non-uniformities of heating which for volumetric heating is totally unacceptable. Therefore, loss factors between the limits $10^{-2}<\varepsilon''<5$, would present materials which, in general, are good candidates for microwave heating applications (Meredith and Metaxas, 1983 and Bradshaw, 2002).

For some materials the increase in loss factor with temperature can be significant. Hence, a material that will not respond to microwave radiation at low temperatures may become treatable if first pre-heated by other means. The positive temperature coefficient of the loss factor may result in thermal runaway, particularly where a phase change causes a sudden increase in loss factor. Table 2.1 shows loss factors for some common materials at various frequencies (Hulls, 1992).

Table 2.1 Loss factors for some common materials (after Hulls 1992)

MATERIAL	27.12MHz	900MHz	2450MHz
Pork Fat	51	17	2.7
Polyethylene	<0.1	<0.1	0.001
PVC	<0.1	<0.1	0.1
Salt Water	900	29	19.6
Pure Water	0.4	3.9	10.7
Dry Wood	0.4	0.3	0.3
Wet Wood	1.2	0.9	1.4
Asphalt	0.4	0.3	0.2

2.4.2. Measurement Techniques

Measurement of dielectric properties requires specialized techniques and dielectric properties often vary with frequency, temperature, composition and density. Different methods are available for the measurement of dielectric properties, which continue to be refined to overcome new measurement problems. They can be classified under four main groups: bridge or Q-meter, resonant cavity, coaxial line and free space techniques (Tinga, 1992). The bridge and Q–meter methods are usually employed for frequencies below 100 MHz and so are not used for microwave heating frequencies. Measurements using coaxial lines, wave-guides or resonant cylindrical cavity techniques are considered to be the most suitable for frequencies above 100 MHz (Meredith and Metaxas, 1983).

The free space technique is suitable for measurement on sheet like samples and is limited for frequencies above 10GHz and so is not suitable at the ISM frequencies of interest. The coaxial line method is accomplished by determining the propagation constant of the electromagnetic wave in the material. The resonant cylindrical cavity method is based on measurements of the change in quality factor and resonant frequency in a cavity when a sample is inserted. It is distinguished by its high measuring precision and simple calculations and does not have a special requirement for ore geometry, size and kind of the sample such as solid, powder or liquid.

2.4.2.1. Coaxial Line Technique

The Roberts and Von Hippel method (Metaxas and Meredith, 1983), also known as the open-ended coaxial line, involves the examination of standing waves in a transmission line or waveguide terminated by a section filled with the dielectric

under investigation. Figure 2.5 illustrates the general form of the apparatus and the standing wave pattern, which is associated with it.

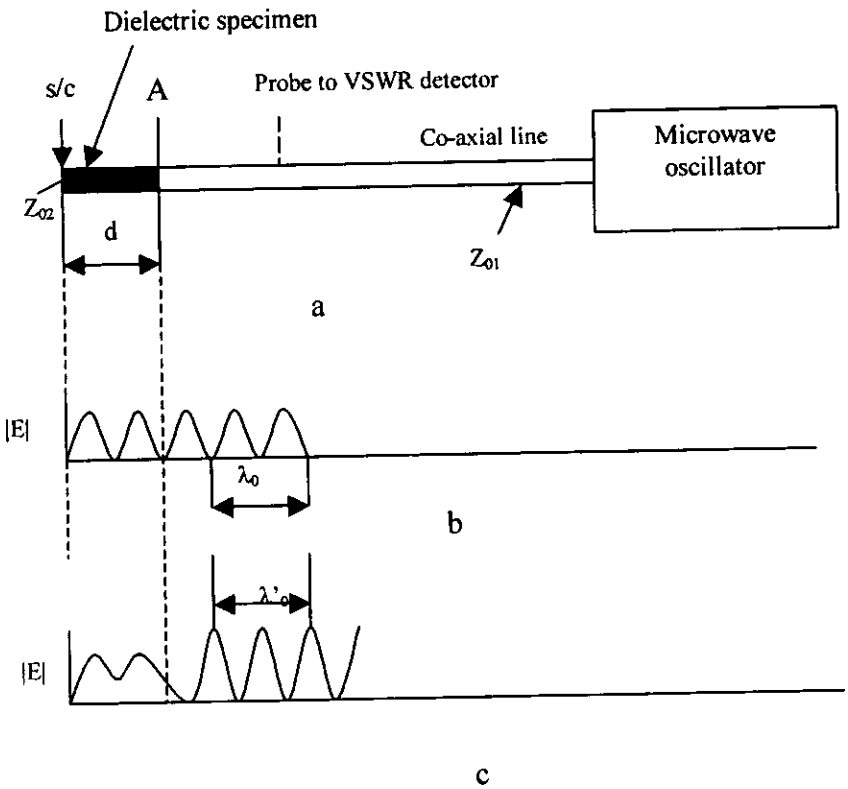

Figure 2.5 The Roberts and Von Hippel method for dielectric measurements. a) General form of apparatus, b) Standing wave pattern with empty slotted coaxial line, c) Standing wave pattern with dielectric specimen of length d at the end of the slotted coaxial line (after Meredith and Metaxas, 1983).

The system makes use of a vector network analyser in conjunction with a reflection test set. The network analyser supplies the signal to the end of the coaxial line. It also measures the magnitude and phase of the applied and reflected signal as well as the impedance at the end of the coaxial line. Comparison of these signals gives the complex reflection coefficient at the end of the coaxial line (Meredith and Metaxas, 1983, Arai et al., 1992 and Salsman, 1992). The complex permitivity can then be determined using the equations:

$$\varepsilon^* = \frac{1-\gamma^*}{j\omega Z_o C_o (1+\gamma^*)} - \frac{C_f}{C_o} \qquad (2.4)$$

$$\gamma^* = \gamma\cos\varphi + j\gamma\sin\varphi \tag{2.5}$$

Where γ^* is the complex input reflection constant, γ the magnitude of the complex input reflection, φ is the phase angle, $\omega = 2\pi f$ is the angular frequency, f is the frequency, C_o and C_f are fringing capacitances associated with the coaxial line, Z_o, is the impedance of the coaxial line and ε^* is the complex permitivity.

The complex input reflection can be expressed by its component, the real and imaginary part, and therefore the real and imaginary components of the complex permitivity.

$$\varepsilon' = \frac{-2\gamma\sin\varphi}{\omega Z_0 C_0(1+2\gamma\cos\varphi+\gamma^2)} - \frac{C_f}{C_0} \tag{2.6}$$

$$\varepsilon'' = \frac{1-\gamma^2}{\omega Z_0 C_0(1+2\gamma\cos\varphi+\gamma^2)} \tag{2.7}$$

Where ε' is the real permitivity or dielectric constant and ε'' is the imaginary permitivity or loss factor. The determination of C_0 and C_f the fringing capacitances are complex. The equations involved are not described and the reader is directed towards the papers of Arai et al., 1992 and Salsman, 1991.

The Robert and Von Hippel technique is primarily suited for use with solids however Williams and Price have adapted it for the measurement of the complex dielectric constant in lossy liquids (Meredith and Metaxas, 1983). Several authors have used the coaxial line probe for measuring dielectric properties of materials (Nelson, 1983 and 1988, Church et al., 1988, Salsman, 1991, Horderfield et al., 1992, Arai et al., 1992 and Fletcher 1995). The technique is mainly used at room temperature. It has been adapted, however, for measurements at higher temperatures (Salsman, 1991, Arai et al., 1992 and Fletcher 1995).

In a system developed at The University of Nottingham sample preparation required for measurement using coaxial surface probe requires the provision of a smooth flat surface of approximately 20mm in diameter (Arai, 1995 and Fletcher, 1995). The end of the probe on which the sample is mounted is inserted into a conventional heated furnace. A water jacket, mounted between the furnace and the conventional microwave components, prevents damage from excess temperature. The surface probe is connected to a vector network analyser, which measures the input reflection coefficient. The system is controlled using a PC computer running a customized program that acts as the system controller. Operation is automatic and the equipment can be left unattended during measurement over the desired temperature range (Arai et al., 1992). Figure 2.6 shows a typical arrangement of the high temperature measurement system used by Salsman (1992), Arai et al., (1992) and Fletcher (1995).

2.4.2.2. Resonant Cylindrical Cavity Technique

Methods based on the electromagnetic field perturbation of a resonant cavity by a small sample inserted in it have been used extensively for measuring the dielectric properties of low loss materials (Meredith and Metaxas, 1983). According to Arai (1995), resonant cavities are the most adaptable arrangement for high temperature dielectric property measurement but the available frequencies normally depend on the choice of resonant modes. This limits the characterization of dielectric properties to a number of discrete frequencies. However, in addition to the relative simplicity of its design its inherent accuracy, particularly for low loss materials, encouraged many workers to use this technique (Arai, 1995 and Hutcheon et al., 1992). In the past, the technique has been used in conjunction with various sample heating arrangements.

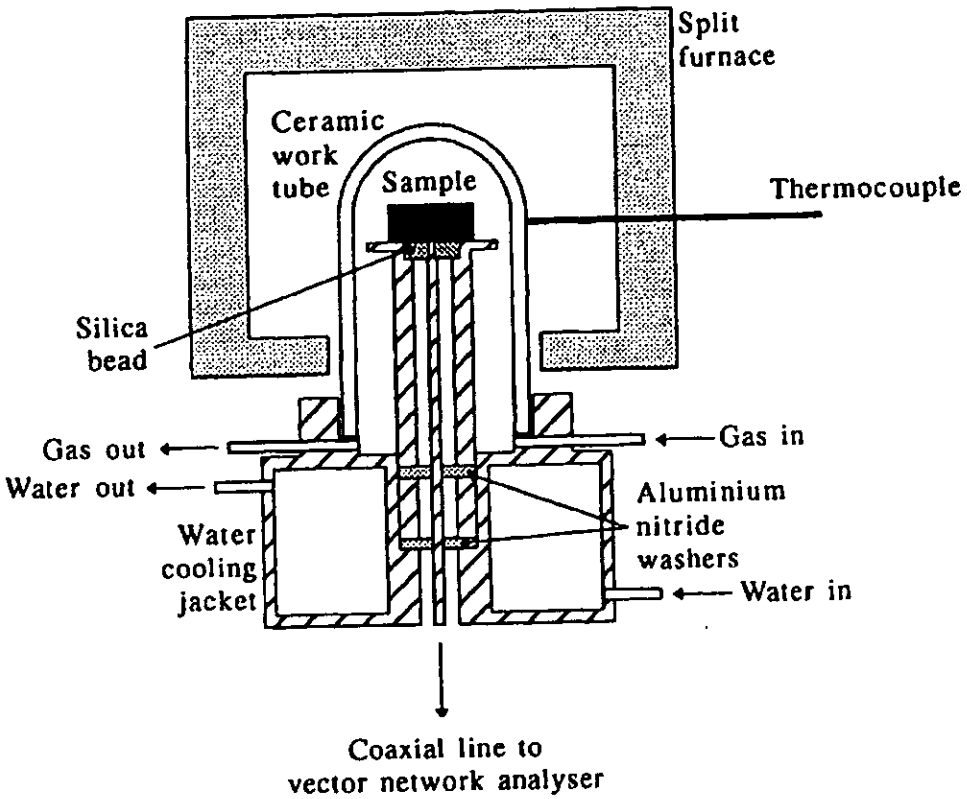

Figure 2.6 High temperature coaxial surface probe and surrounding equipment for dielectric properties measurement, control diagram (after Arai et al., 1992).

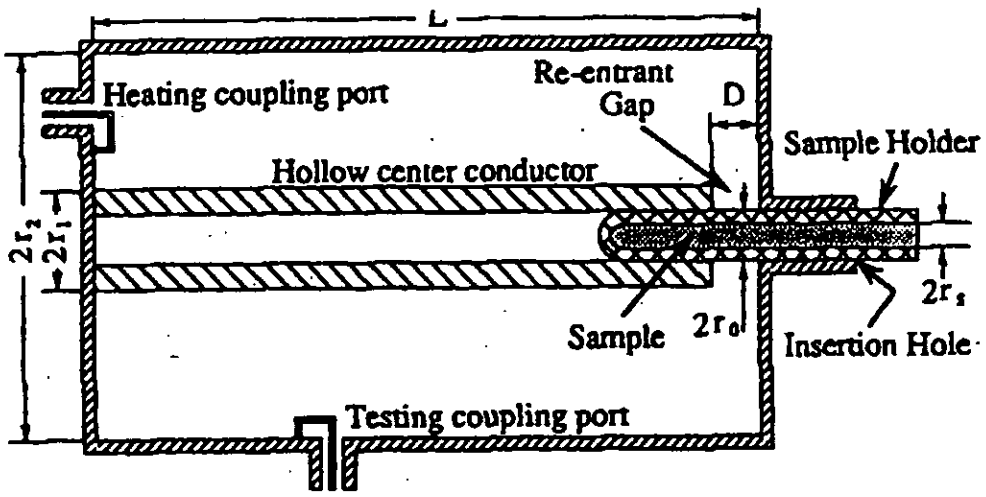

Figure 2.7 Cross section of coaxial re-entrant resonator used as a heating and testing chamber (after Tinga, 1992).

Tinga et al. (1992), in an unusual arrangement, used microwaves to heat the test sample (Figure 2.7). The design had the advantage of providing rapid heating

compared with a system using a conventional furnace and samples can be liquid, solid or pressed powder.

In the most common arrangement, a circular cylindrical cavity is mounted beneath a conventional furnace but insulated from it, as shown in Figure 2.8 (Arai et al., 1993, Fletcher 1995 and Greenacre 1996).

The circular cylindrical resonant cavity is particularly useful for making measurements on lightly compressed powder samples. The sample is held in a fused silica sample holder and the density of the powder is calculated by measuring the volume of the known mass of material.

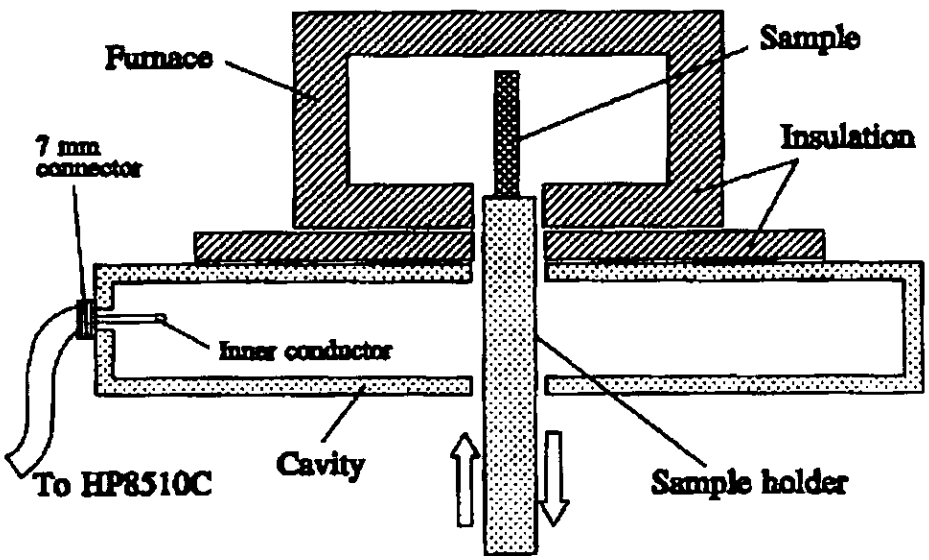

Figure 2.8 Schematic diagram of the resonant cylindrical cavity (after Arai et al., 1993).

A cavity is defined as a dielectric region of any shape completely surrounded by conducting walls. It is said to resonate if the stored electrical energy is equal to the stored magnetic energy. The frequencies at which this effect occurs are called the resonant frequency modes. During resonance, energy is dissipated in the walls of the cavity. This loss gives rise to quality factor (Q) of the cavity (the ratio of total energy stored by the energy dissipated per cycle), which is a direct measurement of its

lossiness. The insertion of a sample into the cavity alters the energy dissipation characteristics of the cavity as well as the resonant frequency and knowledge of these alterations allows the dielectric properties of the sample to be estimated.

The resonant cylindrical cavity technique is based on this simple perturbation theory, which assumes that the change in the stored energy in the cavity between the loaded and unloaded conditions is very small. This means that the electromagnetic fields in the cavity with and without the sample must be approximately equal (Klein et al., 1993). Therefore, for the above effects to be observed, the following criteria should be noted:

- The specimen is very much smaller than the cavity;
- That specimen dimensions are smaller than the wavelength of the radiation used and
- The sample is located in a region of uniform field.

The errors in the measurement of the complex permitivity of a material by the simple cavity perturbation method depend not only upon the accuracy of the measurements of the frequencies and Q-factors but also upon the validity of the approximations made in the determination of the electric field in the interior of the cavity. As a general rule, small samples are chosen to reduce the errors in the perturbation approximation. However, the sample size should not be too small otherwise the changes of the resonant frequency and Q-factor due to the insertion of the sample are too small to be measured accurately and the errors in the estimate of complex permitivity can be very large. This implies that, for a given material, due to the conflicting requirements of small size for small perturbation and large size for small percentage errors in frequency shift and Q value change, an optimum sample size for minimum errors can be found (Klein et al., 1993).

The assumption that the sample is located in a region of uniform electric field is satisfied when a rod shaped specimen is placed along the axis of a large, flat cylindrical cavity resonating in the TM_{0n0} modes (Klein et al., 1993 and Denovan et al., 1993). Cavities operating in the TM_{0n0} modes are useful for this purpose since the electric field is parallel to the direction of propagation and, therefore, along the axis of the material. TM_{0n0} mode resonant cylindrical cavities have their maximum electric field along the axis of the cavity and it diminishes radially to zero at the wall (Meredith and Metaxas, 1983 and Klein et al., 1993). In addition, the magnetic field in a TM_{0n0} mode diminishes to zero at the axis of the cavity, thus a sample on the axis in such mode distribution may be treated as being in pure electric field and effect of the magnetic permeability of the material on the field ignored.

The characterisation of the electromagnetic field in a cylindrical cavity can be obtained theoretically from the solutions of Maxwell's equations. An expression relating the resonant wavelength and dimensions of the cavity is given by (Meredith and Metaxas, 1983):

$$\lambda = 2\left[\left(\frac{2x_{l,m}}{\pi D}\right)^2 + \left(\frac{n}{L}\right)^2\right]^{-1/2} \tag{2.8}$$

Where x_{lm} is the m^{th} root of the first order Bessel function, $J_1(x)=0$, D is the internal cavity diameter and L is the internal cavity height. Making $c=f\lambda$, equation 2.8 may be rewritten as:

$$(fD)^2 = \left(\frac{cx_{lm}}{\pi}\right)^2 + \left(\frac{cn}{2}\right)^2\left(\frac{D}{L}\right)^2 \tag{2.9}$$

Plots of $(fD)^2$ versus $(D/L)^2$ are straight lines with intercept $(cx_{lm}/\pi)^2$ and gradient $(cn/2)^2$ and are called mode charts as shown in Figure 2.9. The above expression thus allows the calculation for the choice of dimensions required for a particular TM

mode resonant frequency within a cylindrical cavity. Therefore, proper design of a cylindrical cavity resonating on TM_{0n0} can be developed and used for measurement of frequency shift and change of cavity Q factor.

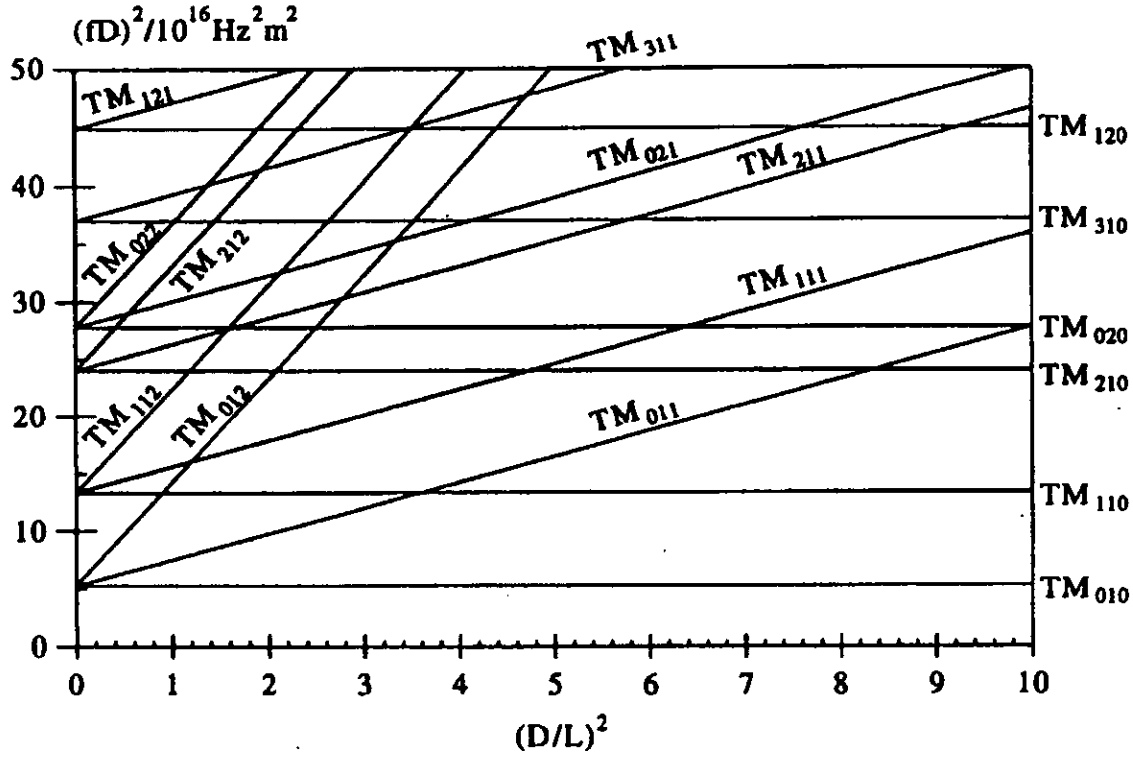

Figure 2.9. Lower order TM_{lmn} mode chart for an empty resonant cylindrical cavity (after Meredith and Metaxas, 1983).

The dielectric properties of any given material can then be calculated from the measured frequency shift and change of cavity Q factor before and after sample insertion, using Maxwell's equations 2.10 and 2.11 developed from the perturbation theory:

$$\varepsilon' = 1 + 2 * J_1^2(X_{l,m}) * \frac{V_c}{V_s} * \frac{f_0 - f_s}{f_0} \qquad (2.10)$$

$$\varepsilon'' = J_1^2(X_{l,m}) * \frac{V_c}{V_s} * (\frac{1}{Q_s} - \frac{1}{Q_o}) \qquad (2.11)$$

Where ε' is the dielectric constant or real permittivity, ε'' is the loss factor or imaginary permittivity, V_c is the volume of the cavity (mm^3), V_s is the volume of the

sample (mm^3), f_o is the resonant frequency of empty cavity (Hz), f_s is the resonant frequency of cavity and sample (Hz), Q_s is the quality factor of cavity and sample, Q_o is the quality factor of empty cavity, J_1 is the first order Bessel function and $X_{l,m}$ is the m^{th} root of J_0.

$$J_0(x) = 1 - 2.249\left(\frac{x}{3}\right)^2 + 1.265\left(\frac{x}{3}\right)^4 - 0.316\left(\frac{x}{3}\right)^6 + \ldots \quad (2.12)$$

$$J_{n+1}(x) = \frac{2n}{x} J_n(x) - J_{n-1}(x), J_{-n}(x) = (-1)^n J_n(x) \quad (2.13)$$

Calculation of dielectric properties of minerals using this technique is presented in Chapter 4.

2.4.2.3. Calculation of Penetration Depth

Microwave heating involves the conversion of electromagnetic energy into heat. As the electromagnetic energy travels through the material to be heated, it is attenuated exponentially at a rate described by the qualitative relationships of absorbed power per unit volume and the depth of penetration, i.e. the distance from the surface into the material at which the power drops to e^{-1} of the original. Figure 2.10 shows the essential features of such propagation. Derivations from Maxwell's equations give the general expression for calculation of penetration depth of materials (Metaxas and Meredith, 1983).

$$Dp = \frac{c}{2\pi f \sqrt{2\varepsilon'(\sqrt{1+(\varepsilon''/\varepsilon')^2} - 1)}} \quad (2.14)$$

For low loss materials ($\varepsilon''/\varepsilon' < 1$) the penetration depth can be approximated by the equation 2.15, (Metaxas and Meredith, 1983).

$$Dp = \frac{c.\sqrt{\varepsilon'}}{2\pi f \varepsilon''} \quad (2.15)$$

Where D_p is the penetration depth of the wave (m), c is the speed of light (m/s) and f is the frequency of the electromagnetic wave (s^{-1}).

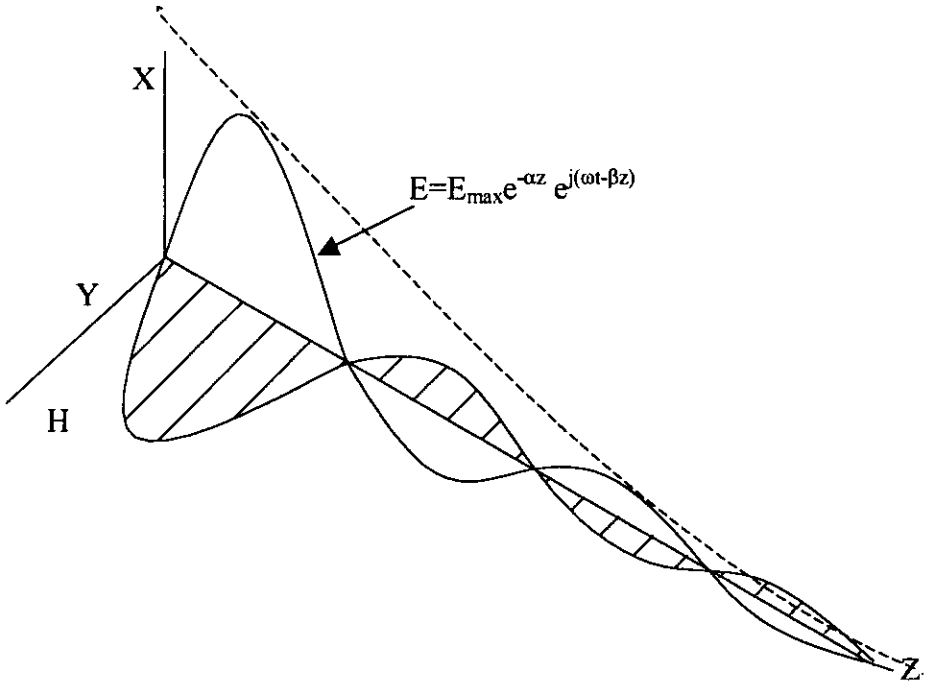

Figure 2.10. Propagation of a plane wave in a lossy medium (after Metaxas and Meredith, 1983).

From equation 2.15 it is important to realise that low frequencies do not necessarily produce greater heating. The penetration may be large but, as the depth increases, the internal electric fields become very small so the heating rate may not increase.

2.4.3 Power Flow And The Power Dissipation Density

Microwave heating involves the conversion of electromagnetic energy into heat. Analogously with ordinary electric circuits, in which the power (watts) is the product voltage x current, the power flow associated with a plane wave can be calculated from the Poynting vector (Meredith, 1998).

According to Meredith (1998), in electromagnetic heating applications, the power flux density in a plane wave is not the power actually dissipated in an absorbing medium, i.e., a material, but is the power incident upon the material. The power dissipation density is the power absorbed per unit volume of the material, has the unit watts per cubic metre and its magnitude is dependent on the dielectric properties of the material.

Therefore, according to Meredith (1998), the power absorbed or power dissipation density by a given material, whereas the electric field is uniform, can be calculated by the following equation:

$$P_d = 2.\pi.f.E^2.\varepsilon_0\varepsilon'' \qquad (2.16)$$

where P_d is the power density in watts per cubic metre, f is the applied frequency in Hertz, E is the electric field strength in volts per metre, ε_0 is the permittivity of free space (8.85×10^{-12}F/m) and ε'' is the loss factor.

It can be seen that heat generation is proportional to the square of the field strength within the material. The equation also shows that the power absorbed varies linearly with frequency and the loss factor.

2.4.4. Calculation of Temperature Change

As the microwave energy is absorbed in a material its temperature increases at a rate dependant upon a number of parameters. The rate of change of temperature of a well-mixed system by conventional heating process is given by the following relationship (Stuchley, 1983):

$$\frac{dT}{dt} = \frac{P_d}{C.\rho} \qquad (2.17)$$

where T is the temperature of the material (°C), t is the duration of heating (s), P_d is the power density of the material (W/m^3), ρ is the density of the material (kg/m^3) and C is the specific heat capacity of the material (J/kg°C).

For a dielectric heating process, assuming a uniform electric field and well-mixed system, equation (2.17) can be seen to change to give (Mingos, 1991):

$$\frac{dT}{dt} = \frac{K.\varepsilon''.f.E^2}{\rho.C} \qquad (2.18)$$

where, K is a constant.

Energy loss due to radiation of heat are given by:

$$\frac{dT}{dt} = \frac{-e.\sigma.A_s}{\rho.C.V_s} \qquad (2.19)$$

Where, e is the emissivity of the sample, σ is the Boltzman Constant, A_s is the sample area and V_s is the sample volume.

The temperature of the sample can, therefore, be seen to depend on the thermal and dielectric properties of the material. In practice though, it is difficult to calculate the power density since the internal field intensity is hard to predict and the dielectric properties of most materials vary with temperature.

2.4.5. Factors Affecting the Dielectric Properties of a Material

As previously demonstrated, the dielectric properties of a material influence the response of that material to an applied microwave field. The dielectric properties are not constant, however, but vary with several factors (Nelson et al., 1990). The dielectric properties of a material are also highly dependent on their chemical composition and more particularly on the permanent dipole moments associated with any molecules making up the material of interest. The dielectric properties of a material also depend on the frequency of the applied electric field, the temperature of the material its density and physical structure. In hygroscopic materials, for example, the amount of water present is usually a dominant factor because of its excellent microwave absorbing properties. In granular or particulate materials, the bulk density

of the air-particle mixture is another factor, which influences the effective dielectric properties.

2.4.5.1. Frequency Dependence

With the exception of some extremely low loss materials, the dielectric properties of most materials vary considerably with the frequency of the applied electric field (Nelson, 1973). An important phenomenon contributing to the frequency dependence of the dielectric properties of most materials is the polarisation arising from the orientation of molecules having permanent dipole moment with the imposed electric field (Whittaker, 1997).

2.4.5.2. Temperature Dependence

The dielectric properties of materials are also temperature dependent, the nature of the dependence being a function of the dielectric relaxation processes operating under the particular conditions and the applied frequency. Dielectric relaxation is defined as the time taken for the dipoles to return to random orientation when the electric field is removed (Nelson et al., 1990). As temperature increases, the relaxation time decreases and the dielectric constant will increase (Bottcher et al., 1978). In addition, according to Bottcher et al., distribution functions have been shown to be useful in expressing the temperature dependence of dielectric properties. However, the frequency and temperature dependence of the dielectric properties of most materials is complex and can best be determined directly by measurement at the frequencies and conditions of interest.

2.4.5.3. Density Dependence

The influence of a dielectric depends on the amount of its mass interacting with the electromagnetic field. Therefore, the mass per unit volume or density will have an effect on the effective dielectric properties of a particular material. This is especially notable in the case of particulate dielectrics such as pulverised or granular materials. Density dependence of particulate materials over a range of bulk densities was studied in depth and linear relationships between the square root and the cube root of the dielectric constant were developed by Nelson in 1983.

2.4.5.4. Influence of Crystallography

The crystallography of materials has been demonstrated to have an effect on dielectric properties. Hematite has been subjected to microwave radiation by various authors (Chen et al., 1984 and Walkiewicz et al., 1988). It was found to be a good absorber of microwave energy, arcing at high temperature. However, Wright, in 1991, found the mineral to be transparent to radiation. The difference in the results can possibly be explained by the different forms of hematite used in the experiments.

2.5. Applicators

The term applicator is used in microwave heating to refer to a device into which a material is inserted for processing. Industrial microwave applicators for processing a variety of materials may be classified into three main categories: travelling wave-guide, multimode and single mode applicators (Meredith and Metaxas, 1983). The design of the applicator depends on the use of the system, shape or type of product. Above all, the applicator must always be efficient and safe. For this reason most applicators are closed metallic boxes that contain both the electromagnetic energy and the product. The microwaves cannot penetrate the metal sheet and the large

amount of reflection with little energy loss ensures that the system is operating as efficiently as possible.

2.5.1. Travelling Wave Applicator

A travelling wave applicator is one in which power is fed into a chamber from the generator and is substantially absorbed by the workload, with the residue being dissipated in an absorbing terminating load (Meredith and Metaxas, 1983). Figure 2.11 shows a sketch of a typical travelling wave applicator. It is characterised by a good input voltage wave standing ratio, VWSR, irrespective of the amount of workload within it and can be operated empty without risk to the generator.

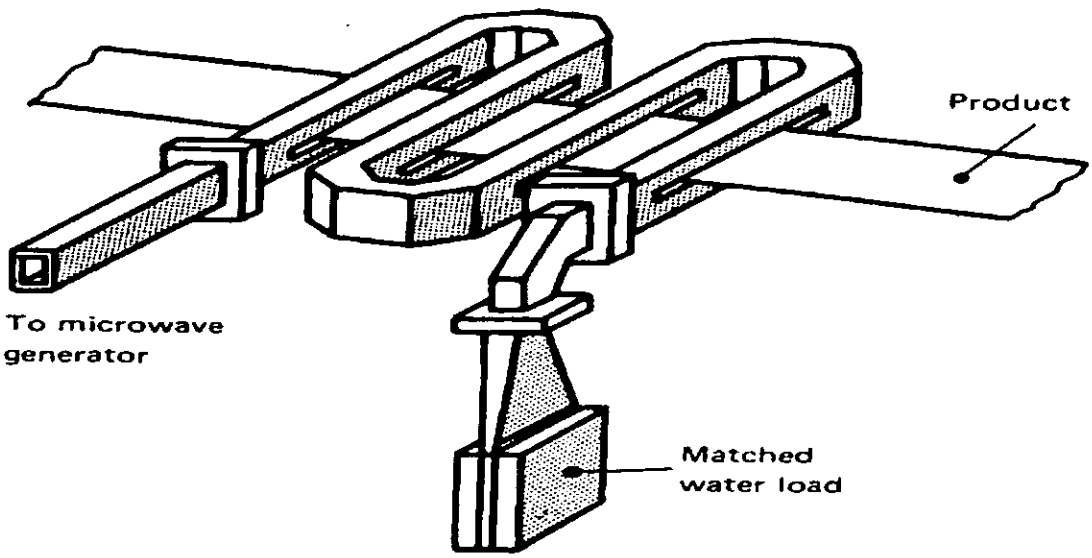

Figure 2.11 Typical waveguide applicator (after Hulls, 1992)

The field distribution in the waveguide decays exponentially with a factor $e^{-2\alpha x}$, where α is the attenuation per unit length and is strongly dependent on the loss factor. The efficiency depends on the permitivity and loss factor values of the workload and its cross sectional area. Due to their design, such applicators are used on continuous flow systems, usually with a conveyor belt. Often they have a balanced symmetrical configuration such that the entry and exit slots for the

workload are at points of minimum wall current, resulting in low levels of energy leakage (Meredith and Metaxas, 1983). A planar material may be processed by being inserted in a slot at the centre of the broad dimension along the waveguide length. The material will thus absorb a quantity of energy from the travelling microwave field dependent upon the loss factor of the insertion (Meredith and Metaxas, 1983).

2.5.2. Multimode Cavities

The multimode cavity is the most commonly used form of microwave heating applicator, comprising well over 50% of all industrial applications and all domestic ones (Fletcher, 1995). Mechanically simple, it is versatile, being able to process a wide range of heating loads (in both size and electrical properties) but uniform heating is often a problem. In principle, a multimode cavity consists of a metal box at least several wavelengths long in two dimensions. Such a box will support a large number of resonant modes in a given frequency range. For an empty applicator, each of these modes is characterized by a sharp resonance response at a given frequency as shown in Figure 2.12 below.

It is important to arrange for as many of these modes as possible to lie near the operating frequency of the magnetron that feeds the microwave energy to the oven applicator. However, when such an oven is partially filled with an absorbent workload, the Q-factor of each mode is reduced from that when it is empty. When the applicator is loaded and the power density is high enough the resonance curves of the modes will overlap in frequency to give a continuous coupling into the load.

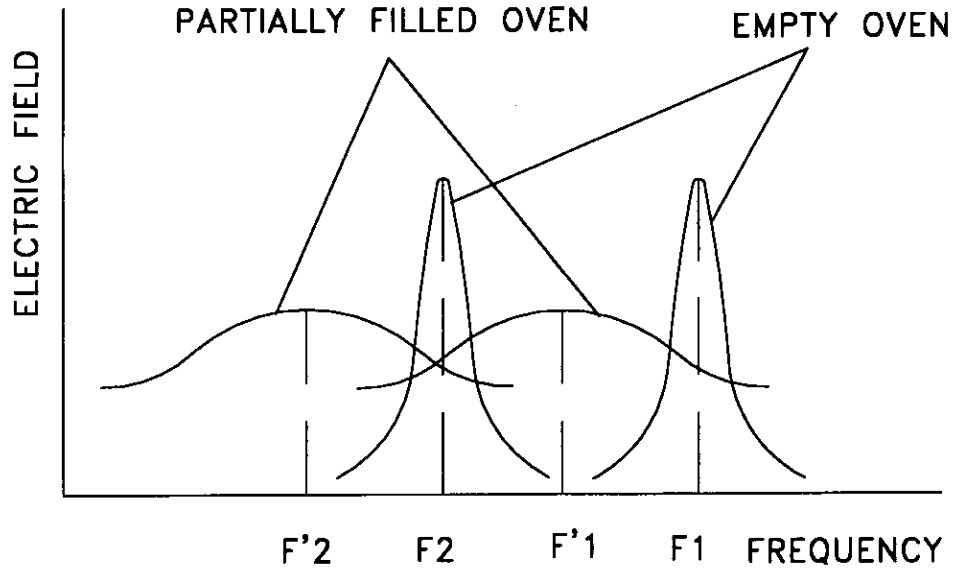

Figure 2.12 Frequency shift and damping of mode patterns due to the loading effect of the dielectric in the multimode cavity (after Meredith and Metaxas, 1983).

As the dielectric constant of the workload is greater than one the spectral density will also be increased from the empty state which gives additional overlap to the modes. This loading effect is also shown qualitatively in the Figure 2.12, where apart from mode damping giving raise to lower Q-factors, a frequency shift of the pattern is seen to occur as well.

In simple terms when the microwaves are launched in to the box they form a complex pattern of high and low areas of electric field strength or modes. In most materials the electric field is responsible for heating the material but, due to the complex distribution of the areas of high electric field strength, achieving high heating rates is very difficult (Meredith and Metaxas, 1983). This helps explain why previous work has reported poor economic balances as extended residence times have been required to induce the desired effects in the treated samples.

2.5.2.1. Field Distribution and Heating Uniformity

Ever since microwave heating was discovered, heating uniformity in a multimode cavity is one of the issues that has drawn much interest. Uneven field distribution creates the so-called hot and cold spots. Hot spots may contribute to the phenomenon of thermal runaway. Cold spots are not welcome as, for example, they may allow harmful bacteria to thrive in food if the temperature is not sufficiently high to kill them.

In a closed rectangular box, the field distribution is given by the sum of all the modes excited at a given frequency. Each mode gives a basic sinusoidal power variation, which results in a spatial non-uniform heating distribution within the multimode cavity. Although the presence of an absorbing material reduces the VSWR of the resultant standing wave pattern, the non-uniformity remains and consideration has been given to minimise its effect. Several methods have been proposed for improving heating uniformity (Meredith and Metaxas, 1983).

Movement of the load is the most obvious and effective technique since the position of the standing waves within the applicator is determined mainly by the cavity walls. It is accomplished by placing the workload on a rotating turntable.

A mode stirrer is a device in the applicator designed to perturb the field distribution continuously and consists of a metal multi-bladed fan rotated inside the applicator. It is capable of contributing to the improvement of non-uniform heating but its operation is quite complex and the overall effect depends on the dielectric loss factor of the load.

Hybrid heating, a combination of conventional and microwave heating, is also used to maintain an even temperature profile throughout the load. The conventional heating minimises losses from the surface of the load by providing heat to its

surroundings, while the volumetric heating, provided by microwaves, heats the load from the inside.

2.5.3. Single Mode Cavities

Single mode microwave resonant structures are widely used at lower power in many fields of microwave engineering, such as frequency counters, interferometers or filters. A resonant applicator consists of a dielectric medium surrounded by conducting walls. The standing wave pattern that will be established can be defined using Maxwell's equations. Their solutions predict electromagnetic fields in time and space that satisfy the existing boundary conditions, also known as the normal modes of the cavity. The resonant cavity in the presence of an external electromagnetic field is characterised by the quality factor Q which, is defined as

$$Q = 2\pi \frac{total\ energy\ stored}{energy\ dissipated / cycle} = \frac{\omega U}{P} \tag{2.20}$$

where P is the power dissipated in the cavity, which includes wall losses as well as loss in the dielectric inserted. The energy stored in cavity, U, is independent of time and can be defined in terms of either the electric or the magnetic fields.

Coupling of the electromagnetic energy into a resonant heating cavity can be experimentally investigated by means of various techniques (Meredith and Metaxas, 1983). These include the measuring, matching and tuning of resonant heating cavities; static measurement of the voltage standing wave ratio as a function of frequency and dynamic measurements of impedance using swept frequency techniques. Dynamic measurement of impedance is accomplished by the use of a network analyser to generate microwave power. In the matching and tuning measurement technique, microwave power is transmitted to the cavity via a slotted line, which incorporates a moveable E-field probe, to sample the field within the

slotted wave-guide. The high frequency signal is rectified and fed into a tuned amplifier calibrated in VSWR readings. Typical values for the VSWR as a function of frequency for resonant cavity are shown in Figure 2.13.

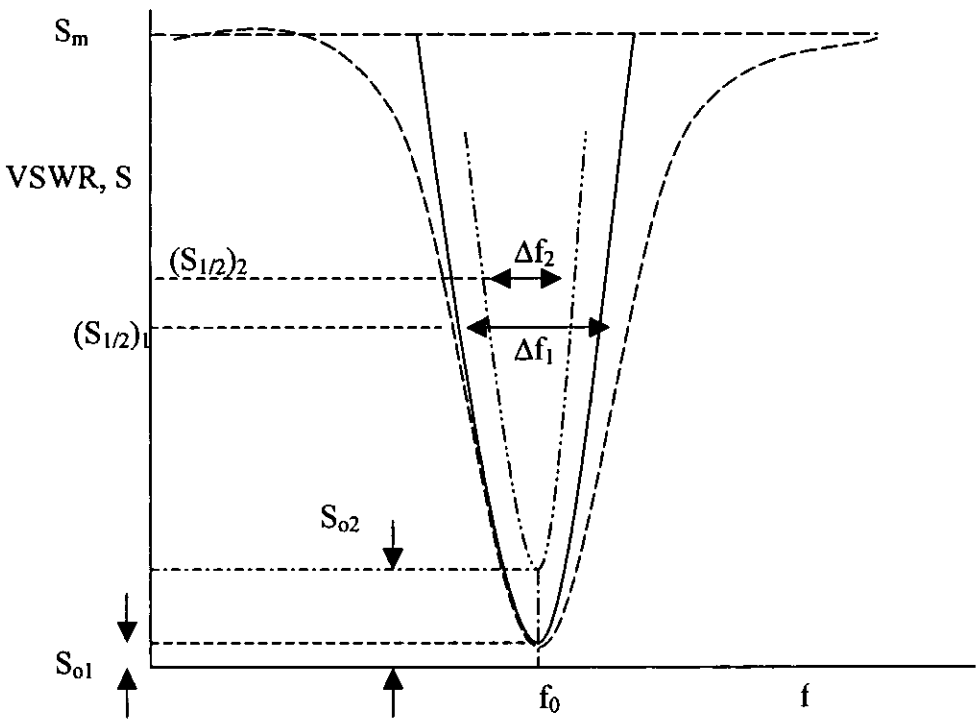

Figure 2.13. Typical voltage standing wave ratios (VSWR), S, verses frequency response for a single mode resonant cavity with a dielectric within it.

The responses are used to calculate the loaded (Q_L) and unloaded (Q_0), Q-factors by determining the corresponding half power width Δf and using the following equation

$$Q = \frac{f_o}{\Delta f} \tag{2.21}$$

A single mode microwave resonant cavity comprises a metallic enclosure into which a microwave signal of the correct electromagnetic field polarisation will undergo multiple reflections. The superposition of the reflected and incident waves gives rise to a standing wave pattern that is well defined in space. Precise knowledge of electromagnetic field configurations enables the material to be placed in the position of maximum electric field strength, allowing maximum-heating rates to be achieved

at all times. A magnetic field is also present inside the cavity with its maximum located at a different position to the electric field maximum and is useful for heating magnetic materials (Meredith and Metaxas, 1983).

For the same applied power, a single mode resonant cavity will generally establish much higher electric field strengths than a multimode cavity and, for this reason, can be useful for the treatment of low loss dielectrics. In the early evolution of microwave heating such cavities saw little use because they lacked the versatility offered by multimode cavities (Meredith and Metaxas, 1983). However, the development of electronic automatic tuning systems now means they are finding favour in industrial situations (Figure 2.14).

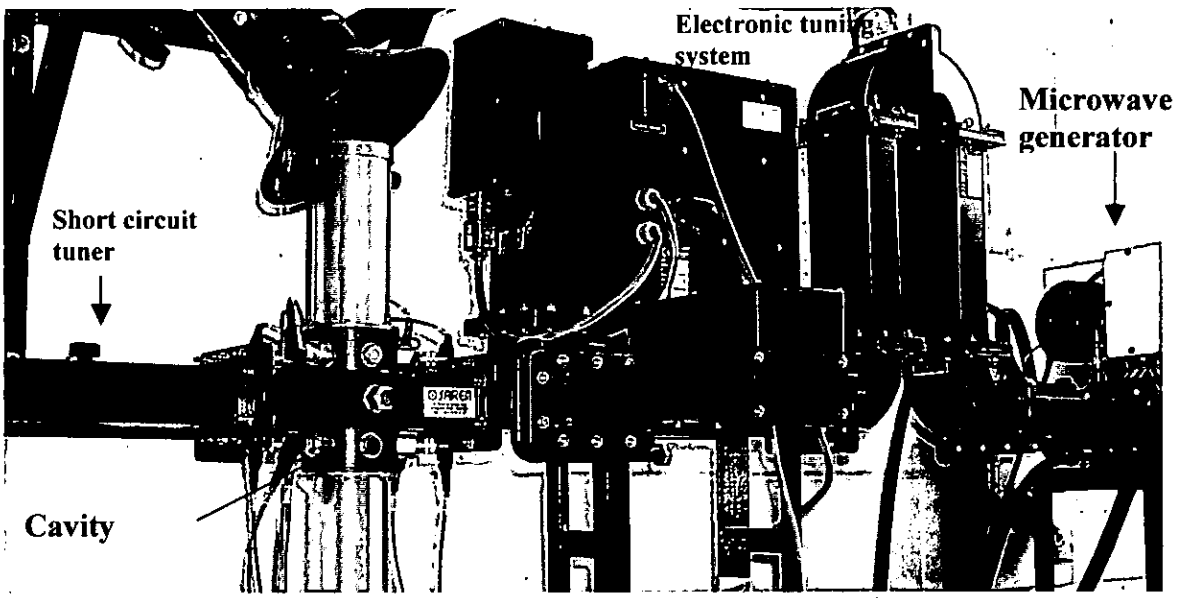

Figure 2.14. Photograph illustrating single-mode microwave heating system.

For a TM_{010} resonant cylindrical cavity coupling the microwave power from the generator via a rectangular wave-guide operating in TE_{10} mode, the frequency tuning could be achieved by ensuring the resonance condition be maintained along the length of the wave-guide. The short circuit plunger at the end of the wave-guide (Figure 2.14) has been used for changing the wave-guide length to maintain the

fundamental resonant mode frequency thus enabling high Q value be achieved within the cavity.

2.6. Conclusions

Microwaves are a form of electromagnetic energy with associated electric and magnetic fields. Microwave heating is different from conventional heating in that, depending upon the dielectric properties of materials some will be heated much faster than others. Various methods for dielectric properties measurement have been developed and the most common are the open-ended coaxial line probe and the resonant cylindrical cavity. The resonant cylindrical cavity is regarded as the most suitable for measurements on powders. In general microwave systems consist of a microwave source, an applicator to deliver the power to the sample, and systems to control the heating. The most common applicators are multimode (e.g., home ovens), where numerous modes are excited simultaneously, and single-mode, where one resonant mode is excited. Multimode applicators are known to have poor heating uniformity, low power density and usually designed for general purpose. While in single mode applicators, heating is more uniform, higher power densities are created, however often they are product specific and in operation can be very sensitive to changes in products properties, geometry and position.

CHAPTER THREE

APPLICATIONS OF MICROWAVE RADIATION IN MINERAL PROCESSING

3.1 Introduction

There is little evidence of research into microwave applications before the commencement of World War Two. However, with the advent of war, rapid growth occurred in the development of microwave systems for telecommunications and radar for military programs (Metaxas et al, 1983, Kingman et al, 1999). Microwave radiation for heating purposes were first developed in 1951 when a large floor standing model was produced by the Raytheon Company of North America (Osepchuck, 1984). Ovens for domestic purposes became available in the early 1960's and an intense market was initiated. Further industrial applications began to be considered and the first attempts included rubber extrusion, plastic manufacture and the treatment of foundry core ceramics. The international shortage of oil and gas in the mid 1970's led to an increase in energy costs and to increased research efforts into the applications of microwave radiation for heating purposes because it was seen as, being potentially, more efficient.

3.2. Microwave Application in the Minerals Industry: Early Work

The first known attempt to expose minerals to microwave radiation was reported in 1978 and resulted in a U.S. patent for coal desulphurisation (Zavitsanos, 1978). Jacobs et al., in 1982 confirmed the results. They demonstrated that non-magnetic pyrite could be converted into magnetic pyrrhotite. In 1984, Chen et al. published a report concerning the relative transparency of minerals to microwave radiation, describing the general

behaviour of a number of minerals exposed to microwave radiation in air. The results were qualitative and descriptive in nature (Table 3.1). Difficulties were reported in making accurate temperature measurements within the commercial multimode microwave cavity. Attempts to measure temperature using infrared camera techniques were inaccurate due to its inability to measure core temperature, which is generally hotter than the surface temperature. However, the results of the study showed that most silicates, carbonates and sulphates, plus some oxides and sulphides, were transparent to microwave radiation and most sulphides, arsenides, sulphosalts and sulphoarsenides heated strongly, emitted fumes and fused.

Table 3.1 Heating responses of various minerals (after Chen et al 1984)

Mineral	**Power (W)**	**Heating Response**
Cassiterite	40	Slight heating
Chalcopyrite	15	Heats well, sulphur fumes
Galena	30	Heats well, sulphur fumes
Magnetite	30	Heats well
Pyrite	30	Heats well, sulpur fumes
Sphalerite	>100	Does not heat

Walkiewicz et al. (1988) overcame the problems of temperature measurement in the microwave cavity by using a metal-sheathed thermocouple. The results provided quantitative data of the microwave heating characteristics of various minerals and compounds. The materials selected were irradiated in a 1kW, 2.45 GHz commercial multimode microwave system, and the heating rates were determined from temperature measurements and exposure times (Table 3.2). This approach, however, has disadvantages of poor heating efficiency of multimode cavity due to an uneven electric field distribution that results in non-uniform heating.

In the same research, Walkiewicz et al. (1988) demonstrated that addition of an absorber to microwave transparent materials promoted microwave heating. Examples reported included the addition of magnetite to improve the conversion of non-magnetic pyrite to magnetic pyrrhotite, compared to microwave treatment without doping. The doping phenomenon is related to the Maxwell Wagner interfacial polarisation in heterogeneous systems, described in Section 2.2.2.3 of Chapter 2.

Table 3.2 Heating responses of various minerals (after Walkiewicz et al. 1988)

Mineral	**Chemical composition**	**Max temp acheived (°c)**	**Time (min)**
Chalcopyrite	$CuFeS_2$	920	1
Galena	PbS	956	7
Magnetite	Fe_3O_4	1258	2.75
Orthoclase	$KAlSiO_3O_8$	67	6
Pyrite	FeS_2	1019	6.75
Quartz	SiO_2	79	7
Sphalerite	ZnS	88	7

Walkiewicz et al (1991) extended this work by exposing ore minerals to microwave radiation. It was found that microwaves heated some minerals in preference to others and, therefore, it was possible to selectively heat ore minerals in a gangue lattice. Furthermore, it was observed that rapid heating of an ore mineral in a microwave transparent lattice caused thermal stresses, which could give rise to micro-cracks within the mineral system. It was suggested that these cracks could give rise to changes in grinding energy requirements, improve liberation of valuable mineral and give rise to better metal recoveries.

The effect of power level on the microwave heating characteristics of minerals has also been investigated (McGill et al., 1988). A heating rate study was completed at four incident power levels ranging from 500 to 2000W at 2.45GHz. Samples were irradiated for seven minutes at 500W increments up to a maximum of 2000W. Tests were terminated if severe melting or arcing occurred or if the temperature stabilised. Similar heating rates to previous authors were found but an increase in power level has shown to increase the heating rate, except for minerals which were very low-loss e.g. quartz and plagioclase feldspar. Low loss materials were found not to heat at any power level. Table 3.3 shows some results of this study.

Table 3.3 Effect of power level on heating rate (after McGill et al.1988)

MINERAL	500W		1000W		1500W		2000W	
	TEMP°C	TIME (M)	TEMP°C	TIME (M)	TEMP°C	TIME (M)	TEMP°C	TIME (M)
Fe_2O_3	60	7	87	7	101	7	130	7
Fe_3O_4	1118	7	1144	3.5	1123	2	905	1
PbS	984	0.5	992	0.4	----	----	----	----
SiO_2	33	7	44	7	55	7	73	7
TiO_2	67	7	109	7	150	7	228	7

3.3. Determination of Dielectric Properties of Minerals

In the past simple multimode cavity tests have been the starting point for the evaluation of an industrial heating process (Chen et al., 1984, Walkiewicz et al., 1988 and McGill et al, 1988). However, the apparent simplicity of this approach often leads to misleading results of interpreting the microwave interaction with materials due to the complexity of the field distribution within the cavity and the variation of the material with temperature, moisture content, density, frequency and structure. In addition, many applications require a specially designed cavity, which necessitates a detailed knowledge of the dielectric

data. Associated with this requirement, a lack of understanding of the behaviour of heterogeneous dielectrics and mixtures has been a hindrance for theoretical modelling. Nevertheless, a number of laboratories worldwide with the capability to make high temperature dielectric property measurements though using different techniques, have developed more accurate methods of acquiring dielectric data.

A considerable amount of data on the variation of complex permittivity with frequency and temperature has been published. This includes dielectric property data of a wide range of inorganic materials (crystals, ceramics, glasses and water) and organic materials (plastics, elastomers, natural resins, asphalts and cements, waxes and wood) in the frequency and temperature ranges of $100<f<10^{10}$ Hz and $-12<T<200$°C respectively (Metaxas and Meredith, 1983). Furthermore, Tinga and Nelson (1973) published a similar list of dielectric properties for food and biological substances. Liao et al (2001 and 2000), Meda et al., (1998) and Mudgett (1996) have also published results of dielectric properties of food.

Pioneering work concerning measurement of the dielectric properties of minerals was reported by Church et al., (1988). Using a technique involving electromagnetic theory and Maxwell's equations of microwave propagation, the permitivity, conductivity and loss factor were measured indirectly through an RF impedance analyzer. The properties were measured in a short section of coaxial wave-guide, filled with the material in question, and the input frequency was measured with an RF analyser. The authors measured the dielectric constant and loss factor of seven groups of minerals including oxides, carbonates, silicates, phosphates, sulphates, halides and tungstates in the frequency range 300 MHz to 1 GHz in 100 MHz steps (Church et al., 1988). The

frequency range, however, despite including 915 MHz, did not include 2.45 GHz. Nelson et al., (1989) measured the dielectric properties of gabbros, basalt and oxide minerals for various bulk densities and an increase in dielectric properties with density was reported. Church et al., and Nelson et al., both measured the dielectric properties at room temperature, using the coaxial line technique.

Salsman (1991) published data on dielectric properties of chalcopyrite and chalcocite as a function of temperature, bulk density and frequency. Using the coaxial line technique, measurements of dielectric properties of powdered minerals were conducted at temperatures up to 325°C and frequencies up to 3GHz. Holderfield et al., (1992) published results on the dielectric properties of minerals including chalcopyrite and chalcocite also using the coaxial line probe. Measurements were taken at 915 MHz and temperatures of up to 325°C. Despite using a similar measurement technique, the results reported by Salsman (1991) and by Holderfield et al., (1992) are quite different. While Salsman reported the dielectric constant of chalcopyrite to be within the range 10-20, Holderfield et al's data shows it to have values of over 100. Holderfield et al., (1992) did not compare their findings with the data presented earlier by Salsman (1991).

The measurement of dielectric properties for ore minerals has been attempted in a further separate study (Florek et al., 1995). A reflection method was used to measure the components of complex permittivity (ε'and ε''). The results suggested that mineral-heating rate was linked to values of the components of the complex permittivity and are shown in Table 3.4. Minerals that are known to be receptive to microwave heating (chalcopyrite, galena and pyrite) can be seen to have the highest values of both ε' and ε''.

Table 3.4 Data for components of complex permittivity at 915 MHz (after Florek et al., 1995)

MINERAL	FORMULA	ε'	ε''
Baryte	$BaSO_4$	0.34	0.05
Magnesite	$MgCO_3$	1.59	0.05
Siderite	$FeCO_3$	1.72	0.08
Magnetite	Fe_3O_4	1.41	0.38
Chalcopyrite	$CuFeS_2$	1.80	2.75
Galena	PbS	3.10	1.85
Pyrite	FeS_2	2.92	2.07

None of the data was comparable with those published earlier by Salsman (1991) and Holderfield et al., (1992) for chalcopyrite. In 1993, at a meeting of the Material Research Society, concern was expressed about the reproducibility of dielectric property measurements published by several authors (Arai et al., 1993). Parallel investigation into high temperature dielectric property measurements using the coaxial line probe and cavity perturbation techniques has been reported (Arai et al., 1993 and Batt et al., 1993). The parallel measurement programme was conducted at three laboratories (AECl of Research Canada, Staffordshire University UK and The University of Nottingham, UK). Alumina ceramic samples were prepared from the same batch and dielectric properties were measured at the laboratories. Good agreement was reported between the different laboratories on the data of dielectric constant, with errors below 10% at temperatures up to 800°C. However, results for loss factor showed poor agreement with differences of about 50% between the different techniques. It was concluded that further work was required on the current techniques, particularly for measurement of loss factor.

Work was undertaken at the National Physics Laboratory UK (Harrison, 1997) and highlighted problems involved with the measurements of dielectric properties and

correlation of the results. It was shown that the measurements must take into account many factors such as composition, density, temperature, moisture and frequency, including the magnetic field portion of the wave that may affect magnetic materials.

3.4. Microwave assisted liberation

Comminution or size reduction is essential in most mineral processing operations in order to liberate the economic mineral for subsequent beneficiation. It is the most energy intensive step in mineral processing and is accomplished by forces applied to the particle externally. It forms the largest proportion of any mineral processing plant's capital and operating costs. Cohen (1983) estimated that 30-50% of total plant energy consumption at most sites and up to 70% for hard rock sites is consumed by comminution. Wills (1992) and Weiss (1985) estimated that for a typical metalliferous concentrator the figure is approximately 50%.

It is clear that there is much to be gained from improving the efficiency of comminution and even slight improvements can result in measurable economic savings. Many attempts have been made to improve efficiency of the process. Improvements can be of two kinds (Napier-Munn et al., 1996):

- Fundamental changes in existing technology or the introduction of novel technology;
- Incremental improvement in the technology, i.e. its application and operating practice.

The latter implies optimisation of equipment design and circuit configuration, such as employing grinding aids and sophisticated classifier recirculation systems, ensuring that

the installed capital asset is exploited as efficiently as possible in an economic sense (Napier-Munn et al., 1996).

Efforts have long being made towards fundamental changes in technology, with both conventional and non-conventional processes being considered in order to increase efficiency and reduce mineral recovery costs. The use of heat to assist in mineral liberation (typically referred to as "thermally assisted liberation", or TAL) has been studied since the early 1900's (Yates 1919, Holman 1927 and Pocock et al., 1998). It has been identified as a potential method to improve comminution and liberation characteristics of ores by inducing grain boundary fracture. Because the constituents of ore typically have very different thermal and mechanical properties (most notably, large differences in thermal expansion coefficients), stresses of sufficient magnitude to create fracture can be developed during heating or cooling. Consequently, TAL has been one of the most intensively studied areas within the comminution of minerals and ores.

The application of thermally assisted liberation to reduce grinding resistance has been investigated by various authors (Fitzgibbon and Veasey 1990, Veasey and Wills 1991 and Pocock et al., 1998). Early research included investigation of the effect of thermal pre-treatment on the Bond Work Index of quartz, tin ore and iron ore. Unfortunately, in each case, it was found that thermal pre-treatment of ore to improve grindability is unattractive because the amount of energy required to reduce the mechanical strength of the minerals was greater than that required for conventional grinding. However, most studies report that thermal treatment improves liberation of valuable minerals in processing the ores and that these improvements may be sufficient to justify the use of thermally assisted liberation. Such improvements included:

- Increased mill capacity and reduced wear
- Better control of mill product size and improved liberation/recovery
- A reduction in slimes production
- Alteration of the physical-chemical properties of ground products.

Different approaches to induce thermal stress have been considered, these include (Walckiewicz, 1988):

- The use of high voltage electrical energy to cause rapid resistive heating to induce thermal stress cracking;
- The use of ultrasonic energy, to produce mechanical vibrations within the particles and solid materials at frequencies of 15 to 60 kHz and
- The use of microwave radiation at a frequency of 0.1 to 100 GHz.

Andres et al., (1999) have recently investigated the use of high voltage electrical energy to induce liberation of minerals. They reported that using high voltage electrical pulses causes disintegration of minerals aggregates due to local explosive plasma streams at the interface of mineral components with different permittivities. Comparative liberation tests on magnetite and hematite concentrates of Kiruna iron ores has shown that high voltage electrical pulses are capable of producing high percentage of mono-mineral particles on disintegration of mineral aggregates. Andres et al., have also shown that the efficiency of recovery was significantly improved when using the new technology for disintegration of rock with components of different permittivties (Table 3.5).

Table 3.5. Recovery of silica (SiO_2) and phosphorous (P) into magnetite and hematite concentrates (after Andres et al., 1999)

Size (μm)	**Mechanical comminution**		**Electrical disintegration**	
	SiO_2 (%)	**P (%)**	**SiO_2 (%)**	**P (%)**
Magnetite				
>500	18.78	16.68	16.31	19.18
500-250	20.57	13.17	10.39	10.04
250-125	16.07	15.33	6.12	7.87
125-38	43.85	44.32	6.50	9.59
Hematite				
>500	3.82	18.83	3.18	17.1
500-250	4.20	7.90	2.04	8.01
250-125	3.22	5.77	1.62	6.94
125-38	3.21	7.80	1.85	11.20

Andres et al., (1999) further suggested that at the existing stage of development, the technology of mineral liberation by high voltage electrical pulses was poorly understood. Better understanding of the mineral liberation process was necessary to develop a convenient mechanism of liberating the targeted minerals from the rock matrices and this should include quantification of energy saving in the disintegration of dielectric by high voltage electrical pulses.

Microwaves have the ability to generate heat within the ores quickly and selectively and have been proven to selectively liberate minerals from the host rock (Walkiewicz, 1991). The interesting results produced by Walkiewicz (1991), suggesting microwave induced thermal stresses, led other authors to further investigate such a potential application (Salsman, 1996; Kingman, 1998; Voster et al, 2000; Wang et al, 2000 and Whittles et al., 2003). It should be noted that Kingman, Andres and Wang used experimental approaches while Salsman and Whittles used a numerical modelling approaches. Kingman (1998) investigated the effect of microwave radiation on the grindability of

three ores (massive ilmenite, massive copper and copper carbonatite). Using a 2.6kW, 2.45 GHz, multimode microwave system, ore samples were irradiated for a range of exposure times and its effect on the mineralogy and Bond work index assessed (Figure 3.1 and 3.2).

It can clearly be seen that microwave pre-treatment has had a significant effect on the Bond Work Index of the ores (Figure 3.1). The reduction of Bond work index was suggested to be due to weakening of ore matrix, owing to the formation of principally intergranular and to a lesser extent transgranular cracks, as illustrated in Figure 3.2.

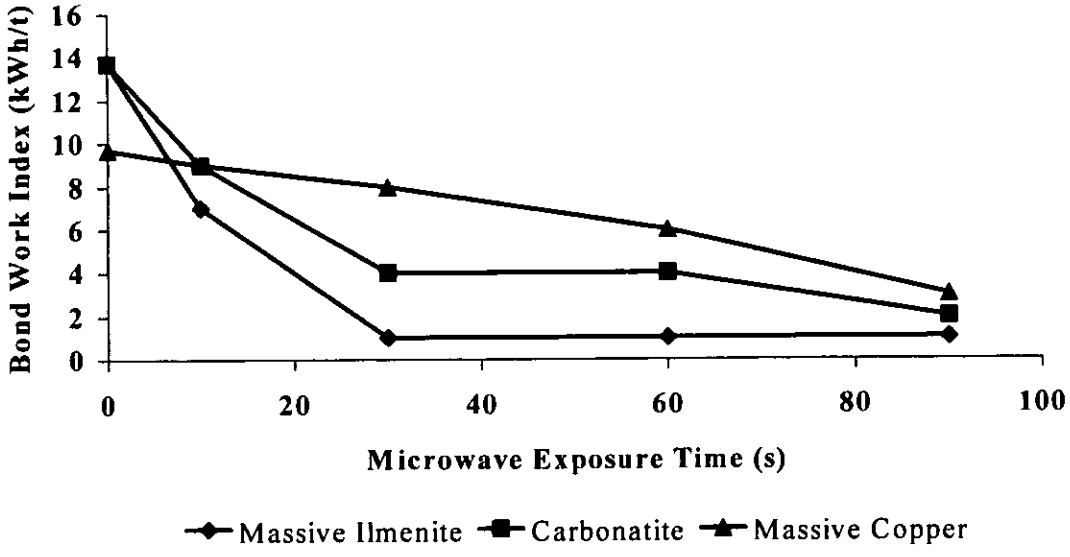

Figure 3.1. Effect of microwave radiation on the Bond Work Index of selected samples (after Kingman et al., 1998)

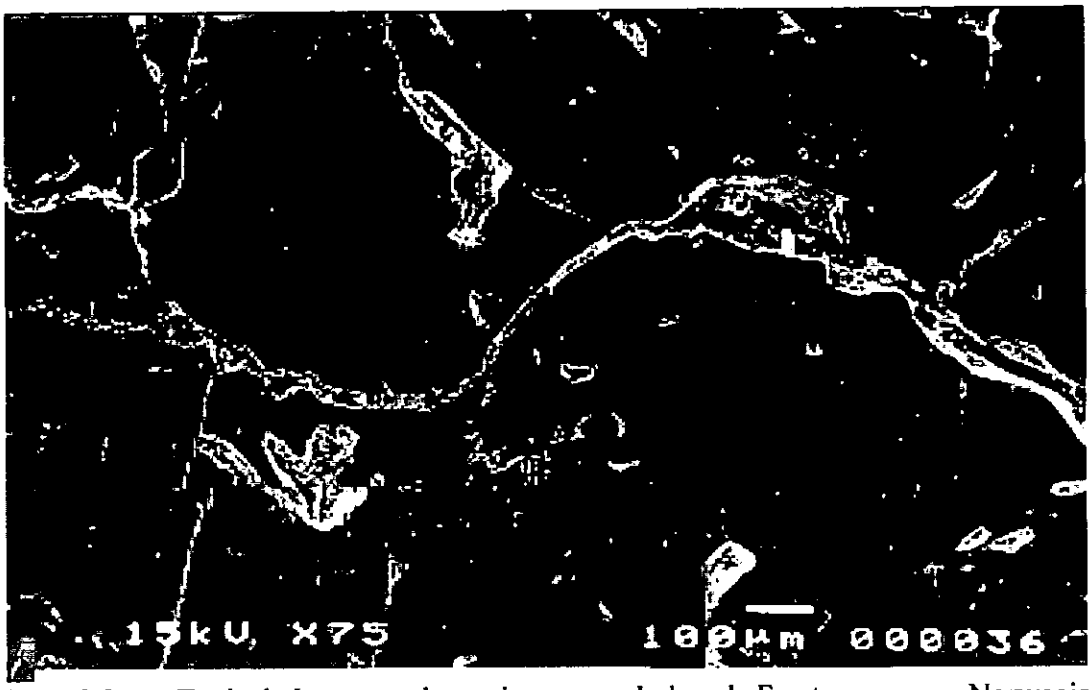

Figure 3.2 Typical Intergranular microwave Induced Fracture on a Norwegian Ilmenite (after Kingman et al., 1998)

Microwave treatment of minerals and ores has two main objectives: firstly to reduce the grinding energy required to mill to an appropriate size and secondly to promote the formation of inter-granular fracture, thus increasing liberation of valuable mineral. Kingman et al. claimed that changes of chemical composition or mineral phase could have the effect of weakening the lattice and reducing the cohesion of the macroscopic structure and thus reducing the grinding energy required. In addition, differential expansion of minerals, due to their different heating rates, will necessarily give rise to different levels of volumetric expansion at the grain boundaries. This differential volumetric expansion in the ore matrix will lead to weakening of the grain boundaries, owing to the formation of inter-granular and trans-granular cracks. This offers possibilities for the liberation of an increase number of whole mineral particles, thus increasing grade of concentrate and recovery of the valuable mineral.

Walkiewicz (1991) and Kingman et al. (1998) have suggested that by improving the grindability, changes occur in the design of the grinding circuit that may decrease comminution costs. If the ore were easier to grind, there would be less wear of the mill per tonne, mill liner, and milling medium. Improved grindability could also result in an increased throughput, and the amount of recycled ore should be decreased. These factors would contribute to reducing comminution costs. However, based on energy saving alone in these studies the use of microwave energy to improve grindability was not cost effective. Overcoming this was suggested as a challenge for the use of microwave energy in thermally assisted liberation.

Wang et al. (2000) investigated the effect of particle size on microwave assisted grinding of four materials (limestone, dolomite, quartz and copper ore). Using a multimode microwave system with a frequency of 2.45 GHz and incident power levels of up to 7kW, ore samples were treated for different microwave exposure times. It was reported that during microwave treatment, conductive heat transfer between minerals phases and the gangue plays an important role as the particle size reduces, resulting in decreased temperature differential. Such decreases of temperature gradient will be less likely to contribute to the formation of cracks and, therefore less reduction in the required grinding energy.

Kingman et al. (2000) also investigated the effect of mineralogy on microwave assisted grinding. They carried out a detailed mineralogical analysis of various commercial ores before and after microwave treatment. The effect of microwave exposure time in work index of each ore was quantified. It was reported that microwave radiation had a significant effect on the work index if the mineralogy of the ore is consistent and

contains a good absorber of microwave radiation in a transparent gangue matrix. However, ores that contained small particles of good absorbers that were finely disseminated in discrete elements were found to respond poorly to microwave treatment in terms of reductions in required grinding energy.

Salsman (1996), using theoretical analysis, studied the feasibility of using short pulse microwave radiation as a pre-treatment step in comminution. The thermo-mechanical responses of pyrite crystals in a calcite host rock, during microwave heating were predicted, using finite-element analysis. The predictions suggested that stresses would occur in the particles that far exceeded the individual particle strengths. The models also indicated that pulsed radiation developed more stress in the gangue. An extremely simplified energy balance is also presented which suggests that the energy required for comminution can be decreased from 10-12kWh/t to 0.8kWh/t for a typical porphyry ore (Salsman, 1996). It should be noted, however, that the assumptions made for this energy balance were quite considerable and experimental work is required to prove the models in question.

Whittles et al., 2003 used a numerical modelling and simulation technique to predict the influence of power density on microwave-assisted breakage. The ore consisted of a microwave-absorbing mineral (pyrite) in a low absorbing matrix (calcite). Simulations were undertaken using finite difference modelling techniques for a theoretical 15 x 30 mm sample of calcite host rock containing 10 vol.%, 1 mm^2 particles of pyrite. The positions of the pyrite particles within the model domain were randomly generated to provide a relatively disseminated ore body (Figure 3.3).

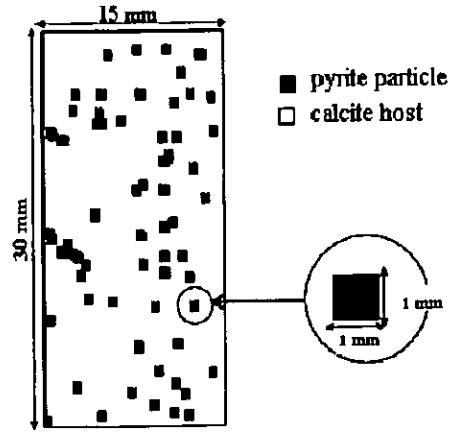

Figure 3.3. Model of the Pyrite Calcite ore sample (after Whittles et al 2003).

The simulations modelled the microwave volumetric dissipation, thermal conduction, expansion, thermally induced fracturing, strain softening and uniaxial compressive strength to predict the effect of microwave heating on the strength of ore. Models were run with different microwave treatment power levels to allow comparison to be made. They simulated high power density ($1x10^{11}$ W/m^3) microwave heating process for short exposure time and compared it to a low power density ($1x10^9$ W/m^3) for a long exposure time (Figures 3.4 and 3.5). They reported high temperature gradients between the mineral phases when using high power density for a short exposure time, while at low power density and with a long exposure time, low temperature gradients were formed. This is because microwave energy is preferentially deposited into pyrite phase and short exposure means that heat transfer by conduction into the calcite is negligible (Figure 3.4). A long exposure time allows greater conduction between minerals phases, resulting in increased temperatures in the calcite (Figure 3.5).

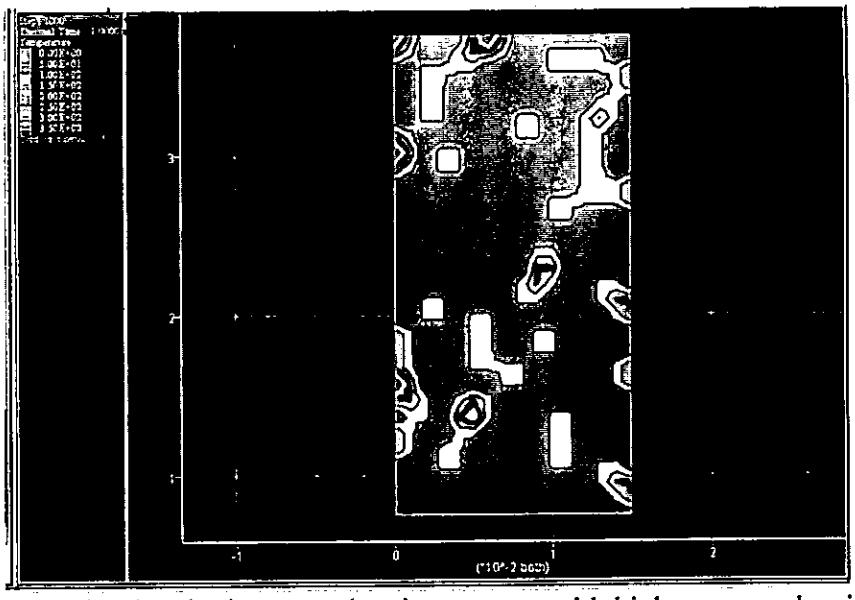

Figure 3.4. Simulated microwave heating process with higher power density 1x 10^{11} W/m^3 (after Whittles et al 2003).

A high temperature gradient between adjacent mineral phases mean that the induced thermal stress at the grain boundaries will also be high, which should result in greater weakening of the material. To further investigate this, Whittles et al. (2003) modelled the UCS test for the model domain for different simulated heating times. They then used the well known relationships developed by Broch and Franklin, 1972 and Bieniawski, 1975 to calculate the point load index (Is(50)) from the modelled UCS data. The equation used was:

$$Is(50) = UCS/K \quad (3.1)$$

Where Is(50) =Point load strength corrected to 50mm core.

K = 24

UCS = Uniaxial compressive strength

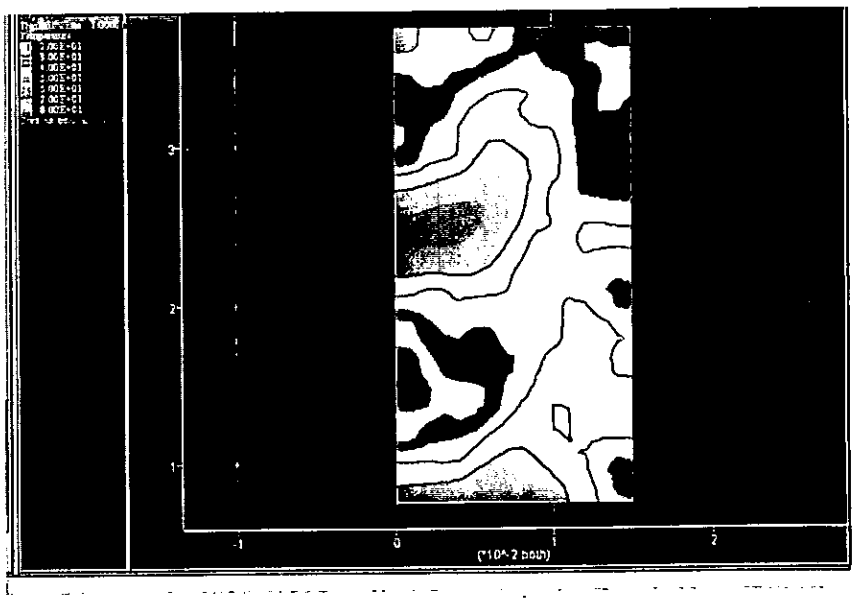

Figure 3.5. Simulated microwave-heating process with low power density between 3×10^9W/m^3 and 9×10^9W/m^3 (after Whittles et al 2003).

The results of this analysis are shown in Figures 3.6 and 3.7. Figure 3.6 shows the influence of microwave heating time on point load index for the lower power density. It can clearly be seen that as microwave exposure time is increased the point load index decreases significantly. This is also true in Figure 3.7, which shows the effect of microwave-heating time on point load index for the ore exposed to the higher power density. As the test is related to UCS tests, the reductions in point load index are particularly significant at the higher power density with a reduction from 5.25 for non-treated to 1.25 after just 0.2 seconds.

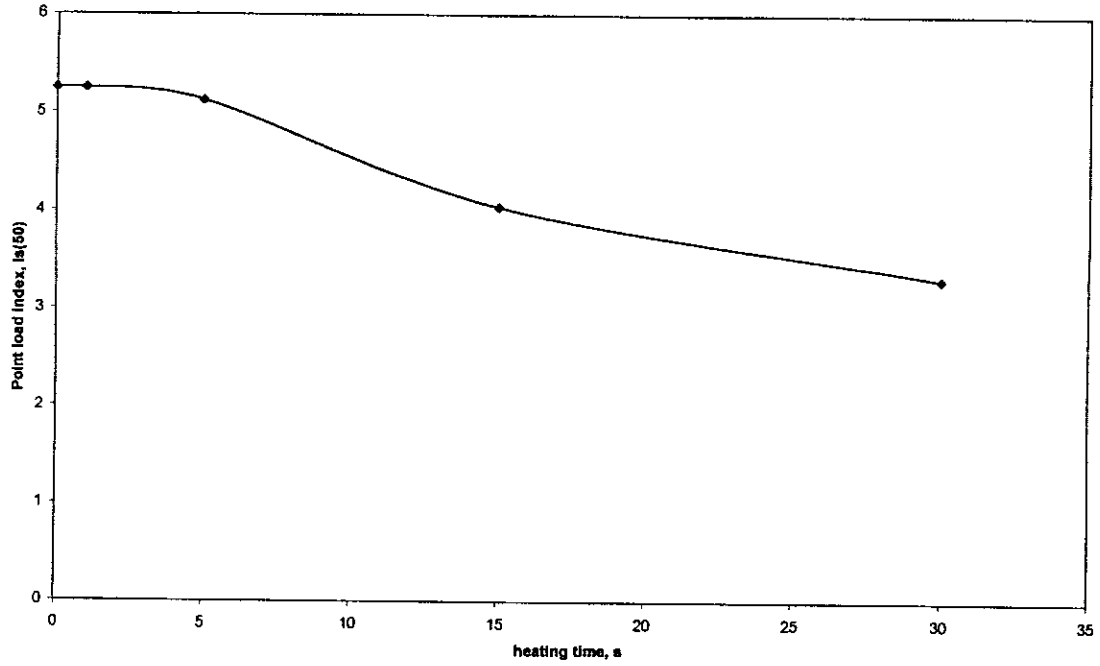

Figure 3.6 Point Load Index versus Microwave Heating Time (2.6 kW 2.45 GHz power density between 3×10^9W/m^3 and 9×10^9w/m^3) (after Whittles et al., 2003).

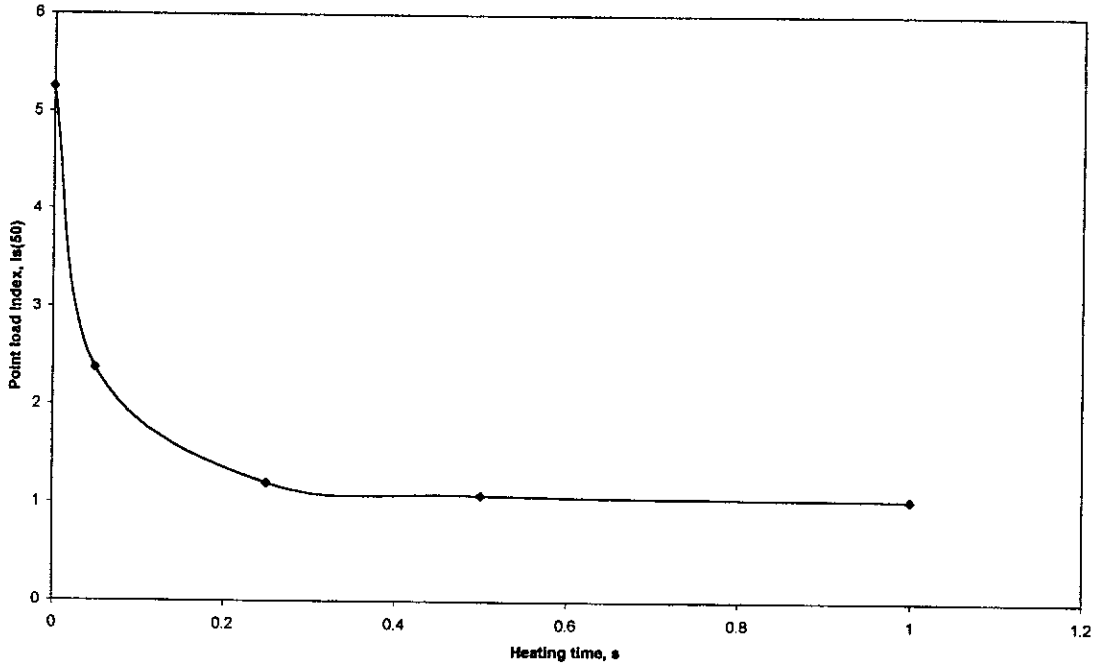

Figure 3.7. Point Load Index versus Microwave Heating Time (Power Density =1x 10^{11} watt/m^3) (after Whittles et al., 2003).

Whittles et al (2003) further illustrated the amount of energy added due to microwave treatment, by assuming the mass of material heated was 1 kg and the sample energy input for each case was for the multimode cavity type, 2.6 kW microwave power, treated sample heated for 30 s:

2.6 x 0.5/60 x 1000/1 = 125 kWh/t

And for the single mode cavity type, 15 kW, treated sample heated for 0.2s:

15 x 0.2/3600 x 1000/1 = 0.8325 kW h/t.

This clearly has shown the influence of power density on the ore strength. The results show that a sample treated on a single mode cavity type, 15kW and 0.2 s exposure time, the ore strength is reduced by 75% and the added energy is about 0.83 kWh/t, compared to strength reduction for about 40% with added energy of 125 kWh/t on sample treated on a multimode cavity type. They suggested that experimental work was necessary to validate the findings.

3.5. Effects of Microwave Radiation on Mineral Properties

Various authors have studied the effects of heat treatment on minerals (Blackburn, 1983), but, to date, very little data exists on the effects of microwave radiation on mineral properties. The material available concentrates mainly on effects on surface area, relative grindability and magnetic susceptibility.

3.5.1. Effect of Microwave Radiation on Mineral Surface Area

The effect of microwave pre-treatment on oxidised ilmenite concentrates was investigated and compared to conventional reduction methods (Kelly et al., 1995). Two

oxidised ilmenite concentrate samples were reduced by microwave heating with carbon in a nitrogen atmosphere. The reduction process was carried out in a variable power (0-1500W), 2.45GHz microwave applicator. Duplicate control samples were also reduced at temperatures over the range 700 to 1000°C in a conventional muffle furnace. The specific surface area of each sample was calculated using a nitrogen absorption technique and it was concluded that after microwave treatment the extraction of iron from the samples could be increased by up to 300%. This was suggested to be partly due to an increase in surface area but it also reflects a decrease in ilmenite grain size. It was also suggested that the extraction of titanium from microwave reduced samples increases with the extent of the reduction. In microwave reduced samples an increase in porosity was reported as well as an increase in surface area.

In a study by Harrison et al. (1996) various minerals were irradiated in a 2.45GHz, 650W microwave applicator. Again, the specific surface of the mineral was determined by nitrogen absorption techniques. All minerals increased their specific surface area after irradiation but, in general, the minerals that were more responsive to microwave exposure showed a much larger increase. For example, chalcopyrite, a good heater, shows a much larger increase in specific surface area than feldspar, a poor heater.

3.5.2. Effect of Microwave Radiation on the Magnetic Properties of Minerals

The effect of microwave radiation on the magnetic susceptibility of minerals has been investigated for minerals containing Fe^{2+}, Fe^{3+} and Cu^{2+} ions (Harrison, 1996). The minerals were treated at 2.45GHz and exposed to various powers ranging from 650-

4500W. Changes in field strength of minerals after irradiation were reported. However, no explanation was given by the authors for the changes in field strength, although, it is thought that the changes are most likely due to change in chemical species of the mineral e.g. magnetite undergoing oxidation to hematite at 350°C.

Florek et al (1996 and 1997) investigated the effects of microwave radiation on the downstream magnetic processing of various ores. Both studies investigated the mechanism of thermal decomposition of minerals after microwave treatment. It was suggested that for ores containing iron and copper microwaves could increase magnetisation and therefore, the recovery of economic mineral. This was considered to be primarily due to the oxidation of sulphide specimens present.

Kingman et al. (1998, 1999 and 2000) published studies of the effect of microwave radiation on the magnetic properties of minerals. Various ores and minerals were exposed to microwave radiation at various exposure times and power. It was reported that long exposure times might be detrimental to downstream processing.

3.6. Applications of Microwave Radiation in Extractive Metallurgy

Previous research, already reviewed, has indicated that some minerals, particularly oxides and sulphides, are good absorbers of microwave radiation. Others researchers have extended this work and have suggested the applications of microwaves to enhance pyrometallurgical and hydrometallurgical processes.

In 1985, whilst attempting to dry a mixture of brown coal and chalcopyrite, researchers observed the formation of a black mass in which the copper was rendered completely soluble in a dilute ammonia solution (Al-Harehsheh et al., 2003). Later it was found that metallic copper had been formed by reduction. Similar results were obtained with

mixtures of carbon and hematite, with fine sponge metal being formed. Since then many pyrometallurgical applications have been proposed, ranging from the production of iron-nickel alloys from a low grade sulphide ore to the reduction of tungsten ores at temperatures of up to 3000°C (Warner et al., 1989). After considerable research, various researchers, have identified significant benefits of microwaves over conventional pyrometallurgical methods such as:

- Volumetric heating enhances uniform heating throughout pellets and thus alleviates the problem with "cold centres" observed when using conventional heating.
- Large masses could be heated much faster than with conventional methods.
- Some phase changes occurred on reduction, possibly enhancing heating rates.
- A possible lowering of activation energy.
- Significant increase in reduction rates.

It was also suggested that making reasonable assumptions of capital and operating costs, the cost of the microwave route maybe up to 50% lower than any conventional process (Standish et al., 1990).

Various attempts to investigate the influence of microwave radiation on typical leaching reactions have been reported (Florek et al., 1995, Balaz et al., 1995; Haque et al., 1986; Woodcock et al., 1989 and MacDougal et al., 1997). This had included microwave assisted leaching of gold, copper, nickel, zinc, lead, cobalt and manganese ores. Several review papers can be found in this area such as Xia and Pickle, (1997), Kingman and Rowson (1998) and Haque (1999). The most recent review on microwave assisted leaching has been presented by Al-Harehsheh (2003). The review suggested that

microwave application to enhance hydrometallurgical process has potential advantages over the current processes such as autoclave, roasting and bio-oxidative leaching. However the lack of understanding of the microwave effect on the leaching process limits its development into industrial applications. A comparative economic analysis was also presented and among the various benefits of microwave radiation it showed that capital and operating costs of microwave assisted leaching are low compared to current processes in practice.

3.7. Applications of Microwave Radiation in the Processing of Coal

Research into microwave pre-treatment for coal beneficiation has probably been the most significant application of microwave radiation in the mining industry. Various authors have published material that falls mainly into the categories of drying, pyrolysis, desulphurisation, grinding and dielectric properties.

Coal has been found to be transparent to microwave radiation while moisture and pyrite contaminants are good absorbers (Marland et al., 2001). Microwaves have been shown to enhance uniform drying of coal due to preferential heating of water. Drying efficiencies of up to 97% for various type and sizes of coal were reported (Chatterjee et al., 1991; Lanigan, 1989 and Marland et al., 2001). It has also been reported that microwave radiation enhanced coal desulphurisation. Coal desulphurisation is an important process from the standpoint of environmental protection and can be accomplished by magnetic separation (conversion of pyrite in to pyrrhotite) and preferential dissolution of sulphur by molten caustics (Zavitsanos, 1979 and Rowson et al., 1990). Microwave treatment of coal has been used to enhance pyrite to magnetic

pyrrhotite for coal desulphurisation by high intensity magnetic separation (Zavitsanos, 1981; Kelland, 1988 and Viswananthan, 1990).

Coal desulphurisation using molten caustics has also been reported (Zavitsanos, 1979). Pyritic and organic sulphur were removed from pulverised coals by contacting the coal with molten alkali caustics. Molten caustics were demonstrated to be excellent absorbers of microwave radiation and thus the sulphur rich areas of the coal were heated to high temperature. This caustic heating gave rise to a water-soluble form of sulphur, which was easily removed by washing. Other researchers have continued this work and promising results have been obtained. High sulphur coals were treated at 500W and 2.45GHz for up to one minute in the presence of 300g/l caustic solution. After washing and low gradient magnetic separation a 70% removal of sulphur was reported (Rowson et al. 1990). Other studies have considered the role of microwave irradiation in molten caustic desulphurisation e.g. Butcher et al. (1995).

Microwave assisted grindability of coal has also been investigated. Various authors have demonstrated that reductions in the amount of energy required to grind coal are possible after microwave irradiation (Lyttle et al., 1992; Herbst, 1981; Viswananthan, 1990; Harrison et al., 1996 and Marland et al., 2001). Among the benefits suggested of microwave compared to conventional heating methods are the reduction of sulphur and ash contents and the required grinding energy in the order of 20-30%.

3.8. Conclusions and further work

The studies presented have shown that microwave assisted liberation can be effective in weakening ore matrices. However, long exposure times have an adverse effect on the process economics as well potentially interfering with downstream processes. It has been

shown that use of numerical modeling technique can be an important research tool for a theoretical investigation of microwave treatment. Nevertheless, the lack of basic data on dielectric properties of minerals constitutes a severe hindrance for full exploitation of numerical modeling technique.

Therefore, future research on application of microwave radiation in the mineral industry should include an investigation of the dielectric properties of minerals and their variation with the various factors such as frequency, temperature, density and composition. Measurement of dielectric properties of minerals will not only contribute to the understanding of microwave interaction with minerals but also assist the effective use of numerical modeling techniques and aid the design of material specific microwave heating cavities.

The majority of research carried out on microwave treatment of minerals has utilized multimode cavities, similar to these found in a domestic microwave oven. As described in Chapter 2, multimode cavities suffer from poor efficiency and low electric field strength, both vital for high power absorption. Low electric field strength requires large microwave energies to induce thermal stress and are, therefore, high cost of energy. Salsman (1996) and Whittles et al (2003), using numerical simulation, have shown that high electric field induces high power density within ore. High power density could create large stresses at low energy input and therefore lower the cost of operation. An experimental program to investigate the effect of high power density and short exposure times on mineral liberation is therefore necessary. These requirements will form the basics for the experimental program in this thesis.

CHAPTER FOUR

Dielectric Properties Of Minerals

4.1. Introduction

An experimental investigation into the dielectric properties of minerals has been carried out using the resonant cylindrical cavity perturbation technique. As mentioned earlier in Chapter 2 this method is suitable for measurement of dielectric properties of lightly compressed samples, an area where the coaxial probe present some difficulties, as it is not always possible to characterize the surface of such samples. To further investigate the variation of the results of dielectric properties with temperature, experiments were also carried out using thermo-gravimetric analysis.

4.2. Measurement technique

A resonant circular copper cavity of diameter 373mm and height 37.3mm, resonating in TM_{0n0} modes, similar to the one described early in Chapter 2, was used for the measurement of dielectric properties (Arai et al, 1992; Fletcher, 1995 and Greenacre, 1996). By making the height of cavity a tenth of the diameter it is possible to excite TM_{0n0} modes up to n=5 without interference from crossing modes, the lowest resonant frequency crossing mode being at TM_{111}. The copper resonant cylindrical cavity measured frequencies for the empty cavity are shown in Table 4.1, for resonant modes up to n=3, which frequency is close to the heating frequency of 2.45GHz (Arai et al, 1992). Table 4.1 shows as well the value of calculated first order Bessel function and the m^{th} root of J_0 for the resonant modes up to n=3.

Table 4.1 Calculated first-order Bessel function for dielectric measurement

Standard resonant Mode	Copper cavity resonant frequency (GHz)	$x_{1,m}$ (Equation 2.11)	$J_1(x_{1,m})$
TM_{010}	0.6154	2.40483	0.51915
TM_{020}	1.4127	5.52008	-0.34026
TM_{030}	2.2160	8.65373	0.27145

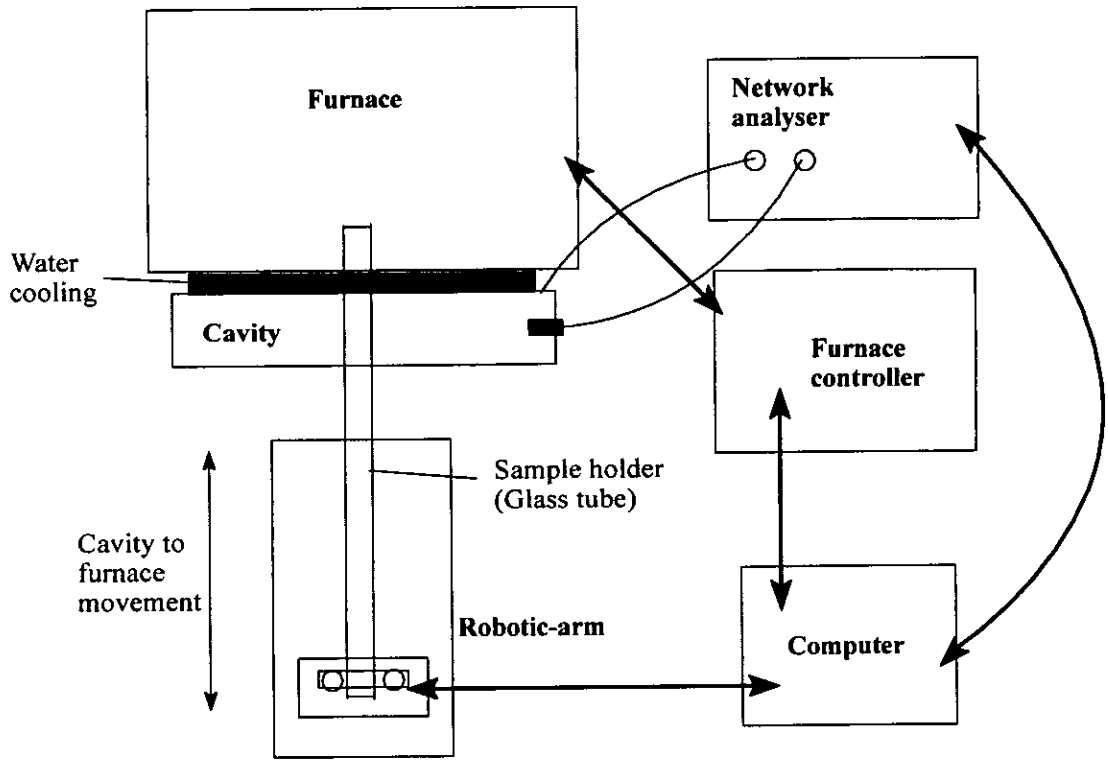

Figure 4.1. Diagrammatic representation of the measurement system (after Greenacre, 1996).

A schematic diagram of the measuring system is shown in Figure 4.1. The circular cylindrical cavity is mounted immediately below a conventional furnace capable of controlled heating up to 1600°C. A Hewlett Packard 8753C vector network analyzer used with a Hewlett Packard 85047A S-parameter test set transmits high frequency

signals via a coaxial line to a loop antenna within the cylindrical cavity. A second coaxial line, connected to a second loop within the cylindrical cavity, returns the signal to the vector network analyzer. The resonance frequency of the transmitted signal into the cavity can be detected and measured by the network analyzer. When a sample is inserted a frequency shift will occur, and typical displays are shown in Figure 4.2 for the empty cavity, the cavity with the empty sample holder and the cavity with a sample held within the fused quartz tube.

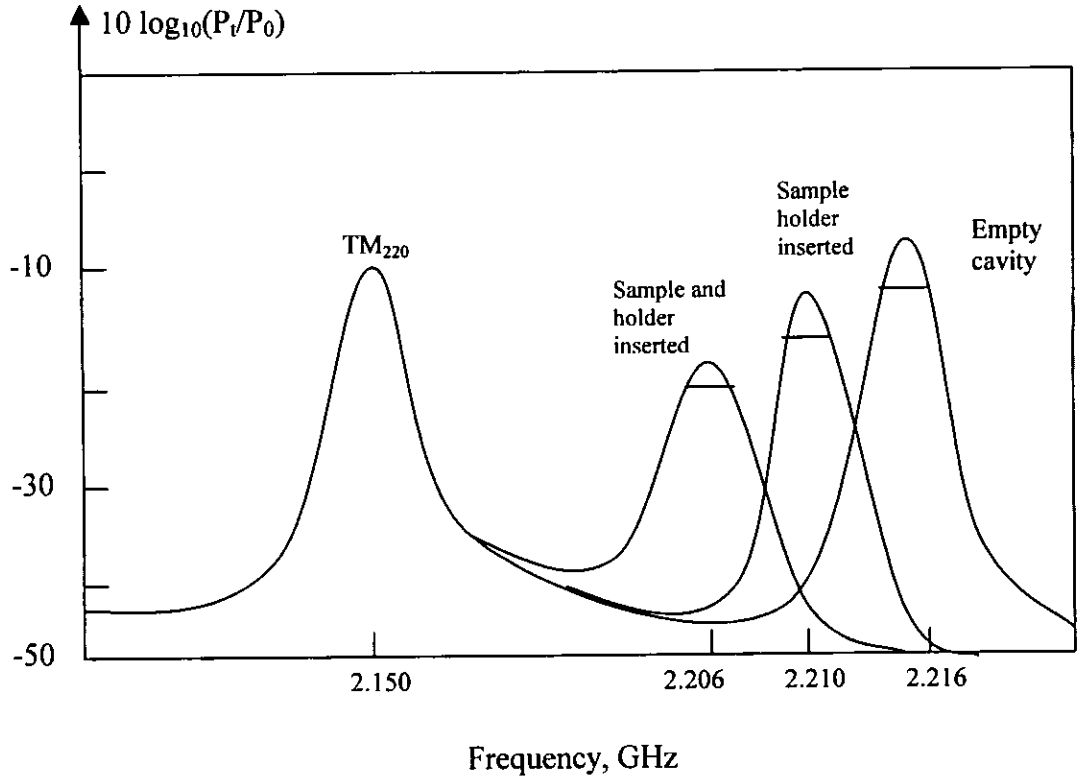

Figure 4.2. Typical displays from the vector network analyzer connected to the resonant cylindrical cavity showing the effect of sample insertion on the TM_{030} mode (after Metaxas et al, 1983).

From the displays such as those shown in Figure 4.2, the frequencies at which resonance occurred within the cavity can be easily measured. To measure the Q value of the resonant mode within the cavity, the frequencies at which the y-axis values are 3dB lower than at the maximum peak are measured. By dividing the frequency of the maximum peak with the difference between the 3dB frequencies at

either sides of maximum peak the value of Q is obtained. With the measurements of the changes in resonant frequency and Q-factor and using standard perturbation technique, the dielectric properties of material can be calculated from Maxwell equations 2.9 and 2.10.

A robotic arm mounted below the cylindrical cavity, with computer controlled stepper motor, is used to move the sample holder between the cavity and the furnace. A Visual Basic program, customized by the University of Nottingham, ultimately controls the system. To prevent cavity distortion at high temperatures, a water jacket is mounted between the cylindrical cavity and the furnace.

4.2.1 Experimental procedure

4.2.1.1. Sample preparation

Selected mineral specimens of galena (PbS), chalcopyroite ($CuFeS_2$), sphalerite (ZnS), pyrite (FeS_2), chalcocite (Cu_2S), magnetite (Fe_3O_4), hematite (Fe_2O_3), cassiterite (SnO_2), ilmenite ($FeTiO_3$), wolframite ((Fe, Mn)WO_4), quartz (SiO_2) and orthoclase ($4KAlSi_3O_8$) supplied by Gregory Bottley & Lloyd, London, were used for all measurements. The purity of the samples was established using X-ray diffraction. Sample preparation consisted of crushing and grinding the minerals to -200μm, using a cone crusher and a Raymond laboratory hammer mill respectively. A 4-mm internal diameter quartz tube was first filled with a small and compressed amount of silica fibre as a sample holder. For each mineral, the optimum sample size to provide a sensible change in the frequency and Q-factor was determined by trials, as required by the perturbation theory. The sample was poured into the tube and shaken to settle and the average length determined. The mass of the sample was then determined to four significant figures. By taking the average sample length and

internal diameter of the tube, to obtain the average volume of the sample and the average sample mass, the density of the sample inside the tube is determined such as:

$$\rho = \frac{m}{V} \tag{4.1}$$

Where ρ is the density (g/cm^3) m is the average mass (g) and V is the average volume of the sample (cm^3).

4.2.1.2. Dielectric properties measurement

A compressed pellet of mineral sample, encased within a quartz tube, was raised into the cavity. Measurement of the frequency shift and quality factor was made at three selected resonant frequencies, i.e. 0.615, 1.413 and 2.216 GHz. The quartz tube was mounted on a computer operated robotic arm, used to raise and lower the sample between the cavity and the furnace so that the temperature of the specimen could be varied.

The sample holder was placed in the furnace and the temperature increased at a rate of 1°C per minute. It was then maintained at the chosen level for 5 minutes to stabilise the temperature within the sample pellet before each measurement was taken. Measurement time was approximately 15 s, and it is assumed that heat loss from the sample during this period is small. All experiments were carried out within an air atmosphere and measurements were taken between 25°C and 600°C at 25°C intervals.

4.2.1.3. Thermo-gravimetric analysis

Thermo-gravimetric analysis of each mineral sample was carried out in order to provide data on phase or chemical changes of samples during heating. The changes were determined by continuous monitoring of the sample mass. The samples were heated in a Perkin Elmer Pyris 1 Thermo-gravimetric Analyser, in which about 50-100mg of each sample was heated from ambient to 600°C at a rate of 20°C per

minute. The sample was then held at 650°C for a further 20 minutes. The experiment was carried out using air and then nitrogen to observe any changes as a result of an inert atmosphere. The gas flow rate was kept constant at 30cc/min.

4.3. Calibration and Validation of the Technique

4.3.1 Procedure

The measurement of the dielectric properties of quartz and distilled water (low and high loss materials) were conducted for calibration purposes. Hand picked samples of quartz, as earlier described, were first analyzed using X-ray diffraction. The sample was then crushed and ground using a cone crusher and a Raymond laboratory mill. Thereafter, the sample was sieved into narrow particle size ranges and measurements were made on three different particle size ranges: <45μm, +90μm - 125μm and +180μm -250μm. A 4 mm internal diameter quartz tube was used to hold the samples during measurements. For the measurement of dielectric properties of water, being a high loss material, a 3 mm internal diameter quartz tube was used. The quartz tube was sealed at the bottom and the measurement of the shift of frequency and Q-factor was conducted on the empty tube before it was filled with water. Thereafter, the tube was filled with double distilled water. The height used for the calculation of volume of the sample was the height of the cavity (37.3mm).

4.3.2. Example calculations

The Table 4.2 below shows the measurements of frequency shift and Q-factor on the empty tube and filled with sample (quartz powder). Measurements were carried out in three modes. For each mode, and using equations 2.9 and 2.10, dielectric constant and loss factor can be calculated. The volume of the cavity is 4075833 mm^3 and the

volume of the sample filled in 4 mm diameter tube and height 37.3 mm is 468.7 mm^3.

Table 4.2. Readings of frequency shift and Q-factor

	Empty Tube		Tube + Sample	
Modes	Frequency (MHz)	Q-Value	Centre (MHz)	Q-Value
TM_{010}	615.3307	2901.15	615.2297	2892.87
TM_{020}	1411.418	2723.21	.1410.862	2680.05
TM_{030}	2211.511	2876.55	2210.079	2867.24

An example for calculations on the first mode is given below, for measurement taken at room temperature. This procedure was used in results of dielectric properties in the following Sections.

$$\varepsilon' = 1 + 2 * J_1^2(x_{1,m}) * \frac{V_c}{V_s} * \frac{f_0 - f_s}{f_0} = 1 + 2 * 0.51915^2 * \frac{4075833}{468.7} * \frac{615.331 - 615.229}{615.331} = 1.78$$

$$\varepsilon'' = J_1^2(x_{1,m}) * \frac{V_c}{V_s} * (\frac{1}{Q_s} - \frac{1}{Q_0}) = 0.51915^2 * \frac{4075833}{468.7} * (2892.87^{-1} - 2901.15^{-1}) = 0.002$$

4.3.3. Results

The results of measurements of dielectric constant and loss factor of quartz powder are shown in Figure 4.3 and 4.4. It has been found that the dielectric constant of quartz at theoretical density was 3.5, while the loss factor was almost zero. The results also show that the dielectric constant of quartz does not change with temperature, although it is density dependent. The results of measurements for double distilled water are shown in Figure 4.5. The results show that there is a significant variance in the values of dielectric properties over the measured temperature range. The dielectric constant and loss factor are both affected by temperature.

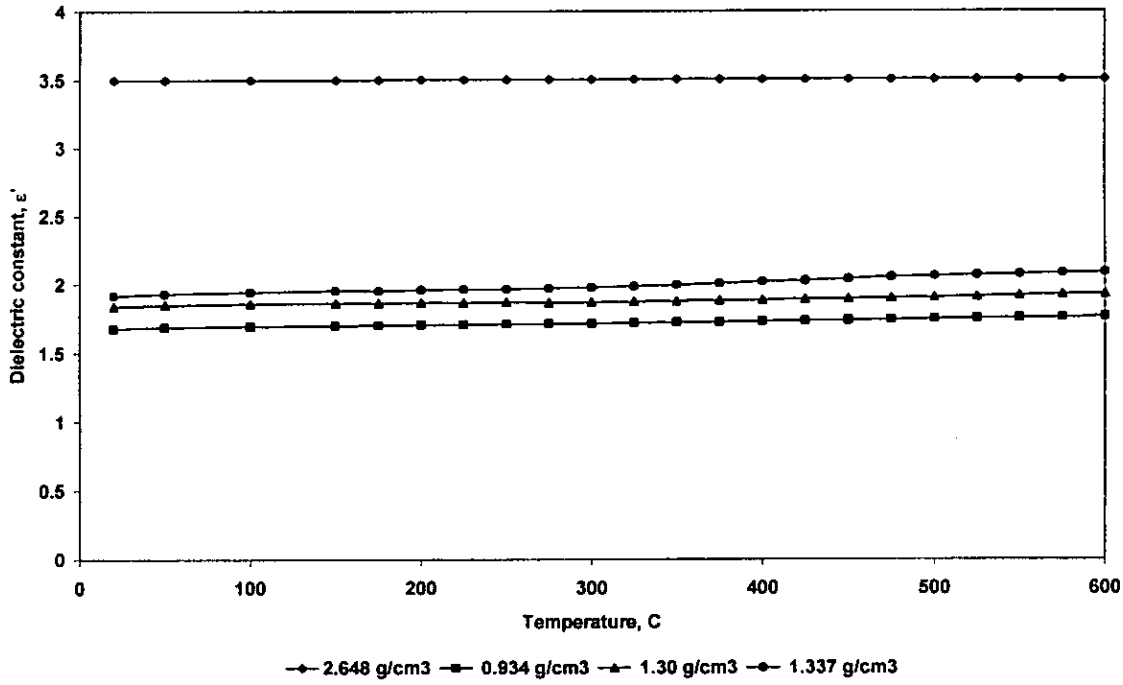

Figure 4.3. Effect of temperature and bulk density on the dielectric constant of quartz.

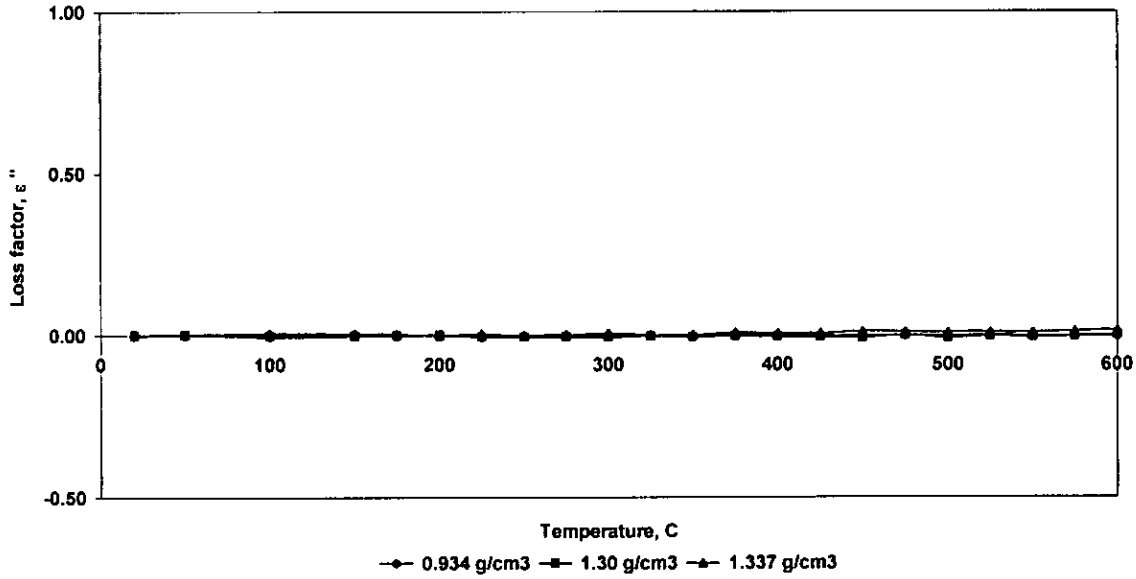

Figure 4.4. Effect of temperature and bulk density on the loss factor of quartz.

4.3.4 Discussion

The dielectric properties of materials are temperature and density dependent, the nature of the dependence being a function of the dielectric relaxation processes operating under the particular test conditions and the applied frequency (Nelson, 1973 and Boucher, 1999).

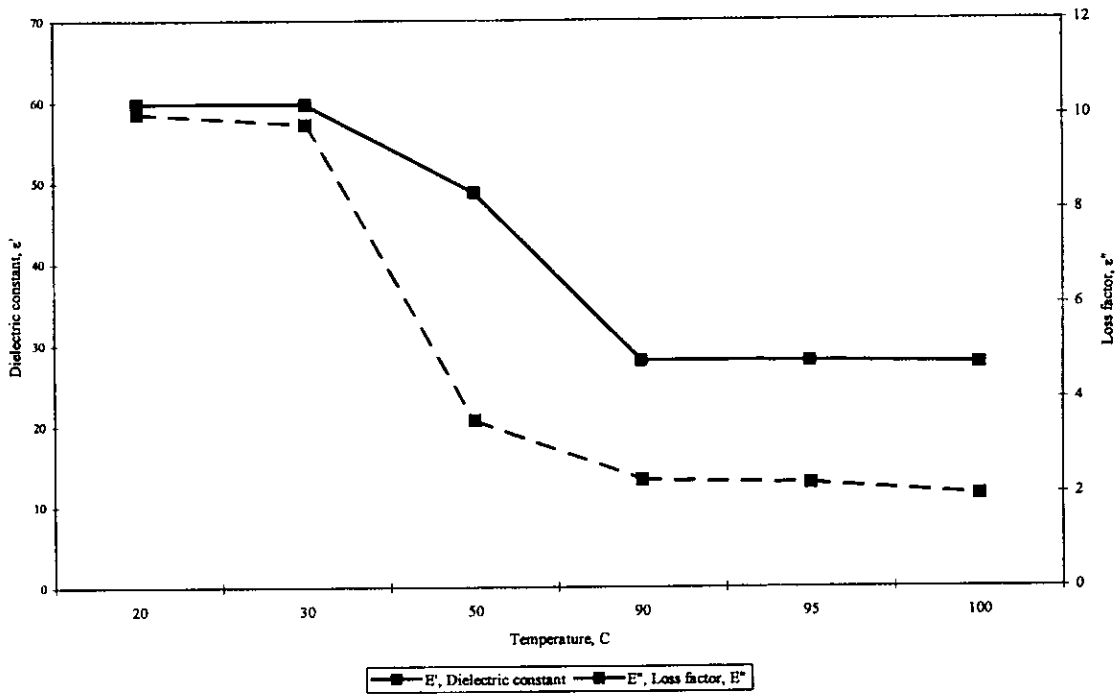

Figure 4.5. Effect of temperature on the dielectric constant and loss factor of double distilled water.

4.3.4.1. Effect of Temperature on the Dielectric Properties

The effect of temperature and frequency on the dielectric properties of water has been reported by Buchner et al (1999). According to Buchner et al., (1999) as the temperature increases, the strength and extent of the hydrogen bonding both decrease. This lowers both the dielectric constant, facilitates movement of the dipole and allows the water molecules to oscillate at higher frequencies. This reduces the friction and, hence, the loss factor. Furthermore, Buchner et al., suggested that indicative values of dielectric constant and loss factor between 0°C and 100°C are

within the ranges 88–50 and 10-2 respectively at a frequency of 1.5 GHz. Meredith (1998), published data regarding water dielectric properties across a range of temperatures and frequencies. This is shown in Figure 4.6.

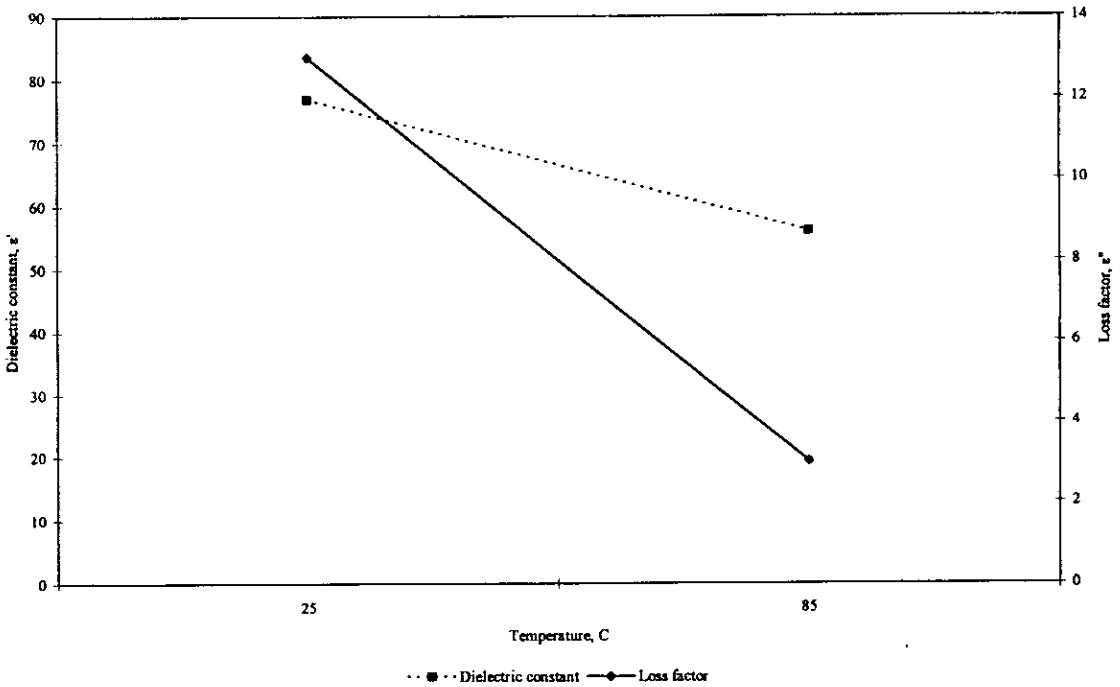

Figure 4.6. Effect of temperature on the dielectric constant and loss factor of distilled water (after Meredith, 1998).

There are some differences in the results measured in the present research and those published in the literature, however the trends in decrease of dielectric constant and loss factor with temperature are similar. The differences are due to the use of perturbation theory for high loss material, $\varepsilon''>5$. On measuring dielectric properties using the resonant cavity technique care is recommended in selection of a reasonable volume of material to ensure a sensible change of resonant frequency and quality factor (Klein et al., 1993). High differences in the changes in the resonant frequency and quality factor reduce the accuracy of measurement.For the measurement of dielectric properties of quartz, 4 mm diameter quartz rod and quartz powder were used. Published data of the dielectric properties for quartz indicates that the dielectric

constant varies from 2.82 to 5.0, while the loss factor varies from 0.02 to 0.04 (Church et al, 1988, Florek et al, 1989 and Harrison, 1997). It is worth noting that Church and Florek did not specify the conditions of the experiments while Harrison measured the dielectric properties using an Open Ended Coaxial Line Sensor on fine powdered material. Nevertheless, the results obtained in the present study are within the specified range.

4.3.4.2. Modeling Bulk Density Effect on Dielectric Constant

Mineral ores are heterogeneous mixtures of multiple mineral phases and, under typical processing conditions, are often present in powder form following comminution. Prediction of mixture properties from pure mineral data, or the variation of complex permittivity with density from a single datum is a valuable tool. There exist a considerable number of dielectric mixture formulae. Tinga et al. (1973) summarize many of these.

Nelson (1988) has investigated relationships to allow prediction of the complex permittivity of granular or pulverized materials at different bulk densities. It was found that dielectric proprieties could be expressed in terms of a powder-air mixture by the following empirical relationships:

$$\varepsilon'^{1/k} = a\rho + 1 \qquad (4.2)$$

$$\sqrt{\varepsilon'' + e} = c_1\rho + c_0 \qquad (4.3)$$

Where k can take the value 2 or 3 depending on the material, a, c_0, c_1 and e are constants for a specific material at a given frequency and ρ is the density of the powder-air mixture. These relationships are valid only for a powder-air mixture, where $\varepsilon' = 1$ and $\varepsilon'' = 0$ at zero density.

In this research, Nelson used data from earlier studies on the density dependence of the dielectric properties of particulate materials to see how well they might support the relationships. The data included measurements taken on pulverized coal, goethite and hard red winter wheat at frequencies of 150 MHz and 11.7 GHz at a temperature of 22 °C. After plotting the experimental points (ρ, $\sqrt{\varepsilon'}$) a straight-line fitting was obtained by linear regression analysis, which provided the intercept, A_0, and slope, A_1, for equation 4.4 (after Nelson 1983).

$$\varepsilon'^{1/2} = A_0 + A_1\rho \qquad (4.4)$$

An attempt to use a similar approach with the data obtained in the present research has been made. Experimental data points using measurement of the dielectric constant of quartz at four densities were plotted against the density using k=2 and 3. The experimental data are a result of measurement of dielectric properties of quartz powder samples at three densities and the fourth was a rod quartz sample.

The results are shown in Figures 4.7 and 4.8, where straight lines were obtained by least squares curve fitting with the (1, 0) point included. More detailed information about the coefficients of empirical equations, obtained by linear regression analysis that provided the intercept A_0 and slope A_1 relating dielectric constant and density of quartz at a range of temperature and frequency is given in Table 4.3.

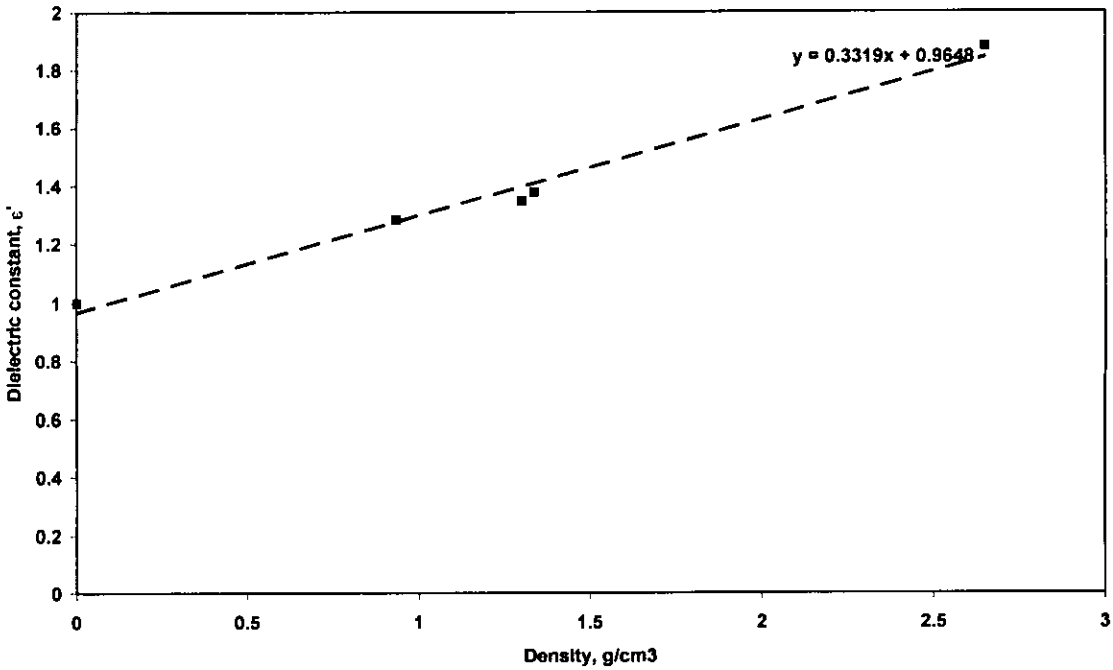

Figure 4.7. Relationship between bulk density and dielectric constant of quartz for k=2

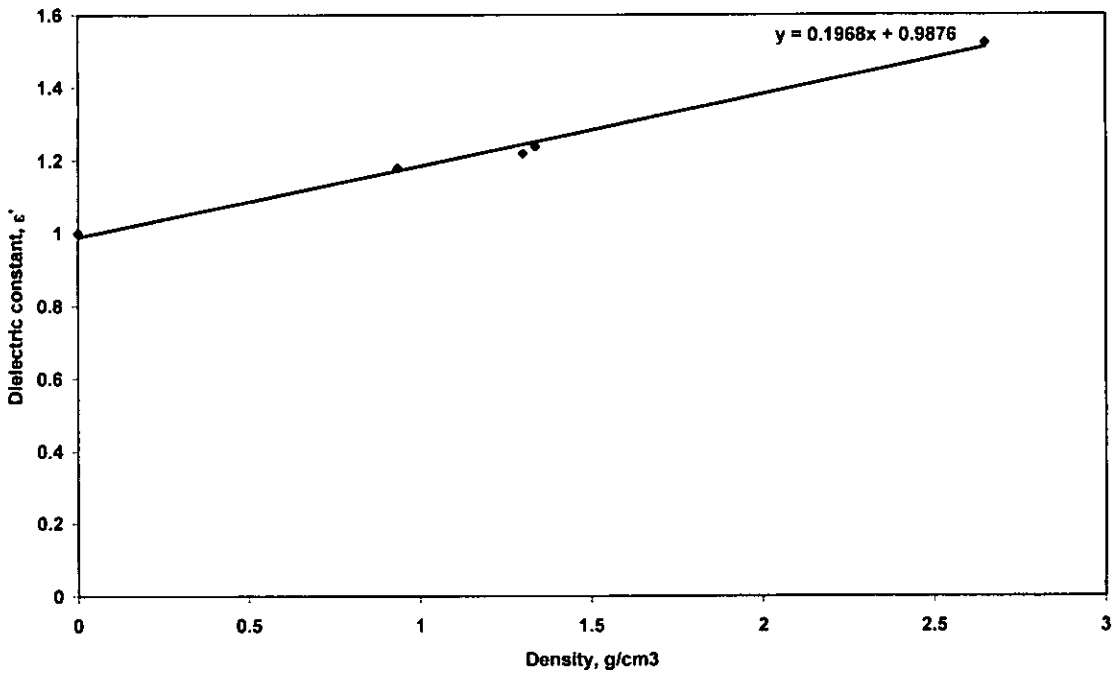

Figure 4.8. Relationship between bulk density and dielectric constant of quartz for k=3

Table 4.3. Coefficients of empirical equations relating the dielectric constant (ε′) and bulk density (ρ) of quartz.

Regression model	Temperature, °C	Measurement frequency, MHz					
		615		1410		2210	
Coefficient		A_0	A_1	A_0	A_1	A_0	A_1
$\sqrt{\varepsilon_r'} = A_0 + A_1\rho$	100	0.9534	0.3304	0.965	0.331	0.978	0.327
	200	0.9573	0.3308	0.968	0.331	0.981	0.327
	300	0.964	0.3305	0.971	0.331	0.983	0.327
$(\varepsilon_r')^{1/3} = A_0 + A_1\rho$	100	0.980	0.196	0.987	0.196	0.996	0.194
	200	0.994	0.196	0.989	0.196	0.997	0.194
	300	0.986	0.196	0.991	0.196	0.998	0.194

Standard deviation analysis for the developed models was carried out. The results are shown in Table 4.4. It has been found from the correlation coefficient that k=2 gives better results than k=3.

Table 4.4. Standard deviation for experimental and calculated dielectric constant based on equation 4.2 for k=2 and k=3 model.

Density, g/cm^3	**Dielectric constant**		
	Experimental	**Calculated, k=2 model**	**Calculated, k=3 model**
0	1.00	0.96	0.95
0.934	1.65	1.61	1.64
1.3	1.81	1.92	1.96
1.337	1.90	1.96	1.99
2.648	3.54	3.43	3.39
Standard deviation, %		**3.81**	**5.15**

Therefore, the k=2 model will be used to calculate the relationship between density and dielectric constant of minerals in the following sections.

4.4. Dielectric Properties of Sulphides

The measurement of dielectric properties of various sulphides has been carried out. The mineral samples were hand picked specimens, as mentioned in section 4.2.1.1.

The purity of the samples was confirmed using X-ray diffraction and data illustrated in Appendices, Figures A1.1 to A1.12. Sample preparation and the experimental procedure were the same as described in Section 4.2.1.

4.4.1. The Nature of Sulphides

Sulphides are complex minerals in terms of both their chemistry and origin. They are usually deposited from aqueous solutions in fracture zones of the crust, located in or near the large, deep igneous bodies called batholiths (Deer et al., 1962). Great effort has been made to understand the origins and properties of the sulphides because they are amongst the most valuable of all economical minerals. Their compounds give rise to many of the metals used by mankind.

A sulphide is, essentially, an oxygen free compound of sulphur and one or more metals. In the simplest form the sulphide structure can be regarded as a spherical packing of sulphur atoms with the smaller metal atoms in the spaces in between. The chemical bonding is, in varying degrees, a mixture of metallic, ionic and covalent bonds. Most sulphides have a metallic appearance, with a strong colour and metallic lustre. The majority are opaque, have high densities and many of them are brittle, which easily distinguishes them from the native metals (Deer et al. 1962)

Pyrite (FeS_2) is the most abundant of sulphide minerals. It occurs in a wide variety of geological conditions, but, in many cases, its mode of origin is uncertain (Deer et al 1962). It is found in large masses or veins of hydrothermal origin, both as primary and as a secondary mineral in igneous and in sedimentary rocks. Large masses of pyrite may also be found in contact with metamorphic ore deposits, often associated with sulphides of copper and of other metals, some of which have been formed by replacement of pyrite. Differential thermal analysis of pyrite has been carried out by a number of investigators. Asensio and Sabatier (1958) observed a large exothermic

peak corresponding to oxidation of the mineral at 450°C –650°C (with components at 510 and 550°C).

Chalcopyrite ($CuFeS_2$) is an important copper bearing ore mineral. It is found, together with other sulphides, among primary ores of magmatic origin in close association with intrusions of basic igneous rocks (Deer et al, 1962). Chalcopyrite is oxidized to sulphates of iron and copper on exposure to air and water or with slight heating. When heated in air chalcopyrite shows an exothermic peak due to oxidation, which is centred on about 500°C (McLaughlin, 1957; Levy, 1958). In general, chalcopyrite and other sulphides that originate at high temperatures can first tolerate a wide range of solid solution but, on cooling under favourable conditions, ex-solution of separate phases may occur (Deer et al, 1962). Furthermore, Sugaki and Tashiro, 1956, reported when chalcopyrite is heated, development of a lamellar intergrowth of bornite occurs followed by conversion of chalcopyrite to pyrrhotite and a solid solution of bornite with chalcocite.

Sphalerite (ZnS) is a colourless mineral but almost all specimens found in nature are coloured through the presence of iron and other elements (Deer et al, 1962). Sphalerite is the most common of the zinc bearing minerals and its occurrence, often in vein deposits associated with galena, is widespread. The less common form of ZnS, wurtzite, is stable only at high temperatures. On heating in air, sphalerite is oxidized to zinc sulphate, but if much iron is present ferric and ferrous sulphates are also formed and at high temperatures (above 1000°C) zinc ferrites result. According to McLaughlin (1957) the differential thermal analysis pattern of sphalerite shows a large exothermic peak corresponding to oxidation at about 1000°C, which masks any peak that may occur through the sphalerite-wurtzite transition at about 1020°C.

Galena (PbS) is the most widely distributed of the sulphide minerals and is the most important of the lead minerals. It occurs most frequently together with sphalerite, and these lead zinc ores often contain recoverable amounts of copper, silver, antimony and bismuth. The main types of occurrence of lead zinc sulphides include deposits of low, intermediate and high temperature origin. Thus galena of high temperature origin is found in veins and replacements in pegmatites, calcico-silicates rocks, limestones and other sediments. In addition to various sulphides, commonly associated minerals include barites, fluorite, quartz and calcite (Deer et al, 1962). According to McLaughlin (1957) on heating in air, galena is oxidized to lead sulphate and it melts at 1115°C.

4.4.2. Results

4.4.2.1. Dielectric Properties

From the data of the frequency shift and Q-factor measured at three resonant frequencies of the copper cylindrical cavity, dielectric constant and loss factor were calculated using equations 2.9 and 2.10. An example of the results of the temperature dependence of dielectric constant and loss factor of sulphides at a frequency of 2.21 GHz are shown in Figures 4.9 and 4.10 respectively. It has been found, as shown in Figure 4.9, that the dielectric constants of pyrite and chalcopyrite have similar trends along the range of temperature used. It is constant between 50 and 375 °C and then a positive slope is observed from 375 till 500°C, from which it remains steady.

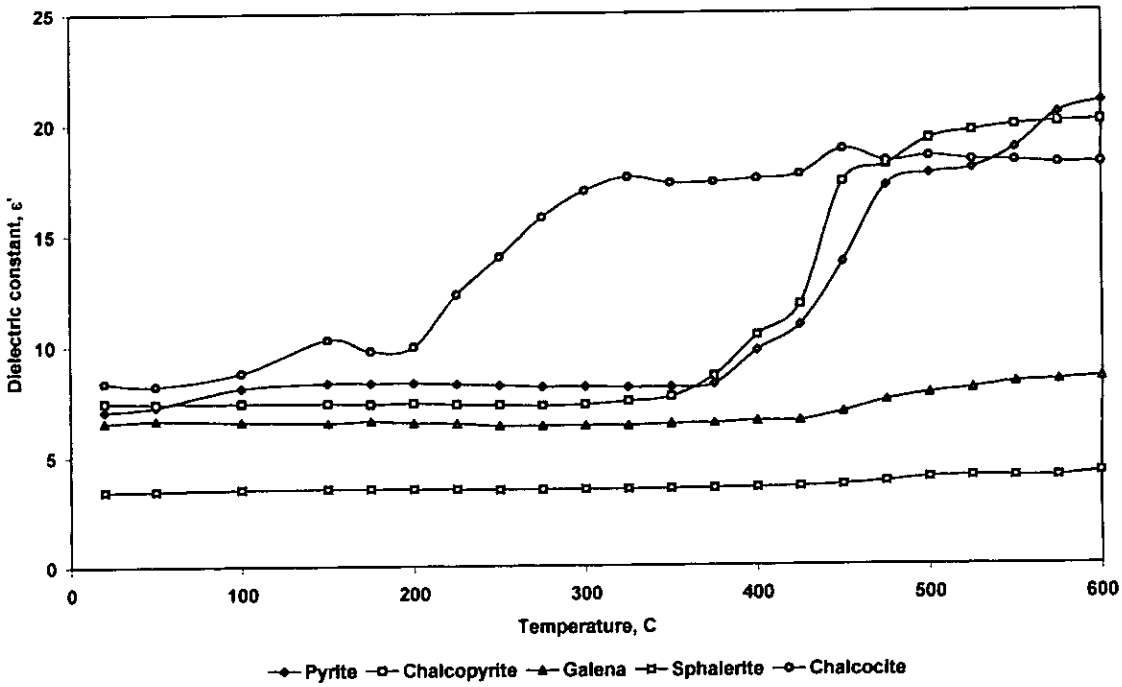

Figure 4.9. The dependence of dielectric constant of sulphide minerals with temperature measured at the frequency of 2.21 GHz.

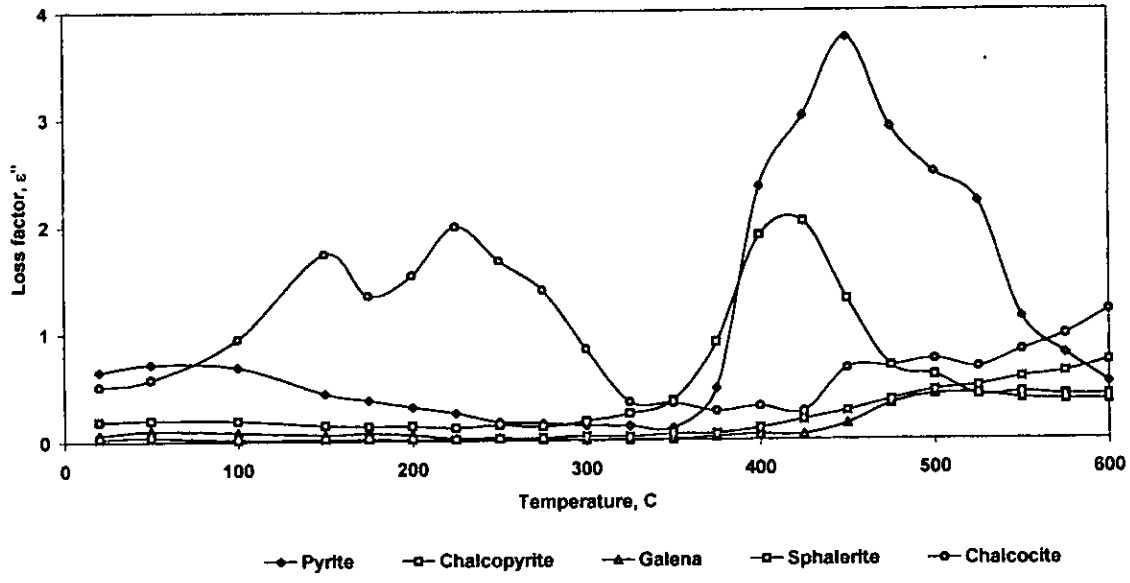

Figure 4.10. The dependence of loss factor of sulphide minerals with temperature measured at the frequency of 2.21 GHz.

The loss factor of chalcopyrite and pyrite also show similar trends for both minerals. It is steady up to 350°C thereafter the loss factor exhibits a peak at the temperatures of 400°C and 450°C for chalcopyrite and pyrite respectively. Such behaviour was

observed during conventional heating. Chalcocite exhibits similar trends but the positive slope occurs in the temperature range 200-350°C. The loss factor shows two peaks at temperatures of around 150°C and around 250°C. The other sulphide minerals, galena and sphalerite are thermally stable up to 425°C. The dielectric constant and loss factor for these minerals are steady throughout this temperature range. However, above this temperature both galena and sphalerite show a positive slope. Similar trends of variation of dielectric constant and loss factor with temperature at frequencies of 615 MHz and 1.410 GHz are shown in Appendices A1.13-17.

4.4.2.2. Thermo Gravimetric Results

The results of thermo-gravimetric analysis of sulphide minerals carried out on air and nitrogen atmospheres are shown in Figures 4.11 and 4.12. It has been found that galena and sphalerite are stable over the temperature range of the experiment and, regardless, of the atmosphere during differential thermal analysis, the minerals are stable at temperatures up to 500°C, as shown in Figures 4.11 and 4.12.

Thermo-gravimetric analysis of pyrite, chalcocite and chalcopyrite show a variation of weight during heating. However, the trends of weight variation depend on the prevailing conditions during heating. When heating in air, an increase of weight is observed for chalcocite and chalcopyrite while pyrite shows a loss of weight (Figure 4.11). When heating in a nitrogen atmosphere, however, a significant loss of weight is observed in all three minerals, with chalcopyrite reporting loss of up to 10% (Figure 4.12).

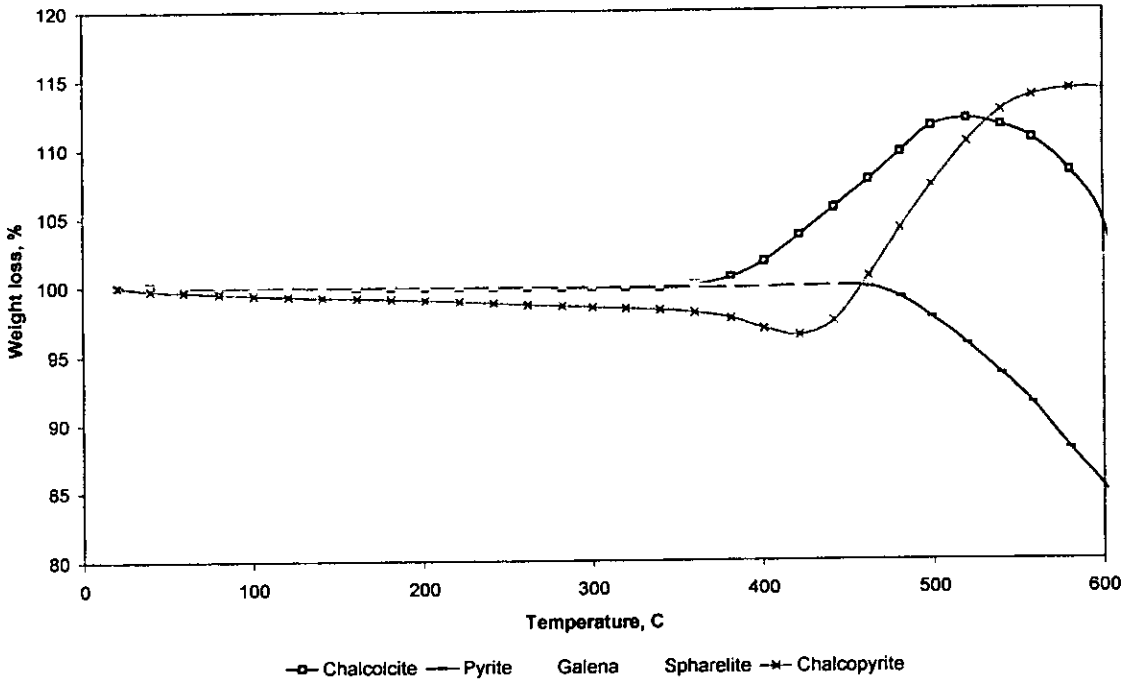

Figure 4.11. Thermo-gravimetric analysis of sulphides in air.

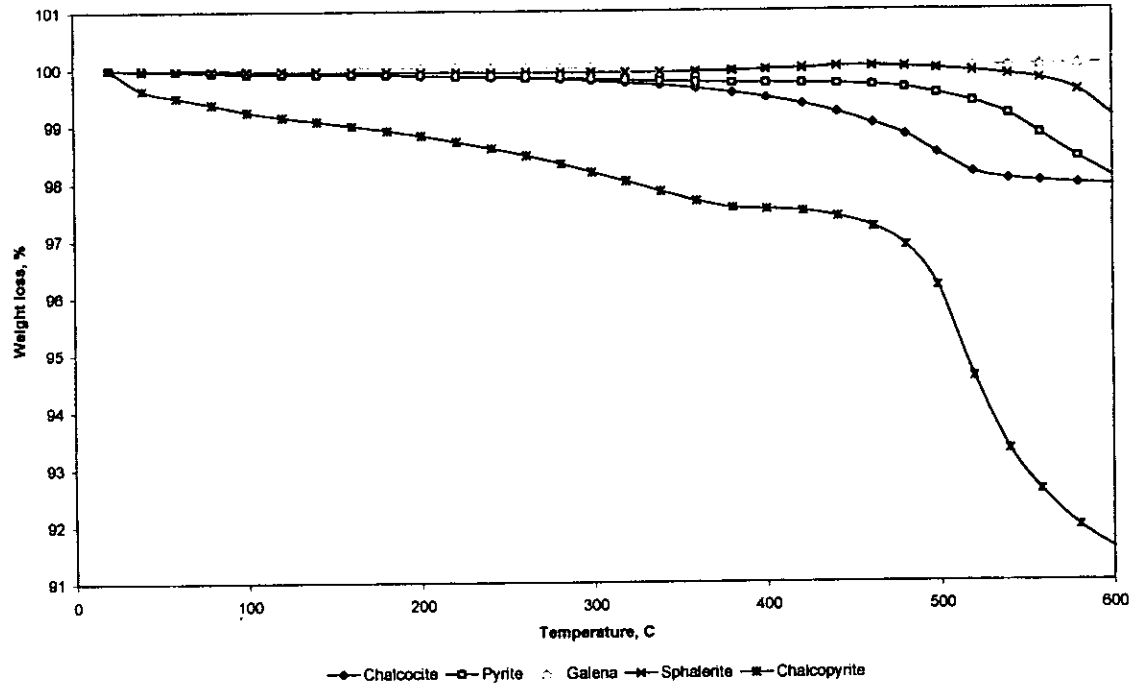

Figure 4.12. Thermo-gravimetric analysis of sulphides in a nitrogen atmosphere.

4.4.3. Discussion

4.4.3.1. Modelling Bulk Density Effect

The bulk density effect on the dielectric properties of sulphide minerals has been investigated. The results for quartz showed the square root model gave the best fit

and this has been applied to the investigation of the relationship of bulk density and dielectric constant of sulphides. Figure 4.13 show the bulk density effect on dielectric constant of sulphides measured at room temperature and a frequency of 2.21GHz. A summary of linear relationships between density and dielectric constant measured at the temperature of 25°C developed for other sulphide minerals at different frequencies are given in Table 4.5. From the developed linear relationship it is possible to extrapolate the dielectric constant of the solid mineral. Comparison of the calculated values of dielectric constant of sulphides and literature are given in Table 4.6.

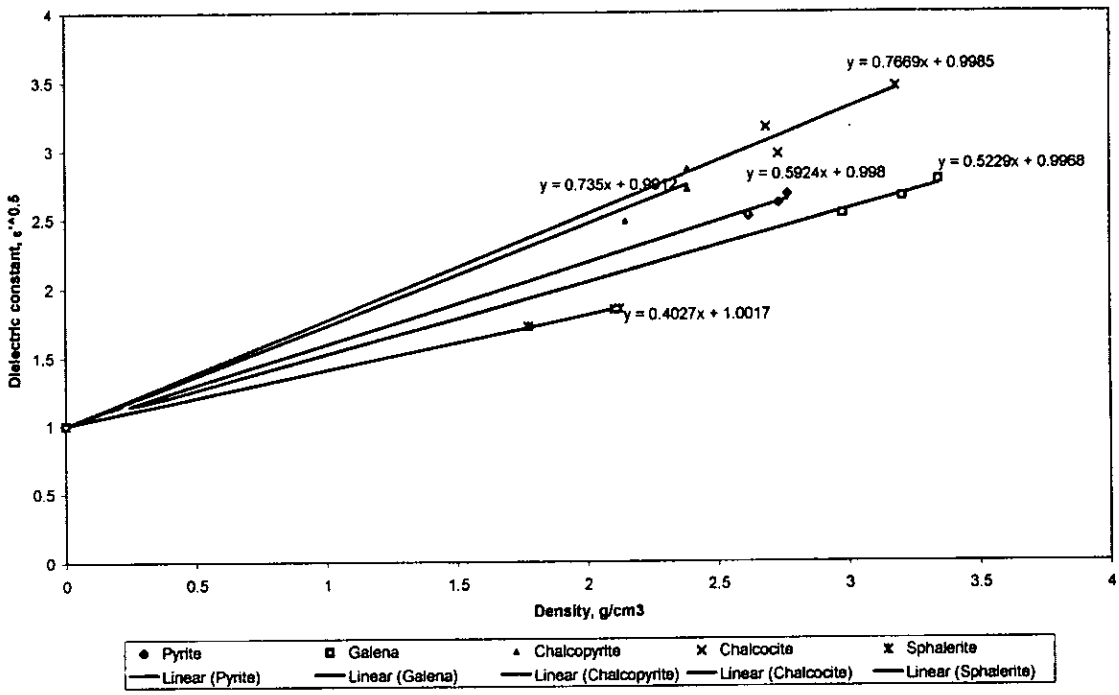

Figure 4.13. Effect of bulk density on dielectric properties of sulphides measured at room temperature.

The experimental data were obtained on the present research and multiplied by the permittivity of free space (8.85×10^{-12} F/m). Holderfield and Salsman's data is assumed to have already been converted. Salsman's data for chalcopyrite has been clearly identified as relative dielectric constant, therefore it was converted and data

from the Handbook of Physical properties of rocks are absolute values. Apart from the result for galena, the differences between experimental and literature values for chalcocite, chalcopyrite and sphalerite is up to 12%.

Table 4.5. Coefficients of empirical equations relating the dielectric constant ($\sqrt{\varepsilon'}$) and bulk density (ρ) of sulphides.

Regression model	**Mineral**	**Measurement frequency, MHz**					
		615		**1410**		**2216**	
Coefficient		A_0	A_1	A_0	A_1	A_0	A_1
$\sqrt{\varepsilon_r'} = A_0 + A_1\rho$	Chalcocite	1.007	0.8016	0.9985	0.767	1.000	0.7738
	Chalcopyrite	0.9885	0.7514	0.9912	0.735	0.992	0.7414
	Galena	0.9968	0.5229	0.9978	0.5302	0.993	0.5301
	Pyrite	0.998	0.5924	0.9975	0.5729	0.998	0.5753
	Sphalerite	1.001	0.379	1.001	0.386	1.001	0.4027

Table 4.6. Dielectric properties of sulphides

Mineral	**Density, g/cm^3**	**ε' (Experimental) 10^{-12} (F/m)**	**ε' (Literature) 10^{-12} (F/m)**
Chalcocite	5.793	282.6	250[a)]
Chalcopyrite	4.200	152.8	100[a)] 146[b)]
Galena	7.598	223.73	158[a),c)]
Pyrite	5.011	142	-
Sphalerite	4.089	62	69.7[c)]

a) Holderfield and Salsman, 1993; b) Salsman, 1991 and c) Clark, 1966.

An attempt to model the relationship between loss factor and density for sulphides was made but was not successful. A possible explanation is the fact that the cavity perturbation technique becomes less accurate for the evaluation of loss factor for high loss materials. As reported in Batt et al. (1995), discrepancies in the value for

loss factor using different measuring techniques could be up to 50% at high temperature. With such an error it is likely that values obtained will be scattered and so it would be difficult to obtain a linear relationship. When using the cavity perturbation technique for measurement of dielectric properties, high loss materials cause high frequency shift and flatten the peak making it difficult for the network analyzer to register it precisely. Smaller amounts of material can improve matters but this is not a complete solution. This is a problem that has to be solved when using the resonant cylindrical cavity based on perturbation technique for measurement of dielectric properties of high loss materials.

4.4.3.2. Effect of Frequency

According to Nelson (1973), with the exception of some extremely low loss materials the dielectric properties of most materials vary considerably with the frequency of the applied energy. An important phenomenon contributing to the frequency dependence of the dielectric properties of most materials is the polarization arising from the orientation of molecules, which have permanent dipole moments with the applied electric field. To better illustrate the dependence of dielectric properties with frequency an analysis has been carried out for pyrite. The dependence of dielectric properties of pyrite with frequency measured at 25°C is shown in Figure 4.14. The results show little variation in the relationship between dielectric constant and loss factor with frequency while the penetration depth shows a negative slope as would be expected as D_p is proportional to f^{-1}.

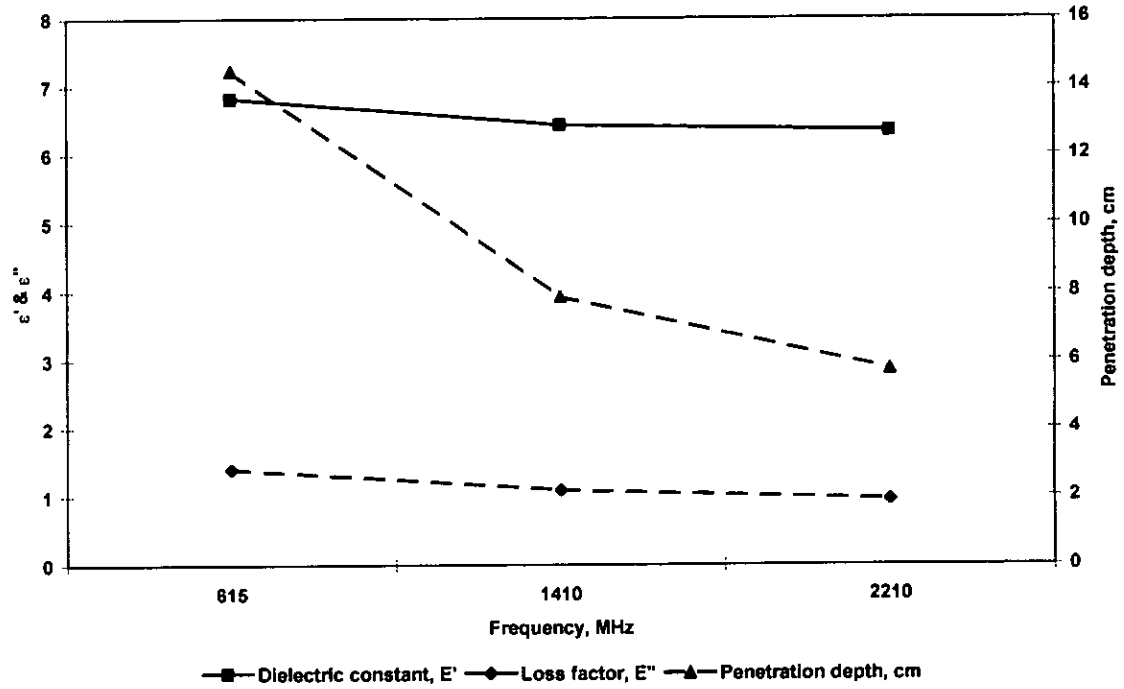

Figure 4.14. Effect of frequency on dielectric properties of pyrite measured at room temperature.

4.4.3.3. Effect of Temperature

Several authors have reported the effect of temperature on the composition and mineral phases of sulphides (Deer et al., 1962; Stolen et al., 1990 and Large et al., 1995). From the results shown in the Figures 4.9 and 4.10 such an effect has been observed on the dielectric properties. Furthermore, thermo-gravimetric analysis has been carried out and the results shown in Figure 4.11. The thermo-gravimetric analysis curve results in Figure 4.11 shows general trends of material mass loss during heating. To further investigate the critical points where such changes occur a derivative function known as differential thermal analysis is required. The results of differential thermal analysis for sulphide minerals are shown in Figure 4.15 for experiments carried out on air.

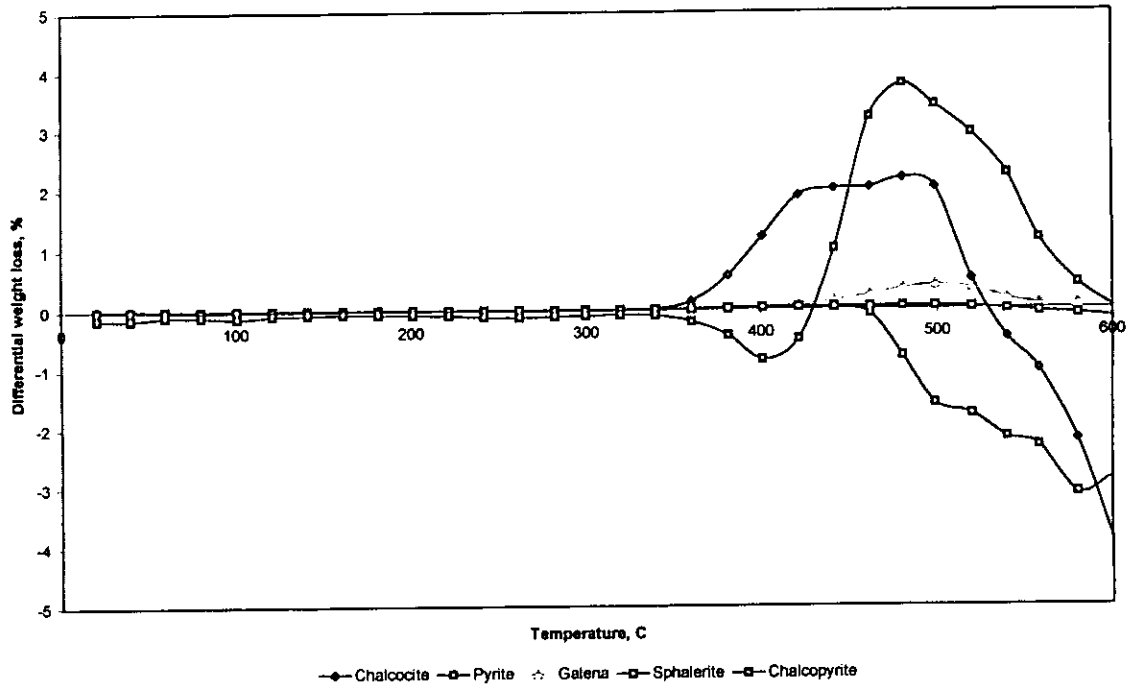

Figure 4.15. Differential thermo-gravimetric analysis of sulphides.

It has been found from the heating experiment in air that a critical temperature of weight changes for chalcocite is observed at 350°C, below which it is stable. An increase in weight is observed above this temperature, up to 500°C, which could be related to the oxidation of chalcocite. Results for chalcocite in a nitrogen atmosphere show a decrease in weight at temperatures above 350°C. The dielectric property results show an increase of dielectric constant at temperatures between 200°C and 350°C. In addition, the results of loss factor show two regions of high microwave absorption between 100°C to 275°C and above 400°C that could be related to complex phase transformation within the mineral during heating.

However, in published data for dielectric properties of chalcocite by Salsman (1991), variation of dielectric constant with temperature shows a different trend. It shows a peak at a temperature of around 100°C and then it decreases up to 300°C. A further paper by Holderfield and Salsman (1992) on the dielectric constant of chalcocite shows a different trend.

Despite these results, there could be some complex phase transformation occurring during heating that cannot be explained by the mass variation for this particular mineral. Furthermore, it has long been reported that in (copper + sulphur) the region from Cu_2S to $Cu_{1.75}S$ shows a wide variety of phases and phase transition of complex nature (Gronvold et al. 1987). Such a variety of phases and phase transformation are likely to have an effect on the dielectric properties but they cannot be detected through differential thermal analysis.

In contrast to chalcocite, the dielectric properties of pyrite, galena, sphalerite and chalcopyrite are quite consistent with the thermo gravimetric results. For example, the results for pyrite show that the mineral is quite stable up to 350°C and above this temperature a loss of weight is observed. It is interesting to note that loss of mass occurs regardless of the heating conditions in an air or nitrogen atmosphere. The present finding could suggest that during phase transition from pyrite to pyrrhotite free sulphur is formed, which is further liberated as sulphur dioxide or sulphur fumes depending on the atmosphere.

Although chalcopyrite exhibits similar trends to pyrite for dielectric constant and loss factor, it shows a different thermo gravimetric curve pattern. The differential thermo gravimetric curve of chalcopyrite (Figure 4.15) shows that the mineral is stable up to 350°C. Between 350°C and 400°C there is a phase transition similar to the process occurring during the phase transition of pyrite to pyrrhotite. This finding is consistent with results of loss factor for chalcopyrite where a maximum value is observed at a temperature of 400°C (Figure 4.10). Furthermore, the results suggest that the increase in loss factor observed for pyrite and chalcopyrite in this temperature range is due to the presence of a similar mineral phase with high absorption of microwave radiation. Above a temperature of 400°C, chalcopyrite undergoes an oxidation process that

results in a stable mineral phase that eventually decomposes with sulphur dioxide liberated at temperatures above 500°C. The liberation of free sulphur at temperature above 500°C was observed on the thermo gravimetric analysis results of chalcopyrite during heating in a nitrogen atmosphere.

The results of thermo gravimetric analysis of galena and sphalerite show that both minerals are thermally stable at temperatures up to 500°C and above this temperature small variations in mass have been observed. The data of loss factor of galena and sphalerite suggest that when cold, they have little response to microwave radiation. Only at temperature above 400°C do they become receptive to microwave radiation (Figures 4.9 and 4.10). However, a thorough examination of the loss tangent, the parameter that shows how well a material will absorb microwave energy and to convert it as heat, showed relatively high values compared to sphalerite (later discussed in Chapter 6).

Overall, the present findings are consistent with differential thermal analysis data on sulphide minerals reported by a number of investigators. These findings suggest that, during heating in an oxidising environment, pyrite is converted into pyrrhotite with the liberation of sulphur fumes and chalcocite and chalcopyrite are converted into Cu or Cu-Fe sulphates. The results are also fully in accordance with observations reported by Chen et al in 1984. Chen et al carried out microwave heating experiments on minerals and observed the heating response and product examination. It was reported that pyrite and chalcopyrite when exposed to microwaves heat readily with emission of fumes. The product examination revealed the presence of pyrrhotite and sulphur fumes when heating pyrite and Cu-Fe sulphides and sulphur fumes for chalcopyrite product.

4.5. Dielectric Properties of Oxides

Measurement of dielectric properties of several oxides has been carried out. The sample preparation and experimental procedure, including the X-ray diffraction analysis to confirm purity, were carried out the same way as described in section 4.2.1. Data of X-ray diffraction are given in Appendices, Figures A1.1 to A1.12.

4.5.1. Nature of Oxides

Hematite (Fe_2O_3) is a very important ore of iron occurring mainly in sediments and their metamorphosed equivalents. It is also found in soils and as a weathering product of iron bearing minerals. The common massive ore is red hematite. On heating in air, hematite dissociates to Fe_3O_4 at about 1390°C. At 500°C a change occurs in the crystal structure of outgrowths formed on hematite single crystals by heating in air: this change is apparently due to migration of some cations (Deer et al., 1962).

Magnetite (Fe_3O_4) is one of the most abundant oxide minerals in igneous and metamorphic rocks and is the main magnetic ore. It occurs typically as an accessory mineral in many igneous rocks but is occasionally concentrated in magmatic segregations or crystal settling, sometimes forming magnetite bands (Deer et al, 1962). The differential thermal analysis curve for magnetite shows two characteristic exothermal peaks, both being considered to be due of Fe^{+2}. The first stage forms a film of Fe_2O_3 around the particles at temperature of 200°C and the second, immediately following the Curie point (the temperature at which, on heating, the ferromagnetism is lost and the substance becomes paramagnetic), at 578°C (Schmidt and Vermaas, 1955). From studies on the hematite-magnetite series, Lepp (1957) concluded that during rapid oxidation of magnetite there are three stages: (1) $4Fe_3O_4 + O_2 = 6\gamma\text{-}Fe_2O_3$, commencing at about 200°C and ending at 375°-400°C; (2) γ-

Fe_2O_3 = α-Fe_2O_3, starting at about 375°C and ending at 525°-550°C and (3) $4Fe_3O_4+O_2 \rightarrow 6\alpha$-$Fe_2O_3$, starting at 550°-575°C, the temperature of completion depending on the extent of reaction (1).

Ilmenite ($FeTiO_3$) is a common accessory mineral in many igneous and metamorphic rocks and may occur in veins and disseminated deposits, sometimes of large extent, in association with gabbros, norites and anorthosites. Bailey et al (1956) recognized three successive stages of alteration of ilmenite: patchy ilmenite, amorphous iron titanium oxide and leucoxene. Karkanavala and Morin (1959) showed that on oxidation in air at 850°C ilmenite is converted to a mixture of hematite, pseudobrookite and rutile. At 650°C oxidation gives hematite and rutile only and some oxidation occurs at temperature as low as 100°-200°C.

Cassiterite (SnO_2) is the most important ore of tin and is typically found associated with acid igneous rocks, such as granites, micro-granites and quartz porphyries. It occurs frequently in high temperature hydrothermal veins closely associated with granite or in granite pegmatites (Deer et al, 1962). It is often found associated with such minerals as wolframite, chalcopyrite, tourmaline, topaz, lepidolite and fluorite and various Bi, Pb, Ag and Mo minerals as inclusions. Although often found as an alteration product of other tin bearing minerals cassiterite is a relatively stable mineral (Varlamoff, 1948).

4.5.2. Results

From the data of the frequency shift and Q-factor measured at three resonant frequencies of the copper cylindrical cavity, dielectric constant and loss factor were calculated using equations 2.9 and 2.10. Summarised data of dielectric properties of oxides are given in Figures A1.18 to A1.23 in the Appendices. An example results of

the dielectric constant and loss factor of oxides, variation with temperature at the frequency of 2.21 GHz are shown in Figures 4.16 and 4.17 and determined by the method shown in Section 4.3.

Apart from hematite, the dielectric properties of magnetite, ilmenite, wolframite and cassiterite have been found to be constant along the temperature range used. The dielectric constant of ilmenite is high compared to the other oxides. The loss factor of hematite exhibits a peak across the temperature range of 200 and 400°C. This temperature range in which hematite exhibits its peak in loss factor is similar to the one reported by Lepp (1957) during his studies of oxidation of magnetite to hematite, where γ-hematite transforms to α-hematite during heating.

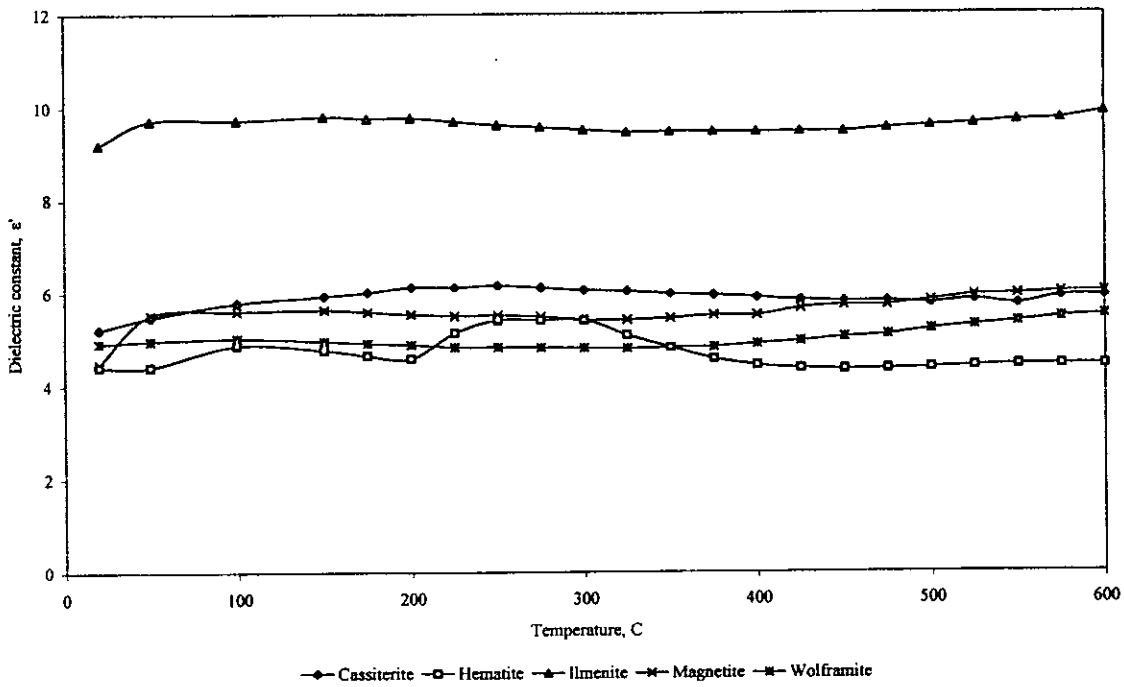

Figure 4.16. Effect of temperature on the dielectric constant of oxides.

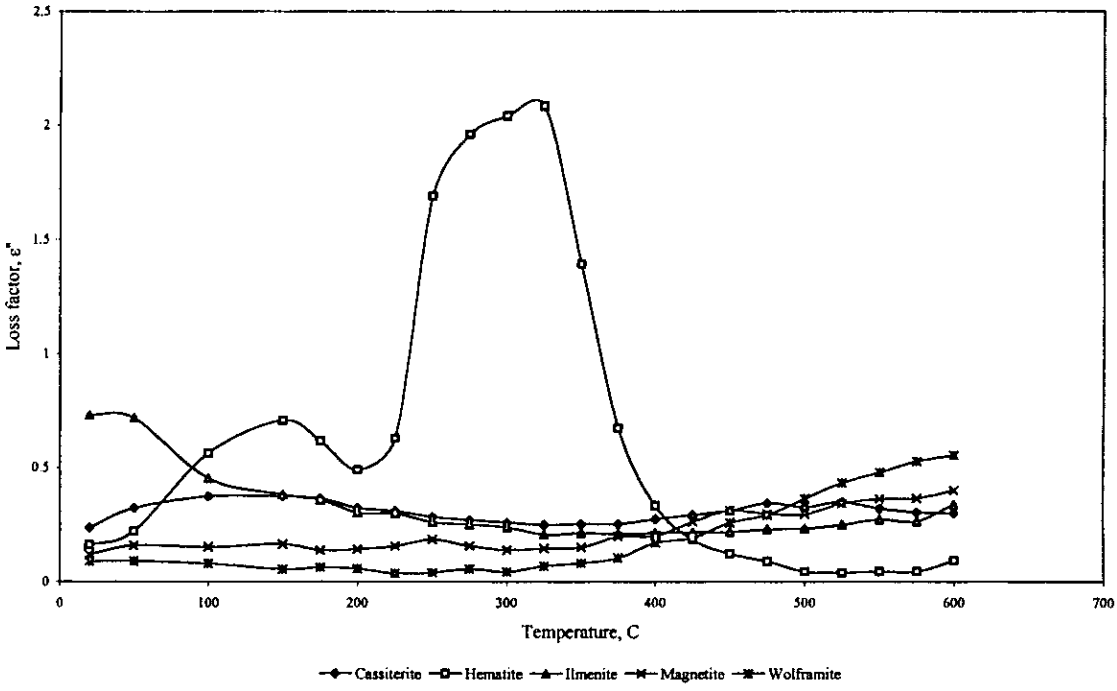

Figure 4.17. Effect of temperature on the dielectric loss factor of oxides.

4.5.3. Discussions

The present results are quite surprising since one would expect magnetite to have high values of dielectric constant and loss factor compared to ilmenite and hematite. Magnetite is well known to have high heating rates (Walkiewicz et al, 1988 and McGill et all, 1988). However, in the present investigation this has not been suggested and it has been found that magnetite has similar loss factor values to other oxides. A possible explanation for the high heating rates observed in the previous experiments is the fact that magnetite, being a ferromagnetic mineral, in the presence of an electromagnetic field the contribution for its lossiness is due to both the electric and magnetic fields. However, the assumptions made for the development of the resonant cylindrical cavity is that the sample is placed on the region of maximum electric field while the magnetic field is nil. This may result on the contribution due to magnetism being neglected.

Work undertaken by Harrison (1996) on the measurement of dielectric properties has recommended that measurement of dielectric properties of minerals should take into account many factors including the magnetic field portion of the electromagnetic wave. However, magnetic materials produce a magnetic resonance, which distorts the field uniformity and therefore the accuracy of measurements. Such effect must be investigated further to improve accuracy.

4.5.3.1. Effect of Frequency

The effect of frequency on the dielectric proprieties of oxides has been investigated. The results are illustrated in Figure 4.18, based on the ilmenite data. The general trends is similar to that observed for sulphide minerals. The dielectric constant and loss factor have been found to be constant over the frequency range. However, the penetration depth decreases with an increase of frequency as would be expected, as D_p is proportional to f^{-1}.

4.5.3.2. Modeling Bulk Density Effect

The effect of density on dielectric properties of oxides has also been investigated. Based on the experimental measurement on three packing densities, the procedure developed by Nelson (1988) was used. A linear relationship between density and dielectric constant was determined and results are illustrated in Figure 4.19 and summarized on Table 4.7. The square root model has been observed on all oxides minerals. An attempt to model the dielectric loss factor with bulk density was made but no linear relationships were found.

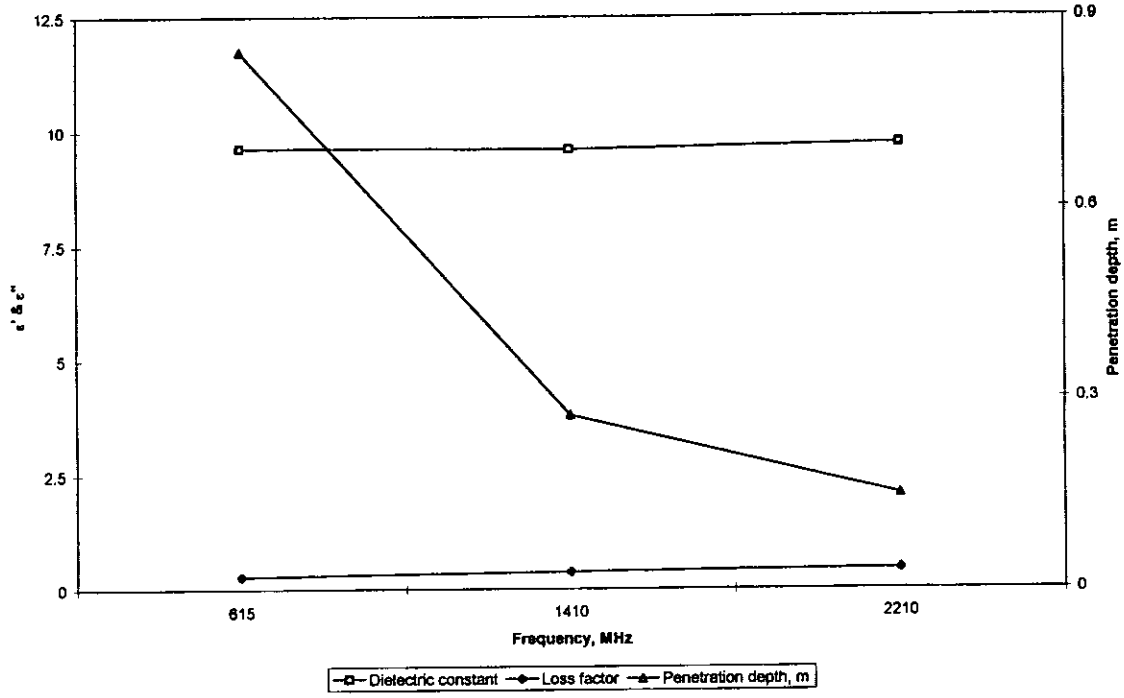

Figure 4.18 Effect of frequency on the dielectric properties of Ilmenite measured at room temperature.

From the developed linear relationship between dielectric constant and bulk density, dielectric constant can be extrapolated. Extrapolated results are shown in Table 4.8, and they have been compared with data from the literature.

Table 4.7. Coefficients of empirical equations relating the dielectric constant ($\sqrt{\varepsilon'}$) and bulk density (ρ) of oxides.

Regression model	Mineral	Measurement frequency, MHz					
		615		1410		2210	
Coefficient		A_0	A_1	A_0	A_1	A_0	A_1
$\sqrt{\varepsilon_r'} = A_0 + A_1\rho$	Cassiterite	1.006	0.3625	1.006	0.361	1.007	0.366
	Hematite	0.9982	0.5255	0.9967	0.4886	0.9965	0.4765
	Ilmenite	1.020	0.6901	1.017	0.6809	1.012	0.6824
	Magnetite	0.998	0.4825	0.9995	0.4881	1.001	0.5005
	Wolframite	1.029	0.3783	1.031	0.3786	1.037	0.3798

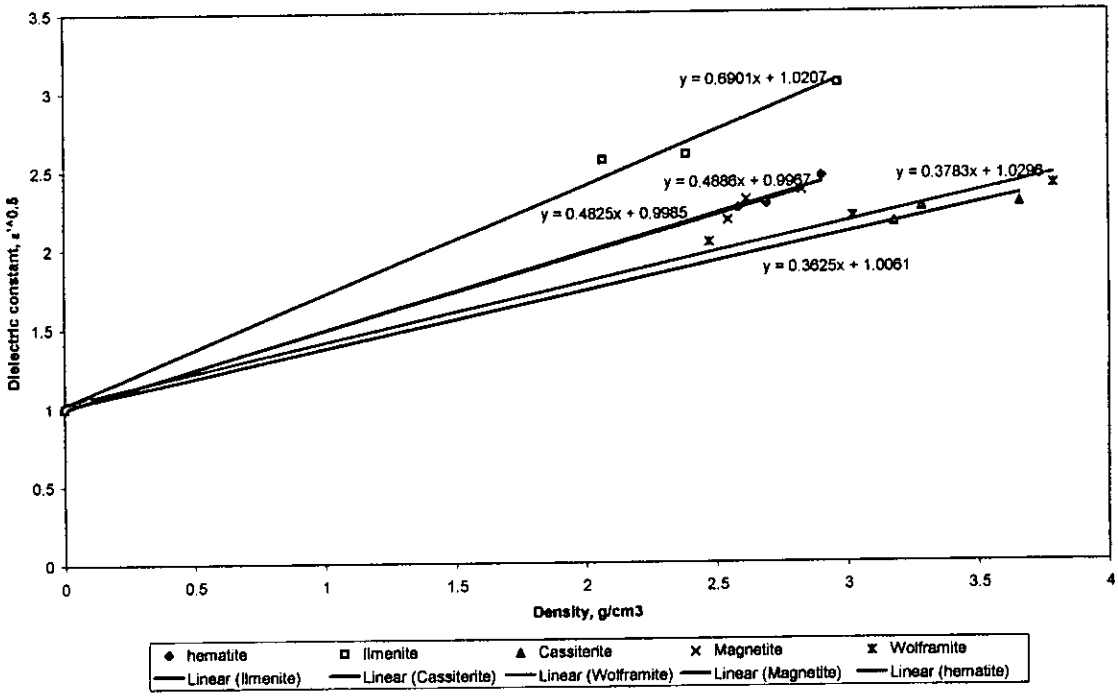

Figure 4.19. Effect of bulk density on dielectric properties of oxides. Data obtained at room temperature and frequency of 615 MHz.

The experimental data were obtained on the present research and multiplied by the permittivity of free space (8.85×10^{-12} F/m). Data from the Handbook of Physical properties of rocks are absolute values and data from Church et al., have been converted.

Table 4.8. Dielectric properties of oxides at room temperature

Mineral	Density, g/cm^3	ε′ (Experimental) 10^{-12} (F/m)	ε′ (Literature) 10^{-12} (F/m)
Cassiterite	6.993	110.6	207 – 212[c)]
Hematite	5.275	127	221[c)]
Ilmenite	4.788	165.5	-
Magnetite	5.2	115	-
Wolframite	7.50	131.2	141.6[d)]

c) Clark, 1966 and d) Church et al., 1988.

4.6. Dielectric Properties of Silicates

Measurement of dielectric properties of two silicate minerals, quartz and orthoclase has been carried out. The purity of samples was confirmed using the X-ray

diffraction technique and data are illustrated in the Appendices, Figures A1.1-A1.12. The sample preparation and experimental procedure were carried out the same way as described in Section 4.2.1.

4.6.1. Nature of Silicates

Quartz (SiO_2) is the most abundant mineral in the earth's crust. It is a common constituent in many igneous, sedimentary and metamorphic rocks, and also occurs as secondary material forming a cementing medium in sediments. Quartz is also a common constituent of hydrothermal veins (Deer et al, 1966) and is a relatively thermally stable mineral with a reverse inversion crystal structure from α to β occurring at temperatures around 573°C.

Orthoclase ($4KAlSi_3O_8$) is a member of the feldspar group of minerals, the major constituents of the igneous rocks. Feldspars are the most important constituents of the simple pegmatites, are common in mineral veins and occur also in many thermally as well as regionally metamorphosed rocks (Deer et al, 1966). The majority of feldspars may be classified chemically as members of the ternary system $NaAlSi_3O_8$-$KAlSi_3O_8$-$CaAl_2Si_2O_8$. These compositions are referred to respectively as sodium, potassium and calcium feldspar. The potassium end-member can exist in a number of different structural states. Those with structures corresponding to the highest temperatures of crystallization are monoclinic and are called sanidines, while a lower temperature monoclinic potassium feldspar is called orthoclase.

4.6.2. Results

Quartz and orthoclase, the most abundant silicate minerals (Deer et al., 1962), were selected for the measurement of dielectric properties. These minerals have been found to be transparent to microwave radiation (Chen et al., 1984, McGill et al.,

1988) with very low values of dielectric constant and loss factor, as illustrated in Figures 4.20 and 4.21.

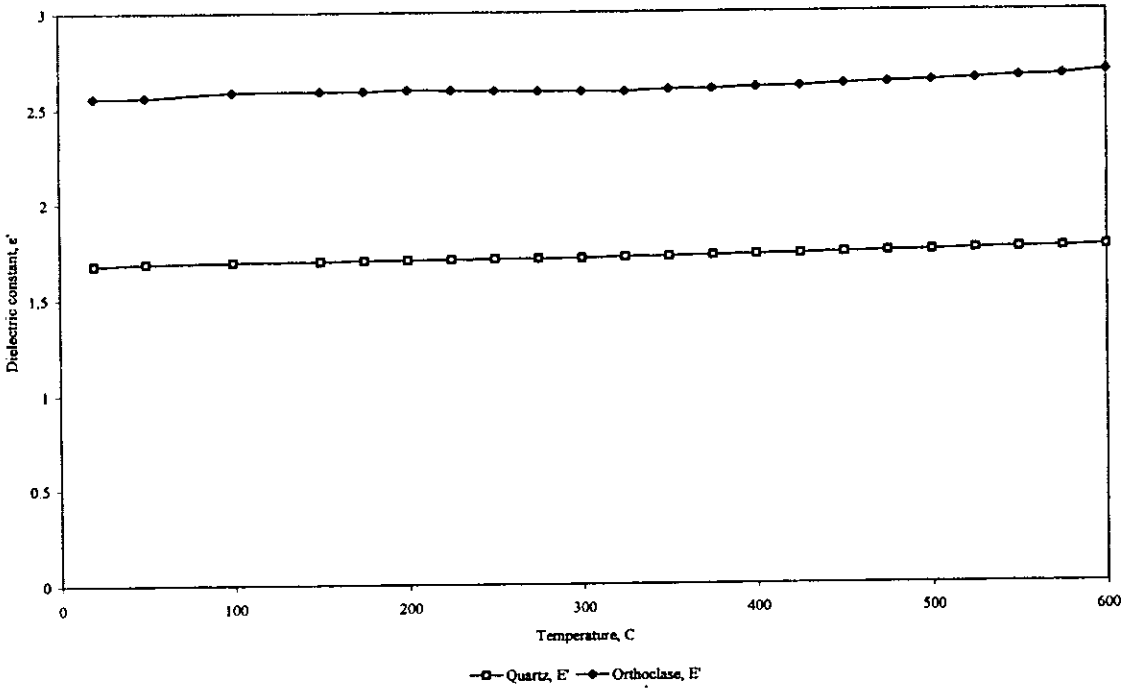

Figure 4.20. Effect of temperature on the dielectric constant of silicates measured at the frequency of 2.21GHz.

4.6.3. Discussion

4.6.3.1. Effect of Temperature

The effect of temperature on the dielectric properties of silicates has also been investigated. Figures 4.20 and 4.21 show the results of measurements of dielectric properties of quartz and orthoclase. Silicates have been found to be stable over the temperature range of measurement and the values of dielectric constant and loss factor are therefore constant. The results show that silicates are relatively transparent to microwave radiation with low dielectric constant and loss factor. The results of thermo-gravimetric analysis as shown in Figure 4.22 suggest that those minerals are thermally stable. Quartz is known to have an inversion temperature around 573°C (Deer et al., 1962) but has not been observed to undergo changes in the dielectric properties around this temperature.

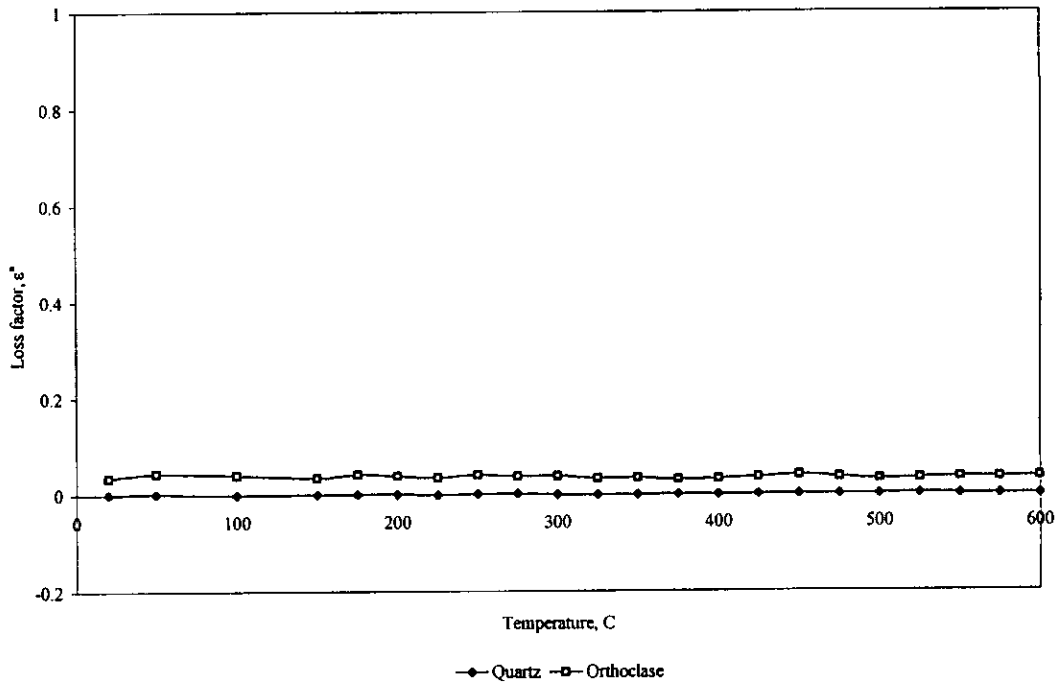

Figure 4.21. Effect of temperature on the loss factor of silicates measured at the frequency of 2.21GHz.

4.6.3.2. Effect of Frequency

The effect of frequency on the dielectric properties of silicates has also been investigated. The results are shown in Figure 4.23. It has been found that within the frequency range 615 MHz and 2.21 GHz the dielectric constant and loss factor are constant. However, the penetration depth decreases with an increase of frequency, which is in accordance with previous results for sulphide and oxide minerals. The low values of loss factor results in high values of penetration depth ranging from 200cm at the frequency of 615MHz to 50 cm at the frequency of 2.21 GHz.

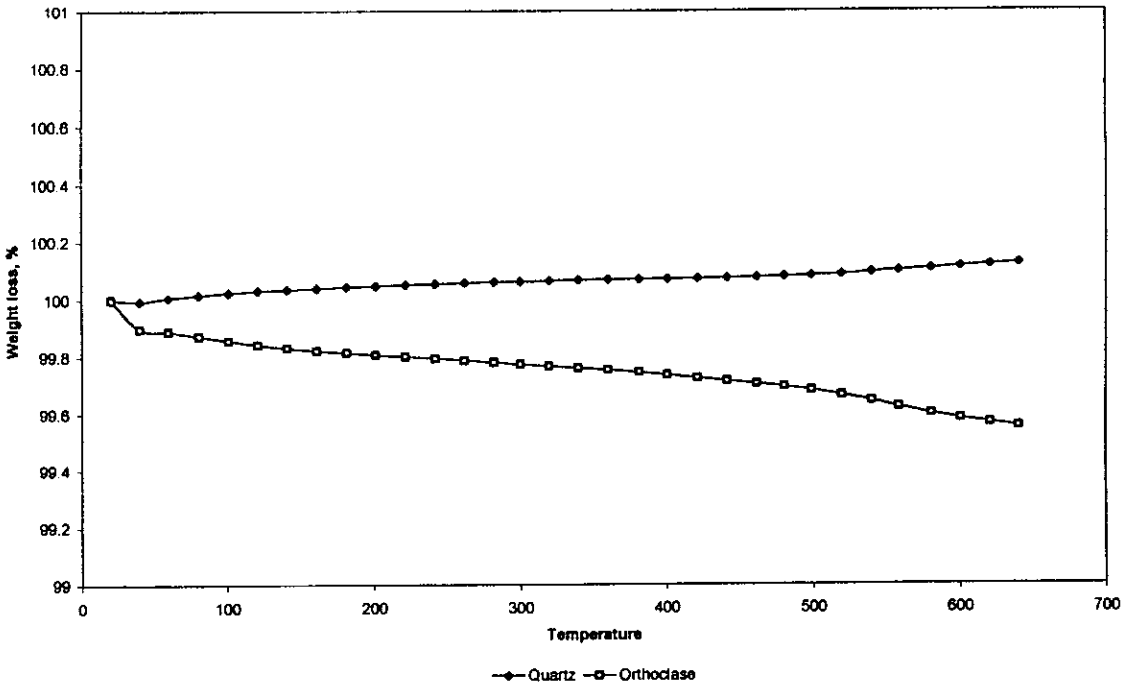

Figure 4.22. Thermo-gravimetric analysis of quartz and orthoclase.

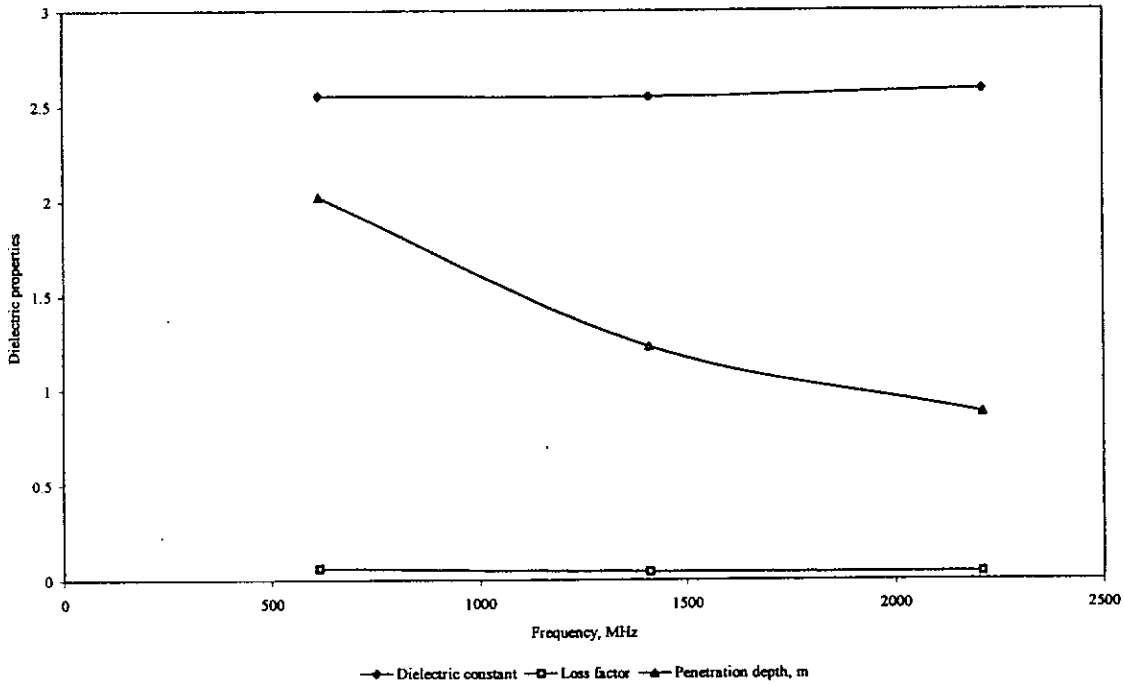

Figure 4.23. The effect of frequency on the dielectric properties of Orthoclase measured at room temperature (25 °C).

4.6.3.3. Modelling Bulk Density Effect

The effect of bulk density on the dielectric properties of silicates has also been investigated. The results are shown on Figure 4.24 and summarized in Table 4.9, for

measurements on orthoclase and quartz at room temperature and frequency of 615 MHz.

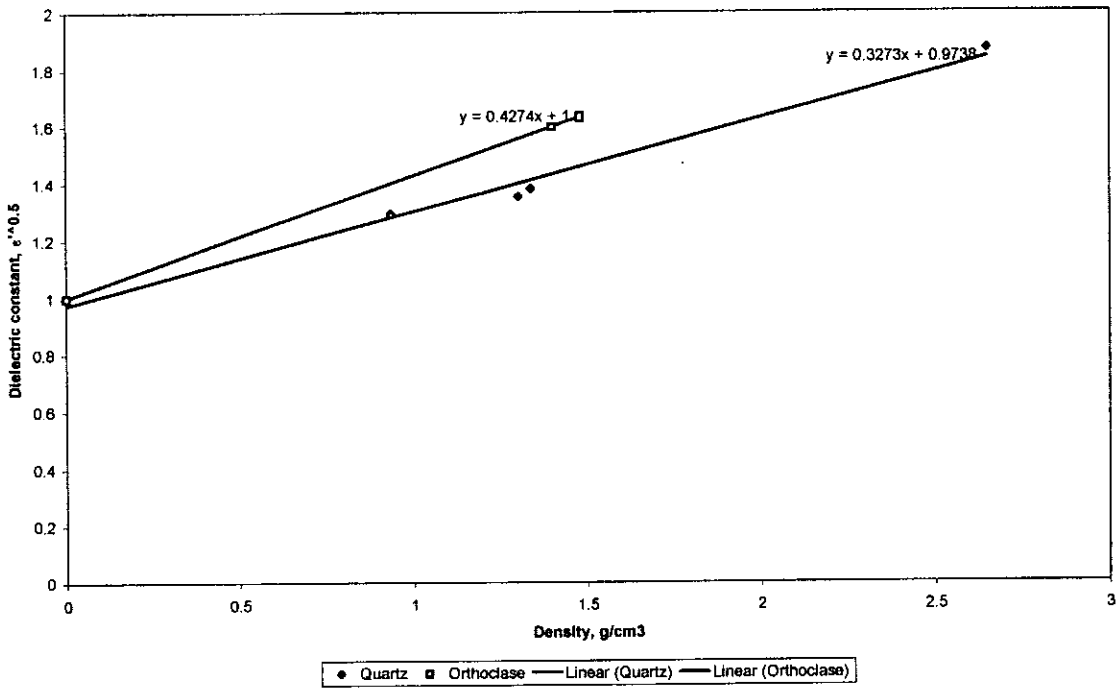

Figure 4.24. The effect of bulk density on the dielectric properties of orthoclase and quartz measured at room temperature (25 °C).

The square root linear relationship model between bulk density and dielectric constant has been observed. Based on measurement made on three different packing densities the dielectric constant of full dense orthoclase was predicted to be 4.4, while for quartz was 3.54. These have been converted to absolute values and compared to data in literature. The results are shown in Table 4.10.

Table 4.9. Coefficients of empirical equations relating the dielectric constant ($\sqrt{\varepsilon'}$) and bulk density (ρ) of silicates.

Regression model	**Mineral**	**Measurement frequency, MHz**					
		615		**1410**		**2210**	
Coefficient		A_0	A_1	A_0	A_1	A_0	A_1
$\sqrt{\varepsilon_r'} = A_0 + A_1\rho$	Orthoclase	1.006	0.427	1.006	0.427	1.007	0.430
	Quartz	0.9782	0.330	0.965	0.331	0.9965	0.327

Table 4.10. Dielectric properties of silicates at room temperature

Mineral	Density, g/cm^3	ε′ (Experimental) 10^{-12} (F/m)	ε′ (Literature) 10^{-12} (F/m)
Orthoclase	2.57[c)]	38.9	39.8 - 51.3[c)]
Quartz	2.648[c)]	31.3	36.4 - 37.8[c)]

c) Clark, 1966.

4.7. Conclusions

A knowledge of dielectric properties, particularly loss factor, is important for an accurate prediction of power loss density, which is known to be dependent on the internal electric field strength, frequency of the microwave radiation and the dielectric loss factor of the materials. With the knowledge of the power loss density, it is possible to model the selective microwave heating of minerals and, thus, the thermal stresses that can be induced in real ores.

Bulk density effects on dielectric properties have been observed and the relationships developed by Nelson (1988) have been found to be valid for quartz with the square root model more accurate than the cube root model. The linearity of square roots and cube roots of dielectric constant of quartz with bulk density are consistent with published dielectric mixture formulae that specify the additivity of the dielectric constants of the constituents of the mixture. The linearity of the k=2 and k=3 relationships for dielectric constant with bulk density provide a means of estimating the dielectric constant of the air and any given material at any bulk density, including solid material, by utilizing a measurement of dielectric constant for the material at any known density and the $\rho = 0$, $\varepsilon'=1$ intercept.

The dielectric properties of a number of sulphide minerals have been measured, including chalcocite, chalcopyrite, pyrite, sphalerite and galena. Galena and sphalerite have been found to be thermally stable at temperatures up to 500°C and their dielectric properties exhibit little variation with temperature within this range.

The dielectric properties of pyrite, chalcocite and chalcopyrite, however show a significant variation with temperature. The changes observed are probably compositional and related to phase transformations during heating.

In addition, the dielectric properties of some oxides have also been measured, including ilmenite, hematite, magnetite, cassiterite and wolframite. It was expected that magnetite a well-known mineral with known microwave heating potential (Walkiewicz et al, 1988 and McGill et al, 1988) would exhibit a high loss factor. However the results obtained in the present research, using the resonant cylindrical cavity, suggest that the mineral is within the class of poor heaters. A possible explanation for such poor result is the suitability of resonant cylindrical cavity based on perturbation technique for measurement of high loss material. Furthermore, the cylindrical cavity resonating in TM_{0n0} modes means that the magnetic field at the region of measurement within the cavity is nil and therefore the magnetic field component of the electromagnetic wave does not contribute to its lossiness.

The measurement of dielectric properties of silicates also has been carried out and included quartz and orthoclase. Silicate minerals constitute the rock forming minerals in most ore deposits have been found to be transparent to microwave radiation with loss factor usually below 0.02. Despite the resonant cylindrical cavity based on perturbation technique for measurement of dielectric properties not being particularly suitable for high loss materials ($\varepsilon''>5$), the present work had shown clearly the differences in the dielectric properties for the variety of mineral classes.

CHAPTER FIVE

Investigation on Microwave Assisted Comminution and Liberation of Palabora Ore

5.1. Introduction

Located 360km north east of Pretoria, close to the Kruger National Park, the Palabora Mining Company is South Africa's leading copper producer. The main shareholders in the company are Rio Tinto plc, which increased its stake to 49.2% in July 2001, and Anglo-American.

Open-pit copper mining commenced at Palabora in 1964. Current integrated copper metal refining capacity is 135,000t/y and the mine is also a major source of vermiculite and baddeleyite (zirconium oxide). However, open-pit mining ceased in May 2002 and has been replaced by an underground operation with a further 20-year life. Development investment in the underground mine is some $410 million. The operation employs around 2,400 people (Rio Tinto Annual Report, 2002).

5.1.1. Geology And Reserves

The complex was formed some two thousand-million years ago as a result of massive volcanic upheavals forcing magma up to the surface. What was left behind has been described as a 'treasure house' of minerals (Aird, 1998) and today is known as the Palabora igneous complex. It is unique in that no other deposit in the world has copper occuring in economic quantities with carbonatites. The complex also contains phosphates, vermiculite, phlogophite, magnetite, titanium, uranium, zirconium, nickel, gold, silver, platinum and palladium.

The Palabora igneous complex consists of a group of 14 distinct rock types, each with their own characteristic mineral assemblages. Of these, carbonatite and foskerite are the two copper-bearing host rocks. These rocks also contain magnetite and apatite. The Palabora igneous complex occurs as a rough figure of eight, which is about 8km long from north to south, and 3.2km wide on its east-west axis. Figure 5.1 shows a cross section of the original Palabora igneous complex (Aird, 1998).

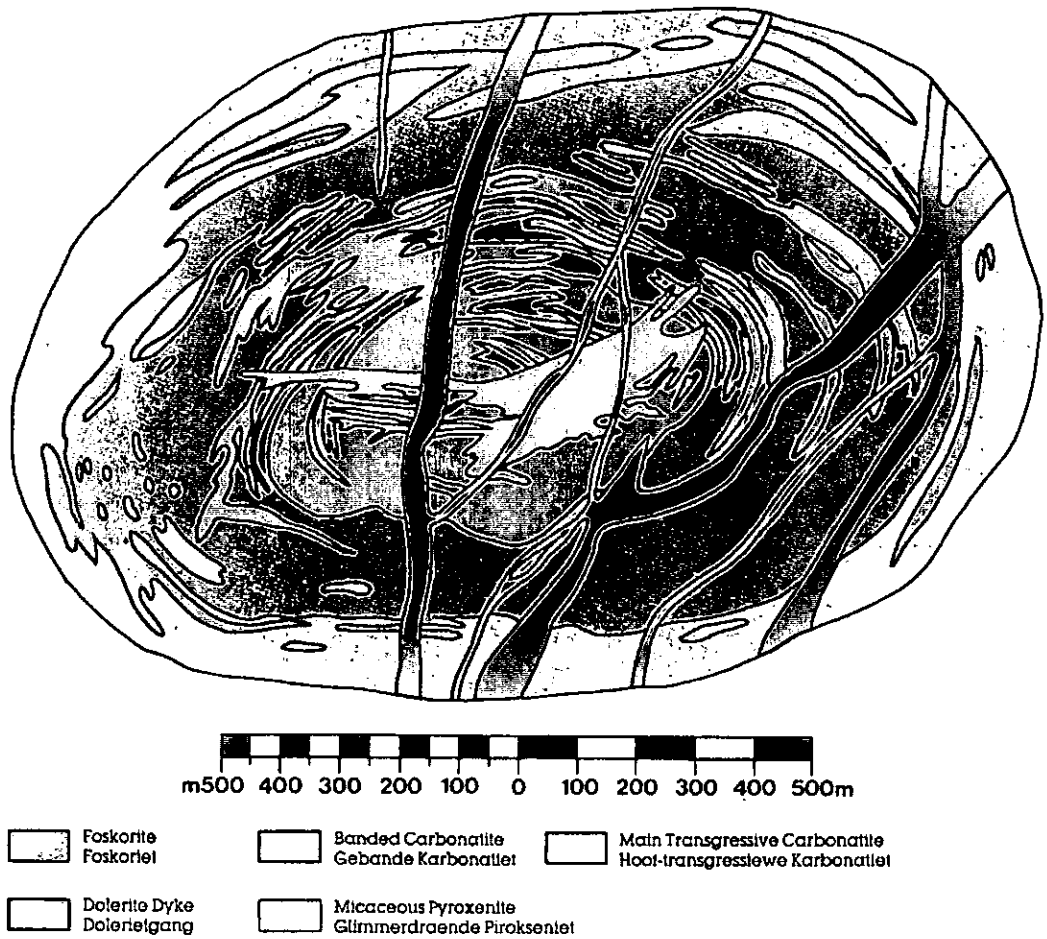

Figure 5.1 Geology of the Palabora igneous complex (Aird, 1998)

The deposit is hosted in an alkaline igneous complex comprising mainly of pyroxenite with occurrences of pegmatites, foskorite and carbonatite. Three separate mineralised zones have been identified within the 20km² surface outcrop of the

complex, of which the most northerly is phosphate-rich while the central (Loolekop) zone forms the basis for Palabora's copper production. The copper orebody is hosted in a carbonatite pipe within which grades are typically concentric and with the highest values (1.0% copper) occurring at the core. The higher-grade mineralisation extends well beneath the centre of the projected final open-pit floor. At the end of 2001, proven reserves were 3.3Mt with and average 0.85% copper in the open pit and 225Mt at 0.7% copper in the underground section of the orebody. Probable underground reserves were 16Mt grading 0.49% copper (Rio Tinto Annual Report, 2002).

5.1.2. Ore Treatment

The flowsheet for processing Palabora copper ore is shown over the page in Figure 5.2. It consists of standard mineral processing unit operations, which are basically crushing, grinding (both conventional and autogenous), flotation and magnetic separation. A detailed description of the flowsheet is available in the literature (Aird, 1998). As well as copper, magnetite, uranium oxide, zirconium oxide, gold, silver and platinum group metals are recovered. Phosphate tails are also processed and a concentrate produced. Table 5.1 illustrates the production statistics for the last three years (Rio Tinto Annual Report, May 2003). Throughput has decreased in the last year due to switch from open pit operation to underground developments.

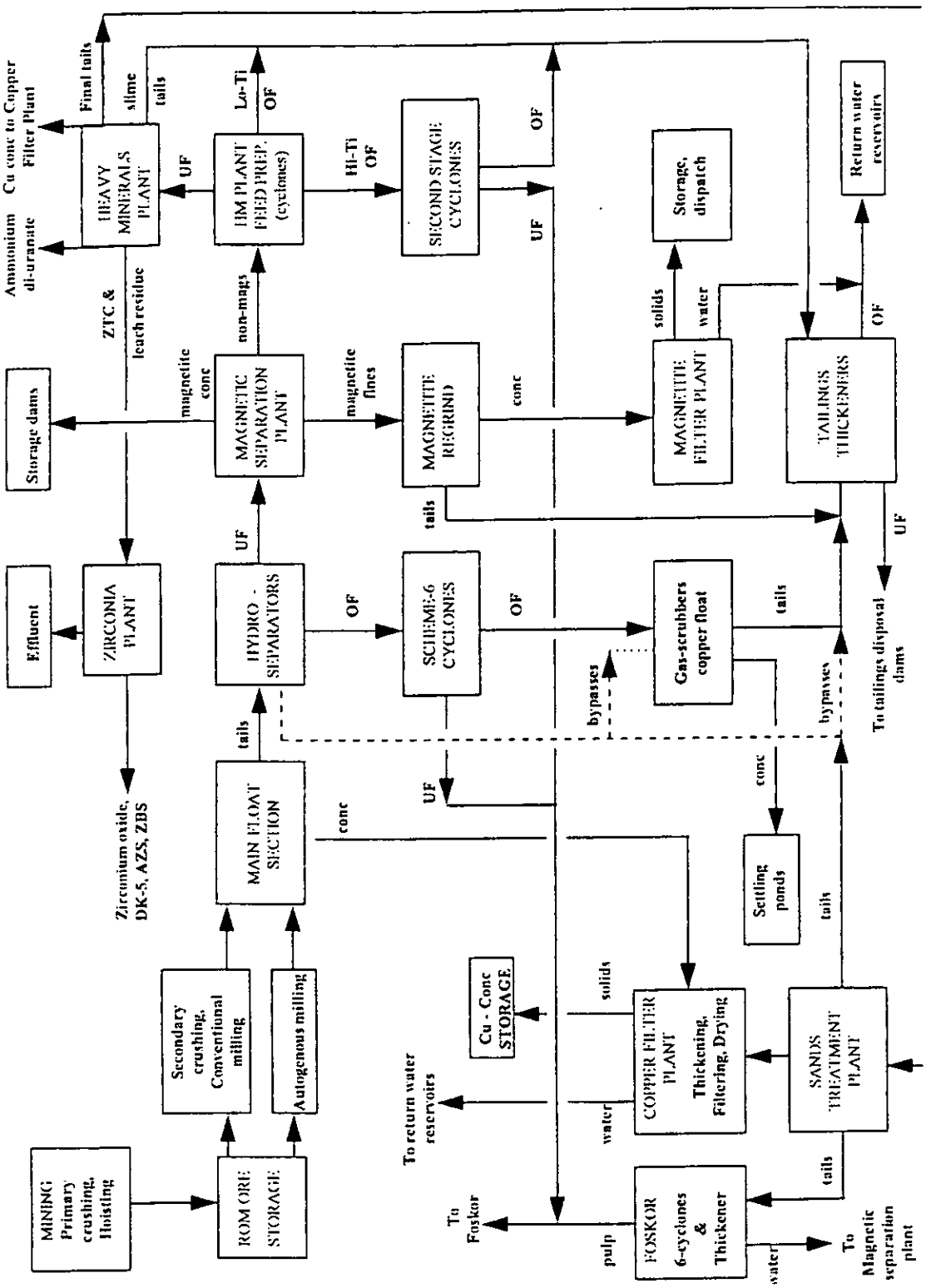

Figure 5.2 Flowsheet for the processing of Palabora copper ore (Aird, 1998).

Table 5.1 Production statistics (Rio Tinto annual report, May 2003)

	1999	2000	2001	2002
Ore milled (Mt)	28.3	25.7	14.5	9.9
Copper head grade (%)	0.47	0.59	0.66	0.63
Copper concentrates produced (kt)	333.4	358.7	233.5	167.9
Contained copper (kt)	111.9	117.0	78.4	52.2
Refined copper produced (kt)	100.1	87.7	86.9	81.6
Uranium concentrates (t)	91.0	95.0	31.0	-
Vermiculite (kt)	208.6	208.4	160.3	223.5
Zirconia products (kt)	11.1	7.9	4.0	-
Magnetite (kt)	190.0	239.0	201.0	172

5.1.3. Palabora Comminution: Current Practice

Palabora has a unique orebody in that it contains most of the valuable minerals known but, unfortunately, some gangue minerals have a major influence on milling rate. The gangue minerals that have the most significant impact are dolerite and magnetite. Dolerite is defined as a medium-grained basic rock with the chemical composition of gabbro, a dark plutonic igneous rock consisting of plagioclase, feldspar, pyroxene and, often, olivine. This type of mineral is illustrated in Figure 5.14. Dolerite has no economic importance, as it is not associated with copper or other valuable minerals. It does, however, have a significant influence on the grinding performance of the mills because of its resistance to comminution. It has a work index of 30kWh/t compared with 12 kWh/t for the average ore.

In the mining operation great, care is taken to segregate the dolerite from the ore but some contamination is inevitable. Records show that, during the past few years, between 120,000 and 320,000 tonnes per year have been ground. In addition, approximately 50,000 tonnes of ore have had to be discarded because of dolerite contamination. The copper content of this ore averaged 0.43% (Sentence, 1998). The

Palabora Mining Company employs two parallel grinding circuits, which handle ore from different areas of the pit. The first grinding circuit is conventional in nature and consists of rod and closed circuit ball mills. This is shown in Figure 5.3.

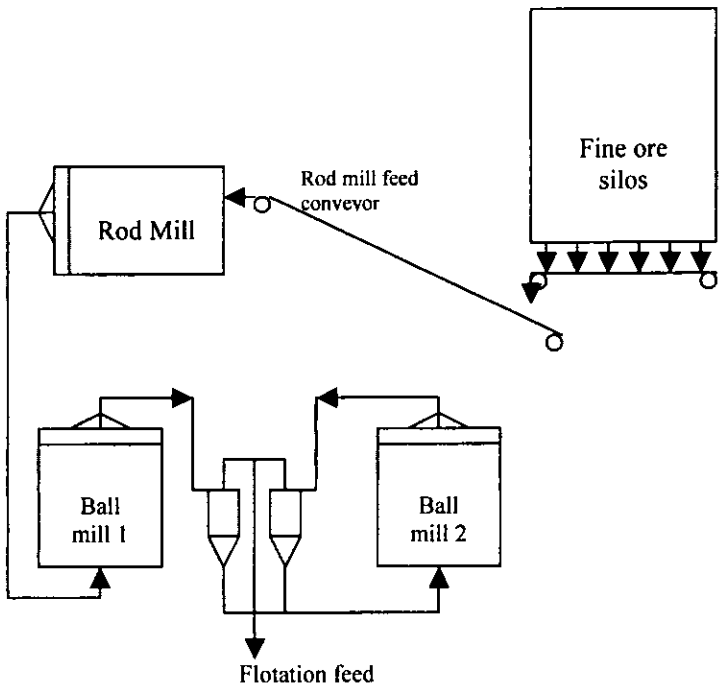

Figure 5.3 Conventional grinding circuit of Palabora Mining Operations (Aird, 1998)

The second grinding circuit (Figure 5.4) is fully autogenous and it is here that dolerite causes particular problems although it is still an issue in conventional milling. Dolerite with its high work index does not grind at the same rate as the rest of the ore, with the result that it builds up a high circulating load within the circuit. The mill eventually becomes filled with coarse dolerite, which upsets the ratio of course grinding media to fines. This will have the effect of dramatically reducing the feed rate through the mill.

Previous work on the effect of microwave treatment on the Palabora ore comminution circuit has been done (Vorster et al. 2000 and Kingman 1998). They investigated the effect of exposure time upon ore mineralogy, grindability and

recovery and showed that the mineralogy of ore plays a significant role in the response of the material. It was found that the work index may be reduced by up to 70% after 90 s of microwave treatment in a 2.6 kW multimode microwave cavity. However, shorter exposure times of up to 10 s can give rise to a reduction in work index of up to 34%.

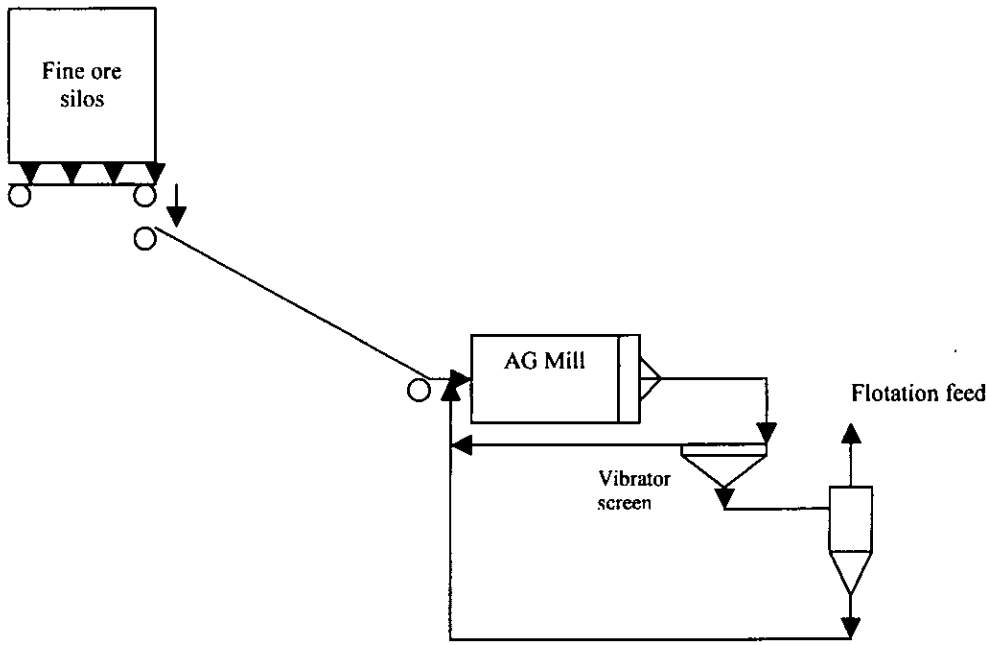

Figure 5.4. Second conventional grinding circuit of Palabora Mining Operation (Aird, 1998).

5.2. Mineralogy of Palabora Ore

A bulk, representative sample was received for analysis and testing. Two kinds of sample were received: 1) autogeneous mill feed consisting of lumps greater than 500mm in size and 2) about 500kg of run of mine feed to the rod mills, consisting of particle size below 19mm.

5.2.1. Sample preparation

Specimens were selected from the larger sample and drilled to give cored test pieces of approximately 37mm diameter and 200mm length, as shown in Figure 5.5. The grain size of test pieces varied widely, with four types visibly identified:

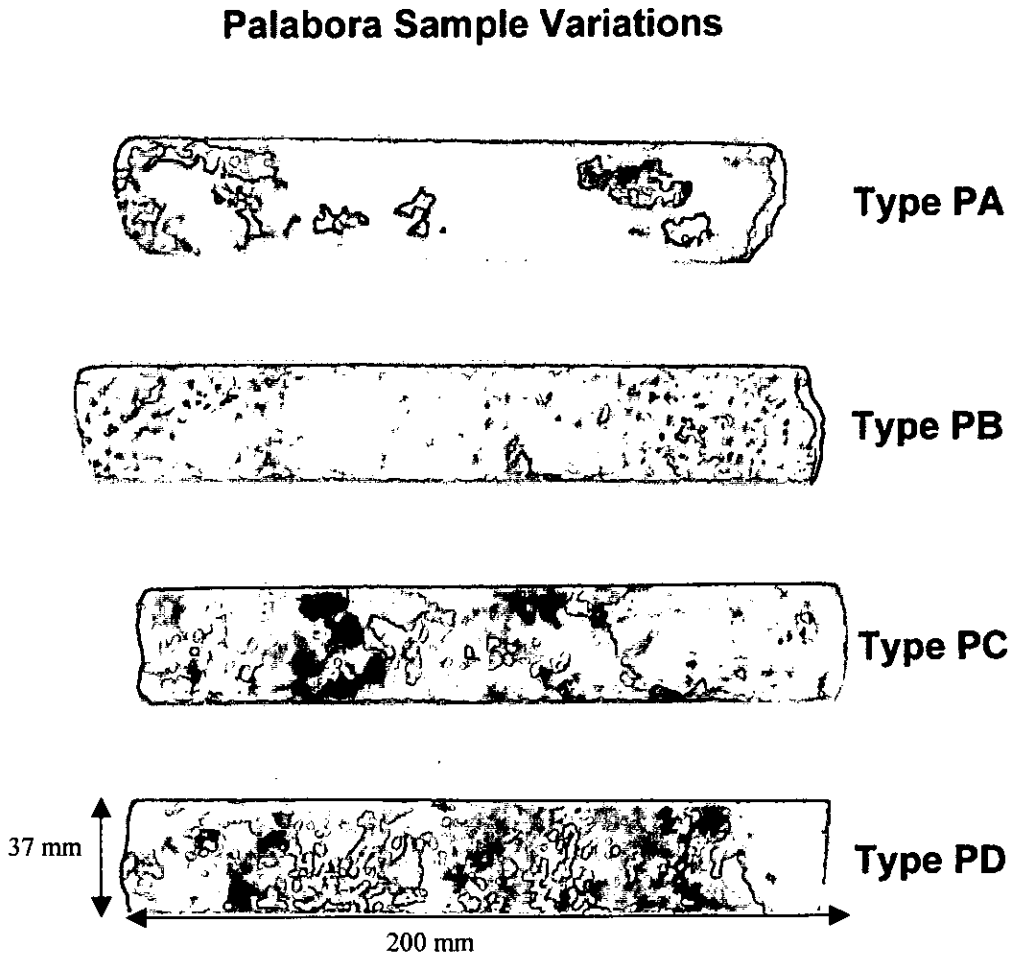

Figure 5.5 Core drill samples of Palabora ore (Rio Tinto Technical Report, 2001).

- Palabora type PA mineralisation consisting of large grains of white calcite with coarse dark inclusions,
- Palabora type PB mineralisation consisting of white matrix with fine grained inclusions,

- Palabora type PC mineralisation with large grains of dark brown with white inclusions and
- Palabora type PD mineralisation consisting of homogeneous grain size distribution.

Mineralogical characterization of the drill core samples was conducted and it focused on the contained phases, degree of dissemination and grain size. Each of the drill cores was sectioned using a diamond saw with numerous polished sections being prepared from each (Rio Tinto Technical Report, 2001).

5.2.2. Methods of investigation

Each polished section was systematically examined using conventional reflected light microscopy techniques. The individual opaque phases were identified on the basis of their optical properties. A number of reflected light photomicrographs were also captured using a Buehler Omnimet 'Enterprise' image analysis system and Rio Tinto Technical Services aided to the evaluation.

A selected number of the polished sections were also systematically examined using qualitative scanning electron microscopy techniques. This provided additional information on the compositions of individual phases and served to confirm their identities. A number of false colour, computer enhanced backscattered electron images were also prepared to illustrate important mineralogical features of the ore.

5.2.3. Mineralogical Results

Mineralogical examination of the samples of drill core confirmed that they consist predominantly of magnetite, vermiculite, apatite, zirconium, titanium and copper sulphide. This is shown in the Figures 5.6-5.18.

5.2.3.1. Transparent Gangue

The head sample was found to be dominated by the presence of a significant amount of transparent gangue. Qualitative SEM analysis of the transparent gangue minerals revealed that they consisted of various combinations of calcite ($CaCO_3$), dolomite ($CaMg(CO_3)_2$), apatite ($Ca_5(PO_4)_3(F,Cl, OH)$, olivine ($Mg_3Si_2O_5(OH)_4$, phlogopite ($KMg_3AlSiO_{10}(F, OH)_2$), serpentine ($Mg3Si_2O_5(OH)_4$), pyroxene and plagioclase feldspar. Minor amounts of brucite were also found.

Figure 5.6. False colour backscattered computer enhanced images of a head sample of Palabora open pit ore.

Figure 5.7. Head sample, false coloured backscatter image showing apatite and dolomite grains. Also shows chalcopyrite lamellae in bornite grains and fine grains of chalcocite.

Figure 5.8 Head sample, false coloured backscatter image

A false coloured computer enhanced image illustrating the nature of ultra-fine inclusions of spinel in magnetite. Ilmenite lamellae are also present in the magnetite. Baddelyite, apatite, dolomite and minor vallerite grains are also present.

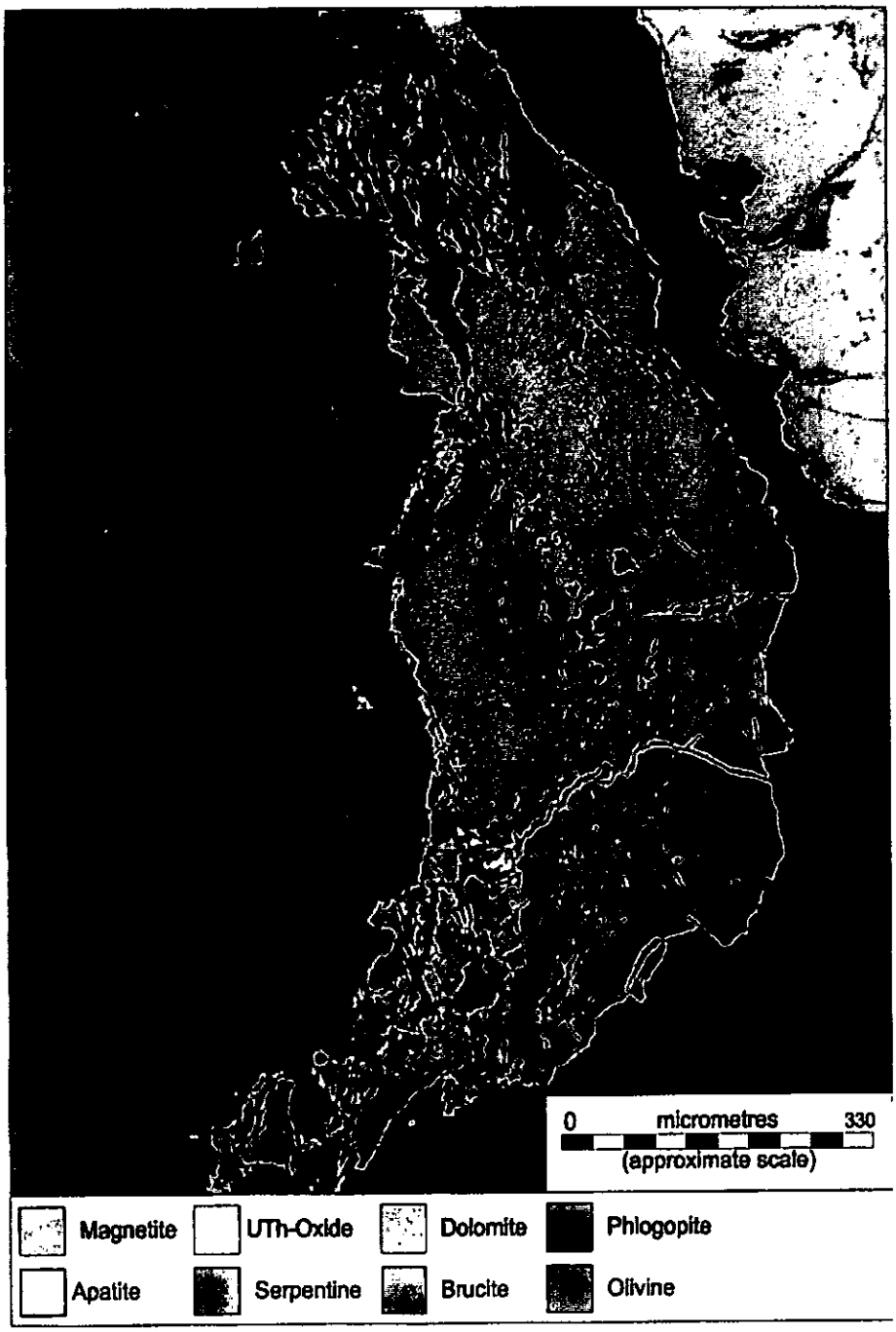

Figure 5.9 Head sample, false coloured backscatter image

A false coloured computer enhanced image illustrating complex associations between apatite, magnetite and dolomite. The apatite is extensively fractured. The magnetite is extensively intergrown with phlogophite and an olivine grain that has under gone replacement by serpentine. Minor amounts of uranite are also present.

Figure 5.10 Head sample, false coloured backscatter image.

A false colour computer enhanced image illustrating typical relationships between apatite, magnetite, phlogopite and ilmenite. Olivine has been replaced by serpentine.

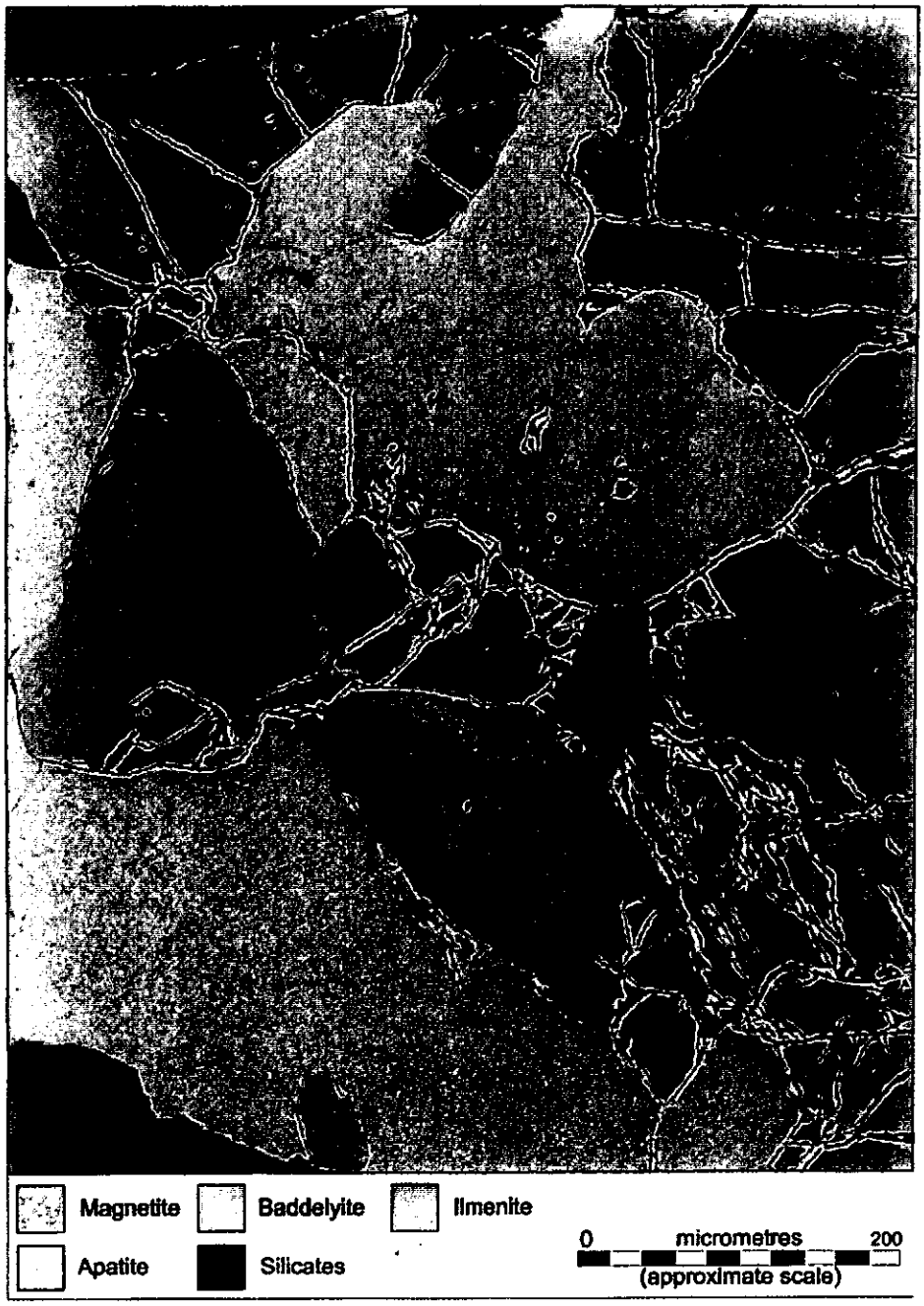

Figure 5.11 Head sample, false coloured backscatter image

A false coloured computer enhanced image illustrating the associations between magnetite, apatite, baddelyite, ilmenite and undifferentiated silicates.

Figure 5.12 Head sample, false coloured backscatter image.

A false coloured computer enhanced image illustrating the ocuurrance of a magnetite grain and also late stage magnetite that is present along margins and grain boundaries of a bornite and chalcocite aggregate. Magnetite and olivine are also present.

Figure 5.13 Head sample, false coloured backscatter image

A false colour computer enhanced image illustrating the occurrence of a fine grained vallerite aggregate that extensively replaced a bornite aggregate. Relict olivine has been extensively replaced by serpentine that is also present along fractures in the apatite.

Figure 5.14 Head sample, false coloured backscatter image

A false colour computer enhanced image illustrating the occurrence of euhedral crystals of baddelyite in serpentine. The serpentine has extensively replaced olivine. Vallerite is shown replacing a former bornite grain. It also found in fine veinlets within the serpentine.

Figure 5.15 Head sample, false coloured backscatter image

A false colour computer enhanced image illustrating the nature of a typical rock fragment. The microgabbro (dolerite) consists predominately of plagioclase feldspar and pyroxene. Skeletal crystals of Ti-magnetite together with minor amounts of ilmenite are also present within the gabbro.

Figure 5.16 Head sample, false coloured backscatter image.

A false colour computer enhanced image illustrating the nature of a chalcopyrite and bornite aggregate that was found along the margins of a magnetite grain. Late stage, granular magnetite is also present along grain boundaries and within fractures in the sulphide aggregate.

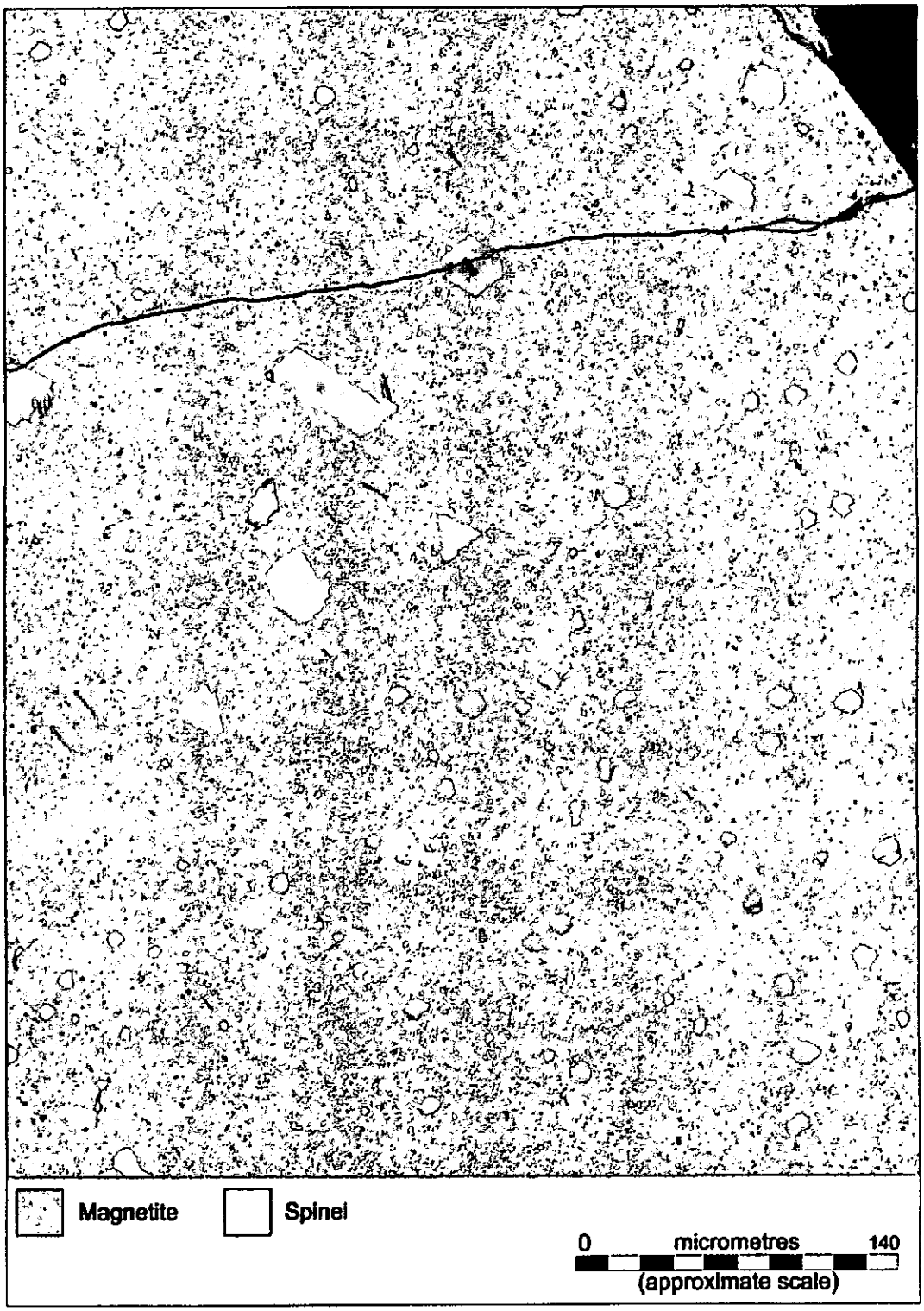

Figure 5.17 Head sample, false coloured backscatter image.

A false colour computer enhanced image illustrating the occurrence of finely disseminated, euhedral crystals of spinel that are present within a magnetite grain.

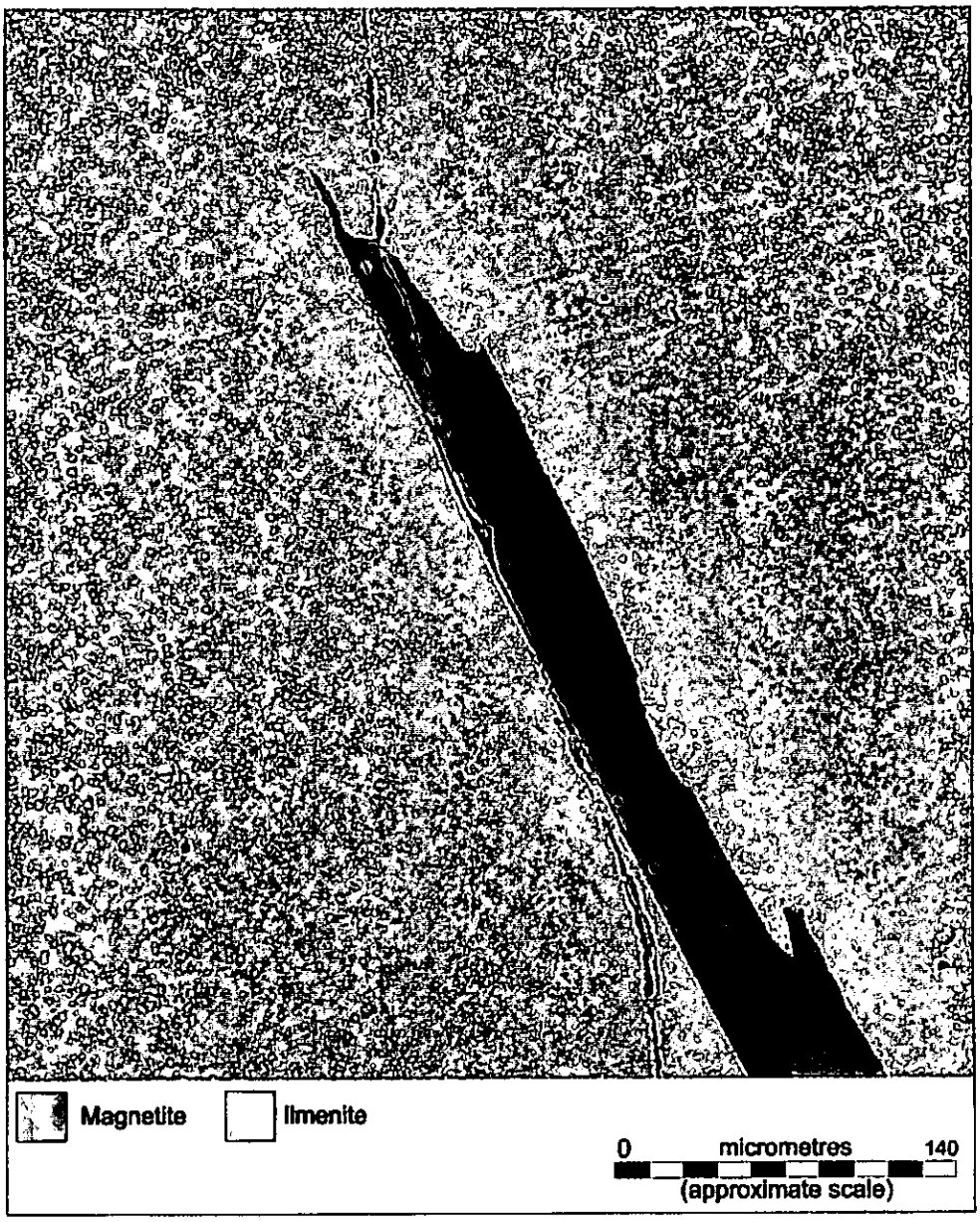

Figure 5.18 Head sample, false coloured backscatter image.

A false colour computer enhanced image illustrate the depletion of ultra-fine Ti-rich exsolution bodies around the margins of an ilmenite grain. The lath-like ilmenite grain is present within a former Ti-magnetite grain that has exsolved tiny ilmenite bodies during cooling. Carbonate minerals were found to be particularly abundant and consisted predominately of calcite and dolomite. Both minerals were found to occur as intergrowths with magnetite, sulphides and the transparent gangue. The bulk of the dolomite and calcite grains ranged in size from a lower limit of 300μm to

grains that exceeded 8mm in size as illustrated in Figures 5.6-5.8. This kind of mineralogy is potentially suitable for microwave treatment, since the magnetite with loss factor 0.3 and sulphide minerals with an average loss factor 0.5 will absorb most of the microwave energy than the transparent gangue with an average loss factor of 0.02 as determined in Chapter 4. Because the grains are relatively large, there will be less heat dissipation between mineral phases thus large thermal stresses induced.

Despite mineral grains having large size that exceed 8mm, penetration depth of microwave radiation will not be a restriction as shown in Figure 5.19. Penetration depth of calcite has been found to be an average 1300mm while pyrite, a typical sulphide mineral has penetration depth of about 200mm.

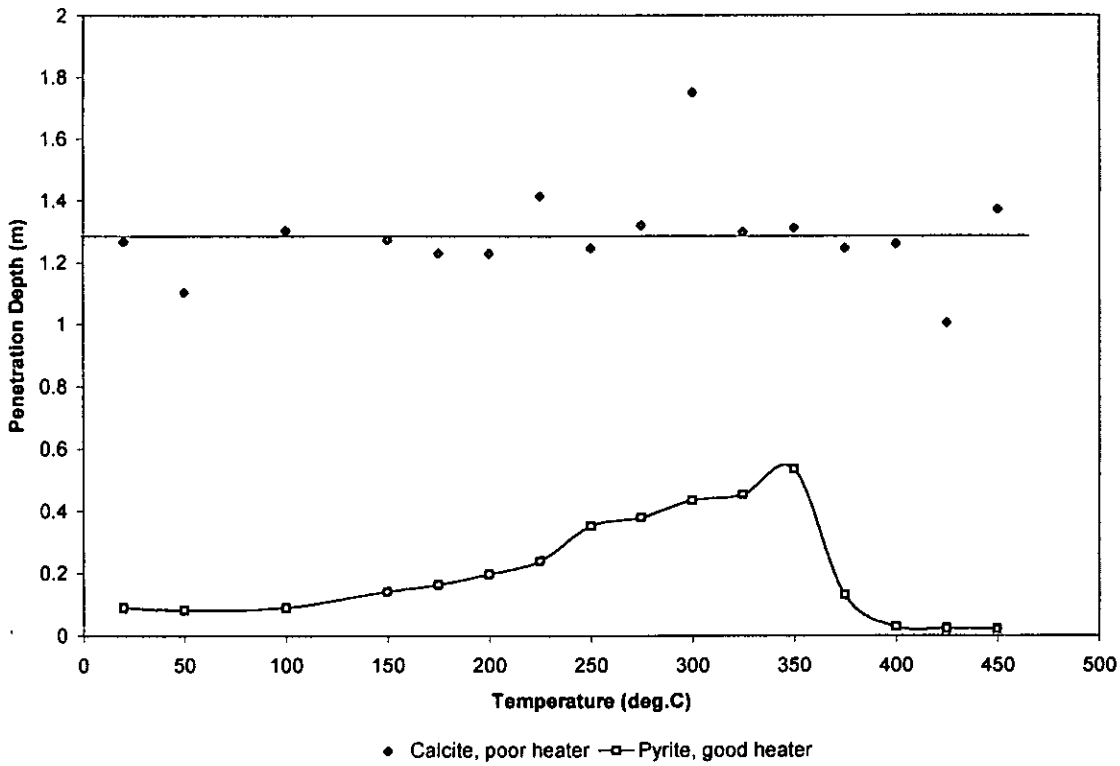

Figure 5.19. Plot of penetration depth of calcite and pyrite at the frequency of 2.21GHz.

Apatite was found to be particularly abundant and it was found to represent the major phosphorous bearing mineral. It was found largely to consist of rounded or sub-

rounded grains that were associated with transparent gangue, magnetite and various sulphide minerals. The grains ranged in size from an effective lower limit of 150μm to grains that exceeded 8mm in size, as illustrated in Figures 5.7-5.13. It was often found in a fractured state, with the fractures filled with magnetite or serpentine. This is illustrated in Figures 5.9-5.13. Qualitative SEM analysis of the apatite confirmed that it contained calcium, phosphorous and oxygen together with minor amounts of chloro.

Olivine was found to be present in moderate amounts in the head sample. The bulk of the olivine was found to be partially or extensively replaced by serpentine and this is shown in Figures 5.9-5.14. The serpentine typically formed fine-grained aggregates that partially filled fractures in apatite or magnetite. The olivine fine-grained aggregates ranged in size from an effective 80μm to grains that exceeded 5mm as shown in Figures 5.10 and 5.13. Phlogophite, magnesium-rich mica, was found to be a common accessory mineral within this ore. It was typically found in flakes associated with one or more of the transparent gangue minerals and, to a lesser extent, the sulphide minerals. The bulk of the phlogophite exhibited grain sizes of between 160 and 1200μm, as shown in Figures 5.9 and 5.10. Brucite was found to be present in only very minor amounts, intimately intergrown with dolomite and apatite grains. The bulk of brucite grains exhibit a restricted size of between 20 to 500μm. It is also dependent on the size of aggregate as shown in Figure 5.9.

5.2.3.2. Microgabbro Rock Fragments

Figure 5.15 shows a false colour, computer-enhanced image of a micro-gabbro rock fragment. The sample contained plagioclase feldspar, pyroxene and skeletal crystals of magnetite, which were always noted together in the form of aggregates. These

represent fragments of microgabbro, present as intrusions in the ore body that commonly exceed 2mm in size. The skeletal crystals of titanium-magnetite and crystal lamellae of ilmenite ranged in size from a lower limit of 70μm to more than 200μm, in the form of intrusions within the micro-gabbro (dolerite). This kind of mineralogy is suitable for microwave treatment, since the skeletal crystals of Ti-magnetite and ilmenite, with an average loss factor of 0.4, couple more readily to microwave radiation than plagioclase feldspar with loss factor equal 0.02. Because, ilmenite and Ti-magnetite will heat faster than plagioclase feldspar and pyroxene, thermal stresses may be induced and result in the development of micro fissures that will weaken the aggregate.

5.2.3.3. Magnetite

Magnetite was found to be abundant within the sample. It occurred as discrete liberated grains and to a lesser extent as intergrowths with transparent gangue. Optical microscopy analysis of the magnetite structure reveals that the granular aggregates consist of discrete magnetite grains that ranged in size from an effective lower limit of 50μm to grains that exceeded 5mm as shown in Figures 5.6, 5.9, 5.10, and 5.12. Copper sulphide mineral phases were found along the grain boundaries of the magnetite and are shown in figure 5.16. Qualitative SEM examination of the magnetite confirmed that it contained predominately iron and oxygen with magnesium and titanium being present in smaller amounts. A significant proportion of the magnetite was found to contain spinel ($MgAl_2O_4$) inclusions. The grain size of the spinel inclusions was restricted to 10 to 250μm and is shown in Figure 5.17. Ilmenite is also intimately associated with the magnetite, and was found to occur as granular intergrowths, laths, lamellae and inclusions. The ilmenite grain size is also

dependant on the size of the granular aggregate, which ranged in size from 10μm to 250μm, as shown in Figures 5.8 and 5.18. Microwave treatment will potentially have little effect on this kind of mineralogy, since the minerals all have similar dielectric properties (Magnetite, 0.3, ilmenite 0.4, and chalcopyrite 0.5). During microwave treatment little differential heating will be induced and the particles will simply heat and cool without any change in strength on grain boundaries.

5.2.3.4. Sulphide Minerals

The sample of head material was found to contain minor amounts of copper bearing sulphide minerals. These included cubanite ($CuFe_2S_3$), chalcopyrite ($CuFeS_2$), bornite (Cu_5FeS_4) and chalcocite (Cu_2S). Vallerite, an extremely rare copper mineral was also found to be present, particularly along fractures and grain boundaries. It was also found in association with one or more of the copper bearing sulphides and magnetite. Vallerite is an alteration product that has formed, at least in part, as a result of the breaking down of one of the copper bearing sulphides. It was commonly found in association with bornite and chalcopyrite.

The bulk of the chalcopyrite was found to be present as intergrowths with bornite and, to a lesser extent, with chalcocite and cubanite. Figures 5.7 and 5.16 show chalcopyrite forming lamellae within bornite and chalcocite grains. The discrete chalcopyrite lamellae were found to range in size from a few tens of micrometres, to tens of millimeters.

Chalcocite was found to be present in lesser, but still significant amounts, largely occurring as intergrowths with chalcopyrite, bornite and vallerite. The discrete chalcocite grains occurred as intergrowths ranging in size from 10μm to 200μm, as shown in detail in Figure 5.12. The bulk of the bornite and vallerite exhibited a grain size between 300μm and 2mm. It is largely dependant on the size of the aggregate, as shown in Figures 5.7, 5.13, 5.14 and 5.16.

5.2.3.5. Accessory Minerals

Baddelyite was found to be the most common accessory mineral, normally being found as euhedral crystals or rounded grains. The nature and occurrence of discrete baddelyite grains that range in size from a lower limit of 200μm to the large grains that exceed 2mm is shown in Figures 5.8, 5.11 and 5.14. The baddelyite was often associated with unranium thorium bearing oxides and rare earth bearing minerals, including monazite ($(Ce,La,Nd,Th)PO_4$). Other accessory minerals were observed in minor amounts, including pyrite, siderite and rutile in restricted grain sizes of tens of micrometres.

5.3. Effect of Microwave Treatment on Ore Mineralogy

5.3.1. Previous Work on the Effects Microwave Treatment on Palabora Ore

Research into the effect of microwave radiation on the mineralogy of Palabora ore has been reported (Kingman, 1999 and Vorster et al. 2000). Using a 2.6kW multimode cavity, Palabora ore samples were microwave treated at a number of different exposure times. Polished sections of the treated samples were prepared and examined using optical and scanning electron microscopy. It was reported that long exposure times were required in order to induce micro fissures in grains or grain boundaries. However, long

exposure times also resulted in the chemical decomposition of certain mineral phases and new compounds being formed as shown in Figures 5.20, 5.21 and 5.22.

Figure 5.20. 240 Second treated sample, false colour backscattered image (after Kingman 1999).

A false colour, computer-enhanced image illustrating the partial melting of a magnetite grain. A significant amount of the magnetite contained within the sample appears to have been affected by the microwave treatment.

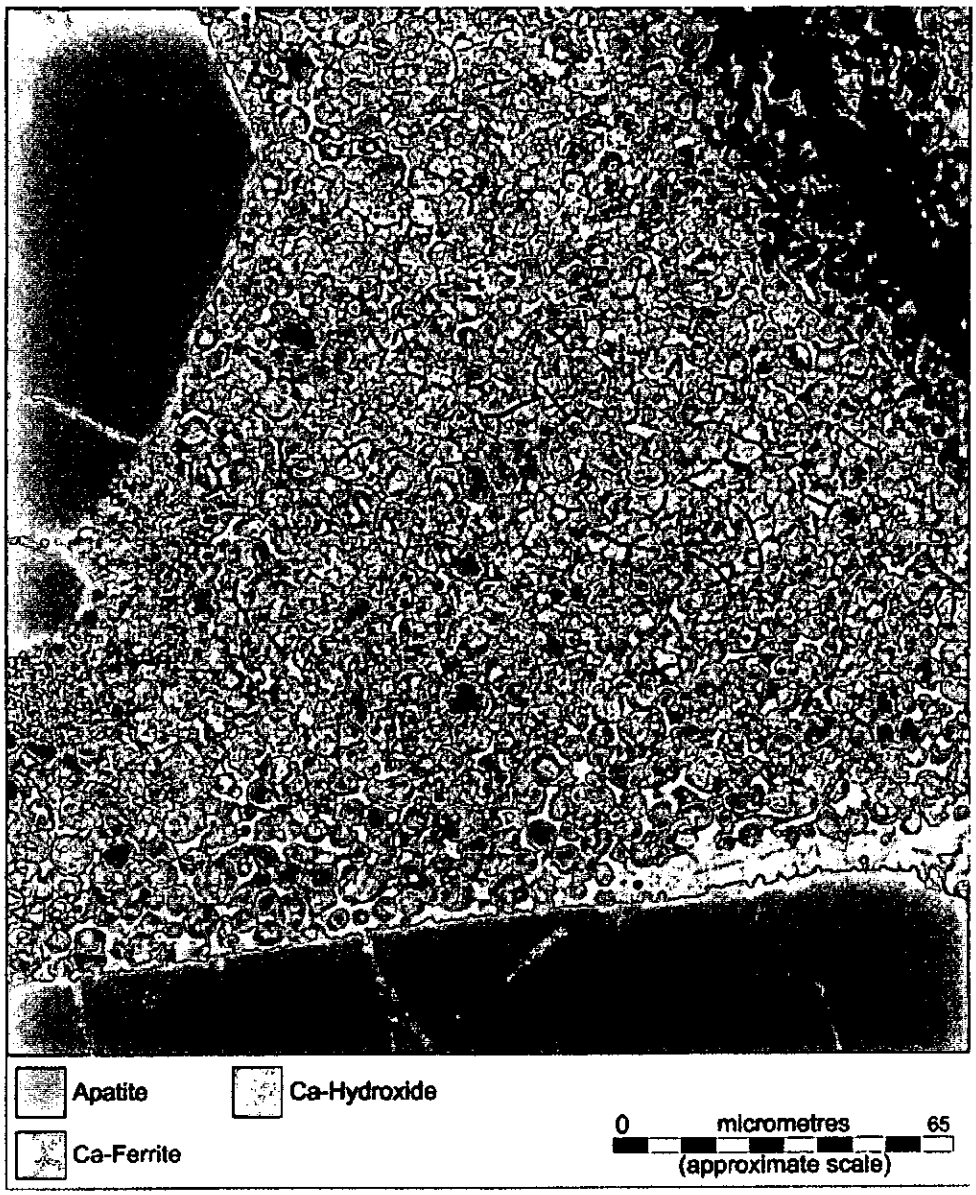

Figure 5.21. 240 Second treated sample, false colour backscattered image (after Kingman, 1999).

A false coloured computer enhanced image illustrating the occurrence of Ca-ferrite that is intergrown with Ca-hydroxide. The Ca-ferrite forms a complex web-like intergrowth

that appears to occur along grains boundaries of the Ca-sulphate. Relict apatite grains are also present in the field of view.

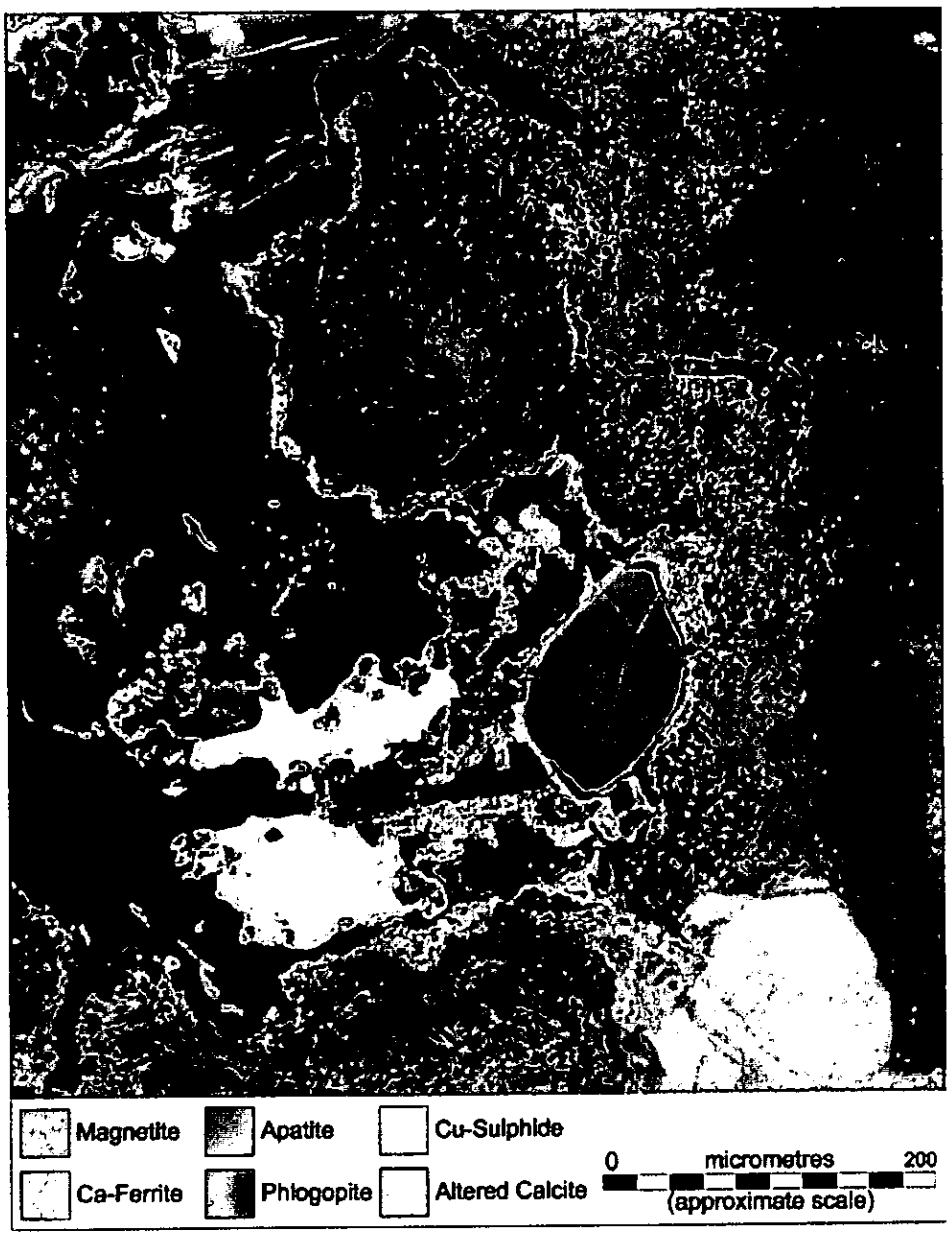

Figure 5.22. 240 Second treated sample, false colour backscattered image (after Kingman, 1999).

A false coloured computer enhanced image illustrating the occurrence of a fine grained and porous Ca-hydroxide aggregate that represents a former calcite grain. The Ca-ferrite

intergrowths represent the reaction products of the former calcite and the magnetite. The Cu-sulphide is also a reaction product formed as a result of the microwave treatment.

5.3.2. Sampling and sample preparation

A sub-sample was taken from the bulk sample >500mm particle size, received from Palabora mine. The first stage of treatment was crushing to give particles 100% passing 63mm. The upper particle size was selected to reproduce the feed size to the autogenous grinding and tertiary crushing circuit. The sample was then sieved into narrow sieve size ranges as follows: -63+53mm, -53+45mm, -45+37.5mm, -37.5+31.5mm, -31.5+26.5mm, -26.5+22.4mm, -22.4+19mm, -19+16mm, -16+13.2mm, -13.2+9.5mm, -9.5+6.7mm, -6.7+4.75mm, -4.75+3.35mm and <3.35mm.

5.3.3. Microwave treatment

Microwave treatment was carried out in a system that is capable of being operated with both single and multimode applicators manufactured by SAIREM. The microwave generator 2450 MHz operating frequency a variable output power from 3 to 15kW. The system can absorb a maximum of 5 kW reflected power and will reduce the forward power automatically should this be reached. It is connected to the applicator through a TE_{10} waveguide with internal dimensions 110mm width and 55mm height. The system already described in Chapter 2 could be coupled with a multimode or single mode resonant cavity.

The system comprises a power supply, microwave head, remote control, an automatic magic-T tuner and the applicator. The power supply is integrated with the control unit. The microwave head is mounted in a separate case and consists of a magnetron with

launcher and circulator, arc sensor and air-cooling circuit. Also built in the microwave head is a reflected-power measuring system. This is made up of a water-cooling circuit an isolator to protect the magnetron against the absorption of excessive reflected power. The remote control is built in the multimode cavity and is used for safety during operation. The automatic magic T tuner is used from impedance matching when using single mode applicator.

5.3.3.1. Heating Experiments with Multimode Cavity

The multimode cavity consists of a rectangular metallic box, with internal dimensions 43cm width and 55cm height (Figure 5.23).

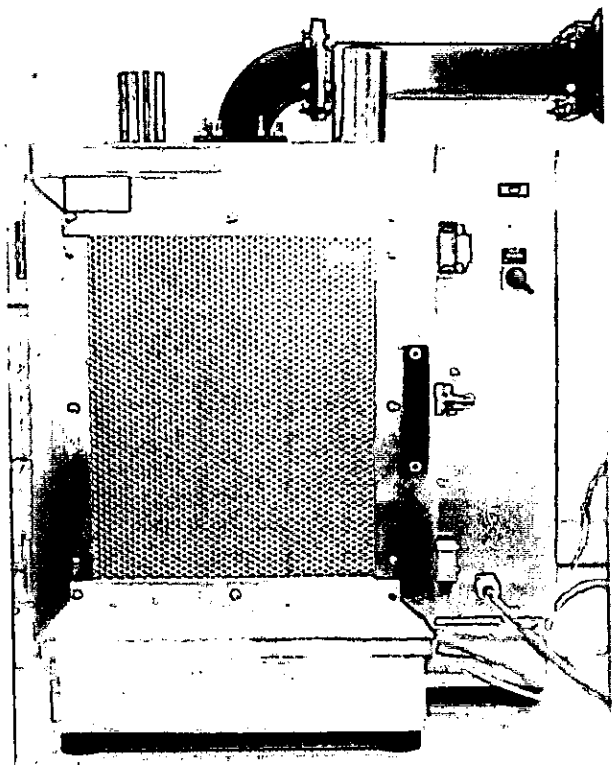

Figure 5.23. Multimode cavity used for microwave treatment.

It has a rectangular flange with equal dimensions as the wave-guide used to launch the microwave radiation. When the microwaves are launched within the box, they will

undergo multiple reflections at the cavity walls. To help improve heating uniformity a turntable plate is fitted at the centre of the cavity floor. Microwave treatment in this cavity consisted of placing the sample in five-litre capacity Pyrex beaker, which was then exposed at the desired microwave power level for various exposure times. The samples to be treated were irregular pieces of ore classified in a base as described in Section 5.3.1. The microwave treated samples were then quenched in water and left overnight to dry.

5.3.3.2. Heating Experiments using a Resonant TE_{10} Cavity

Heating experiments using a single mode resonant cavity, similar in design to the one described in section 2.5.3.4, operating at a frequency of 2.45GHz were also carried out. The cavity, illustrated in Figure 2.14, consisted of an aluminium cylindrical cavity of internal diameter 83.0mm, capable of resonating in TM_{010} mode and microwave power coupling via a TE_{10} waveguide with internal dimensions 110mm width and 55mm height. Such a resonant cavity produces a transverse electric field and a circumferential magnetic field.

Single mode microwave treatment procedure, consisted of placing a sample in a borosilicate glass tube, 70mm internal diameter. Thereafter, the tube and sample were placed into the cavity using a piston as shown on the sketch in the Figure 5.24. The rate of descent of the piston was variable and was adjusted to give the desired microwave dwell time in the cavity.

When a microwave signal is launched with an absorbent material placed in the cavity a standing wave can be formed. The standing wave length varies depending on the dielectric properties of the material to be treated and its particle size and using the short

circuit tuner fitted at the end of the wave-guide is used to restore resonance and optimize conditions in the cavity, as illustrated in Figure 2.14, and schematically represented in Figure 5.24. Before each experiment, a small representative sample of equal size distribution of the batch to be treated was packed in the borosilicate tube and placed within the center of the cylindrical cavity and a microwave signal of 3kW power was launched. The position of the short circuit tuner was varied to fine-tune the microwave signal for the minimum reflected power.

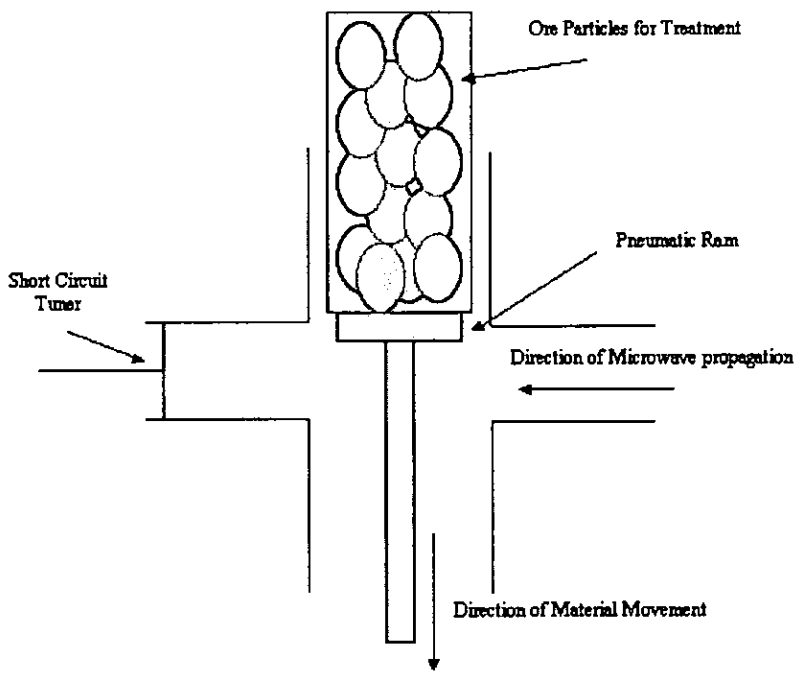

Figure 5.24. Schematic diagram of the arrangement for test in single mode cavity.

5.3.4. Results and Discussion

For a qualitative investigation of the effect of microwave power density on the mineralogy of palabora ore, samples were exposed on multimode and single mode

cavities at the same power level. Because of the nature of standing wave in single mode cavity, the power density generated within the material lattice is higher than the power density generated by the multimode cavity for equal forward power level. Figures 5.25-28 shows the effect of power density on the mineralogy of Palabora ore.

Figure 5.25 illustrates a specimen of Palabora ore exposed for 1 second at 15kW microwave power in the multimode cavity. Some heating has occurred but the power absorbed was not sufficient to induce visible thermal stress cracking.

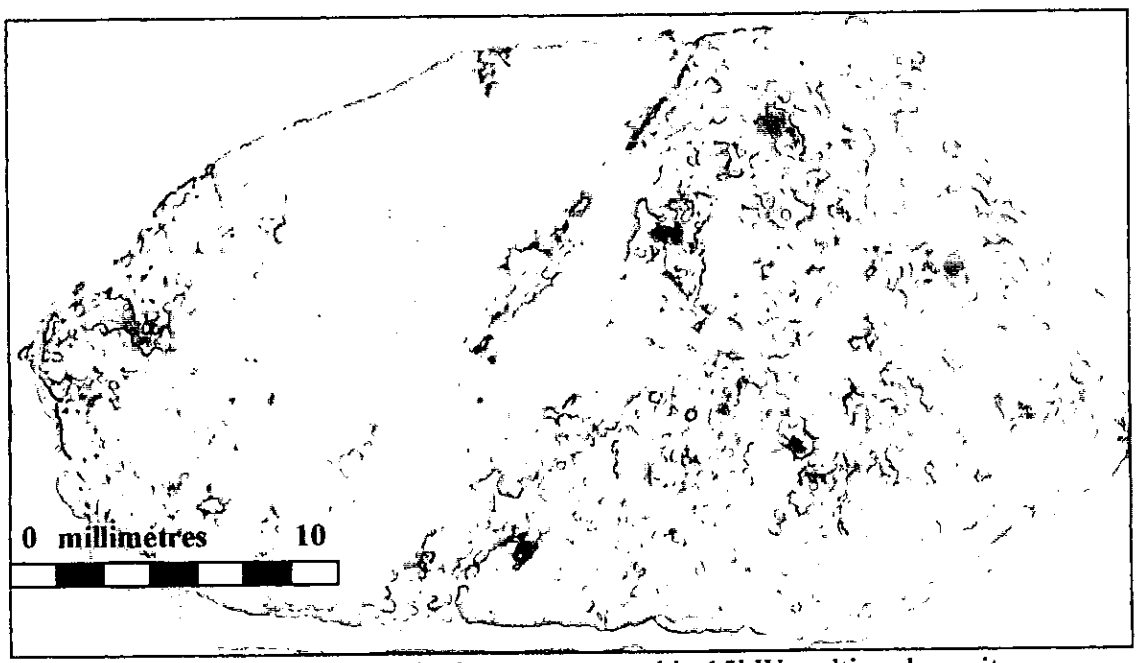

Figure 5.25. 1 Second microwave treated in 15kW multimode cavity.

Figure 5.26 illustrates a specimen of Palabora ore exposed for 5 seconds at 15kW microwave power in the multimode cavity. Again, despite inclusions of minerals such as chalcopyrite (yellowish grains) with good coupling to microwave radiation within a matrix of calcite, the specimen did not absorb enough power to induce significant thermal stress cracks.

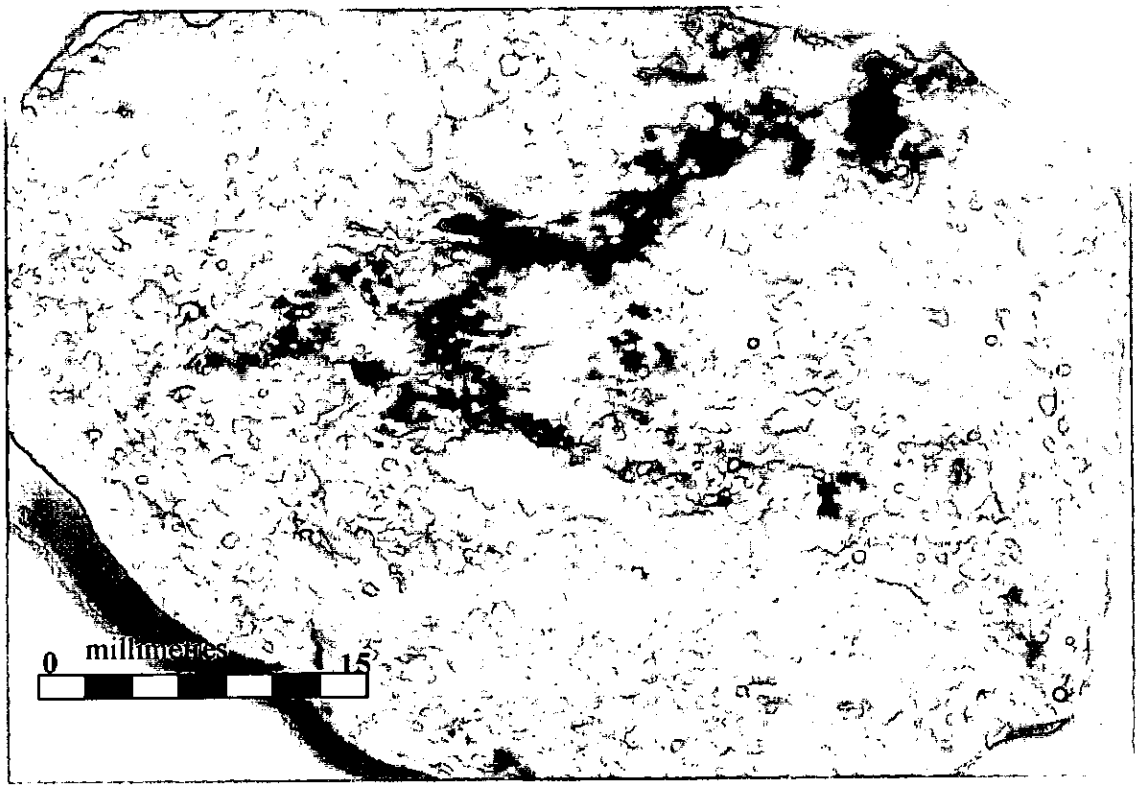

Figure 5.26. 5 seconds, 15kW multimode treated Palabora ore sample.

Figure 5.27 illustrates Palabora ore specimen that has been treated at 15kW in the single mode cavity for 0.5 seconds. It shows clearly that heating developed near grains of absorbing minerals like pyrite, chalcopyrite and magnetite and cracks developed along the interfaces between these minerals and the gangue. No attempt was made to investigate possible changes of mineralogy due to oxidation or decomposition. The experiment was intended to visualize the degree of damage on ore specimens due to microwave treatment and its consequent effect on the comminution process.

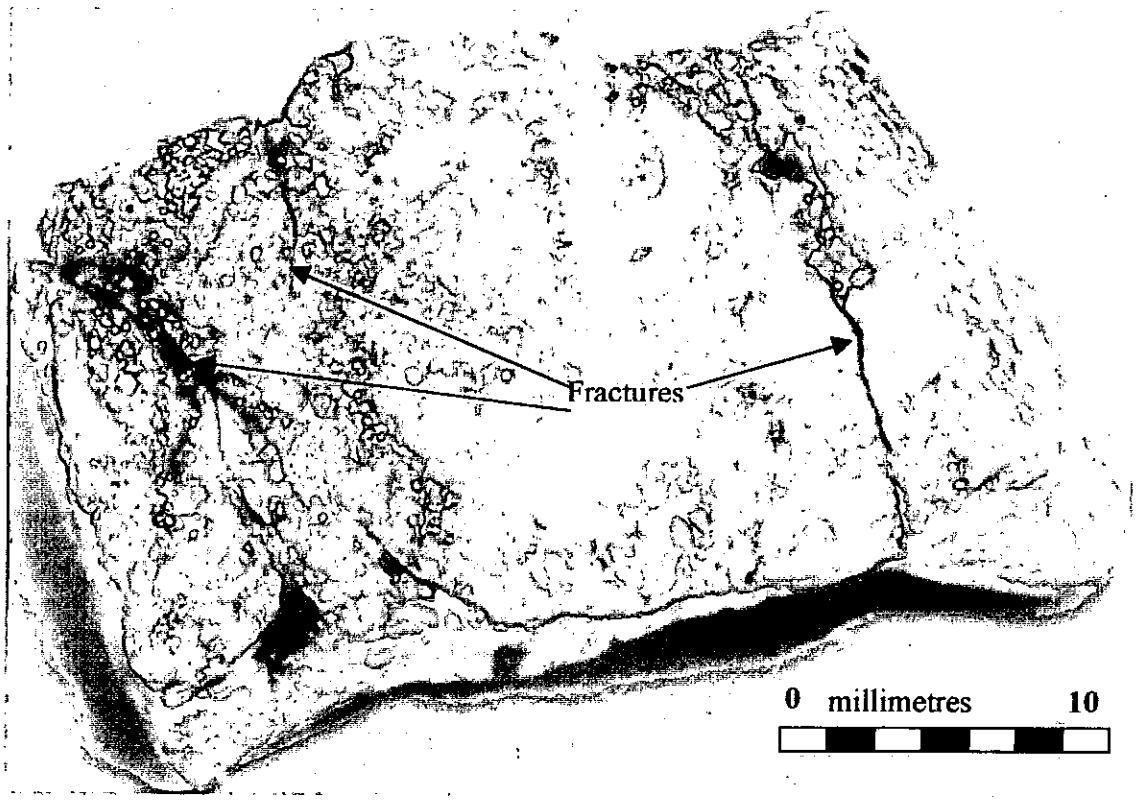

Figure 5.27. 0.5 Second, 15kW single mode treated sample of Palabora ore. Fractures occur on grain boundaries.

Figure 5.28 shows a Palabora ore specimen that has been microwave treated at 15kW in the single mode cavity for 0.2 seconds. Like the previous specimen, shown in Figure 5.27, significant damage is noted on grain interfaces. Melted spots are also observed and could be a result of concentration of power density on a grain of a high loss mineral (magnetite). It is therefore evident that ore specimens microwave treated in the single mode cavity even for short exposure times are more damaged than ore specimens treated in the multimode cavity at the same power.

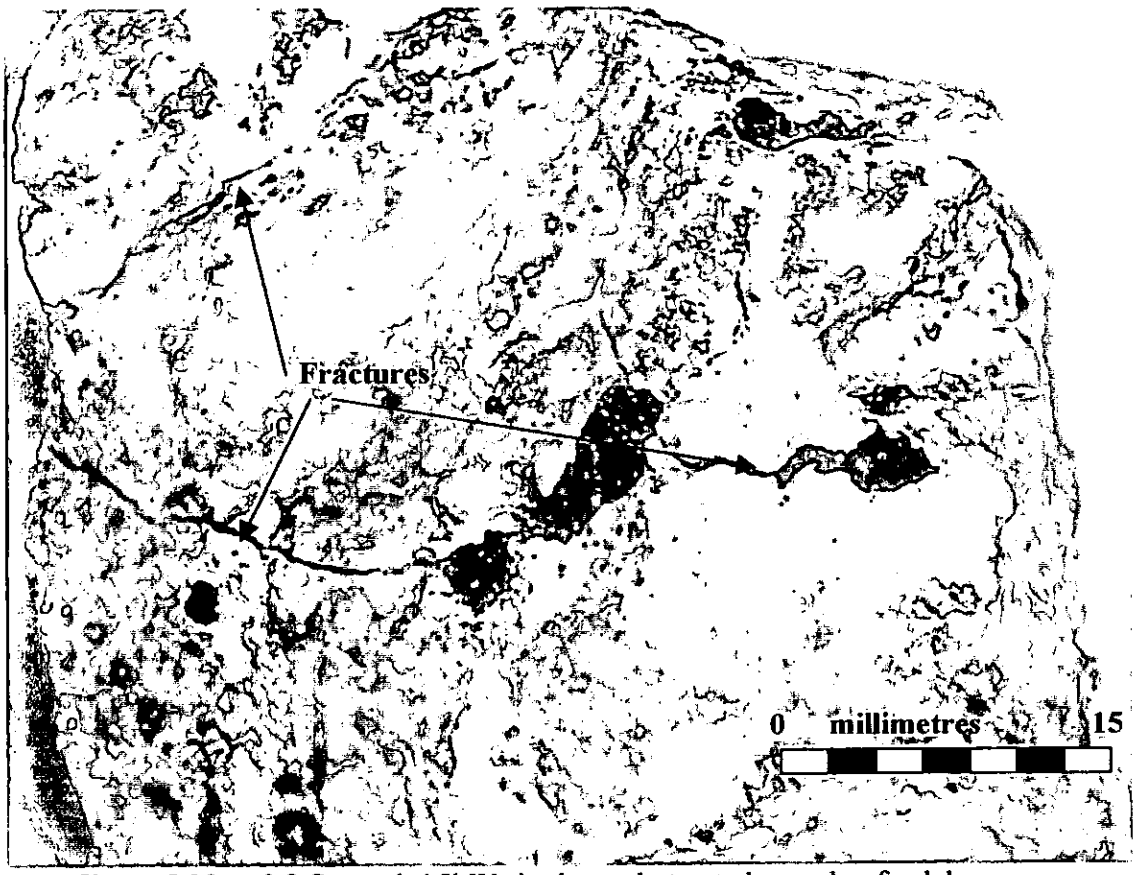

Figure 5.28. 0.2 Second, 15kW single mode treated sample of palabora ore.

5.4. Influence of Microwave Power on Ore Comminution

5.4.1. Introduction

The study of ore comminution has historically been regarded as relating energy input to the degree of size reduction, expressed as a percent passing size or proportion of final product generated. Therefore energy and degree of size reduction are related by equation 5.1 (Lynch 1977):

$$dE = -\frac{kdx}{x^n} \qquad (5.1)$$

Where dE is the incremental energy required to produce an incremental change dx in size, x is the initial particle size and k and n are specific parameters that depend on the ore type.

The quantification of the relationship between energy and size reduction of rock can be conducted using a variety of standard tests. Uniaxial compression of cylindrical specimens prepared from drill core is the most widely performed test on rock. It is used to determine the uniaxial or unconfined compressive strength (σ_c) and the elastic constants Young's modulus, and Poisson's ratio. Fracture toughness, Brazilian disc indirect tensile strength and point load strength comprise some of the standard rock mechanics tests. They provide information on the stress required to cause failure under a particular mode of loading in the form of a single hardness or strength parameter. The Brazilian disc is an indirect measure of tensile strength (Hondros 1959), which relies upon the diametral compression of a rock disc. The Point Load Test is a portable method of estimating rock strengths. Initially used with sections of core, it has been developed so that it can be used with irregularly shaped specimens (Bieniawski, 1975 and Bearman et al., 1991). The Point Load Test has the advantage of requiring no sample preparation so that a statistically sound test sample can be rapidly processed.

Whilst changes in strength are useful for comparative purposes, they are difficult to interpret in terms of process efficiency. In comminution studies, it is more important to identify the product size distribution resulting from applying a particular breakage mechanism to a given feed size and the energy input required to generate the desired product size. In particular it is the energy input size reduction relationship, that has been the main focus of the laboratory tests developed to assist in comminution equipment specification and circuit design and optimization (Napier-Munn et al., 1996).

One such approach for the investigation of the energy input size reduction relationship is the Bond work index test. Bond (1952) published the approach that has continued to be the major comminution design tool used by industry, particularly the equipment manufactures. Such an approach has also served as a useful operating tool to evaluate and optimize crushing and grinding circuits. According to Bond's 'third theory of comminution', the work input is proportional to the new crack tip length produced. It is represented by:

$$W = 100 * Wi * (\frac{1}{\sqrt{P_{80}}} - \frac{1}{\sqrt{F_{80}}}) \quad (5.2)$$

And,

$$P = T * W \quad (5.3)$$

Where W, is the work input (kWh/t); Wi, is the work index – a material specific constant (kWh/t); P_{80}, size at which 80% of the product passes (μm); F_{80}, size at which 80% of the feed passes (μm); T, throughput of new feed (t/h) and P is power draw (kW).

The work index is a comminution parameter that expresses the resistance of the material to grinding. Empirically, it is the kWh per tonne required to reduce the material from a theoretically infinite feed size to 80% passing 100 microns.

Another approach for characterising the energy size reduction relationship is single particle breakage. Single particle breakage is a process where one particle is crushed between two hard surfaces. It has been developed for the separate estimate of the material specific properties (breakage function) and the machine specific properties (the breakage rates or selection function). Farhernwald et al (1938) used a twin pendulum device to conduct early breakage studies under controlled conditions. Further work by Whiten and Awachie (1983) and Narayanan (1985) led to the development of the drop weight test procedures for the separate estimate of the breakage or appearance function by the controlled breakage of single particles.

5.4.2. Research Plan

A variety of methods available for conducting laboratory investigations into the comminution process have been reviewed in the introduction of this section. With the nature and amount of samples available, a thorough research plan was designed. The previous work by Kingman (1998) and Whittles at al (2003) showed that applied microwave power and exposure time were the two important variables that must be considered when investigating the effect of microwave pretreatment on comminution. Furthermore, applied microwave power will have a different effect depending on the form it is presented to the material, i.e. multimode or single mode cavities. Available methods for conducting material breakage characterization also differ and can be classified for the purpose of this research as: rock strength, crushing and rate of grindability.

It would have been ideal to carry out a detailed investigation into the effect of microwave power, exposure time and cavity type for each test method. However, the resources available restricted the options available in this research. It was therefore decided to use the rock strength as a preliminary characteristic to assess the effect of

microwave power, exposure time and cavity type. From the results of the assessment of ore strength, exposure time and applied microwave power would be fixed for a detailed investigation of the specific rate of breakage, material specific breakage function and liberation.

5.4.3. Influence of Microwave Treatment on Rock Strength

5.4.3.1. Uniaxial Compressive Strength

Uniaxial compression of cylindrical specimens prepared from drill core is the most widely performed test on rock (Brady and Brown, 1993). Figure 5.29 below shows a typical example of a stress versus strain plot for the uniaxial compression of cylindrical rock (after Jaeger and Cook 1979). At point A the material is said to yield and corresponding value of applied stress is the yield stress (σ_0). The point B denotes the transition from ductile to brittle behaviour and the stress at this point (C_0) defines the uniaxial compressive strength (UCS). The point C denotes the residual strength.

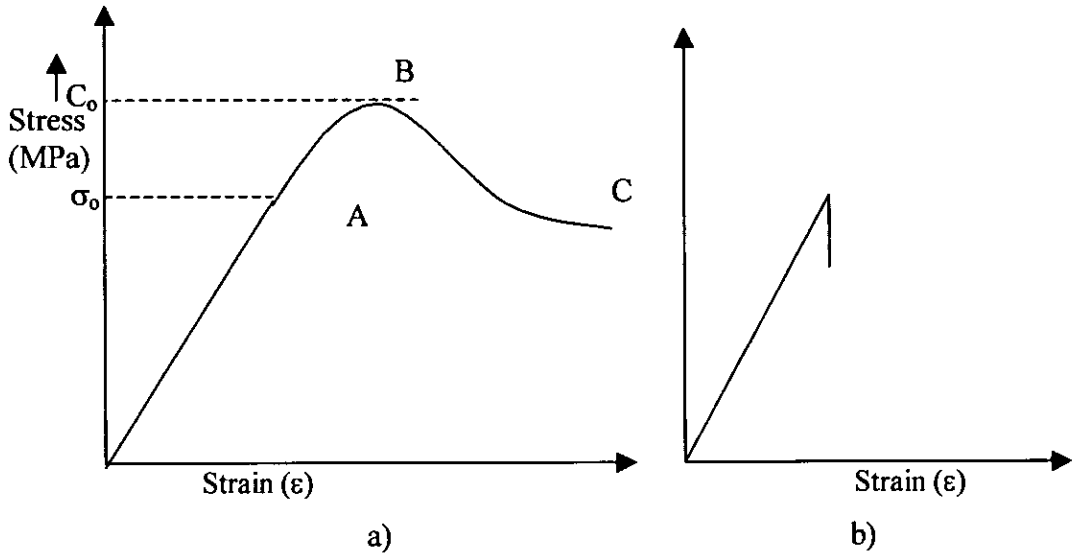

Figure 5.29. Typical example of a stress versus strain plot for the uniaxial compression of cylindrical rock (after Jaeger and Cook 1979). a) Ductile deformation process and b) brittle fracture process.

The UCS, the maximum stress recorded at the point of ductile-brittle transition, is a measure of strength that is important in designing structures in mining and civil engineering. Another important parameter is the Young's modulus defined as the slope of the elastic region of the stress versus strain. Young's modulus values range from <10 GPa for marble and weak sedimentary rock types to >70 GPa for certain quartzite and igneous rocks capable of sustaining high stress with restricted longitudinal strains. Poisson's ratio is defined as the ratio of the circumferential strain to the longitudinal strain.

Despite the apparent simplicity, interpreting results obtained from uniaxial compressive strength test requires great care. The results depend on the nature and composition of the rock and on the conditions of the test specimens. For similar mineralogy, σ_c (uniaxial compressive strength) will decrease with increasing porosity, increasing degree of weathering and increasing degree of microfissuring. Suggested techniques for determining the uniaxial compressive strength and deformability of rock material are given by the International Society for Rock Mechanics Commission on Standardization of Laboratory Field Tests (ISRM commission, 1979).

5.4.3.1.1. Sample preparation

Lumps of ore were randomly selected from the bulk sample and core drilled to give core samples of approximately 37mm diameter and 200mm length as shown in Figure 5.30. As shown earlier in Figure 5.5 the grain size of Palabora core samples can vary widely, therefore, to carry out a statistical sound test series it would require large amount of samples. Type PD samples were used for the investigation of the effect of microwave treatment on UCS. Cored test pieces were sectioned using a diamond saw to give samples of approximately 37mm diameter and 74mm length.

Two cored samples were microwave treated in both single mode and multimode cavities, both at 15kW microwave power for 1s exposure time.

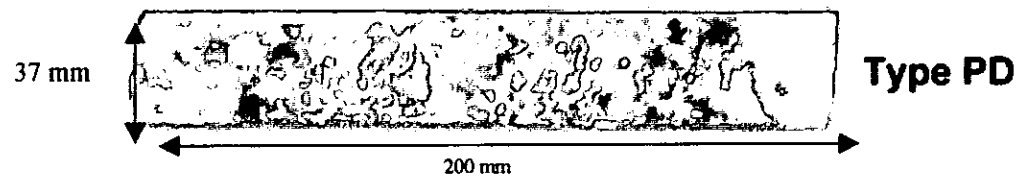

Figure 5.30. Core drill sample of palabora ore.

5.4.3.1.2. Test Procedure

Uniaxial compressive strength tests were carried out using a RDP-Howden 1MN stiff universal loading frame. The tests were conducted in strain control, i.e. at a constant rate of cross head movement (0.00625 mm/s) irrespective of the applied force. Three core samples were tested, one untreated and the other two microwave treated at 15kW microwave power for 1second on a multimode and single mode cavities. The apparatus is shown in Figure 5.31.

5.4.3.1.3 Results and Discussion

Recorded data of applied force versus strain were converted to stress, by dividing force by the cross sectional area of the sample. Results of the uniaxial compressive strength test carried out are shown in Figure 5.32. The plot illustrates the stress versus strain curve treated and untreated specimens. It was found that UCS for the untreated specimen was approximately 128MPa, the multimode treated specimen was about 90MPa and the single mode treated specimen was approximately 65 MPa.

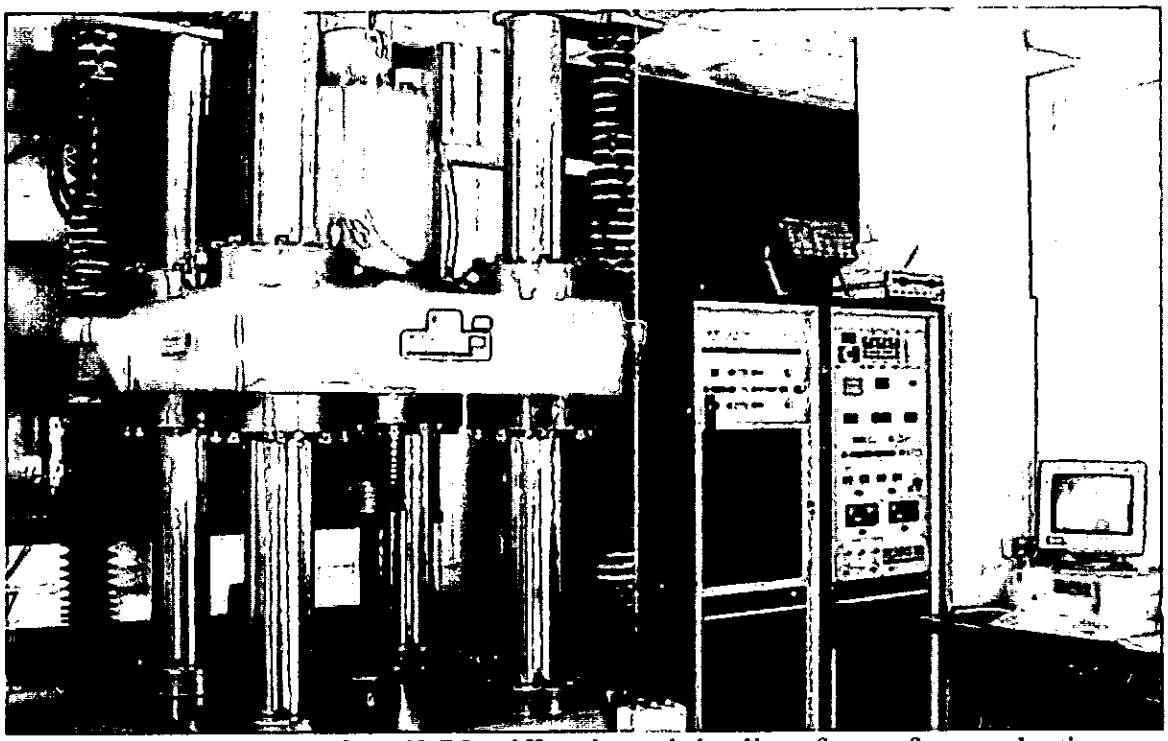

Figure 5.31. RDP-Howden 1MN stiff universal loading frame for conducting uniaxial compressive strength.

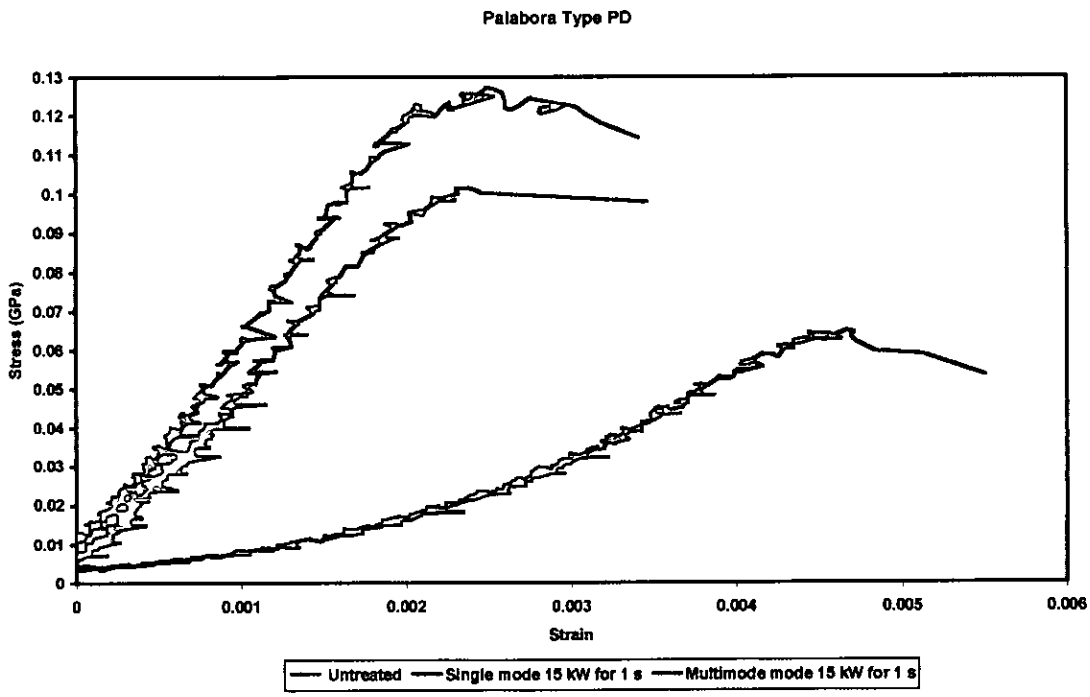

Figure 5.32. Plot of stress versus strain of Palabora type PD core drilled samples.

The limited number of tests means that the results must be treated with considerable caution but significant strength and stiffness reduction can be clearly seen, viz. about

30% with the multimode cavity and about 50% for the single mode cavity for the some exposure time.

5.4.3.2. Point Load Test

Aspects of the point load tests as used in determining rock strength, have been discussed by a series of authors, including Goodier (1933), Hondros (1959) and Protodyakonov (1960). The main themes of the discussions can be divided into two groups: tests on irregularly shaped specimens and cubes and tests carried out on rock cores. The work carried out by Protodyakonov in 1960 was later recommended by the International Bureau for Rock Mechanics in 1961 as a suggested method for testing irregular lumps of rock (Broch, 1971). It was recommended that specimens with a ratio of the longest to the smallest diameter of about 1.5:1 should be used. In addition it was recommended that the specimen should be tested parallel to its longest axis and perpendicular to the plane of the laminations. Despite criticisms by Hobbs in 1963, the test procedure was successfully used by Diernat and Duffaut (1966) in classifying rocks. Diernat and Duffaut also reported that scattering is slightly greater on irregular specimens than when testing regular specimens (cubes, prisms or cylinders).

Duffaut (1968) and Duffaut and Maury (1970) further investigated the Protodyanokov test in depth. Duffaut showed that results from the test are influenced by weight, size or shape effects and specimen orientation. Duffaut and Maury studied thirteen plane models and concluded that the failure load is highly dependent upon the specimen orientation and recommend that testing across their large length should be avoided.

When conducting a point load test on a regular specimen such as a core, two parameters are measured: the failure load, P, applied by the tips, and the distance

between the tips where the specimen is failing, D. The result of point load test is expressed as strength index (Is) and is defined as:

$$Is = P/D^2 \qquad (5.4)$$

The magnitude of this index is not only material dependent, but also on the size and shape of the specimens and, to some extent, on the testing conditions. The number of test pieces recommended by many authors to determine the rock strength is ten or more to be within a 96 per cent confidence interval of the mean strength. In addition, from a practical point of view, it has been recommended as well that size of specimen for testing should be between 25 and 50mm diameter (Broch, 1972) and 50mm should be adopted as standard (ISRM commission, 1979).

Therefore, when conducting point load test on specimens of a different diameter (Figure 5.33), the results need to be presented as an index known as Is(50) or the equivalent index value at 50mm diameter. Several empirical equations have been developed to convert the test data to Is(50) and then to an approximation of compressive strength (Hoek and Brown, 1980). The equation used in this work is given below:

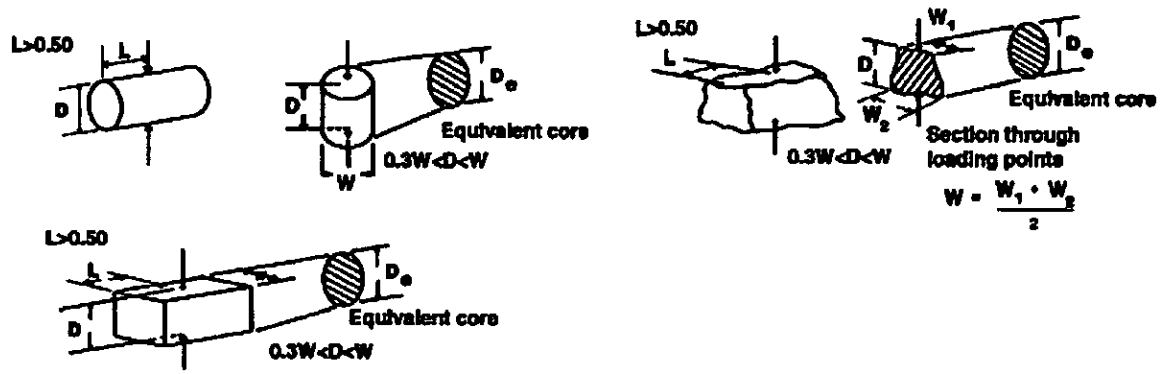

Figure 5.33. Suggested sample dimensions for point load testing (Hudson, 1993)

$$Is(50) = \frac{\left(\frac{Depth}{50}\right)^{0.45} \times Force}{\frac{4 \times Width \times Depth}{\pi}} \qquad (5.5)$$

Is(50) in this case is the equivalent point load strength index of an irregularly shaped specimens equivalent to that of a 50mm diameter cylindrical specimen.

Broch and Franklin (1972) found that the Is can be correlated with the uniaxial compressive strength of the material in question. For core diameter equal 50mm it was found that

$$\sigma_c \approx 24Is \tag{5.6}$$

And for other values of D, a size correction is necessary and the following approximate relation between σ_c, Is and the equivalent core diameter, D, measured in millimetres:

$$\sigma_c = (14 + 0.175D) * Is \tag{5.7}$$

Most recently, the test has been adapted for the rapid prediction of Mode I fracture toughness (Bearman, 1999) and comminution behaviour in rocks (Bearman et al., 1997).

5.4.3.2.1. Sample Preparation

Following sample preparation described in section 5.3.2, representative samples within the ranges –53+45mm and -37.5+31.5mm were selected for point load test and the other fractions were saved to be used for drop weight test, abrasion test, ball mill rate of breakage and Bond Work index test.

For each test 10 particles of ore were used. After a thorough mixing of the particles, a random selection of the required number of particles for each set was made. The microwave power was set for 5, 10 and 15kW and exposure time set for 1, 5 and 10seconds in the multimode cavity and 0.1, 0.5 and 1s in the single mode cavity. The conditions of sample preparation are summarized on Table 5.2.

5.4.3.2.2 Test Procedure

Suggested techniques for determining the uniaxial compressive strength of rock material are given by the International Society for Rock Mechanics Commission on Standardization of Laboratory and Fields Tests (ISRM Commission, 1979). The essential features of the recommended procedure and adapted for the present situation is the use of a suitable machine for applying and measuring axial load to the specimen. The machine should be of sufficient capacity and capable of applying load at a rate conforming to the requirement of the test procedure.

Table 5.2. Sample description for point load test

Cavity type	Sample size	Power (kW)	Exposure time (S)			
Multimode	37x31 mm	15	10	5	1	0
		10	10	5	1	0
		5	10	5	1	0
Single mode	37x31 mm	15	1	0.5	0.1	0
		10	1	0.5	0.1	0
		5	1	0.5	0.1	0
	53x45 mm	15	1	0.5	0.1	0
		10	1	0.5	0.1	0
		5	1	0.5	0.1	0

In the Point Load test, measurement of width and depth of the specimen near the loading point is recorded. Then the specimen is placed and loaded between the two shaped and hardened steel platens in the apparatus (Figure 5.34). The force, P, at which the specimens breaks is determined from the peak pressure recorded on the pressure gauge and the known cross sectional area, using a correction formula usually specific for each equipment. For the equipment used the following relationship was used:

$$Force = \frac{9.835 * P - 344}{1000} \tag{5.8}$$

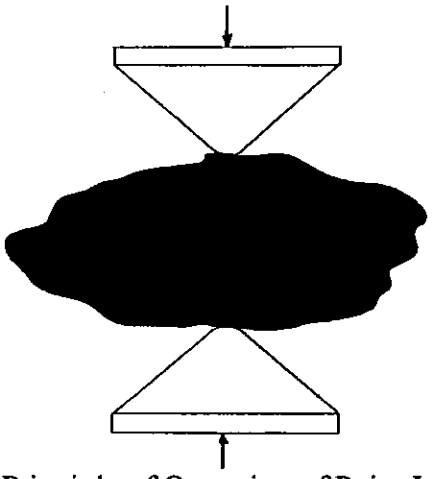

Figure 5.34. Principle of Operation of Point Load Apparatus.

5.4.3.2.3. Point Load Test Results and Discussion

As mentioned previously, the aim of characterization by ore strength in general and point load index in particular was to assess the effect of microwave power, exposure time and cavity type. In addition, it is well known that rock strength varies with specimen size. Therefore, for preliminary assessment of the combined effect of microwave power and specimen size, experiments were carried out on samples microwave treated on single mode cavity. Samples on the size range –37.5+31.5mm and –53+45mm were used. The samples were microwave treated in a single mode cavity for 0.1, 0.5 and 1second exposure time and microwave power of 5, 10 and 15kW. For each size range, a similar sample set was tested without treatment as a comparison.

Equations 5.6 and 5.5 were then used to convert the data into point load index Is(50). The results are shown on Table A2.1 and in Figures 5.35 and 5.36, plotted as percentage of original Is(50) (treated/untreated*100) versus microwave exposure time.

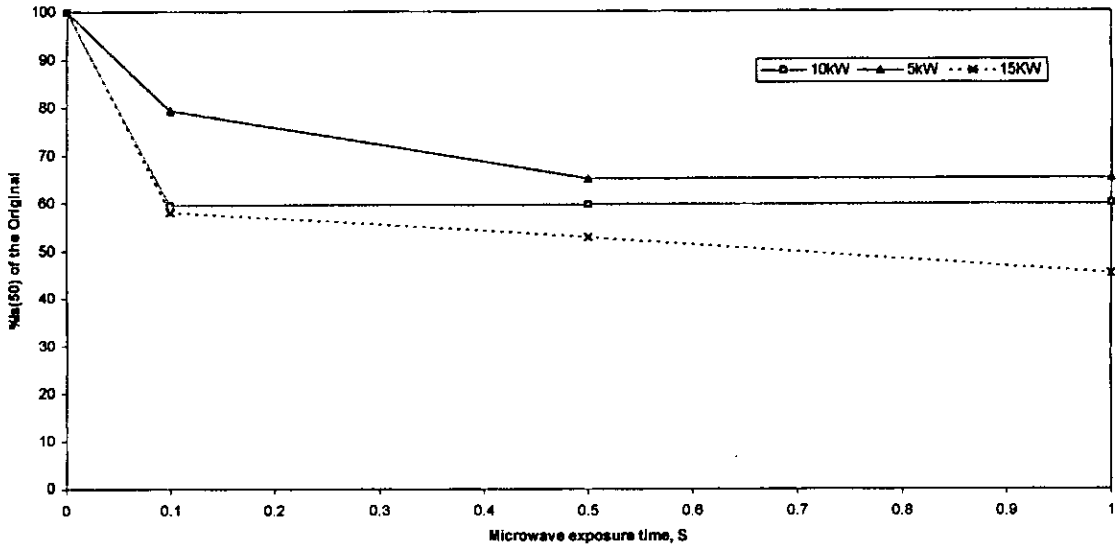

Figure 5.35. Effect of Single mode microwave treatment on the Point Load Test index for Palabora ore –37+31mm particle size.

The average Is(50) for the untreated material has been found to be 2.88±1.06MPa for the –37.5+31.5mm size and 3.31±0.87MPa for the –53+45mm size, as shown on Table A2.1. Also shown on Table A2.1 are the mean value for Is(50), median and range for each mode of treatment, microwave power and exposure time. In both Figures 5.35 and 5.36 it can clearly be seen that microwave treatment has a significant effect on the ore strength, with short exposures of 0.1 seconds giving rise to up to 45% and 55% reductions in Is(50) for the –37.5+31.5mm and –53+45mm respectively, for 15kW microwave power. These results also show that particle size has an effect on the microwave-induced stress. The amount of microwave power deposited into the material will have an effect on the induced stress cracking and, therefore, on the ore strength. More micro-fractures are developed in the bigger particles than in the small ones. Furthermore, the trends of the curves on both plots are similar suggesting that exposure time does not have a significant effect on generation of thermal induced stress cracks.

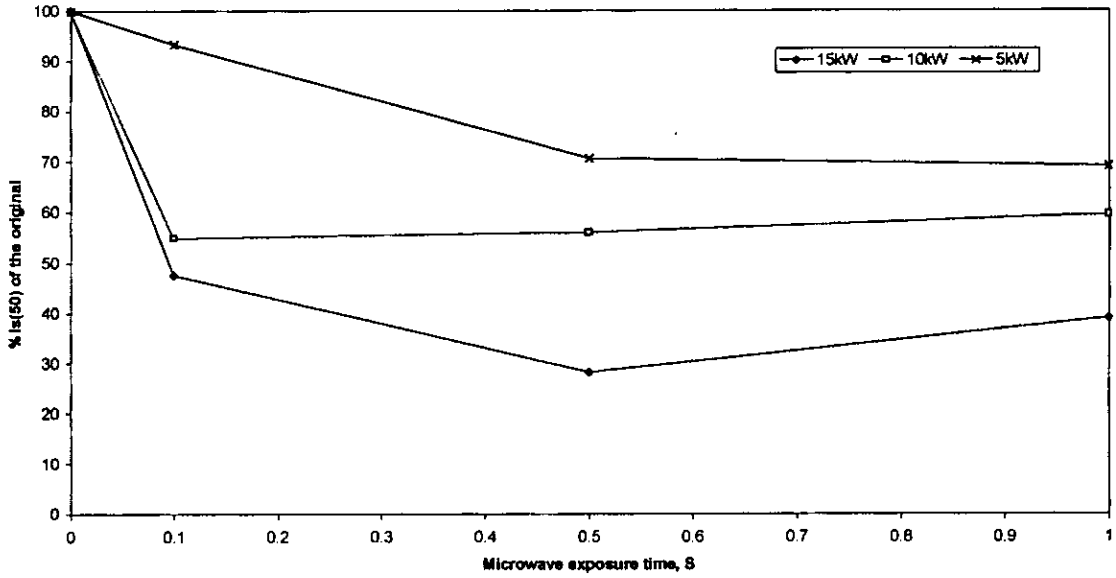

Figure 5.36. Effect of Single Mode microwave treatment on Point Load test for Palabora ore, -53+45mm particle size.

The results from the single mode tests showed similar trends in the microwave power versus exposure time relationship, regardless of the particle size effect. It was considered that tests using the multimode cavity were necessary but that tests on only one particle size, –37.5+31.5mm were needed to demonstrate the lower level of effect. Three samples with 10 test specimens each were microwave treated for 1, 5 and 10 seconds at 5, 10 and 15kW.

Figure 5.37 shows a plot of percentage of original Is(50) verses microwave exposures times for these tests. It can be clearly seen that the trends of the curves are quite similar with those observed with single mode microwave treatment. However, the significant effect on the strength of the ore is observed after 1second exposure time for multimode treatment with reduction to up to 45% while for single mode with even short exposures of 0.1 seconds giving rise to up to 45% reductions in Is(50).

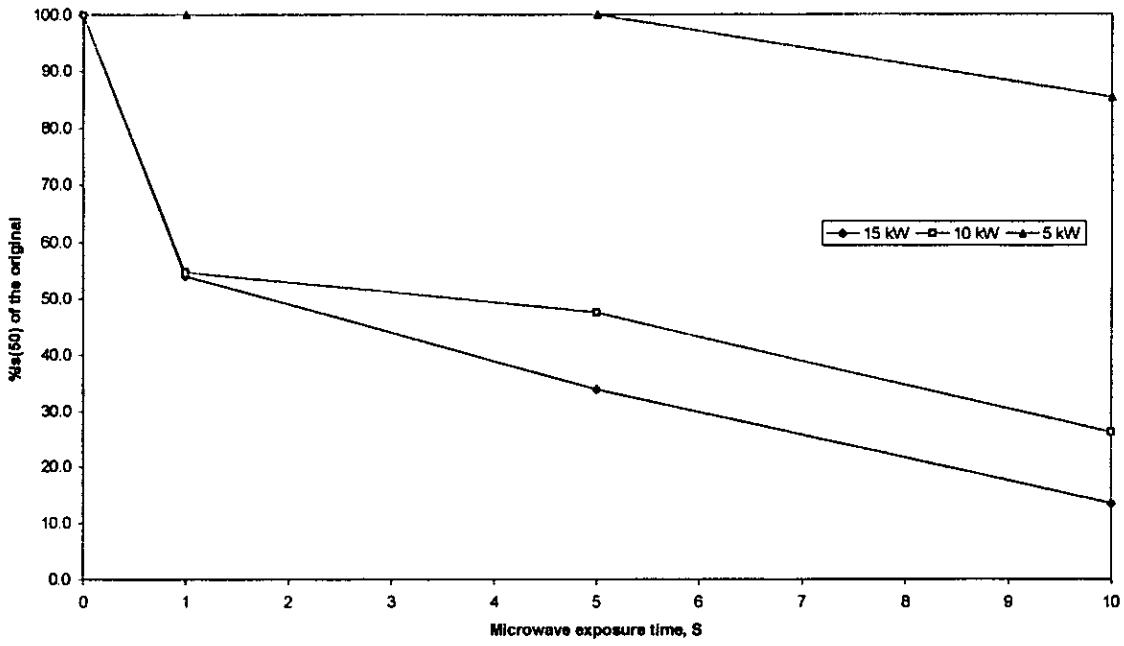

Figure 5.37. Effect of Multimode microwave treatment on Point Load test for Palabora ore, -37.5+31.5mm particle size.

Interestingly for 0.1 seconds exposure, similar results are obtained for samples treated at both 10 and 15kW in the single mode cavity. Similar results were obtained for samples treated for 1second at both 10 and 15kW in the multimode cavity. It can be seen however that as exposure time is increased to 0.5 seconds approximately 70% reductions in strength are achieved for samples treated at 15kW compared to only 55% reduction for samples treated at 10kW in multimode cavity. For all exposure times 5kW gives the smallest reduction in strength with only approximately 30% reduction occurring after 1 second in a single mode microwave cavity and 10 seconds in a multimode microwave cavity only giving rise to 20% reduction.

The present findings are not new. Previous work (Kingman 1999) has shown reductions in ore strength (Bond work index) to be related to microwave exposure time. In the present research the results, however, are highly significant as previous

work showed that at least 10 seconds (and often 180 seconds) were required to achieve small reductions in ore strength. In this study significant reductions in strength are demonstrated for an exposure time of 0.1 seconds in a single mode cavity, up to 1800 times less than that previously used.

A recent study, already referred to in Chapter 3, by Whittles et al. (2003) using a numerical modeling approach has shown very clearly that if the preferential dielectric material can be made to absorb the majority of the applied energy significant reductions in compressive strength can be achieved. The model domain consisted an area representing a 15 mm wide by 30 mm high section, which was subdivided into individual square zones of 1 mm sides. The positions of the pyrite particles within the model domain were randomly generated to provide a relatively disseminated ore body (Figure 3.3). This type of ore mineralogy (pyrite particles in the calcite matrix) has great difference on response to microwave power, as illustrated by their dielectric properties (Figure 5.38).

The differences between the loss factors of the two minerals clearly suggest that pyrite will preferentially absorb microwave energy. Whittles et al. (2003) further simulated the effect of power density versus exposure time on the heating process. They simulated high power density ($1x10^{11}$ W/m^3) microwave heating process for short exposure time and compared it to a low power density ($1x10^9$ W/m^3) for a long exposure time (Figures 3.4 and 3.5). They reported high temperature gradients between the mineral phases when using high power density for a short exposure time, while at low power density and with a long exposure time, low temperature gradients were formed. This is because microwave energy is preferentially deposited into pyrite phase and short exposure means that heat transfer by conduction into the

calcite is negligible. A long exposure time allows greater conduction between minerals phases, resulting in increased temperatures in the calcite.

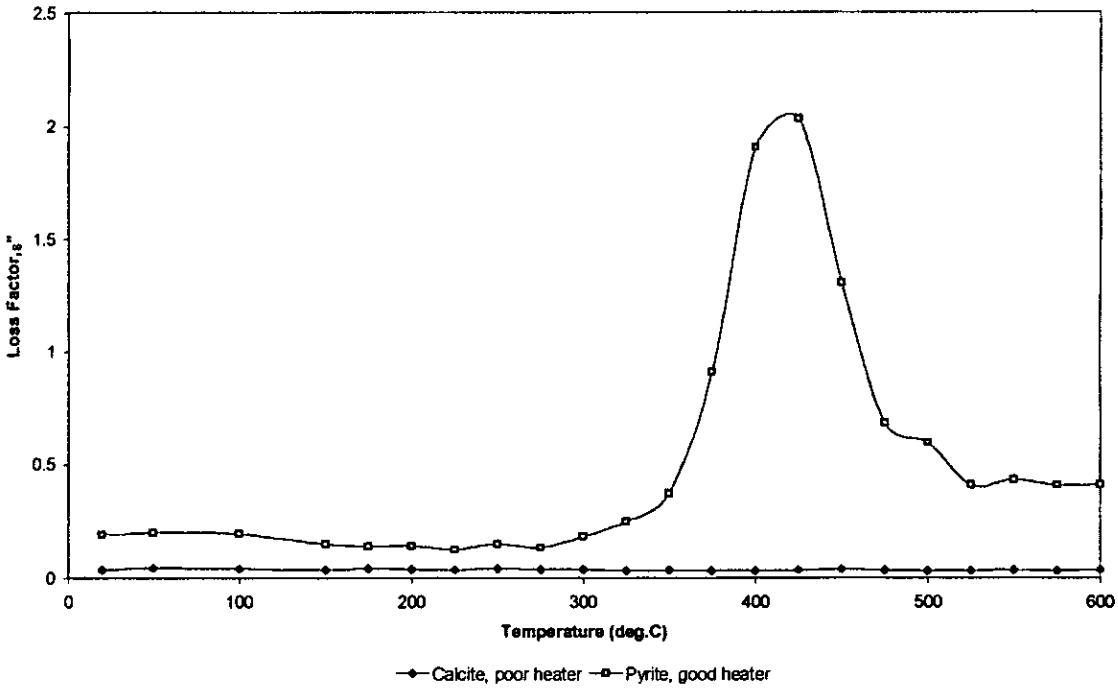

Figure 5.38 Loss factor of Pyrite and Calcite.

A high temperature gradient between adjacent mineral phases mean that the induced thermal stress at the grain boundaries will also be high, which should result in greater weakening of the material. To further investigate this, Whittles et al. modelled the UCS test for the model domain for different simulated heating times. The results are shown in Figures 3.6 and 3.7.

Figure 3.6 illustrates the influence of microwave heating time versus unconfined compressive strength for the lower power density ($1x10^9$ W/m^3). It can clearly be seen that as microwave exposure time is increased the UCS decreases. This is also true in Figure 5.36, which shows microwave-heating time versus UCS for the ore exposed at the higher power density. However, while at lower power density the maximum decrease in UCS is achieved at 30s, at the higher power density a greater reduction is achieved after only 0.05s.

It is interesting to compare the model prediction with the experimental data in Figures 5.35-37, i.e. the shape of the curves and even reductions in strength. The shape of the curve for test carried out using 5kW microwave power is similar to that observed on modeled results for lower power density, with reduction accounting for about 30% as shown in Figures 5.35, 5.36 and 3.6. In addition, the shape of the curve for test carried out using 10 and 15kW microwave power (Figure 5.35 and 5.36) is similar to that observed on modeled results for higher power density (Figure 3.7).

5.4.4. Influence of Microwave Treatment on Crushing

The breakage of material in cone type gyratory crushers and SAG/AG mills is traditionally regarded as relying upon single particle breakage (Evertsson and Bearman, 1996). Single particle breakage may occur by impact, slow compression and shear. The mechanism of single particle breakage by impact has been used to study the relationship between comminution energy and size reduction. Several devices have been developed for experiments on single particle breakage such as twin pendulum device, drop weight tester and Hopkinson pressure bar.

5.4.4.1. Single Particle Breakage Techniques

The twin pendulum device (Figure 5.39) has been used to study the effect of velocity on single particle breakage under controlled conditions (Fahernwald et al 1938). Fahernwald et al found that an increase in impact velocity increased the production of fines resulting from breakage of a particle. It has also been used by other authors to determine the impact crushing strength under controlled conditions (Bond, 1946, Gaudin and Hukki, 1946, Yashima et al 1981 and 1982).

The use of a twin pendulum testing to determine the breakage function for crusher modeling has been reported. Awachie (1983) investigated single particle breakage using a twin pendulum test and the product was compared to that generated by a crusher and found to be similar. The twin pendulum test was further developed (Narayanan 1985 and Narayanan and Whiten 1988) and used for conducting single particle breakage tests from which the comminution energy, defined as the energy available for the breakage of a particle, could be determined, together with the product size distribution. The development included the modeling of the ore specific breakage functions for cone crushers and SAG/AG mills.

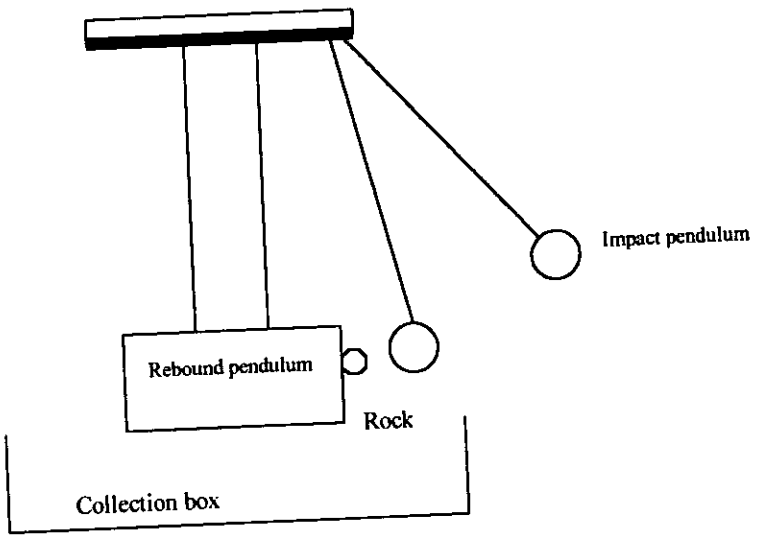

Figure 5.39. Schematic of a twin pendulum device (after Napier-Munn, 1996).

The Hopkinson pressure bar (HPB) test is used to determine material properties under extreme loading conditions (high pressure and strain rate) using induced wave propagation along a metallic elastic bar to measure the pressure produced during dynamic testing. Bertram Hopkinson developed the test around 1914 when studying the shape and evolution of stress pulses as they propagated along rods (Kuokkala et

al. 2003). The method is used to examine material properties such as fracture toughness, compressive and tensile strengths.

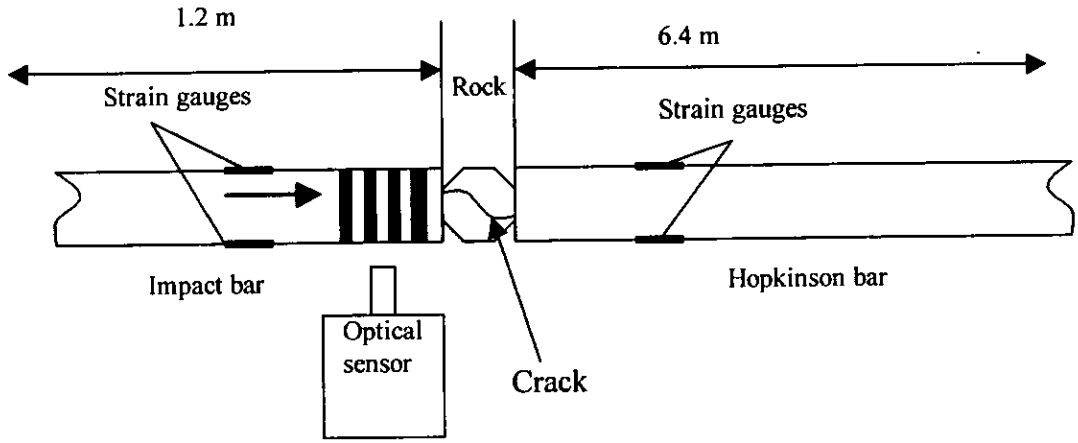

Figure 5.40 Schematic set up of Hopkinson Pressure Bar experiment and wave signal plotted as a function of time (after Kuokkala et al., 2003).

The HPB (Figure 5.40) experiment is basically composed of two separate bars placed horizontally, with the sample to be tested sandwiched in between the two bars. The impact bar is mounted on linear bearings and is attached to a spring mounted at the opposite end of the bar. The spring is compressed to a known distance to control the impact velocity and then input energy is determined by measuring the speed of the impact bar at the point of impact, using an optical sensor. Upon contact with sample, the force exerted between the ends of the two bars during the collision propagates as longitudinal strain wave down the impact and Hopkinson bars. These waves are measured by strain gauge bridges on both bars. The integration of the force-time profiles from both the Hopkinson and impact bars allows lost strain energy to be subtracted from the input energy, so that the actual energy responsible from breakage can be calculated (Napier Munm, 1996). A specifically developed software interface is used to process the signals and convert them into forces and velocities and specimen strength be calculated.

Drop weight testers of various kinds have been described in the literature. According to Napier-Munn (1996), early forms of drop weight tester were reported by Gross (1938), Piret (1953), Fairs (1954), Schonert (1972), Van der Waeden (1982) and Pauw and Mare (1988). In the early stage of development, a particle was dropped from a known height and the size distribution of the broken product measured. The breakage energy was assumed to be the potential energy, in Joules. For simulating breakage of ores in crushers and tumbling mills in which high energies are believed to dominate, this procedure, however, is not practical.

Morrell and Morrison, 1989, in their research at the Julius Kruttschnitt Mineral Research Centre (JKMRC) suggested a new approach: to drop a suitable weight on the particle. Such an approach has resulted in the development of an alternative to the twin pendulum device for determining the ore specific parameters in comminution models. A schematic diagram of the drop weight device is shown in Figure 5.41. It comprises a weight that is raised by a winch to a known height from which it falls under gravity onto a rock particle resting on a steel anvil. The unit is enclosed in Perspex to prevent any broken fragments from being lost. The input energy is calculated from the mass of the drop weight head, the distance through which it falls in breaking the rock and the mass of the rock to be broken.

The data from the drop weight test can be used to yield quantitative information about the relationship between input energy and resultant size distribution (Napier-Munn et al, 1996). According to Bourgeois and Banini (2002) the drop weight tester, however, does not give information about the actual energy used during breakage and it is not possible to derive or estimate ore properties such as strength and fracture toughness. This has led to new comminution models being developed (Valery, 1997; Dukino et al., 2000 and Banini et al., 2000) that make use of increasingly

fundamental ore breakage properties and the physics of the process, separate from comminution process they are subject to (Bourgeois and Banini, 2002). Dukino et al. (2000) and Banini et al. (2000) have indicated the possibility of predicting the broken mass of the surface impact breakage process, often referred to as attrition, from fundamental mechanical properties, including fracture toughness and material hardness.

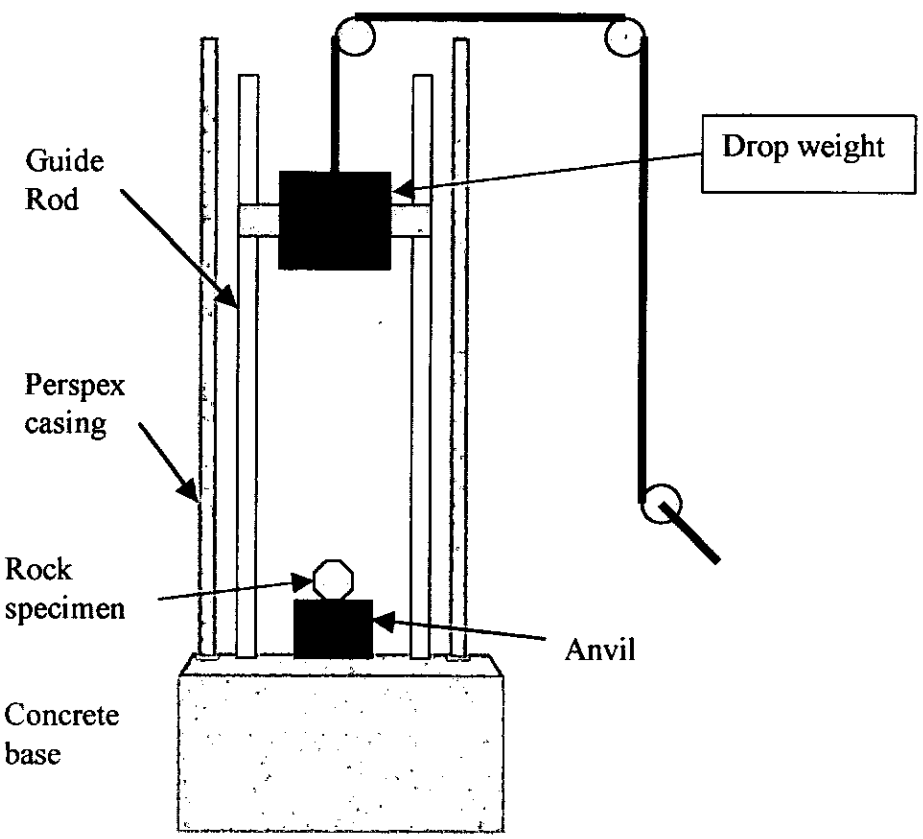

Figure 5.41. Schematic diagram of drop weight tester (after Napier-Munn et al., 1996).

According to Banini et al. (2002) this necessary evolution must be supported by experimental techniques that can provide fundamental information about ore breakage properties. In addition, such fundamental ore breakage characterization techniques must be developed so that they become available to industry.

Over two decades, another type of drop weight testing device incorporating some features of the classic Hopkinson pressure bar was reported by Weichert and Herbst, 1986, and referred to as the Ultrafast Load Cell (UFLC). The UFLC can provide information about detailed energetic aspects of single particle breakage such as compression, compressive force, tensile strength, material stiffness, energy absorbed, energy at first fracture, and energy absorption during fragmentation (Hoffler and Herbst, 1990; Bourgeois et al, 1992; Tavares and King, 1998 and Bourgeois and Banini, 2002).

Despite the existence of such a variety of techniques to conduct single particle breakage tests, in the present research a drop weight tester developed by JKMRC was used. At present, industry and specialized laboratories use the drop weight tester on a routine basis, associated with JKSimMet, a steady state mineral processing plant simulator (Napier Munn, 1996). JKSimMet has been designed as a powerful aid to perform steady state simulation of a range of comminution and classification operations such as cone crushers, jaw, gyratory and rolls crushers, autogenous and semi-autogeneous mills, rod and ball mill, vibrating screen and hydrocyclones.

5.4.4.2. Drop Weight Test Procedure

A standard drop weight test comprises breaking five narrow size ranges of particles, each size range at three different energy levels, making a total of 15 size/energy combinations. The size ranges chosen lie in a fourth root of 2 ranges as specified in Table 5.3.

5.4.4.2.1. Sample Preparation

The sample is mixed as thoroughly as possible and then sieved to generate particles in the size ranges detailed in Table 5.3. Random selection of the required number of

particles for each set is then made. In addition, samples for an abrasion test and relative density measurement should be made. The abrasion test, used for the assessment of the resistance of the ore to abrasion, requires tumbling of a 3 kg sample of 55 x 38 mm material in a 300 x 300 mm mill for 10 minutes at 70% critical speed.

Table 5.3 Complete drop weight test typical size energy combinations

Size particle, mm	No of particles	Nominal energy, kWh/t		
63x53	10	0.4	0.25	0.1
45x37.5	15	1.0	0.25	0.1
31.5x26.5	30	2.5	1.0	0.25
22.4x19	30	2.5	1.0	0.25
16x13.2	30	2.5	1.0	0.25

The product is then sized to –38 μm on a $\sqrt{2}$ series of sieves so that the t10 can be calculated. For the measurement of relative density, it is required weighing 30 randomly selected ore particles in the size range 31.5 x 26.5 mm. The weighing for each particle is conducted in air and in water. The data is used to calculate the relative density using the following expression:

$$\rho = \frac{m_d}{m_d - m_{wet}} \tag{5.9}$$

Where ρ is the relative density (g/cm^3), m_d mass of the particle in air (g) and m_{wet} mass of particle in water (g).

5.4.4.2.2. Procedure for Drop Weight Test

Following sample preparation, the mean mass of each set of particles to be broken is calculated. Based on the required specific input energy for each test, the drop weight heights from which the drop weight is to be released are calculated from the following equations (Napier-Munn et al., 1996):

$$h_i = \frac{\bar{m} * E_{is}}{0.0272 M_d} \quad (5.10)$$

Where h_i is the initial height (cm) from which the drop weight is released, $\bar{m}$ is the mean particle mass (g), E_{is} is the specific input energy and M_d is the mass of drop weight (kg).

The height from which the head is released should be adjusted to compensate for the fact that the drop head finishes some distance above the anvil due to the presence of the crushed particle. The average offset h_f can be measured for each samples of particles broken and the effective applied energy calculated:

$$E_{is} = \frac{0.0272 * M_d (h_i - h_f)}{\bar{m}} \quad (5.11)$$

The broken product from each set of particles is sized on a root 2 sieve series down to the sieve size smaller than the t_{100} size and the results reported together with the energies applied. This information is sufficient to provide the model parameters, which reflect the impact resistance of the ore under test.

5.4.4.2.3. Data Analysis

The results from the drop weight tests provide an energy input-feed size-product size relationship. The analytical procedure is based on the assumption that product size distributions are a function of input energy or specific comminution energy. To model the breakage process the JKMRC developed a method of relating energy to geometric size reduction. This relationship is analyzed using a set of curves, known as t parameter, to describe the size distribution resultant from breakage events of increasing size reduction or energy input. Each product size distribution curve is normalized with respect to the input size to give percentage-passing figures t_2, t_4, t_{25}, t_{50} and t_{75} for various fractions. Therefore, t_2 is the percentage passing ½ of the original feed size, t_{10} is the percentage passing 1/10th of the original feed size and t_{75}

is the percentage passing 1/75 of the original feed size. For each feed size, the size distribution curves from the breakage events are normalized by conveniently representing as one-parameter family of curves of the percentage passing figures t_2, t_4, t_{25}, t_{50} and t_{75} versus t_{10}, also referred to as appearance function, shown in Figure 5.42 (Narayanan and Whiten, 1988).

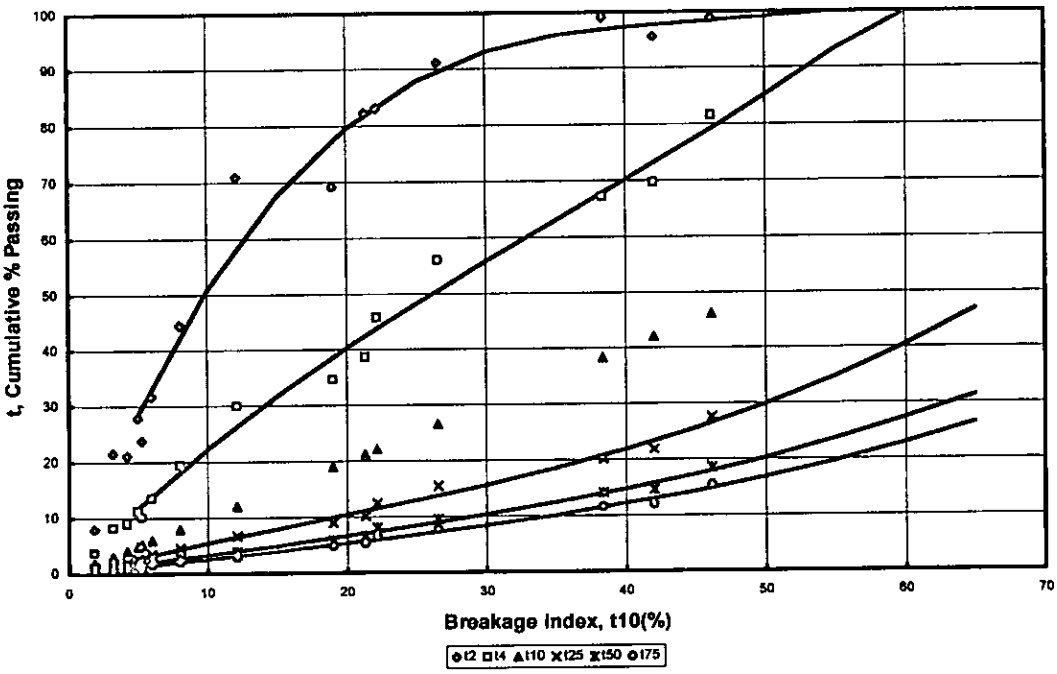

Figure 5.42. Appearance function relating t versus t10 (after Narayanan and Whiten, 1988).

From the resultant data it is also possible to derive the relationship between the breakage index t_{10} and the energy input, referred to as specific comminution energy by the equation:

$$t_{10} = A(1 - e^{-b.Ecs}) \tag{5.12}$$

where t_{10} is the percentage passing $1/10^{th}$ of the initial mean size, E_{cs} is the specific comminution energy (kWh/t) and A and b are ore impact breakage parameters. The value of parameter A, also referred to as the limiting value of t_{10}, indicates that at higher Ecs the size reduction process becomes less efficient (Napier Munn et al.,

1996). The product A*b is the slope of the curve t_{10} versus Ecs at the point of 'zero' input energy and is also known as the impact parameter.

5.4.4.3. Results of Standard Sample Drop Weight Test

A standard sample supplied by the JKMRC was received. The sample consisted of 15 sub-samples ready made to conduct a drop weight test as described on the Table 5.3. The sample weight of each set was taken and relative density measured on 30 particles of –31.5+26.5 size range. Thereafter, the required drop weight and height were calculated using an Excel spreadsheet customized by JKMRC. The drop weight test was then conducted and the breakage product size distributions calculated.

A key concept in analyzing data from the drop weight test and in establishing ore breakage functions is that the product size distributions are a function of the size reduction or specific comminution energy, Ecs (kWh/t). These breakage product size distributions, also known as appearance functions constitute an integral part of one class of mathematical models of industrial comminution equipment.

5.4.4.3.1 AG/SAG Mill Standard Sample Specific Parameters

According to Nappier-Munn (1996) in AG/SAG milling, size reduction occurs both by impact and abrasion. Therefore, the drop weight device provides an effective means for ore characterization for impact energy breakage. The generation of abrasion characteristics is carried out by a tumbling test, in which a quantity of ore is tested autogenously under a standard set of conditions, as described earlier. The AG/SAG mill appearance function for a given material is defined in terms of three breakage and abrasion parameters (A, b and Ta). The appearance function is size-energy dependent and is defined according to the equation 5.12. Ta is the abrasion parameter for AG/SAG mills. Napier-Munn also suggests that the effect of particle

size on the t_{10} versus Ecs relationship is usually negligible in hard rocks, but the A and b parameters may both be dependent on particle size, shape and ore type. Figure 5.43 shows the plot of t10 verses Ecs and the fitted SAG/AG mill parameters A and b for the standard sample supplied by JKMRC.

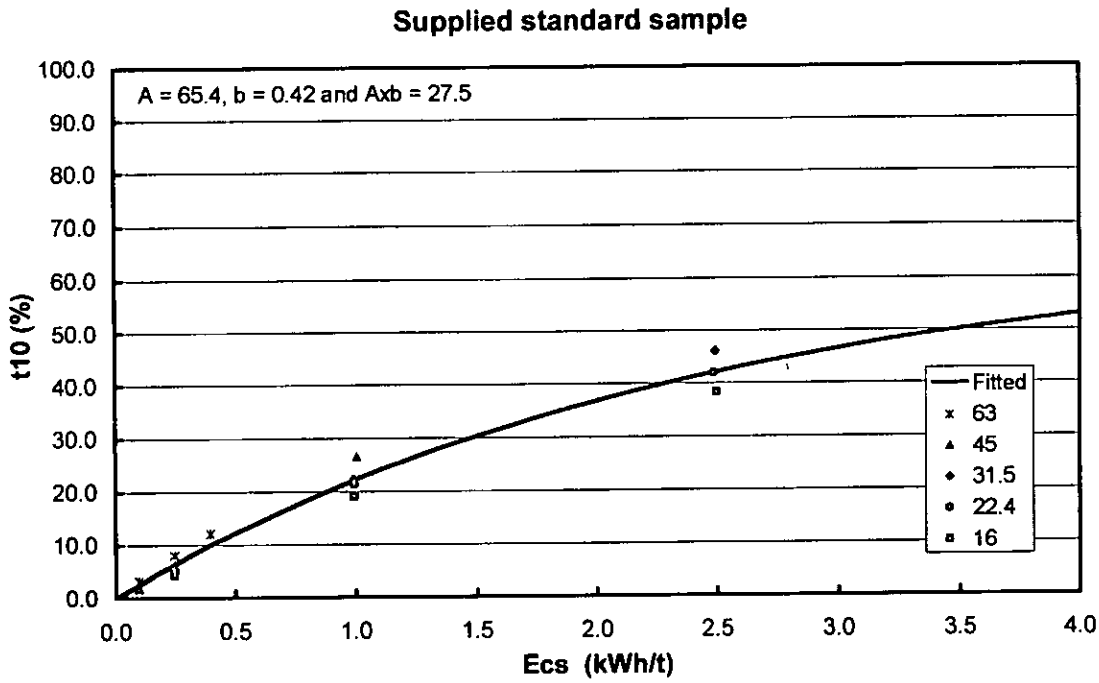

Figure 5.43. Relationship between t10 and Ecs for standard sample used for drop weight calibration and the SAG/AG mill parameters A and b.

5.4.4.3.2 Crusher Model Appearance Function

Unlike the AG/SAG mill, size reduction in a crusher is assumed to occur mainly by impact. The drop weight device is currently used to derive the energy- size reduction results to predict both the breakage and crusher power consumption (Andersen 1988 and Whiten 1974). The crusher model developed by Andersen uses the drop weight test results to determine two sets of ore specific crusher parameters:

- The appearance function which relates the degree of breakage, t_{10}, to the remainder of the size distribution and,

- The size-specific energy relation required to achieve a particular degree of breakage. The obtained results are given in Tables 5.4 and 5.5 for the standard sample supplied for drop weight test calibration purposes.

Table 5.4. Appearance function data, t_n (%)

t_{10} (%)	t_{75}	t_{50}	t_{25}	t_4	t_2
10	2.6	3.3	5.5	22.3	50.7
20	5.3	6.7	10.5	40.3	79.6
30	8.4	10.4	15.7	55.8	93.0

Table 5.5 Crusher Power data

Mean size (mm)					
t_{10} (%)	14.53	20.63	28.89	41.08	57.78
Ecs (kWh/t)					
10	0.50	0.43	0.42	0.35	0.32
20	1.08	0.94	0.90	0.74	0.72
30	1.78	1.55	1.44	1.19	1.19

5.4.4.4. Palabora Ore Sample Preparation

Four sets of Palabora ore samples for drop weight test were prepared. Sieving into the size intervals given in Table 5.3 was then used to generate the required particle size ranges. A random selection of the required number of particles for each set was then made and the mass determined. Then 30 additional particles in the 31.5 – 26.5mm range were selected for density measurements. In addition two sets of 3.0 Kg of ore sample were made for the autogenous grinding test.

Based on the results of point load test the conditions for microwave treatment were determined. Samples were irradiated in a 15 kW microwave treated on a single mode cavity for 0.2 seconds. After irradiation samples were immediately quenched in water to cool and then left overnight to dry.

5.4.4.5. Results and Discussion

The conditions for drop weight test were based on the results of point load test that had shown significant reductions on the strength of the ore. To investigate the effect of the microwave radiation on the breakage of ore, a drop weight test was carried out on two samples, one as received and one after exposure to microwaves. Before breakage, the microwave treated sample exhibited significant amounts of visible fractures and many pieces could be broken by hand. The untreated sample, by contrast was wholly competent. The untreated sample was drop weight tested at standard energy input as shown in Table 5.3 while the microwave treated was drop weight tested at 50% of the original energy input, as results of point load test had suggested, by reducing the nominal energies in Table 5.3 to new values as given in Table 5.6.

Table 5.6 Complete drop weight test with 50% of typical size energy combinations

Size particle, mm	No of particles	Nominal energy, kWh/t		
63x53	10	0.2	0.125	0.05
45x37.5	15	0.5	0.125	0.05
31.5x26.5	30	1.25	0.5	0.125
22.4x19	30	1.25	0.5	0.125
16x13.2	30	1.25	0.5	0.125

It was expected that significant differences would be observed in the appearance function and the subsequent breakage parameters for AG/SAG mill model as well as crusher power data. This, however, was not the case. Detailed examination of the parameter b showed significant differences, 1.83 and 2.48 for the untreated and

treated samples respectively. However the same was not observed from comparison of the crusher power and appearance function data between the untreated and microwave treated samples, as shown on Tables A2.2 and A2.5 in the Appendices. Despite tests conducted at different energy levels, the size distribution of the product as suggested by the crusher appearance function data shown on Tables A2.2 and A2.5 were close. However, the crusher power data did not show similar trend. Figure 5.44 illustrates the calculated percentage change of the crusher power data between the untreated and treated samples. Apart from the particles class with mean size 14.53mm that showed over 50% energy saving, the differences were relatively low compared to those suggested by the parameter b as well as from previous results of ore strength based on the point load test.

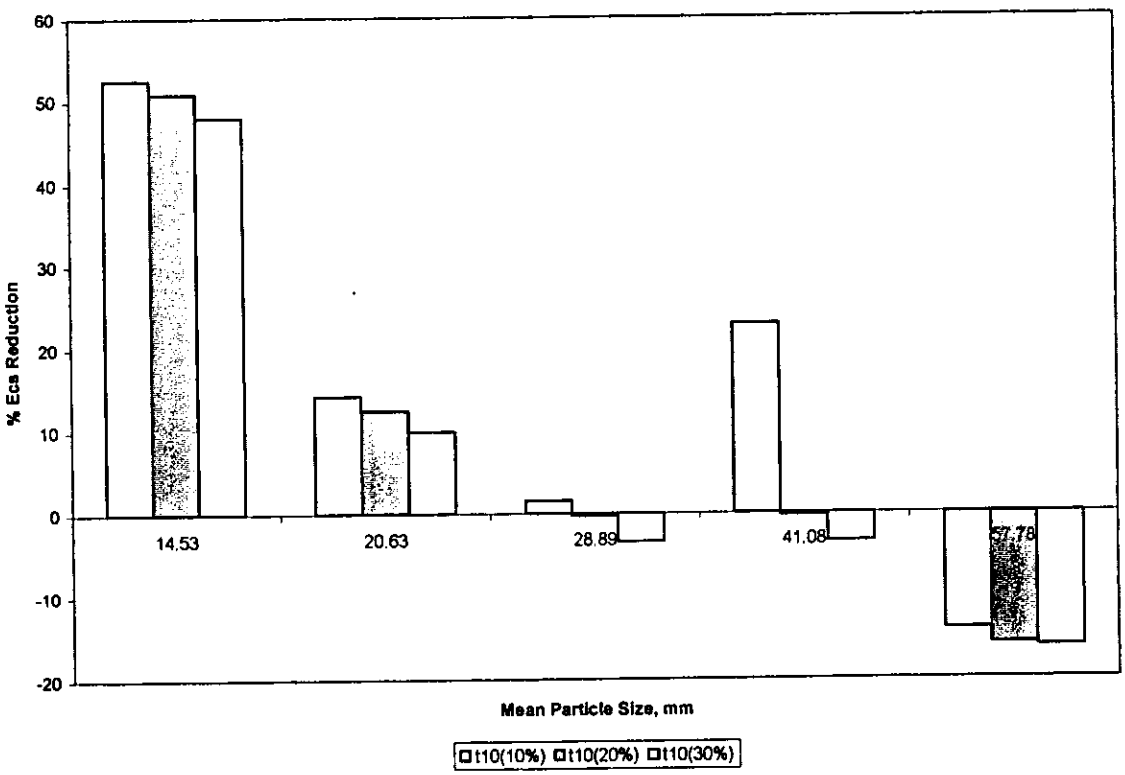

Figure 5.44. Comparative crusher power data of the untreated tested at 100% Ecs and microwave treated samples tested at 50%Ecs.

As stated by Bourgeois and Banini (2002), the drop weight tester does not give information about the actual energy absorbed by the rock particles during breakage

and it is therefore not possible to derive or estimate an ore property such as strength and fracture toughness. The ore strength as shown from the results of UCS and point load test showed significant difference between the untreated and microwave treated samples. After microwave treatment there is clearly significant weakening of the mineral phases and this appears to preferentially occur on grain boundaries as shown in Figures 5.27. It was therefore thought that the energy inputs used to break the ore particles were in excess of that required for breakage and the test could not distinguish between treated and untreated material. To address this problem the tests were repeated for treated and non-treated material at specific comminution energy inputs as shown in Tables 5.3 and 5.6 respectively.

In this experiment parameter b was found to be 1.61 for the untreated sample and tested at 50% of the standard input energy and 2.45 for the microwave treated sample tested at nominal input energies, i.e. no significant differences compared to the previous results (1.81 and 2.48 for untreated and microwave treated samples respectively). The results are shown on Tables A2.3 and A2.4 in the appendices. Comparison between untreated and microwave treated samples drop weight tested at energies levels described on Table 5.6 showed better results as illustrated in the Figure 5.45. Energy saving between 25 to 40% has been obtained.

Figure 5.46 shows the comparison of crusher power data between untreated and microwave treated samples drop weight tested at the standard energy input as described on Table 5.3. Because of the high stressing rates applied, this test could not show significant difference on the specific comminution energy compared to test carried out at low stressing rates (energy input as described on Table 5.6).

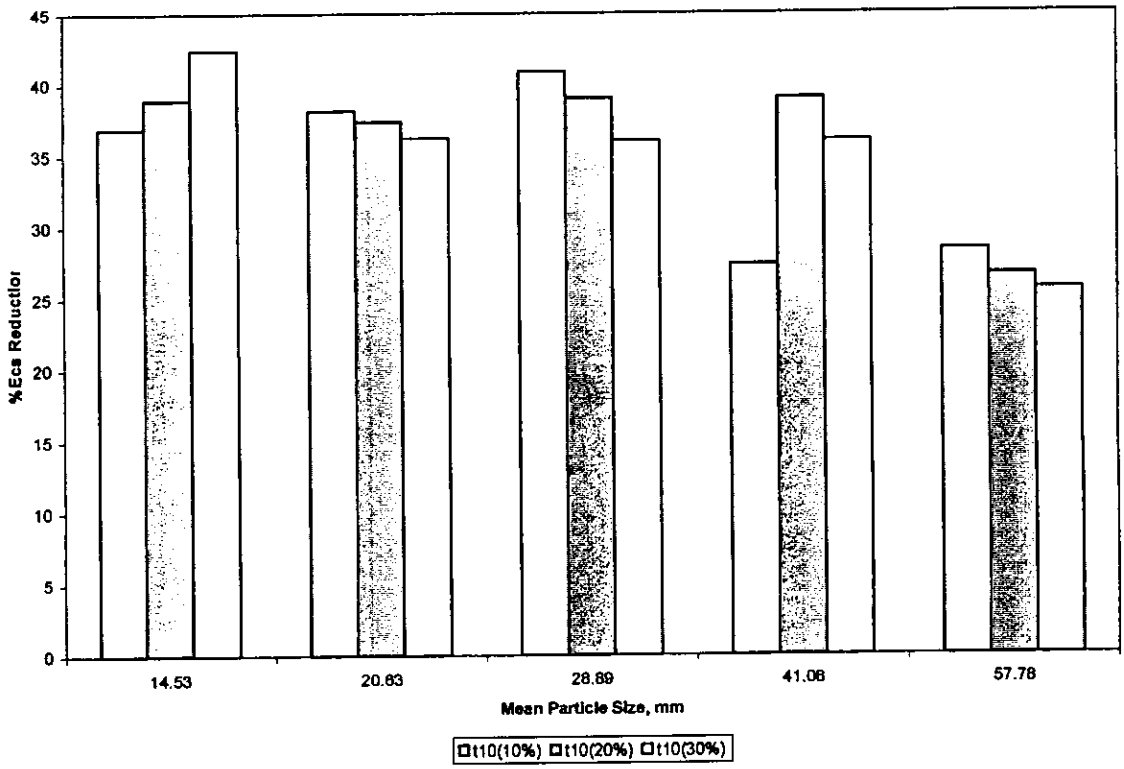

Figure 5.45. Comparative crusher power data for Palabora ore untreated and microwave treated. Drop weight test carried out at 50% of the original energy input (Ecs).

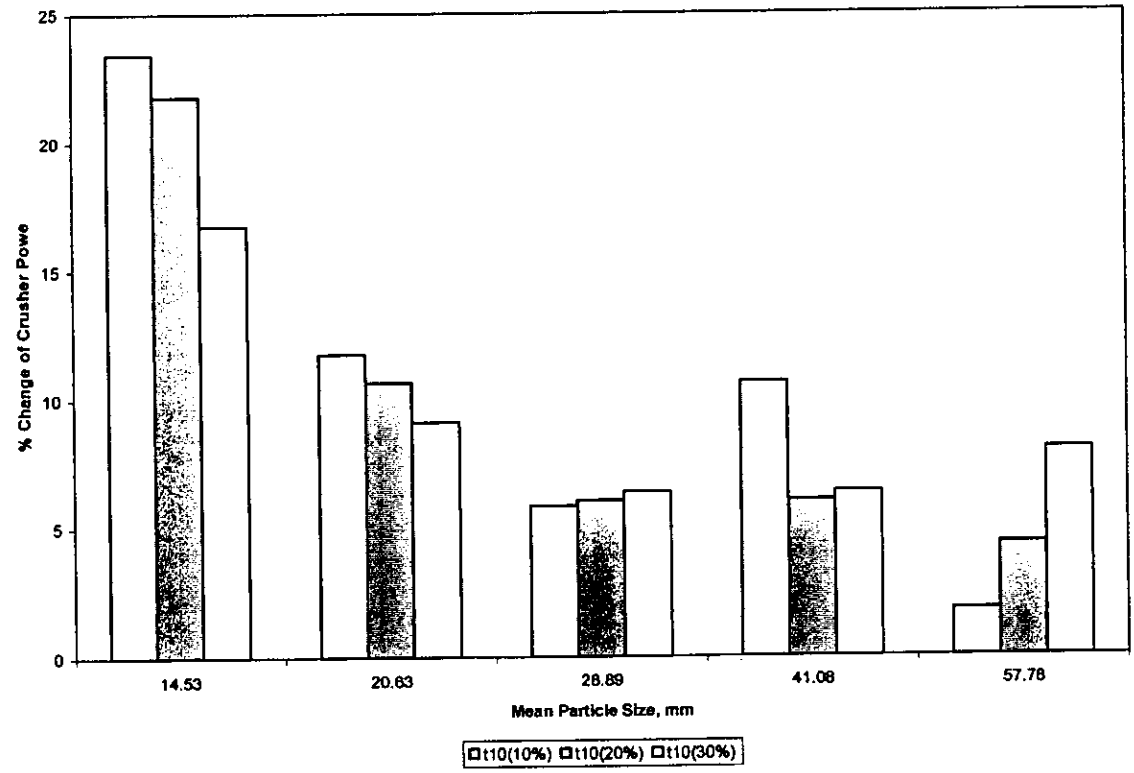

Figure 5.46. Comparative crusher power data for Palabora ore untreated and microwave treated. Drop weight test carried out at the original energy input.

Summarized results of drop weight test parameters A and b for four samples of Palabora ore are illustrated in Table 5.7. The results show higher values of parameter b for microwave treated samples compared to the untreated i.e. when the ore is microwave treated it became softer. Another interesting observation is that of the values of A and b for the two treated samples. They were drop weight tested at significant different energy levels but values of parameters A and b are similar. Therefore, it could be speculated that the actual design of drop weight test uses higher energy levels than those required to produce energy efficient breakage in the material.

Table 5.7. Drop weight test parameters for Palabora ore SAG/AG mills

Test run	Parameters			
	A	b	A.b	Ta
Untreated, full energy	63.2	1.83	115.7	0.64
Untreated, 50% energy	54.3	1.61	87.4	0.64
Treated 15 kW, 1s, 50% Ecs	54.5	2.48	135.2	1.04
Treated 15 kW, 1s, full energy	57.4	2.45	140.6	1.04
Treated 15kW 0.2s, 50% Ecs	52.5	2.35	123.4	0.97

The present findings suggest that drop weight testing may not be suitable for the comparison of particle breakage energy for microwave treated and untreated samples. It is known that the energy applied to break particulate material during comminution is far in excess of the minimum required (Wills and Atkinson, 1993; Hofler, 1991). Fracture and materials engineering literature also documents the fact that fracture paths become less influenced by microstructure at high stressing rates (Yang and Kobayashi, 1990, Freiman, 1984), which is the case of drop weight tester.

Because drop weight tests simulate the stress within comminution machines, it will have a tendency to significantly ignore the influence of the material microstructure. Microwave treatment of rock induces thermal stress cracks at grain boundaries that result in significant weakening of the rock. Test methods capable of distinguishing between mineralogical materials with weaker grain-boundaries are therefore required in place of the drop weight tester. Middlemiss and King (1996) have used the indentation crack technique to investigate fracture of materials with different mineral phases. They used a magnetite/hematite polycrystalline material and determined the fracture toughness, particle strength and energy of failure. They showed that despite the magnetite being a tough material, the grain boundaries were regions of weaker structure and when this material is under stress the fracture will occur at the grain boundary. This result was observed because indentation fracture is a relatively slow (quasi-static) and small-scale phenomenon that is significantly influenced by the microstructure of the material (Middlemiss and King, 1996).

The actual design methods of comminution processes using drop weight test results almost seem designed to ignore the effect of weaker microstructure. Crushers, SAG/AG mills and ball mills are designed ignoring such effects. Middlemiss and King (1996) have suggested that other methods of comminution, such as high pressure roll crushers and vibratory mills, that produce lower stressing rates may induce grain boundary fracture and thus enhance better mineral liberation.

Preliminary testing has been carried out on Palabora samples using the Hopkinson Pressure Bar, in conjunction with Chalmers University of Technology, Sweden. Two samples in the range –26+22.4mm consisting of 30 particles each were tested. One sample was microwave treated on a single mode cavity for 15 kW and 0.2 s exposure time and the second was kept for comparison. When conducting Hopkinson Pressure

Bar test, two parameters are measured: the energy of failure and the width of the specimen near the impact point. The energy of failure is determined from the point of sudden release of force on the force versus stiffness curve registered during the test. Size analysis was then carried out on the tested material on a $\sqrt{2}$ sieve series down to -38μm on each sample. The results are shown in Figure 5.47. It can be seen from the curve that size distribution of the product of the microwave treated sample is much finer compared to that of the untreated sample. It has also been found that the energy of failure for the untreated sample was 19.92±17.31 MPa while for microwave treated the value was 14.24±8.10 MPa, an energy saving of about 28%.

This work still ongoing and it is expected that data obtained from the test may be used to derive the breakage parameters of the JKMRC model and then in the JKSimMet steady state mineral processing plant simulator.

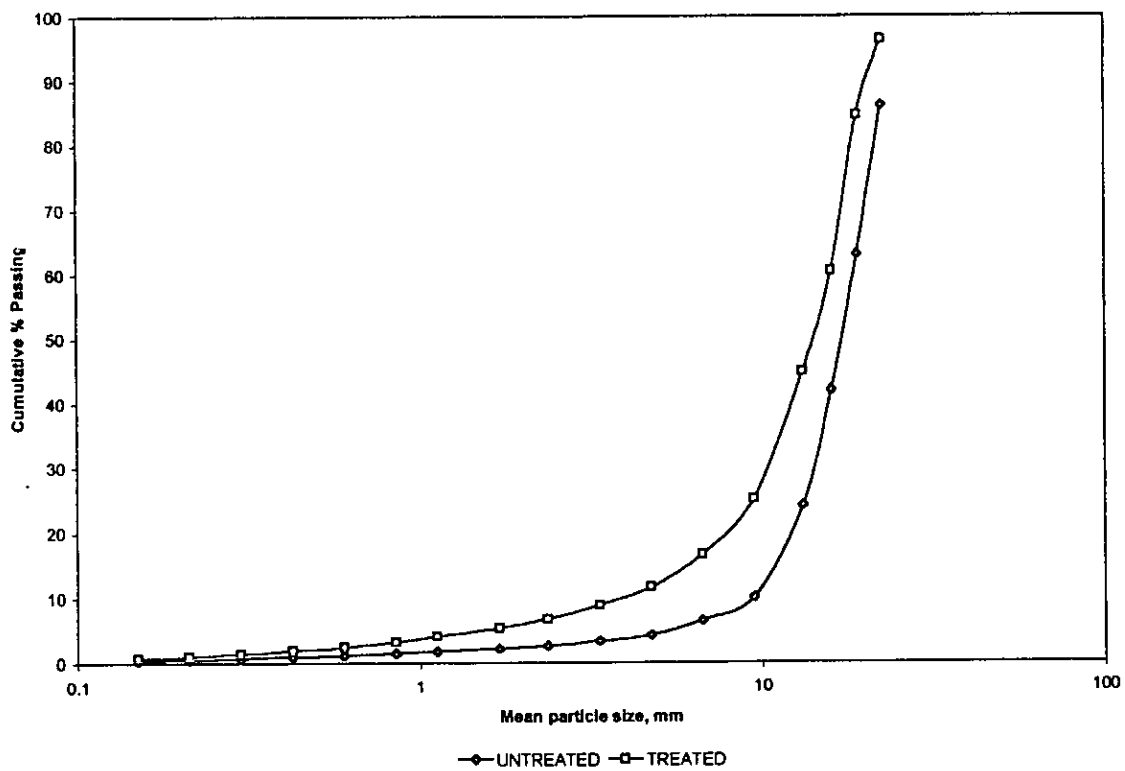

Figure 5.47. Size distribution of Hopkinson Pressure Bar test.

5.4.5. Influence of Microwave on Breakage Rate

Industrial grinding equipments used in the mineral processing industries are mostly of the tumbling mill type. These mills exist in a variety of types: rod, ball and pebble. According to King (2001) several models for characterization of grinding equipment have been developed and in use in the industry and specialized laboratories such as the Austin and Luckie, 1971; Herbst and Fuerstenau, 1980 and the JKMRC model developed by Whiten, (1974, 1976). The process engineering of milling circuits is intimately linked with the kinetic mechanisms that govern the rate at which the material is broken in a comminution machine (King, 2001). The grinding process can therefore be treated as a rate process. The discussion of breakage phenomena in previous sections has been based on the concept of individual impact events in which particles are broken in a single application of compressive stress.

The kinetics of a grinding process can be studied with batch grinding tests on discrete size classes that provide an adequate approximation for practical computation (King, 2001). The typical procedure involves batch grinding the material within a certain size fraction, from which the breakage rate of that size fraction is determined, together with the breakage function of the material. The breakage function is essentially a size distribution resulting from breakage, usually expressed in matrix form. The results of the test are interpreted in terms of the population balance model usually by estimating the values of the selection and breakage functions in the model (Napier-Munn, 1996).

The test material is classified into a specific size fraction usually as $\sqrt{2}$ size interval, and loaded into the mill. The selection of other grinding conditions depends on the objective of the test and should be as close as possible to the conditions envisaged for the final application. The material is discharged at milling times decided prior to the

test. After the product is sieved, the material and grinding media are reloaded into the mill. The test is repeated until a grinding time appropriate to the expected residence time is achieved. For the mono-size fraction tested, if the specific rate of breakage of the particles in the feed is constant, the following equation is valid (Austin and Weller 1982):

$$\frac{dm_1(t)}{dt} = -S_1 m_1(t) \tag{5.13}$$

where $m_1(t)$ is the mass percentage of the feed size at grinding time t and S_1 is the specific rate of breakage of the feed size (minute^{-1}). The integrated form of the equation may be written as:

$$\log m_1(t) = \log m_1(0) - \frac{S_1 t}{\ln 10} \tag{5.14}$$

Thus, by plotting the logarithm of the mass percentage remaining in the top size fraction, $m_1(t)$, versus the grinding time, t, the breakage rate of that size fraction, S_1, can be determined from the slope of the curve, which is usually linear for the ball grinding process. The mono-size grinding test is closely related to the population balance model that can be used to describe the breakage function of the material, Herbert and Fuerstenau (1968) and Austin and Luckie (1971).

After conducting the mono-size grinding test for a number of size fractions, the selection function based on the breakage rates can be estimated and fitted using the following equation (Austin and Brame, 1983).

$$S_i = A\left(\frac{x_i}{x_o}\right)^{\alpha}\left[\frac{1}{1+\left(x_i/\mu\right)^{m}}\right] \tag{5.15}$$

where x_i is the upper size of interval I, and x_o is a standard size. A, μ and m are parameters related to the grinding conditions and α is a characteristic of the material.

The breakage function of the material can be calculated using the population balance model by the equation (Napier-Munn et al., 1996):

$$\frac{dm_i(t)}{dt} = -S_i m_i(t) + \sum_{j=i+1}^{k} b_{ij} s_j m_j(t) \qquad \text{for i =1,2,3,...,k} \qquad (5.16)$$

Where b_{ij} is the discrete size breakage function.

5.4.5.1. Sample Preparation

The mono-size samples, below 19mm, described in Section 5.3.2 were used for testing. Riffling was then used to obtain a 2 kg sub-sample for test-work on each mono-size fraction. Each mono-size fraction was kept separate and riffled in half. One sub-sample was microwave treated in the single mode cavity at 15kW for 0.2 seconds and the other was kept for comparison.

5.4.5.2. Batch grinding test procedure

The mill used for the test was cylindrical in shape with smooth surfaces inside; the joints between the barrel and the end plates were filled in to maintain the integrity of the sample. The mill had the following internal dimensions: D=30.48cm L=30.48cm. The mill was rotated at a constant speed of 70 r.p.m. The ball charge consisted of 279 steel balls with total weight of 19.83kg.The distribution used is shown in Table 5.8.

Table 5.8. Ball charge used for batch grinding

Nominal Ball Size (in)	Number of balls	Weight (g)
1.55	20	5155
1.27	34	5025
1.00	54	3894
0.91	57	2929
0.71	114	2825
Total	**279**	**19828**

A five hundred grams sample of dry ore was placed in the mill, which was run for 35 revolutions at fixed speed of 70 r.p.m. The mill contents were removed, the ball charge screened out and returned to the mill. The product was then screened, using the lower size screen of each mono-size fraction. The undersize was weighed and the mass recorded. Thereafter the undersize and oversize were returned to the mill and then run for another 35 revolutions.

5.4.5.3. Results

The recorded masses of oversize retained for each batch-grinding test carried out for Palabora ore are summarized in the Appendices, Table A2.7. The data were then plotted as the natural logarithm of mass retained against grinding time. The slope of the curves also referred to as the specific rate of breakage (equation 5.13), were determined for each treated and untreated mono-size fractions and are summarized on Table 5.9. As comparative data were required for the analysis the results were then reported as percentage change of rate of breakage of untreated versus the mean particle size for each mono-size fraction. The results are also summarized on Table 5.9 and shown on Figure 5.48.

Table 5.9 Summary of the breakage rate and percentage change results

Mean Particle Size, mm	Breakage rate, s^{-1}		% Change of breakage rate
	Microwave treated	Untreated	
4.05	0.006	0.0054	11
5.72	0.005	0.0041	22
8.1	0.004	0.0026	54
11.5	0.0026	0.0016	62
17.5	0.0026	0.0015	73

Table 5.9 shows the comparative data of rate of breakage between Palabora untreated and microwave treated at 15kW microwave power in a single mode cavity for 0.2 seconds exposure time. Figure A2.6 illustrates graphically the relationship of breakage rate versus mean particle size for the microwave treated and untreated mono-size fractions.

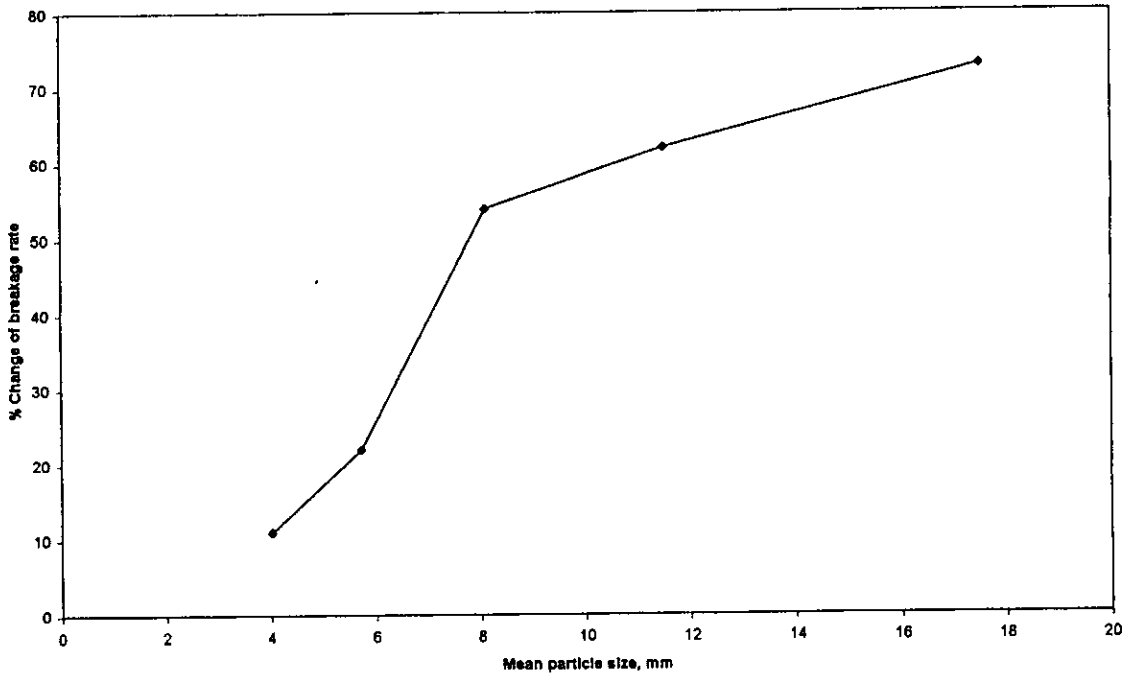

Figure 5.48. Effect of microwave treatment on breakage rate versus mean particle size relationship.

5.4.5.4. Discussion

The results have shown that the particle size has a significant effect on the change in grindability for a fixed microwave treatment. It has been found that microwave treatment has a significant effect on size particle range –19 + 6.7 mm with a change of the breakage rate greater than 50 percent.

The mineralogy of Palabora ore is dominated by the presence of a significant amount of transparent gangue. The bulk of the gangue grains range in size from a lower limit of 300μm to grains that exceed 8mm in size, as illustrated in Figures 5.5-5.13. The

bulk of copper bearing minerals and other accessory mineral grains range from a lower limit of 10μm to grains that may exceed 2mm, as illustrated in Figures 5.6, 5.11, 5.12, 5.13 and 5.17. The variations of grain size will thus have an effect on microwave treatment as well as on the breakage process.

The gangue minerals are effectively transparent to microwave radiation and as they have a low loss factor determined in Section 4.5. Thus, most of the microwave energy will be deposited in the copper-bearing minerals and any other accessory minerals that couple with microwave radiation, such as magnetite. The result is that differential heating may occur and thermal stress would be induced at the grain boundary, weakening the microstructure of the ore.

The results illustrated on Table 5.9 show that breakage rate decreases with increase of particle size and at a certain point it become constant. This suggests that as the particle size increases they are less likely to be broken during any typical impact in the mill. According to King (2001), the specific rate of breakage increases with particle size, which reflects the decreasing strength of the particles as the size increases. This is attributed to the greater density of micro-flaws in the interior of larger particles and to the greater likelihood that a particular large particle will contain a flaw that will initiate fracture under the prevailing stress conditions in the mill. However, the decrease in particle strength does not lead to an indefinite increase in the specific rate of breakage. King (2001) also suggested that as the particle size becomes significant compared to the smallest grinding media, the prevailing stress levels in the mill are insufficient to cause fracture and the specific rate of breakage passes through a maximum and decreases with further increase in particle size. It is interesting to note that large particles show a greater difference in breakage rate between microwave treated and untreated samples. This can be

explained by the fact that microwaves have more probability to create more micro-cracks on large particles than the smaller ones because of the surface area. Large particles have small surface area and therefore less heat dissipation. This results in high temperature gradient between minerals with consequence on high thermal stresses being developed.

5.4.6. Effect of Microwave Treatment on Ore Bond Work Index

5.4.6.1. Introduction

The most widely used parameter to evaluate the comminution energy requirements of ores is the Bond Work Index (Wi) (Mosher and Tague, 2001), also referred to as the correlation between material toughness and power requirement in the comminution machine (King, 2001). The test has been in use since the late 1920's (Mosher and Tague, 2001) and laboratories and operations around world use the procedure as a component of comminution circuit design and evaluation of plant performance. The standard laboratory test for the measurement of the power requirements in the comminution machine, expressed by the empirical Bond (1961, 1962) equation, was designed to produce an index that would correctly predict the power required by a wet overflow discharge ball mill of 2.44 m diameter that operates in closed circuit with a classifier at 250% circulating load (King 2001). Bond (1961 and 1962) developed a theory, which was based on the assumption that the work input is proportional to the new crack tip length produced in particle breakage. Bond's equation can be expressed as

$$W = \frac{10W_i}{\sqrt{P}} - \frac{10W_i}{\sqrt{F}} \qquad (5.17)$$

Where Wi is the Bond Work Index, P is the size in microns which 80% of the product passes, F is the size in microns which 80% of the feed passes and W the

work input in kilowatt hours per ton. The work index is the comminution parameter, which expresses the resistance of the material to crushing and grinding. Numerically it is the energy input (or kilowatt hours per ton) required to reduce the material from theoretically infinite feed size to 80% passing 100μm. Table 5.10 shows some values of Bond Work Index for some common materials.

Table 5.10 Selection of Bond work indices for common materials (Kingman, 1999)

Material	Bond Work Index (KWh/t)
Bauxite	8.78
Coal	13.00
Quartz	13.57
Limestone	12.74
Granite	15.13
Ferro-silicon	10.01
Fluorspar	8.91
Graphite	43.56

5.4.6.2. Sample Preparation

A bulk representative sample, which was 100% passing 3.35 mm was used for the present investigation. Riffling was used to obtain approximately 20kg of material for the test. The sample was then riffled to produce two sub samples of approximately 10kg, as required by the Bond test procedure. One sub-sample was then microwave treated in a single mode cavity, at 15kW for 0.2 seconds, and the other sample was kept for comparison. The test material was then closely sized using a $\sqrt[3]{2}$ sieve progression from 2.8mm down to -45μm. Each fraction was kept separate and the overall size distribution calculated.

Based on the results of rate of breakage tests, which had shown that microwave treatment is more effective on large particles compared to the small ones, a sub-

sample within the size range –19+13.2mm was also prepared. Approximately 10 kg of this fraction was microwave treated in a single mode cavity, at 15kW for 0.2 seconds and was then jaw crushed to produce material that was 100% passing 3.35mm as required by the Bond test procedure. The material was then closely sized using a $\sqrt[4]{2}$ sieve progression from 3.35mm down to -38μm. A summary of sample description and preparation is given in the table below.

Table 5.11 Sample description for Bond Work Index test

Reference	Sample description	Preparation
BWIT_P01	Palabora –3.35mm	Untreated
BWIT_P02	Palabora –3.35mm	Microwave treated at 15kW for 0.2 s
BWIT_P03	Palabora –19+13.2mm	Microwave treated at 15kW for 0.2s and jaw crushed

5.4.6.3. Bond Work Index Test Procedure

The procedure for the determination of the Bond Work Index is as follows (Bond, 1961 and Berry 1966).

5.4.6.3.1. Sample Preparation

A 1000ml graduated measuring cylinder was packed with ore to the 700cm^3 mark. It was then shaken until compact and the mass determined. This "unit volume" of 700cm^3 was selected as the volume of ore always present in the mill during closed circuit grinding. The mass was noted at the beginning of each grinding cycle.

5.4.6.3.2. Test Mill and Charge

The mill used for the test was cylindrical in shape with smooth inside surfaces; the joints between the barrel and the end plates were filled in to maintain the integrity of the sample. The mill had the following internal dimensions: D=30.48cm L=30.48cm. The mill was rotated at a constant speed of 70 r.p.m. The ball charge consisted of 279 steel balls with total weight of 19.83kg.The distribution used is shown in Table 5.8.

5.4.6.3.3. Test Procedure

A "unit volume" (700cm^3) sample of dry minus 3.35mm ore was placed in the standard mill with the specified ball charge. The mill was then run for 50 revolutions at the standard speed of 70 r.p.m. The mill contents were removed and the ball charge screened out; this was returned to the mill. The ground material was then screened on a sieve of 180μm (P_1). The material finer than mesh (P_1) was weighed and the mass of material finer than P_1 produced by grinding calculated. The figure was divided by the total number of mill revolutions to give the grindability figure G (g/rev).

A new feed sample was then weighed. This was of equal in mass to that removed. To ensure that the size distribution of the new material was equal to that of the original feed, riffling was used. The new feed was placed back into the mill along with the circulating load (oversize) and the mill charge. At equilibrium, under standard conditions, 28.6% of the mill discharge should be finer than P_1. This is equivalent to a circulating load of 250%. The number of revolutions to produce an equivalent mill discharge to that at equilibrium is calculated by the difference between mass finer than P_1 at equilibrium and that in the new feed added. The mill is run for the number of revolutions and the procedure repeated. This was then repeated until the net

production of material finer than P_1 (in g/rev) reached a constant value for a minimum of three cycles.

The product (finer than P_1) was riffled to get a representative sample of about 100 grams and then sieved by $\sqrt[3]{2}$ sieve progression and the 80% passing size determined. The Bond Work Index was then determined from the following equation (Bond, 1961).

$$Wi = \frac{4.45}{P_1^{0.22} G^{0.8} (P^{-0.5} - F^{-0.5})} \tag{5.18}$$

Where,

P_1 = size of test product (μm)

G = grindability factor (g/rev)

P = 80% passing size of product (μm)

F = 80% passing size of feed (μm)

5.4.6.4. Results

The results of size analyses of the feed and product are shown in appendices Figures A2.7, A2.8 and A2.9. F_{80} (size particle for which cumulative percentage of material passing is 80%) was found to be 1.500mm. The mass of unit volume was 1455.2g. The working index test was conducted at P_1=180μm particle size. From the size analysis, the percentage of material <180μm was determined.

Tables A2.8 and A2.9 in Appendices show the results of the recorded data during grinding test for non-treated and microwave treated samples. From the plots in appendices Figures A2.7, A2.8 and A2.9 of the size distribution the F_{80} (initial feed) and P_{80} (final product for the untreated and microwave treated samples) were determined and from the Tables A2.8 and A2.9 the grindability of untreated and microwave treated samples. Then the equation 5.18 was applied.

For the untreated sample:

$$Wi = \frac{4.45}{180^{0.22}1.81^{0.8}(135^{-0.5} - 2000^{-0.5})} = 12.89kWh/t$$

For the microwave treated sample:

$$Wi = \frac{4.45}{180^{0.22}2.0^{0.8}(140^{-0.5} - 2000^{-0.5})} = 12.20kWh/t$$

Based on these data, the present result shows a decrease of Bond Work Index of about 5.35%, which follow the trend that has been observed on breakage rate characterization. Therefore, application of microwave treatment at the grinding circuit does not bring any benefit to the process economic compared with the application at the crushing stage.

To further investigate the effect of microwave treatment upon the grindability of Palabora ore, and based on the results of breakage rate characterization an additional Bond Work Index test was carried out. Figure A2.7, in appendix, shows the initial size distribution of the sample BWIT_P03 described on Table 5.11 after microwave treatment and jaw crushing. Table A2.10, in appendices, shows the recorded data during grinding test and Figure A2.10 the size distribution of the final product.

From the plots in appendices Figures A2.10 and A2.11 the F_{80} (initial feed) and P_{80} (final product for the untreated and microwave treated samples) were determined. From Table A2.10 in appendices the grindability of the microwave treated sample P03 was determined. Then the equation 5.18 was applied.

$$Wi = \frac{4.45}{180^{0.22}2.20^{0.8}(135^{-0.5} - 2400^{-0.5})} = 11.43kWh/t$$

The results of Bond Work Index are summarized on the Table 5.12 below.

Table 5.12 Summary of BWI results

Sample ref.	F_{80}	P_{80}	G (g/rev)	BW_i, kWh.t^{-1}
BWIT_P01	2000	140	1.81	12.89
BWIT_P02	2000	135	2.00	12.20
BWIT_P03	2400	135	2.20	11.38

It has been found that BWI for Palabora ore as calculated on the present work is 12.89. The microwave treated samples BWI has been found to be 12.20 and 11.38, about 5.35% and 11.3% change in comparison with the untreated sample.

5.4.6.5. Discussion

A detailed study into the accuracy and reproducibility of the standard Bond Work Index test has been carried out (Laplant 1988). It was found that the main sources of error in the test were the representativity of the sample used and the test itself. It is stated that test errors were likely to originate from screening and grinding. A detailed series of tests found the accuracy to be between 0.2 and 0.33 kWh/t. Reproducibility was estimated to be 0.13kWh/t. In the present research, caution has always been observed in the preparation of representative samples. Using a Russell motorized sieve method had the advantage of a large screening area and, therefore, minimization of the error due to the loss of sample when using small sieves.

Microwave treatment has been found to be more effective when applied to large particles compared to smaller particles. These differences could be explained by the fact that large particles have smaller surface area and therefore less affected by heat dissipation during microwave treatment. This results in high temperature gradient

between mineral phases, which is responsible for developing stress cracking, while small particles have bigger surface area, which result in low temperature gradients and so fewer stress cracks developed.

The present results may also contrast with previous results reported by Kingman 1998 and Vorster et al 2000 where it has been found that Palabora ore Bond Work Index could be reduced for up to 80% on ore microwave treated in a multimode with exposure time up to 240s. The differences may be explained by the fact that long exposure times result on microstructure weakening due to the decomposition of mineral phases due to heat treatment. Long exposures times have been found to cause heat transfer by conduction between mineral phases (Whittles et al. 2003). Since an effect has been observed within the grain size range of mineral liberation, further investigation on down stream processes is needed to evaluate the benefits of long exposure time.

5.5. Effect of Microwave Treatment on Mineral Liberation

Liberation size is defined as the size to which the comminution step must reduce the rock to ensure an economic level of separation of valuable components from the gangue Napier Munn, 1996). To ensure an efficient process, therefore, mineral liberation and its association with size reduction should be well characterized. Understanding and describing mineral liberation requires the characterization of mineral phases within a rock both before and after comminution.

The classical method of characterization of mineral phases in a rock or broken particles has been based on mineral identification, fractionation and counting under a binocular microscope. Recent developments, however, have produced automated

systems for mineral phase identification and determination of the degree of liberation. One such system is the Quantitative Evaluation of Materials using Scanning Electron Microscopy (QEM*SEM), developed by CSIRO (Commonwealth Scientific, Industrial Research Organisation) Division of Minerals (Napier Munn, 1996). The system comprises a computer controlled scanning electron microscope using backscattered electron signals to identify and rapidly locate the particle phase and X-ray detectors to identify the elements and provide their relative proportions. The results are then presented in tabular format on a size-by-size and mineral-by-mineral basis. They are also described pictorially in false colour maps in which the outline of each particle and the phases present are shown. Such maps are helpful in obtaining a qualitative indication of the degree of liberation and nature of locking for a particular process stream.

5.5.1. Sample Preparation

A representative sample was produced from samples previously used for drop weight tests. Two samples, each with 100 randomly selected particles, were made from the mono-size fraction 22.4x19mm. One sample was microwave treated on a single mode cavity, 15kW for 0.2 seconds and the other was kept for comparison. Thereafter, single particle breakage using drop weight tester was carried out on both treated and untreated samples. An equivalent of 2.5 kWh/t was the energy level used for breakage. Then, the samples were screened using 1.0 mm sieve size and the undersize sent for QEM*SEM analysis.

5.5.2. Mineral Liberation Test Procedure

Upon their receipt at the laboratory, a representative sub-samples from each of the samples was obtained by riffling for chemical assay of the head sample. The

remaining were screened into four size fractions *viz.* +500 μm, +150/-500 μm, +38/-150 μm, and –38 μm. Individual size fractions were submitted for chemical assay. Cu, Fe, Pb and Zn were determined by an Inductively Coupled Plasma Mass Spectrometry (ICP).

The size fractions were also submitted for quantitative mineralogical characterization. Representative sub-samples were mounted in chlorinated epoxy resin, polished and carbon coated for analysis by QEM*SEM.

5.5.3. Results and Discussion

In QEM*SEM analysis, three category particle type were defined as described on the Table 5.13 below:

Table 5.13. Palabora ore particle types.

Liberated- >80% liberated	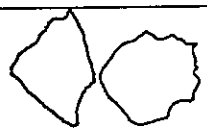
Middling– 30-80% liberated	
Locked<30% liberated	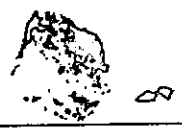

The degree of liberation by random breakage depends on the extent of size reduction and varies with structural features of multiphase particles (Lin et al, 1988). In certain cases, the extent of liberation may be increased due to preferential breakage at phase boundaries, due to weaker interfaces within the particles (Bradt et al., 1995; Middlemiss et al., 1996 and Atkinson and Meredith 1987). The preferential breakage phenomenon, which enhances the degree of liberation, is determined by both particle

size and by the interfacial strength of the mineral phases within the particle. As suggested by Bradt et al., (1995) and Middlemiss and King (1996), in some cases, it would be expected that there exists a critical particle size below which preferential breakage occurs at the phase boundary within the particle, thus yielding liberated mineral phases. However, Middlemiss and King (1996) further suggested that selective fracture in the grain boundary region produces poor liberation at finer particle sizes, because comminution processes have been designed to ignore the effect of material with weaker grain boundaries.

Kingman et al., (1998) suggested two mechanisms of microwave interaction with material:

- The weakening of the mineral lattice and thus reducing the macroscopic cohesion or
- The volumetric expansion that leads to the formation of inter-granular cracks.

The QEM*SEM results, shown in Figure 5.49 are the liberation characteristics of copper sulphides in Palabora ore untreated and microwave treated samples respectively, by grade and particle size.

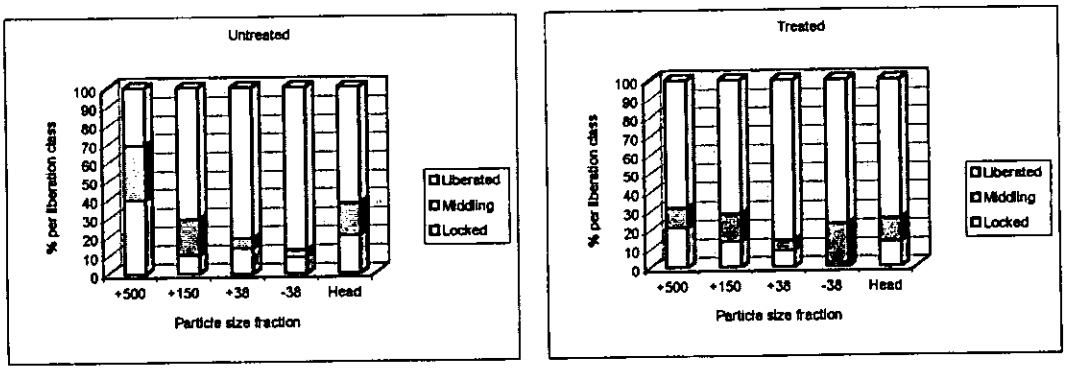

Figure 5.49. Copper sulphides liberation.

It has been found that microwave treatment of Palabora ore improves the liberation of copper sulphides and iron oxide particularly in the +500 μm fraction. The results of chemical assays and ICP are summarized in Appendix, Table A2.11.

For copper-sulphide minerals there is a significant decrease in locked and middling material in the +500 μm fraction for the microwave treated sample. These results, if associated with the mineralogy of the ore as illustrated in Figure 5.5, suggest that microwave radiation induces preferential breakage at grain boundaries. Figure 5.5 shows copper-sulphide lamellae as bornite in a matrix of dolomite. Given the difference in dielectric loss factor for these minerals, it is clear that, under microwave radiation, differential heating will occur and thus induce thermal stress at grain boundaries.

The QEM*SEM results for iron-oxide liberation characteristics for untreated and treated samples are shown in Figure 5.50. For iron-oxide minerals there is an increase in the locked and middling material in the –38 μm fraction in the microwave treated sample compared to the untreated. Therefore, microwave induces a different kind of breakage on these minerals. Whilst in untreated material iron-oxide appears liberated, suggesting a preferential breakage on grain boundaries, in microwave treated samples there is an increase of middling and locked minerals. This suggesting that iron-oxide grains become weaker after exposure to microwave radiation and, therefore, breakage occurs within the grain structures rather than at the grain boundaries.

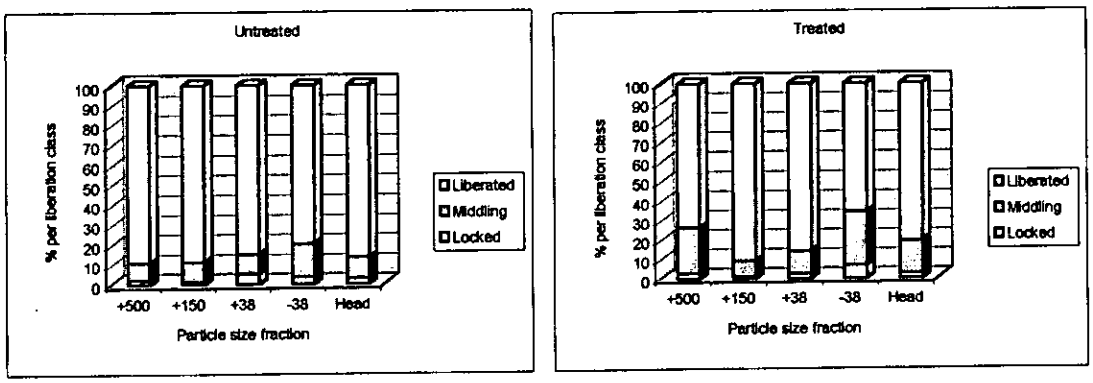

Figure 5.50. Iron-oxide liberation

However, as suggested by Middlemiss and King, the application of comminution techniques based on high stress rates will result in poor liberation of fine particles. It is, therefore, important that a breakage test method that produces lower stress rates, such as the Hopkinson pressure bar and the ultrafast load cell may thus enhance the mineral liberation.

5.6. Conclusions

This study has shown that microwave cavity type has a significant effect on the power density generated within the material under treatment. Single mode cavities have the ability to generate high power densities within the material compared to a multimode cavity because the material can be placed in the region of high electric field strength due to the known position of the standing wave.

The effect of microwave treatment upon the Palabora ore strength has been investigated. Two methods for measurement of rock strength available at the University of Nottingham have been used: the uniaxial compressive strength and point load. It has been found that short exposure times and high microwave power density is the most energy efficient practice for achieving a significant reduction in ore strength. The ability of a single mode cavity to generate a standing wave results

in the material to be treated being positioned at the region of highest electric field. If an ore consisting of minerals with a difference in dielectric properties (loss factor) is exposed to microwave radiation in a single mode cavity, the high loss material will absorb most of the microwave power and high temperature gradients are developed. This results in cracks being induced by thermal stresses that weaken the ore.

In reviewing the present findings it is worth noting the low accuracy of the method used, i.e. the Point Load on irregular particles. It has been reported that results are usually highly scattered, which was also found in this work. Standard deviation of the experimental data is, in many cases, the same order of magnitude of the mean value. Nevertheless, as it was used only for a preliminary assessment of the effect of microwave power and exposure time, the conditions for carrying further tests using more accurate methods can be selected.

A drop weight tester has also been used for characterization of the microwave effect on the comminution machines such as crushers and AG/SAG mills. It has been found that a drop weight tester is not a suitable tool for the investigation of microwave effect. Because of the high stressing rates developed on drop weight tester, assessing the microwave effect was possible by lowering the energy input for up to 50% of the energies recommended by JKMRC. Preliminary tests carried out using the Hopkinson Pressure Bar suggest that this may be the way forward for characterization of the effective energy in comminution machines. The characterization of the rate of breakage in tumbling mills have also been used to assess the effect of microwave radiation in the comminution processes. The test has

shown that significant reductions of breakage rate of over 50% can be obtained in ball mill and these reductions are intimately related to size particles.

Quantification of the effect of microwave radiation on mineral liberation has also been carried out. QEM*SEM data has shown an increase of liberation of copper sulphides on coarse size when applying microwave treatment.

CHAPTER SIX
Investigation on Microwave Assisted Comminution and Liberation of Zinkgruvan Ore

6.1. Introduction

The ore at Zinkgruvan contains minerals of lead and zinc. The most common ore forming lead mineral is galena (PbS) and it is often found associated with other metals such as zinc, silver and copper. The world's major producers of lead are Australia, China and the USA (Gaal & Gorbatschev, 1987). Lead is derived from the Latin word "plumbus"; hence the symbol Pb. Lead is a dense, malleable bluish-grey metal whose physical and chemical properties find application in a variety of uses in the manufacturing, construction and chemical industries.

Zinc ore is commonly associated with copper, lead and gold and is often produced as a by-product in these operations. The main ore mineral of zinc is sphalerite (Zn,FeS). Australia, Canada and China are the world's major producers of zinc. Zinc (Zn) is commonly used for coating iron and steel products in order to make them corrosion resistant. This zinc coating is known as galvanising and represents about 40% of the end use for zinc. Zinc is also a major product in brass alloys, die casting alloys, chemicals and rolled zinc products (Gaal & Gorbatschev, 1987).

6.1.1 Geology And Reserves

The Zinkgruvan ore deposit is located in the Bergslagen district of Sweden (Gaal & Gorbatschev 1987). The stratiform Zn-Pb-Ag ore deposit, as shown in Figure 6.1, consists of several thin ore sheets that have been cut and deformed by various faults and tectonic events (Stephens et al. 1996). The proven and probable reserves of the deposit are 11,900,000 tons at 10% Zn, 4.4% Pb and 90g/t Ag together with an

additional 2,700,000 tons at 3% Cu and 52g/t Ag (North Ltd, Concise Annual Report 1999).

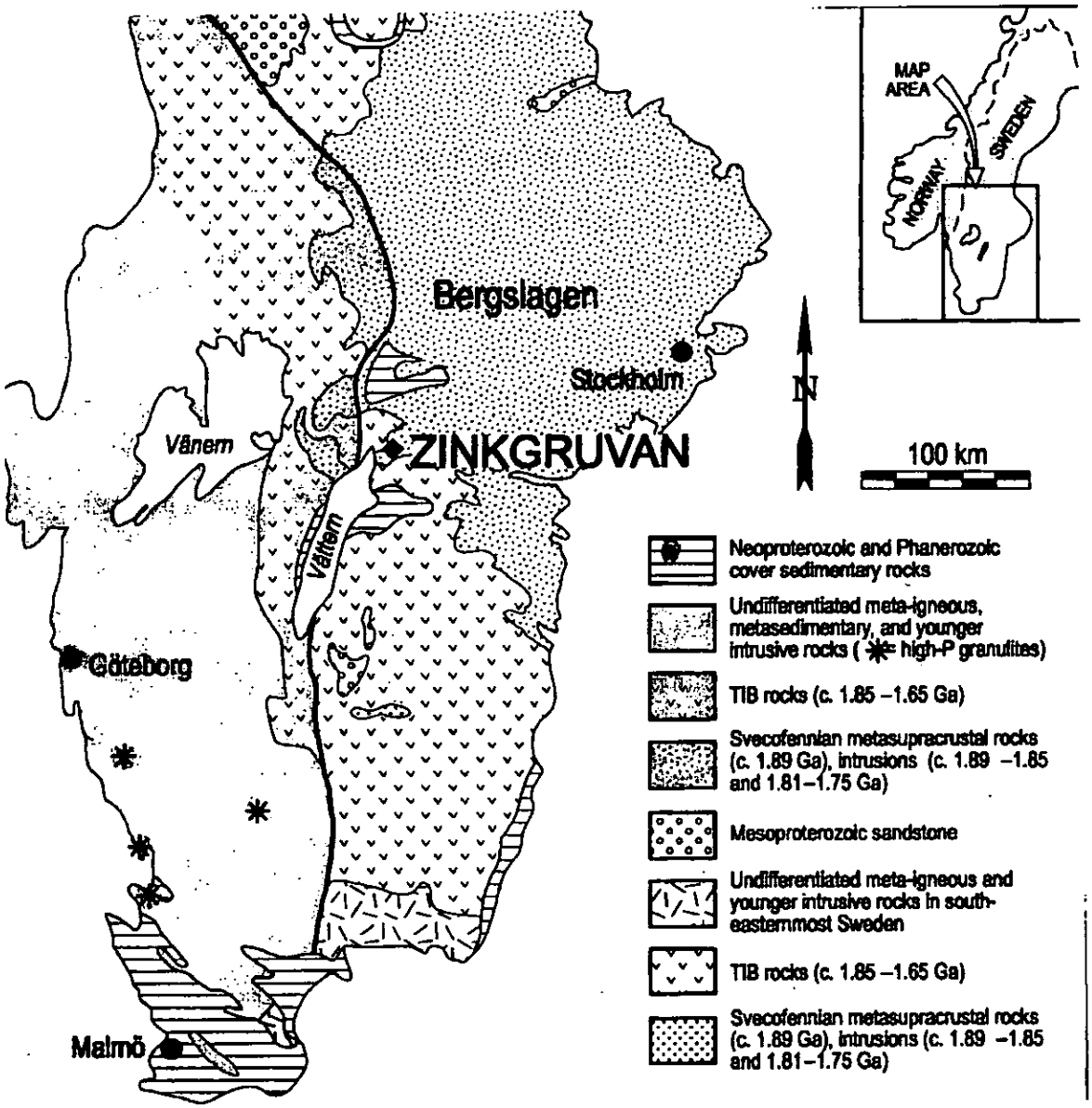

Figure 6.1 Geology of southern Sweden (after Stephens et al. 1996).

The ore genesis event that formed the Zinkgruvan ore deposit is still not well understood. However, the Zinkgruvan ore body has been interpreted as a Broken Hill type deposit (Plimer 1988, Beeson 1990, Parr & Plimer 1993). Broken Hill type

deposits are characterized by the stratigraphic sequence of the host rock package and the associated volcanism and the subsequent high-grade metamorphism.

The Zinkgruvan ore deposit is hosted by a lithological sequence consisting of three rock types, (1) a red, fine grained, massive to foliated quartzofeldspathic rock, (2) the ore bearing, grey, fine grained, massive to foliated, occasionally skarn banded quartzofeldspathic rock and (3) veined gneisses (Figure 6.2).

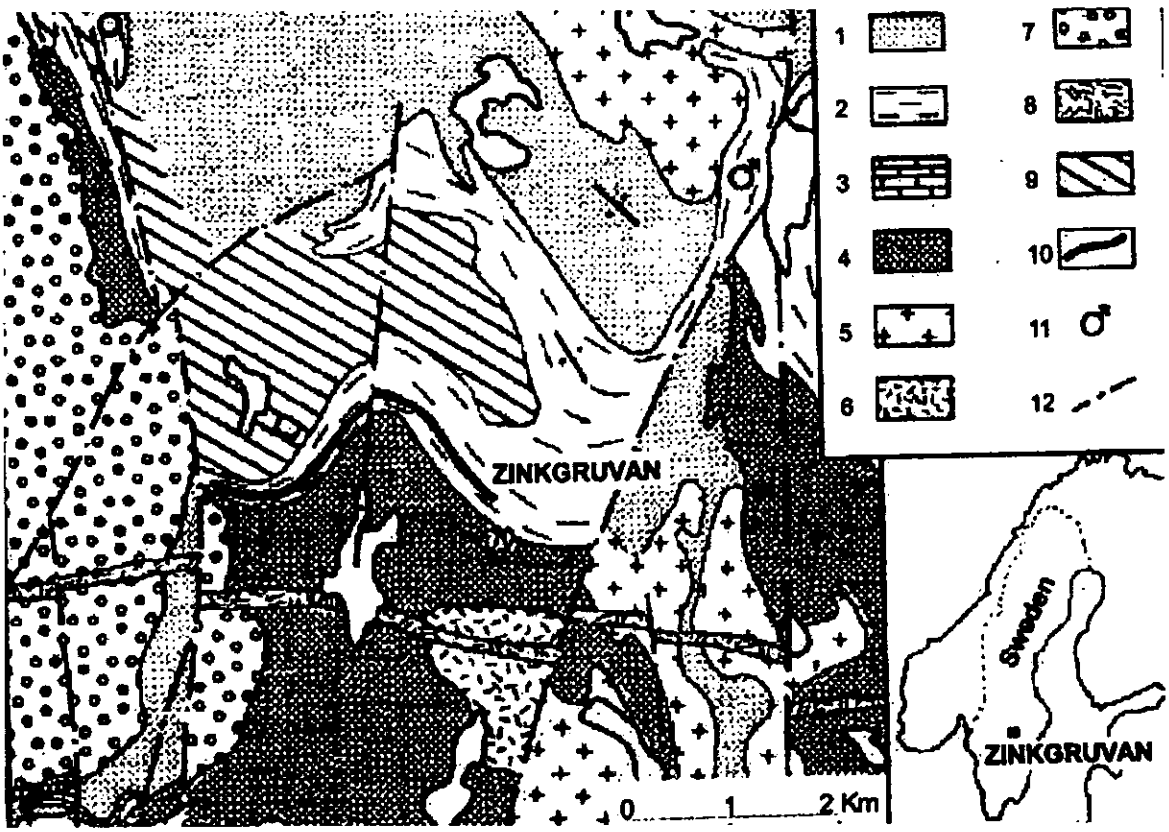

Figure 6.2. Geological map of the Zinkgruvan ore (after Bengtsson, VC 2000).

1-felsic volcanic rock, 2-metatuffite, 3-marble, 4-argilic metasediment, 5-early orogenic granitoids, 6-late orogenic granites and pegmatites, 7-postorogenic granites, 8-dolerite, 9-quartz microcline rock, 10-Zinkgruvan ore, 11-iron oxide mineralisation, 12-fault.

The ore hosting unit that has been interpreted as a metatuffite by Hedstrom et al. (1989) and it consists of a grey, fine grained massive to layered rock, which is

dominated by quartz and feldspar. It also contains accessory minerals and varying amounts of biotite, sillimanite, cordierite, garnet, pyroxene, amphibole, epidote and carbonates. Within the ore-hosting unit there are some thin impure marbles as well as some thin calcsilicate rich layers. Pyrrhotite can also be found disseminated within the ore.

6.1.2. Ore Processing

Autogenous and ball mills liberate the galena and sphalerite minerals, which are extracted by rougher-scavenger flotation followed by pebble regrinding and cleaning. Larox and Svedala pressure filters dewater the concentrates (Johan et al., 2002). The schematic diagram of the grinding circuit is shown in Figure 6.3.

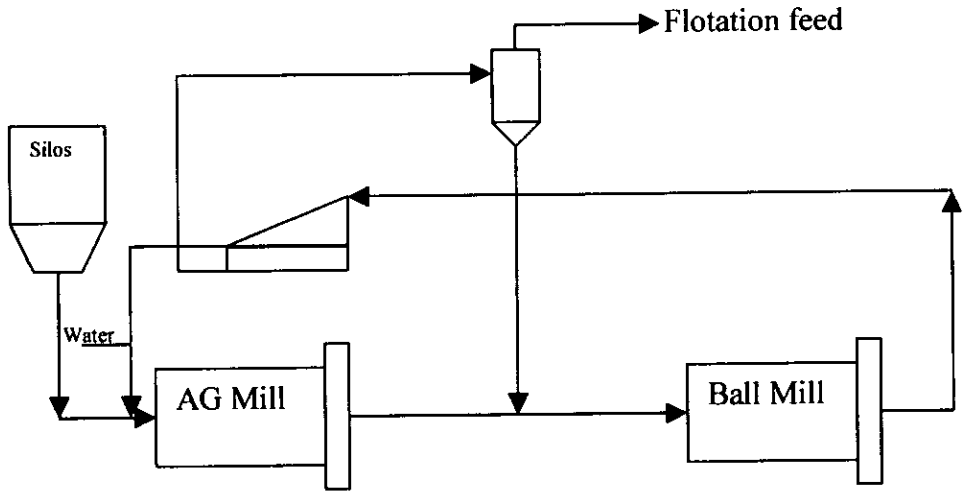

Figure 6.3. Schematic diagram of Zinkgruvan ore grinding circuit (Johan et al., 2002).

Milled tonnage has increased in parallel with greater mine output and zinc-in-concentrate production has been further increased by better recoveries, after switching from rod mill to autogenous grinding in 1998 (Johan et al., 2002). However, during the first half of 2002, difficult mining conditions reduced production. From July 2001 to June 2002, Rio Tinto reported metal-in-concentrate outputs of 53,200t of zinc, 21,500t of lead and 1.38Moz of silver (Table 6.1).

Table 6.1. Zinkgruvan production (after Rio Tinto annual report, May 2003)

	2001	2002
Ore treated, 10^3ton	807	735
Zinc (%)	8.4	7.2
Lead (%)	3.5	3.8
Silver (g/ton)	84	90
Metal concentrate		
Zinc, 10^3 ton	61.8	48
Lead, 10^3 ton	24.5	24.7
Silver, 10^6 ounces	1.496	1,554

6.2. Mineralogy of Zinkgruvan Ore

6.2.1. Sample preparation

A representative sample consisting of lumps >500mm was selected and core drilled to give core samples of approximately 37mm diameter and 200mm length as shown in Figure 6.4.

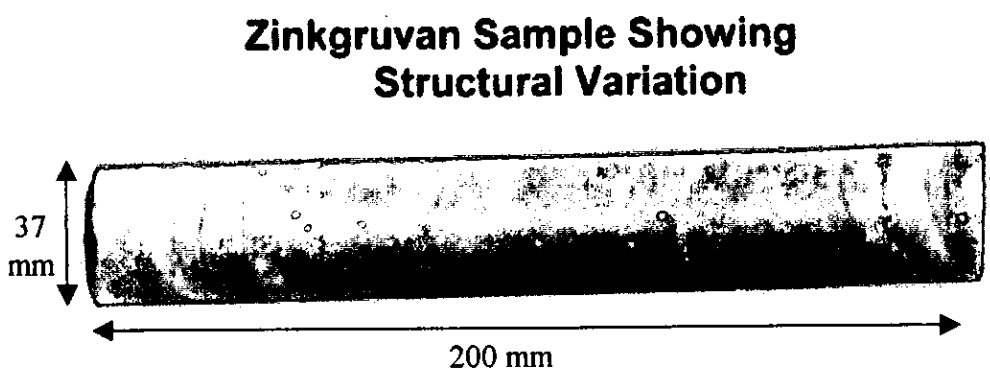

Figure 6.4. Core drill sample of Zinkgruvan

Mineralogical characterization of the drill core samples was conducted in conjunction with Rio Tinto Technical Services Ltd, Bristol and it focused on the determination of contained phases, degree of dissemination and grain size. The drill

core was sectioned using a diamond saw with polished sections being subsequently prepared from each.

6.2.2. Procedure

The polished sections were examined using reflected light microscopy and SEM based techniques, as described in section 5.2.2.

6.2.3. Results and Discussion

Microscopic examination of samples of the sections confirmed that they consisted predominantly of sphalerite and gangue minerals, together with small amounts of galena. Sphalerite was the dominant mineral and occurred as granular aggregates that were intimately intergrown with galena and the transparent gangue minerals. The relative distribution of sphalerite in the ore was found to be highly variable and may be locally abundant, occurring within discrete sphalerite-rich bands that may exceed several millimeters in width (Figures 6.5 and 6.6). Microscopic examination of the sphalerite revealed that the granular aggregates consisted of discrete sphalerite grains that ranged in size from an effective lower limit of 10μm to the largest grains that exceed 100μm in size (Figure 6.7). The bulk of the sphalerite exhibited a more restricted grain size of between 20 and 75μm. The grain size of the sphalerite was also largely dependant on the size of the aggregate. The sphalerite grains in the polycrystalline aggregates typically exhibited polygonal outlines with slightly curved grain boundaries and were characterised by the widespread development of annealing twins.

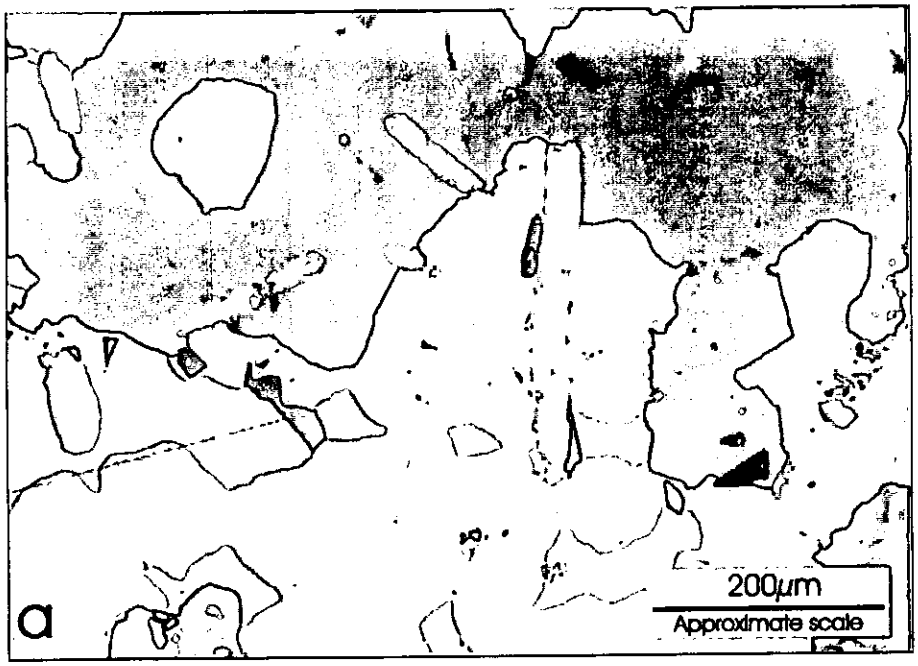

Figure 6.5. A colour reflected light photomicrograph illustrating the presence of graphitic carbon flakes (pale brown). Sphalerite (medium grey), galena (white) and gangue (dark grey) are the phases present in the image.

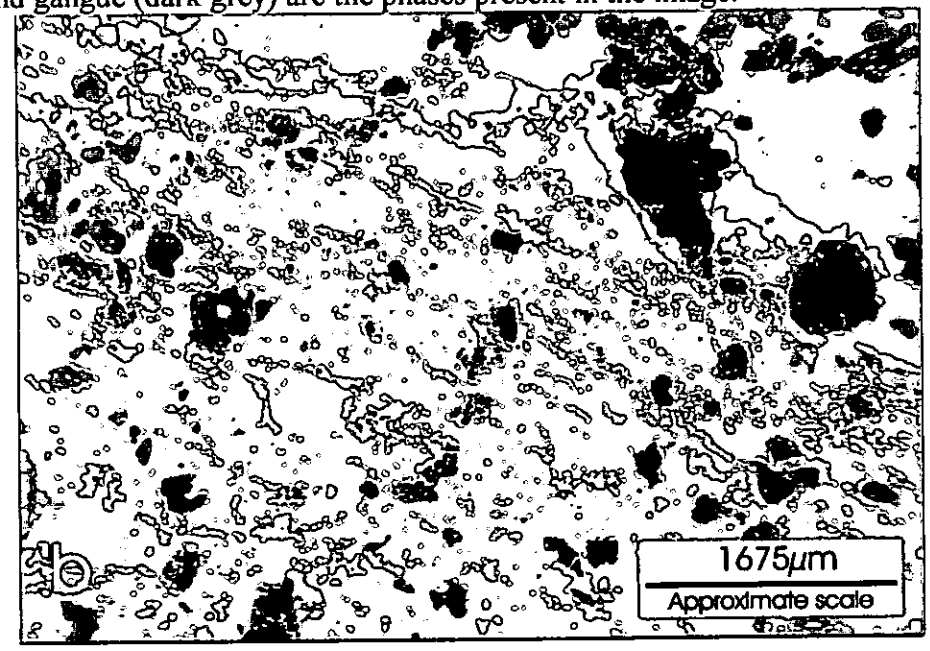

Figure 6.6. A monochrome backscattered scanning electron microscope image illustrating the preferred orientation of film like galena aggregates (white) within a sphalerite band (medium grey). The gangue (dark grey shades) consists predominatly of quartz and K-feldspar.

The larger sphalerite aggregates, essentially devoid of transparent gangue, typically hosted the coarser sphalerite grains. Conversely, interstitial sphalerite aggregates that formed along the margins of transparent gangue-rich areas typically exhibited a

finer grain size. Microscopic examination also revealed that the sphalerite grains commonly exhibited twinning (Figure 6.7). Qualitative SEM analysis of the sphalerite confirmed that it consisted predominantly of Zn and S together with minor amounts of Fe. Galena was found to be locally abundant, occurring as aggregates that commonly exceed 200μm in size (Figure 6.9). The film-like galena aggregates may also exhibit some degree of preferred orientation within the sphalerite bands (Figures 6.6 and 6.8).

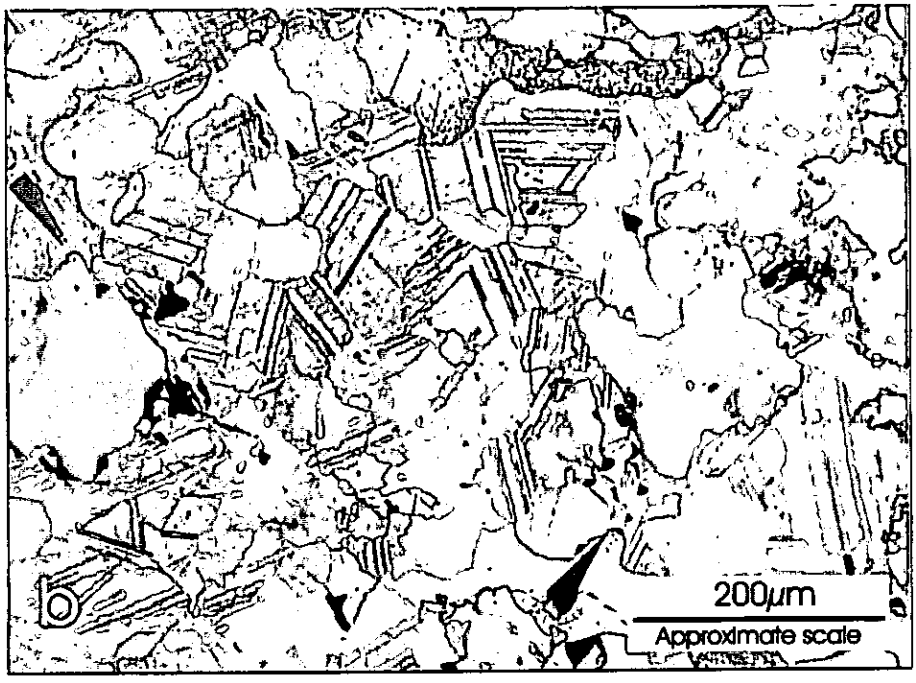

Figure 6.7. A colour reflected light photomicrograph illustrating the granular and twinned nature of the sphalerite aggregates (light and dark brown shades). Galena (silver-blue shades) is present along the margins of the sphalerite grains. Gangue is present (dark grey shades).

Narrow veinlets of galena were found along fractures in the transparent gangue minerals. In transparent gangue-rich portions of the core, extremely fine-grained sphalerite and galena were found finely disseminated throughout the gangue, occurring along grain boundaries and fractures (Figure 6.10). The transparent gangue mineralogy was typically rich in biotite and K-feldspar, but also contained small amounts of epidote, quartz, clinopyroxene, sphene and sericite. Within the

sphalerite- and galena-rich portions of the core, the transparent gangue minerals typically occurred as rounded and sub-rounded aggregates that consisted predominantly of quartz and K-feldspar.

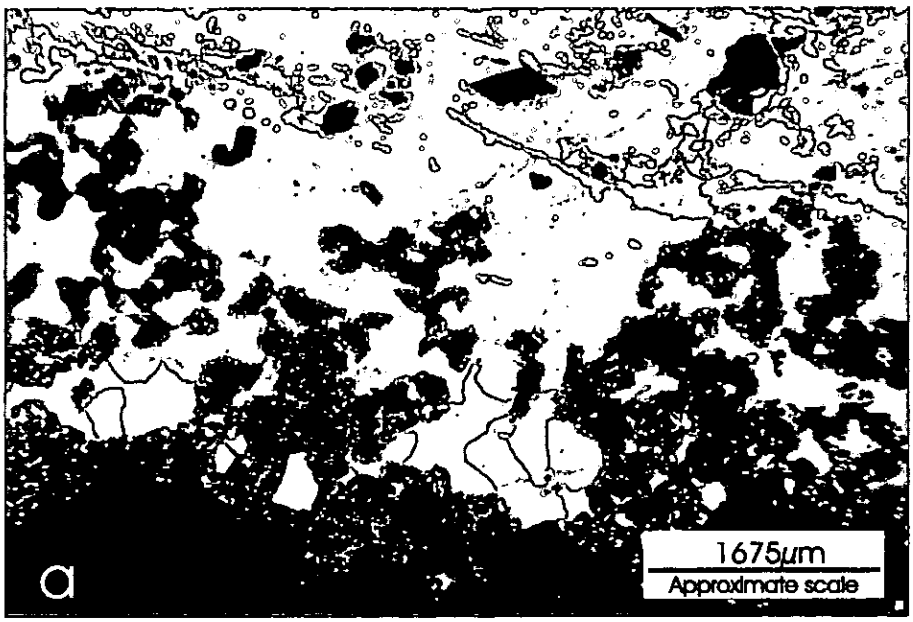

Figure 6.8. A monochrome backscattered SEM image illustrating the preferred orientation of film-like galena aggregates (white) within a sphalerite rich band (medium grey). Discrete gangue layers (dark grey shades) also occur on this image.

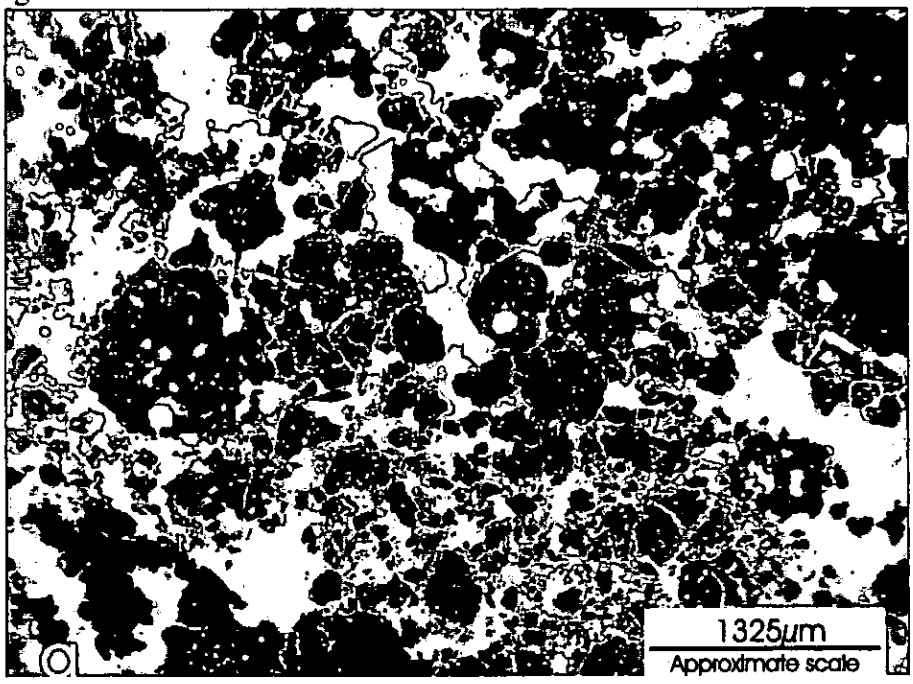

Figure 6.9. Monochrome backscattered SEM image illustrating galena (white) occurring along fractures in the gangue minerals (dark grey shades). Sphalerite (medium grey) is also present.

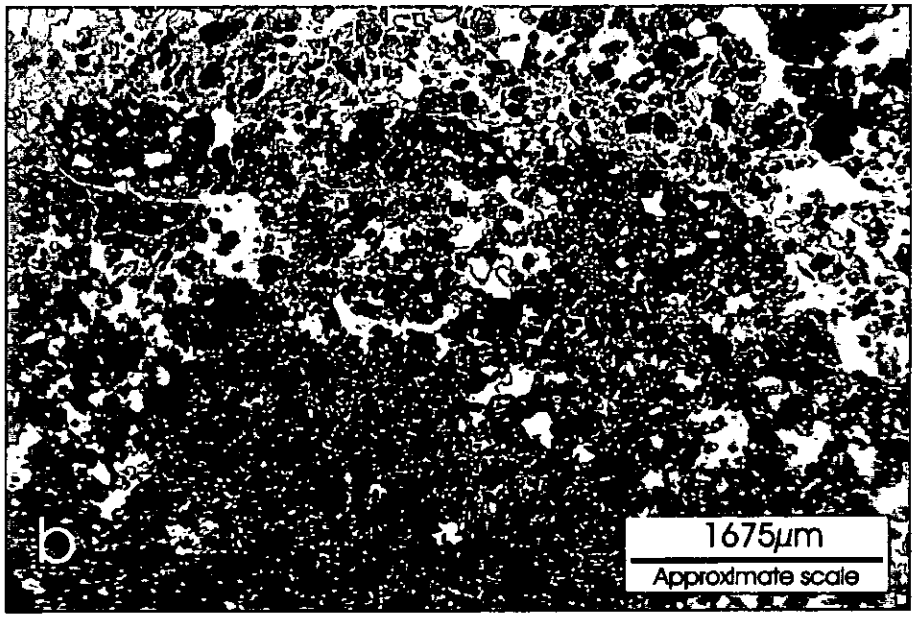

Figure 6.10. Monochrome SEM image illustrating a transparent gangue rich area (dark grey shades), consisting largely of epidote/clinozoisite. Fine grained galena (white) and sphalerite (medium grey) typically occurring along gangue mineral grain boundaries.

A Fe-Ca-Mn-rich variety of garnet was also found to be locally abundant. These subhedral garnet crystals commonly contained abundant quartz inclusions and were found to be extensively fractured. Galena typically occurred along the fractures within the transparent gangue. Clinopyroxene and apatite were common accessory minerals and typically occurred as rounded grains and subhedral crystals. The grain size of the transparent gangue minerals was highly variable. Generally, however, the transparent gangue minerals were medium grained in size, with the bulk of the gangue minerals exhibiting a grain size of between 50 and 150μm in size. Graphitic carbon was also present in minor, but nevertheless significant amounts. The graphitic carbon typically occurred as elongated flake-like grains and granular aggregates that were disseminated throughout the samples of core (Figure 6.4). Discrete graphite flakes was found to exceed 50μm in length. X-ray powder diffraction analysis also revealed the presence of amphibole within sample. The discrete transparent gangue clasts ranged in size from a few tens of micrometres, to

the largest clasts that exceed tens of millimetres in maximum dimensions. The transparent gangue clasts contained intergrowths and inclusions of sphalerite and galena (Figures 6.11, 6.12 and 6.13).

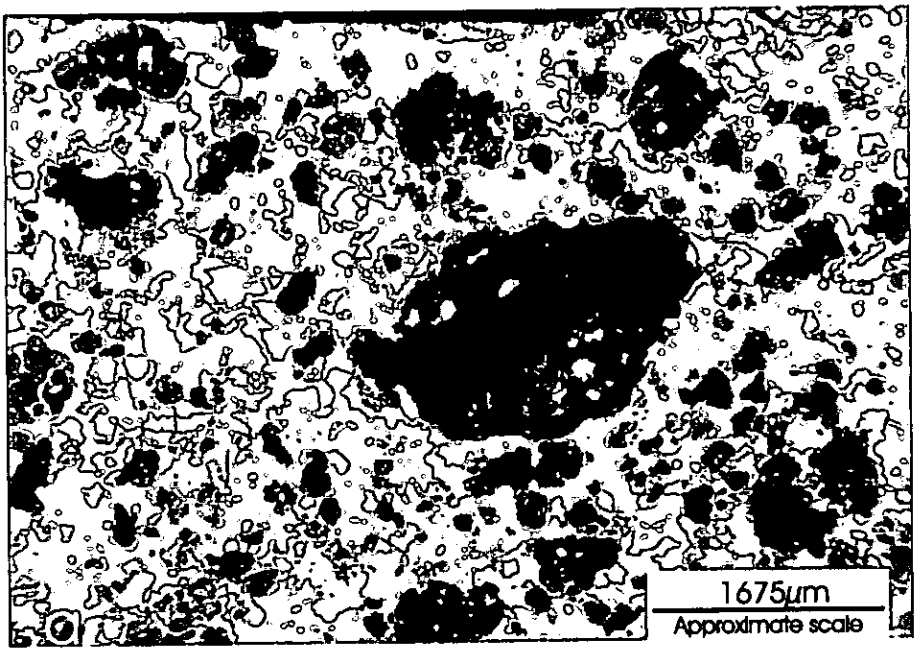

Figure 6.11. Monochrome backscattered electron images illustrating the rounded and sub-rounded nature of transparent gangue mineral clasts (dark grey shades). The galena (white) typically occurs as film-like aggregates along the margins of sphalerite grains (medium grey).

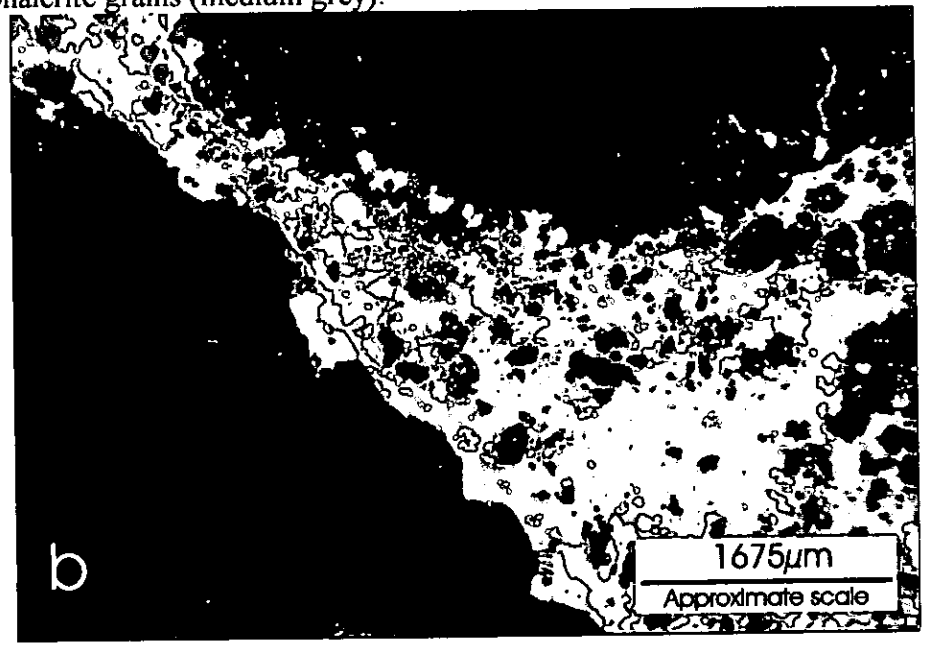

Figure 6.12. Monochrome backscattered electron images illustrating sphalerite and galena occurring between two relatively large transparent gangue mineral clasts. The lower clast consists predominantly of quartz. The upper clast consists predominantly of K-feldspar and clinopyroxene.

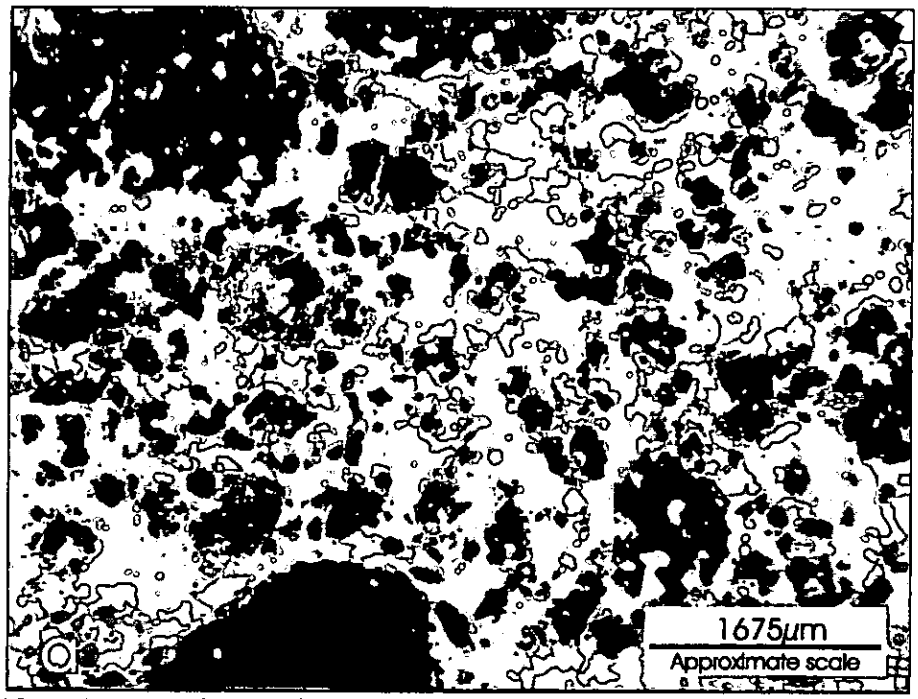

Figure 6.13. A monochrome backscattered electron image illustrating the typical nature and appearance of transparent gangue minerals (dark grey shades), galena (white) and sphalerite grains (medium grey).

6.3. Effect of Microwave Treatment on Ore Mineralogy

6.3.1. Sample Preparation

A sub-sample was taken from the bulk sample received from Zinkgruvan mine. The first stage of treatment was crushing to give particles 100% passing 63mm. The sample was then sieved into the narrow sieve size ranges: -63+53mm, -53+45mm, -45+37.5mm, -37.5+31.5mm, -31.5+26.5mm, -26.5+22.4mm, -22.4+19mm, -19+16mm, -16+13.2mm, -13.2+9.5mm, -9.5+6.7mm, -6.7+4.75mm, -4.75+3.35mm and <3.35mm.

6.3.2. Microwave Treatment

Random selection of ore particles in the –53+45mm size range was made and microwave treatment was carried out in a system that is capable of being operated with both single and multimode applicators, manufactured by SAIREM, as described in section 5.3.3.

6.3.3. Results and Discussion

Previous research (Kingman et al., 2000, Kingman 1999) has shown a close relationship between the effectiveness of microwave treatment and ore mineralogy. It was illustrated that of particular importance was the degree of dissemination of the absorbing minerals within the host rock and also the particle size. It was also shown that long exposure times might result in heat transfer between phases. For a qualitative investigation of the effect of microwave power density on the mineralogy of Zinkgruvan, samples were exposed on multimode and single mode cavities at the same power level.

Zinkgruvan contains gangue minerals disseminated in the valuable minerals as could be seen in Figures 6.5-6.13. The average grains range in size of about 10μm to 1mm. The average grains size of the gangue minerals are typically below 100μm. This kind of complex dissemination will render a significantly different behaviour when exposed to microwave radiation, compared to that observed in Palabora ore where valuable minerals are disseminated within the coarse gangue.

Furthermore, the loss tangent that describes the ability of the material to dissipate electromagnetic energy as heat, of the major constituents is shown on Figures 4.10 (galena and sphalerite) and 4.21 (orthoclase). As suggested by loss factor data, galena and sphalerite do not heat very well at low temperature. However, Walkiewicz (1988) has reported that galena heats readily. Despite the low values of loss tangent, Zinkgruvan ore has been found to be a good absorber of microwave radiation, causing arcing when treated at higher power densities. For better understanding of the phenomena, an analysis of the loss tangent, the ability of the material to heat in an applied electromagnetic field, was carried for galena, sphalerite and orthoclase and the results are shown on Figure 6.14.

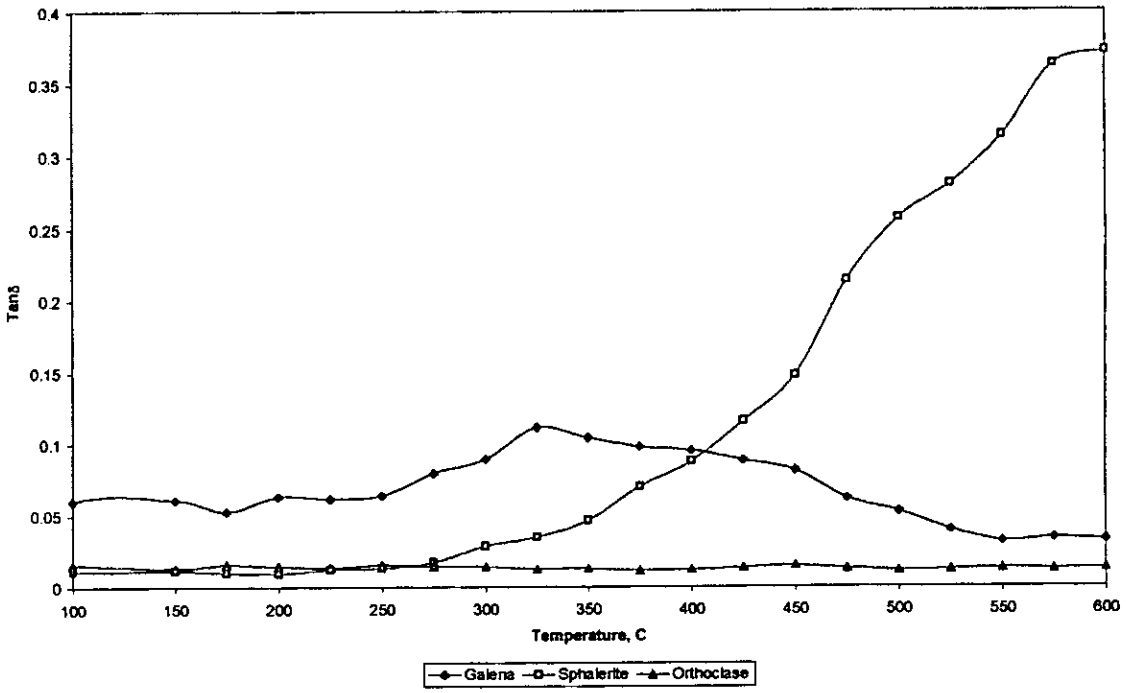

Figure 6.14. Loss tangent of the major constituents of Zinkgruvan ore.

The results of the lost tangent suggest that galena is relatively a good heater throughout temperature range while sphalerite does not absorb microwave radiation at temperatures below 300°C. However, once sphalerite is hot, the loss tangent increases exponentially with temperature and this may result in temperature runaway. This may explain the heating behaviour of Zinkgruvan ore during microwave treatment.

As could be observed from the ore mineralogy shown on Figures 6.11-6.13, most of galena occurs disseminated within the sphalerite matrix. The finely disseminated nature of galena means high surface area and, therefore, high rates of heat transfer between galena and sphalerite grains.

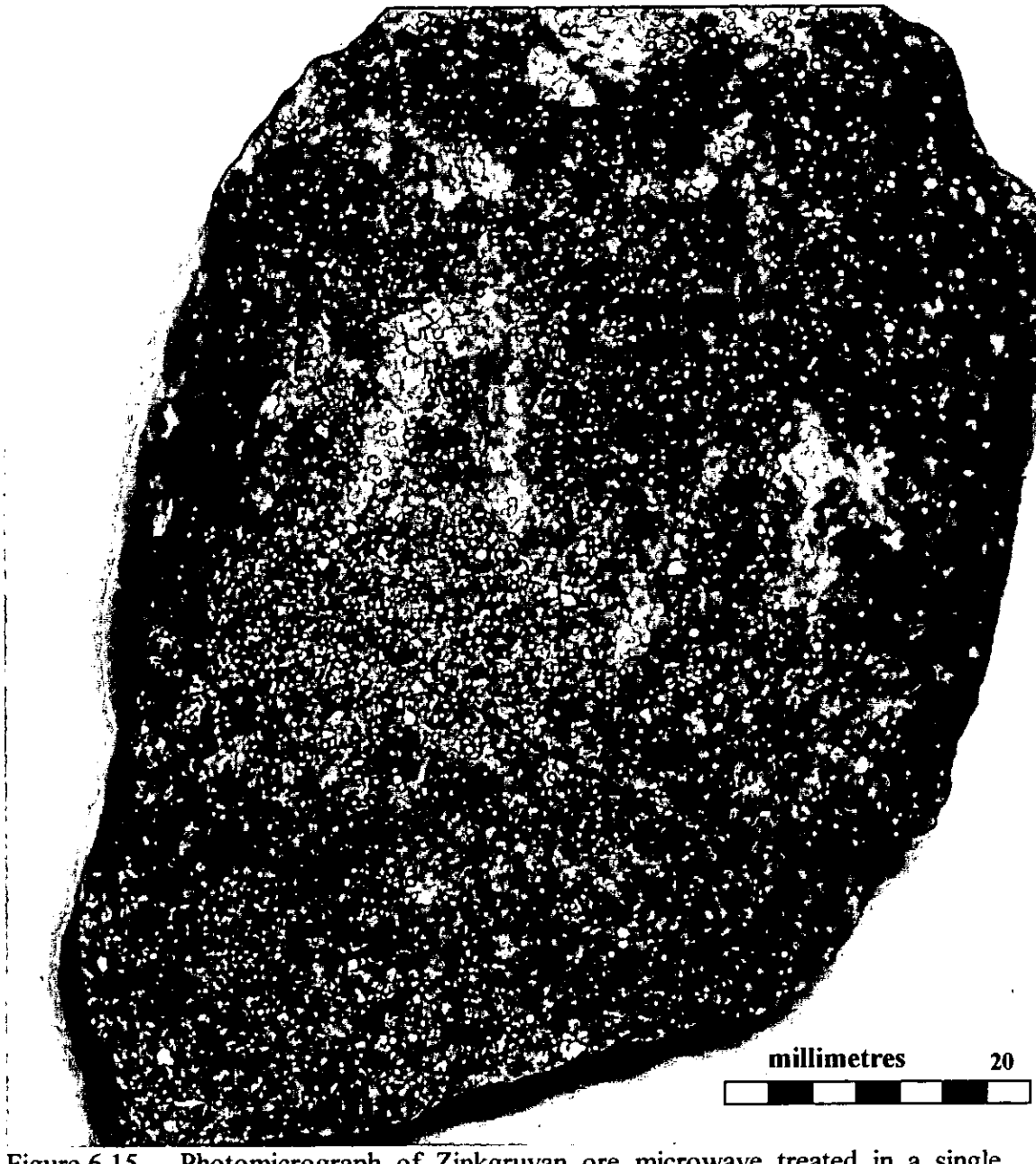

Figure 6.15. Photomicrograph of Zinkgruvan ore microwave treated in a single mode cavity, 10kW, 0.5 s exposure time.

Figures 6.15 and 16 show the effect of microwave radiation on the mineralogy of Zinkgruvan ore. Figure 6.15 illustrates a specimen of Zinkgruvan ore exposed for 0.5 seconds at 10kW microwave power in the single mode cavity. As can be observed, some heating has occurred and stress cracks have developed.

Figure 6.16 illustrates three specimens of Zinkgruvan ore exposed to 15, 10 and 5 kW for 5 seconds in a multimode cavity. Zinkgruvan ore was found to be highly

absorbent and treating samples in a single mode cavity for 15 kW proved very difficulty due to sample arcing.

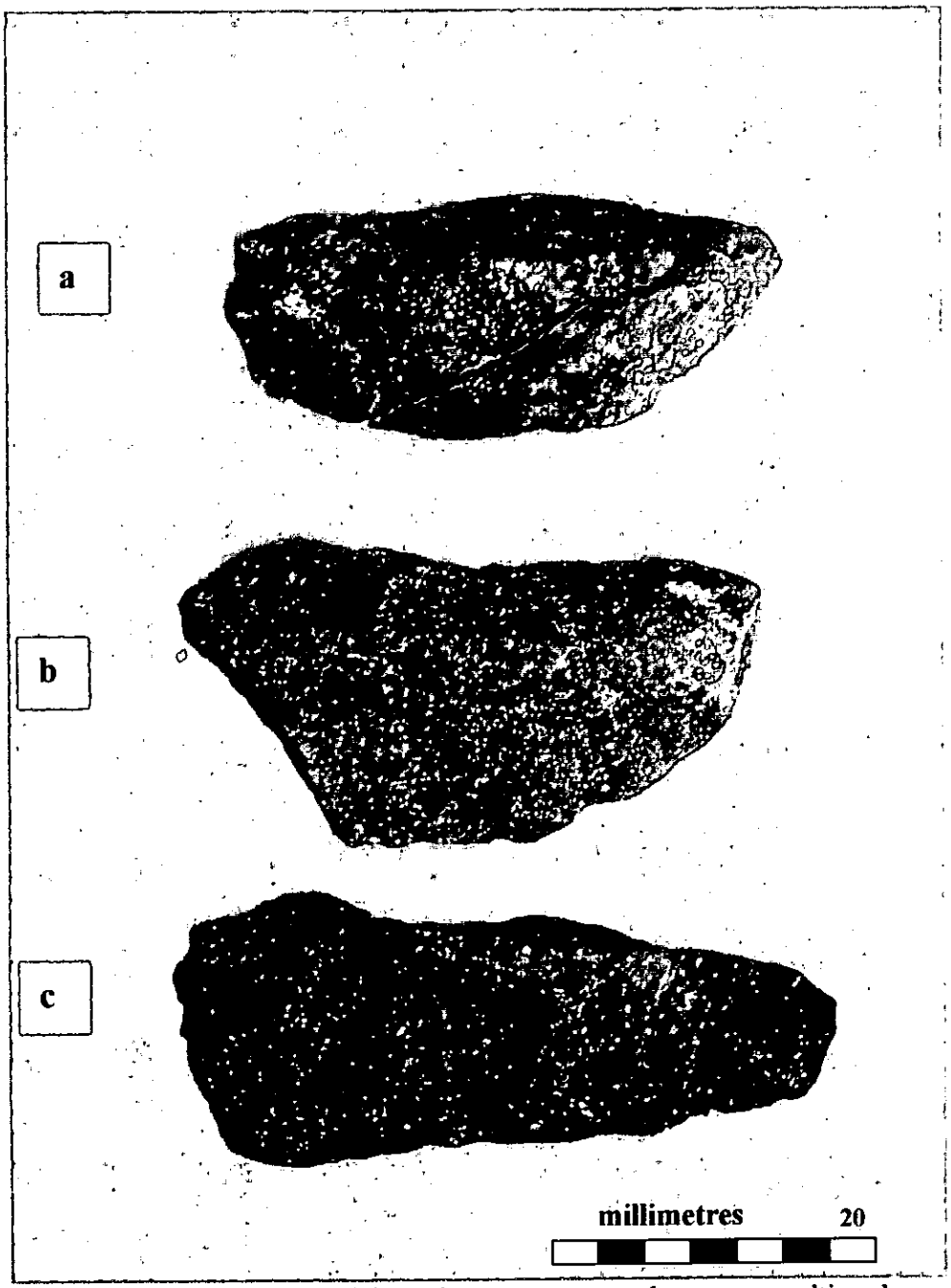

Figure 6.16 Zinkgruvan particle microwave treated on a multimode cavity, exposed for 5 seconds at a) 15kW, b) 10kW and c) 5kW microwave power.

6.4. Influence of Microwave Treatment on Comminution

6.4.1. Introduction

The Zinkgruvan operation employs two grinding circuits, which handles the ore from different areas of the pit. The first grinding circuit consists of autogenous mill and closed circuit ball mills. The second circuit is regrinding stage and consists of a closed circuit ball mills. An investigation was carried out to study the efficiency between primary and secondary grinding and no difference was found regardless the system used (Johan et al., 2002). However, comparison of flotation results showed that the lead flotation was influenced by the grinding method. This resulted in switching the operation from rod mill to autogenous mills on the primary grinding stage (Johan et al., 2002). Regrinding is required, however, to liberate galena and sphalerite. This has been an issue since it results in high operating costs and in some situations over-grinding the ore occurs resulting in more difficulties for handling fines and losses due to slimes.

6.4.1.1. Research Plan

A similar approach was adapted to that used for the investigation of the effect of microwave treatment on the comminution behaviour of Palabora ore. It consisted of the characterization of ore strength by the use of uniaxial compressive strength and point load tests, characterization of material breakage function using a drop weight tester and the characterization of rate of breakage and Bond ball mill work index.

6.4.2. Influence of Microwave Treatment on Ore Strength

6.4.2.1. Sample preparation

Representative samples were randomly selected from the bulk sample and core drilled to give samples of approximately 37mm diameter and 200mm length, as shown in Figure 6.4. Cored pieces were sectioned using a diamond saw to gives samples of

approximately 74mm length. Cored samples were then microwave treated in a multimode mode cavity at 15kW and 1 second exposure time. Samples were also kept untreated for comparison purposes.

6.4.2.2. Test Procedure

Uniaxial compressive strength tests were carried out using a RDP-Howden 1MN stiff universal loading frame. Although standard procedure requires at least 5 cored test pieces for statistically sound test availability of samples made this impossible. Further, at this stage of research, UCS tests were conducted only on two cored samples, one untreated and microwave treated in multimode cavity.

6.4.2.3. Results and Discussion

Results of the uniaxial compressive strength tests are shown in Figure 6.17. The plot shows the stress versus strain curves of treated and untreated specimens.

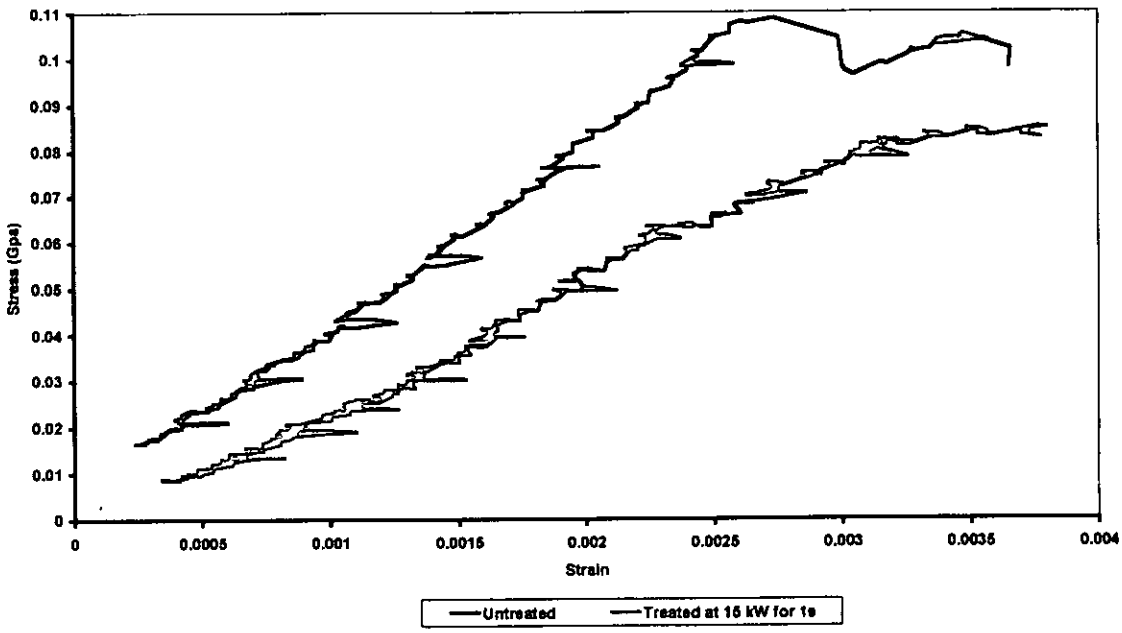

Figure 6.17. Plot of stress versus strain of Zinkgruvan core drilled samples.

The values of stress were calculated from recorded data of force (kN) and then divided by the cross sectional area of the sample. It was found that UCS for the untreated

specimen was approximately 110MPa and the single mode treated specimen was approximately 85MPa. These results should be treated with considerable caution because of the limited number of tests carried out but significant strength reductions can be clearly seen on Figure 6.17. Comparison of the ore strength between the treated and untreated shows a decrease of about 22%.

6.4.3. Influence of Microwave on Point Load Test

For preliminary assessment of the effect of microwaves on ore breakage a quick evaluation of breakage energy reduction was conducted using the point load test. The Point Load Test has the advantage of requiring no sample preparation so that a statistically sound test sample can be rapidly processed and an assessment made of the strength.

6.4.3.1. Sample Preparation

A bulk representative sample of Zinkgruvan ore was received from Sweden. The first stage of treatment was to crush the ore to give particles 100% passing 63mm and then sieving into the size intervals described in section 6.3.1. Following the results obtained for Palabora ore, that showed similar trends of the combined effect of microwave power and specimen size, it was decided to carry out tests on the size range –37.5+31.5mm. A random selection of the required number of particles for each set was then made.

6.4.3.2. Test Procedure

After thorough mixing a random selection of the required number of particles for each set was made. Thereafter, Zinkgruvan ore samples were microwave treated in multimode and single mode cavities at three different power levels and exposure times. Details are shown in Table 6.2.

In the Point Load test, measurement of width and depth of the specimen near the loading point is recorded. The specimen is then placed and loaded between the two shaped and hardened steel platens in the apparatus as described in the section 5.4.3.2.3, and the force at which the specimen breaks determined using equation 5.6. For each test 10 particles of ore were tested and the Is(50) value for each particle calculated. Thereafter the mean, median and range values of Is(50) for the 10 particles were calculated. Results are also reported as percentage reduction in Is(50) of the treated against the non-treated sample versus microwave exposure time.

Table 6.2. Sample description for point load test

Cavity type	**Sample**	**Power (kW)**	**Exposure time (s)**			
Multimode	37x31 mm	15	10	5	1	0
		10	10	5	1	0
		5	10	5	1	0
Single mode	37x31 mm	10	1	0.5	0.1	0
		7.5	1	0.5	0.1	0
		5	1	0.5	0.1	0

6.4.3.3. Results and Discussion

Table A3.1 illustrates the microwave treatment conditions, the mean, median and range of the point load index Is(50) values. The data were then converted into percentage by dividing the value of the microwave treated by the untreated result. Figures 6.18 and 6.19 show plots of percentage of original Is(50) verses microwave exposure time for material in the size range -37+31.5mm. Figure 6.18 shows a plot of percentage of original Is(50) verses microwave exposure time for material treated on a multimode microwave cavity. It can clearly be seen that microwave treatment has a significant effect on the ore strength with short exposures of 0.5 seconds giving rise to up to 60% reductions in Is(50). With exposures time above 1 seconds reduction in strength to up to 80% in Is(50) can be achieved for samples treated at 10 and 15kW.

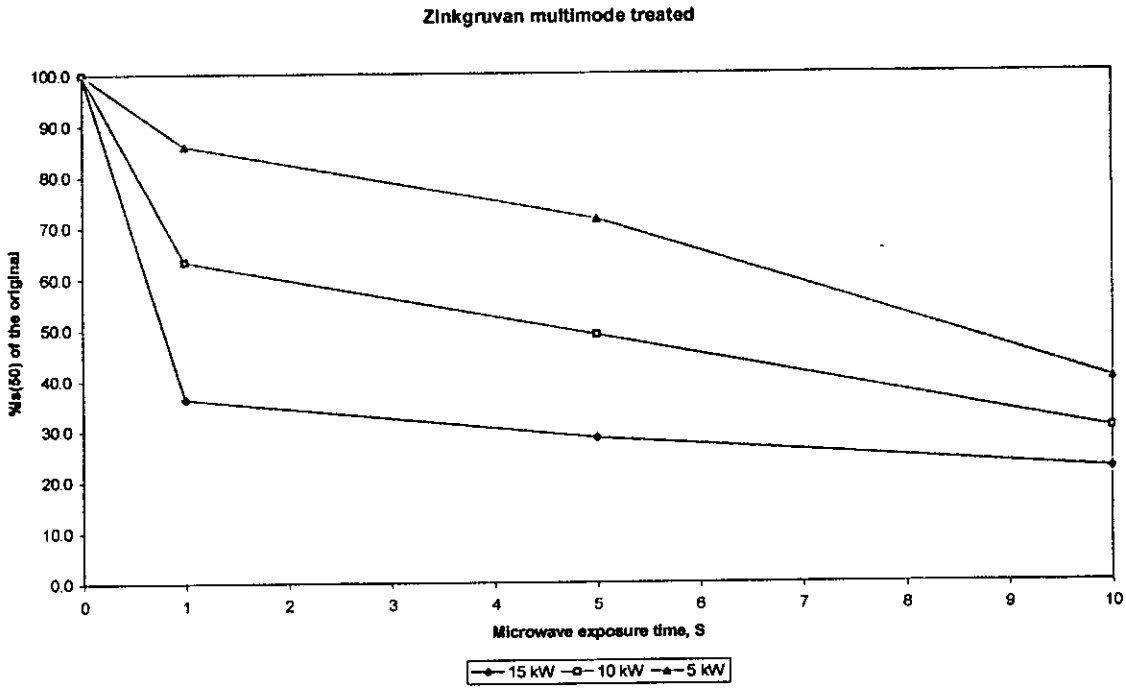

Figure 6.18. Effect of microwave exposure time on Point Load test for Zinkgruvan ore.

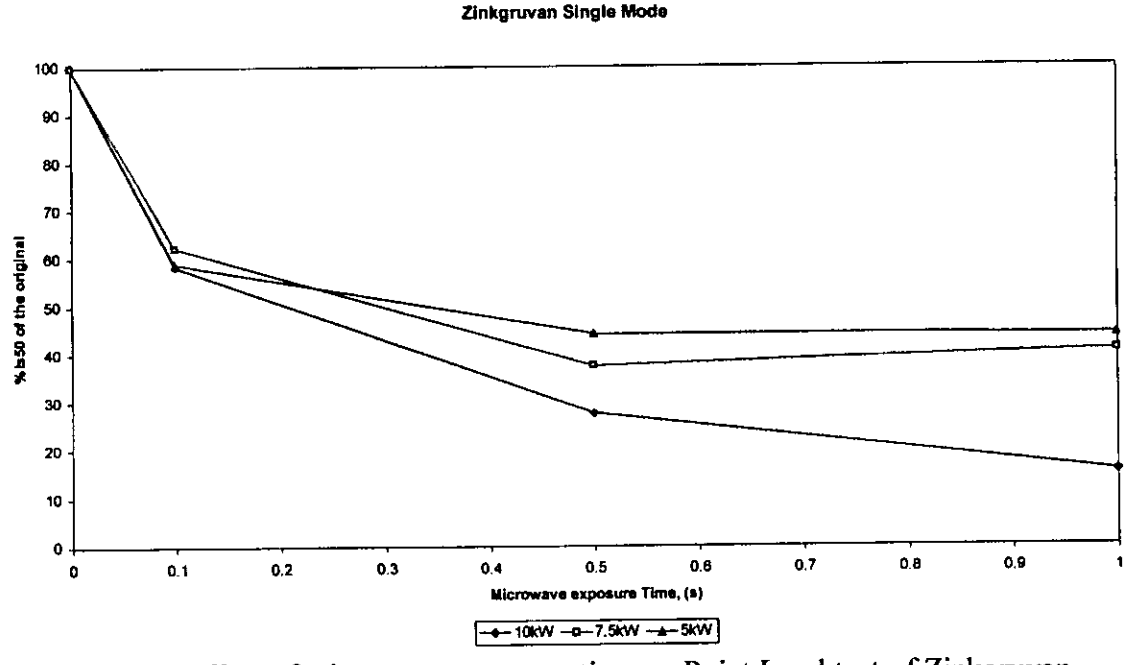

Figure 6.19. Effect of microwave exposure time on Point Load test of Zinkgruvan ore.

Figure 6.19 shows a plot of percentage of original Is(50) verses microwave exposures times for material treated in a single mode microwave cavity. It can be clearly seen that single mode microwave treatment has a more significant effect on the strength of

the ore with even short exposures of 0.1 seconds giving rise to up to 40% reductions in Is(50).

Interestingly for up to 0.1 seconds exposure closest results are obtained for samples treated at both 10 and 7.5kW in single mode microwave cavity. It can be seen however that as exposure time is increased to 0.5 seconds approximately 70% reductions in strength are achieved for samples treated at 10kW compared to only 55% reduction for samples treated at 5kW. For all exposure time 5kW gives the smallest reduction in strength with only approximately 30% reduction occurring after 1 second in a single mode microwave cavity and 5 seconds in a multimode microwave cavity.

The results obtained have shown that microwave treatment can have a significant influence on the amount of energy required for breakage. It has also been shown that the effectiveness of the treatment is related to the power level of the applied radiation. As discussed in the previous literature review, a recent paper (Whittles et al., 2003) has shown that failure in microwave treated samples is a function of electric field strength. It was shown as well, that failure was a result of temperature gradients across grain boundaries and that the higher the value of the temperature gradient between mineral phases and transparent gangue matrix the more effective the failure. To a degree this can be concluded from this test work.

6.4.4. Influence of Microwave Treatment on Crushing

6.4.4.1. Sample Preparation

Three representative sets of Zinkgruvan ore were prepared for drop weight testing. A random selection of the required number of particles for each set of the size intervals given in Table 5.4 was made from particle size ranges prepared in section 6.3.1. Then 30 additional particles in the 31.5 – 26.5mm range were selected for density

measurements. In addition two 3.0 kg sets of ore were produced for the autogenous grinding test.

6.4.4.2. Test Procedure

Based on the results of the point load tests, two samples were irradiated in a 15 kW microwave multimode cavity for 1 second. After irradiation each sample was immediately quenched in water and then left overnight to dry. One untreated sample was kept for comparison. Details are shown in Table 6.3.

Table 6.3. Sample description for drop weight test

Sample	Power (kW)	Exposure time (s)	Input energy
1	Untreated	0	Standard
2	15	1	Standard
3	15	1	60%

6.4.4.3 Results and Discussion

To investigate the effect of microwave radiation on the breakage of Zinkgruvan ore, drop weight tests were carried out on three samples, one as received and two after exposure to microwaves as shown in Table 6.3.

The untreated sample was drop weight tested at the energy inputs as recommended by JKMRC and shown in Table 5.3 while the microwave treated was drop weight tested at 60% of the original energy input. It was therefore expected that significant differences would be observed in the appearance function and the subsequent breakage parameters for AG/SAG mill model as well as crusher power data. This, however, was not the case. Detailed examination of the breakage parameter b showed significant differences, 1.54 and 2.19 for the untreated and treated samples respectively. Results of crusher power and appearance function data are illustrated on Tables A3.2 and A3.3

in the Appendices. Comparison of the crusher power data between the untreated and microwave treated samples is shown in Figure 6.20.

Figure 6.20 shows the effect of microwave treatment on the particle size verses the specific comminution energy (expressed as percent reduction of the original Ecs for the untreated sample). Zinkgruvan samples were microwave treated at 15kW for 1 second exposure time and drop weight tested at 60% of the standard Ecs energy input. The results suggest that, smaller particle are more sensitive to microwave than the bigger sizes for this particular ore, in contrast to what has been observed with Palabora ore.

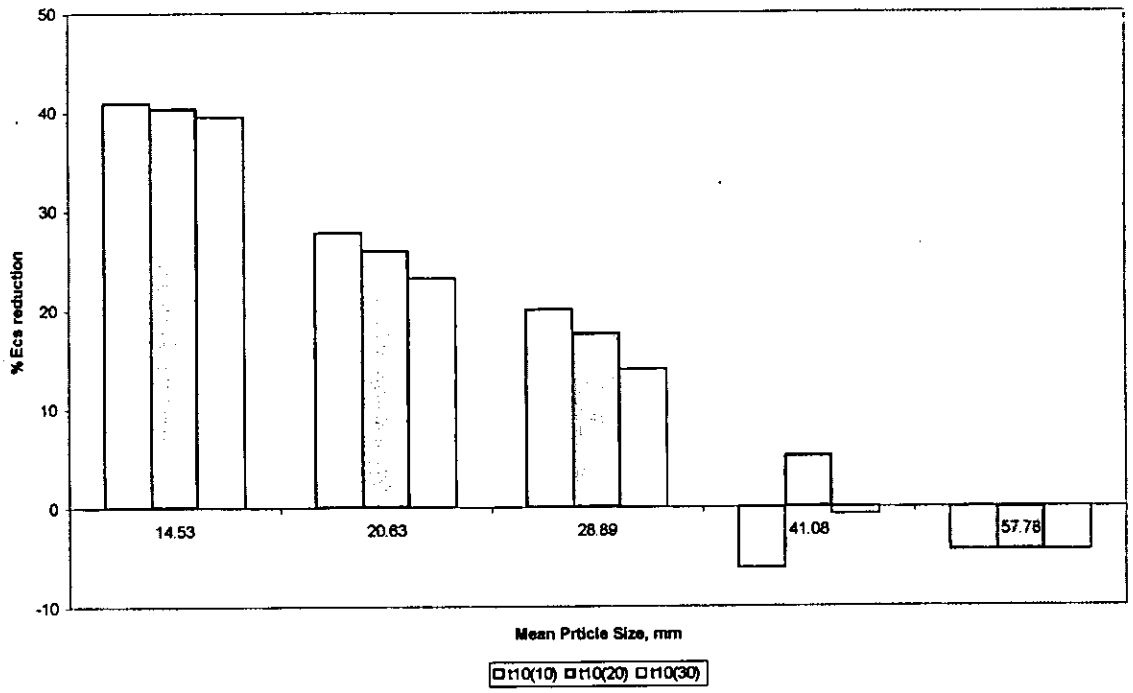

Figure 6.20. Effect of particle size on comparative crusher power data of Zinkgruvan treated and untreated samples and drop weight tested at 60% and standard energy input.

To further investigate the differences, it was therefore thought to address the problem with a similar approach used for the Palabora ore. Additional tests were therefore required however, availability of sample only allowed a retest to be carried out on the treated material and drop weight tested at standard specific comminution energy inputs

as shown in Table 5.3. It was expected that values of breakage parameters could exhibit similar variation compared to those obtained for Palabora. However, a value of 1.74 for the breakage parameter b was obtained for the microwave treated sample and drop weight tested at standard Ecs input energy compared to 2.19 for a sample microwave treated at similar conditions but drop weight tested at 60% of the standard Ecs input energy. Comparisons of the crusher power data between the untreated and treated samples drop weight tested at standard Ecs input energy are shown in Figures 6.21 and 6.22.

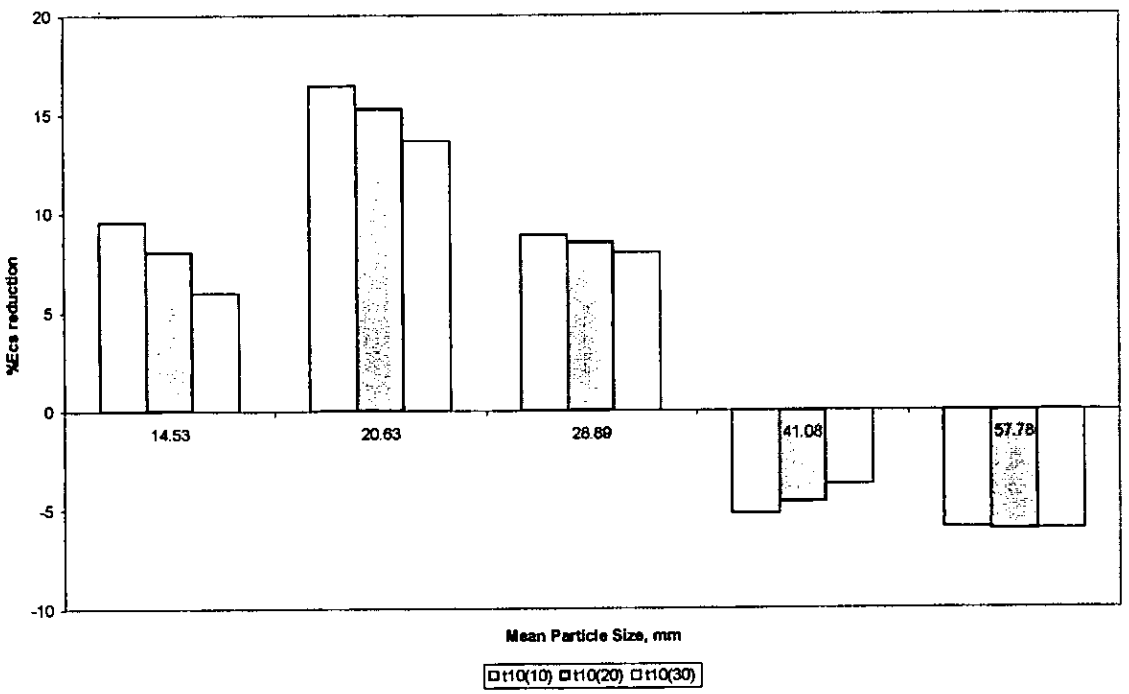

Figure 6.21. Effect of particle size on comparative crusher power data of Zinkgruvan untreated and treated samples and drop weight tested at full Ecs energy input.

Table 6.4 given below shows a summary of the results of drop weight test for microwave treated and untreated Zinkgruvan samples. Due to the availability of ore sample, it was not possible to conduct the drop weight test for reduced energy input on an untreated sample as well as the effect of high electric field for short cavity residence times.

Table 6.4. Zinkgruvan drop weight test results

Test run	Parameters			
	A	b	A.b	Ta
Untreated, full energy	70.5	1.54	108.6	0.80
Treated 15kW 1s, 60% energy	65.6	1.74	114.1	0.93
Treated 15kW 1s, full energy	61.2	2.19	134.1	0.93

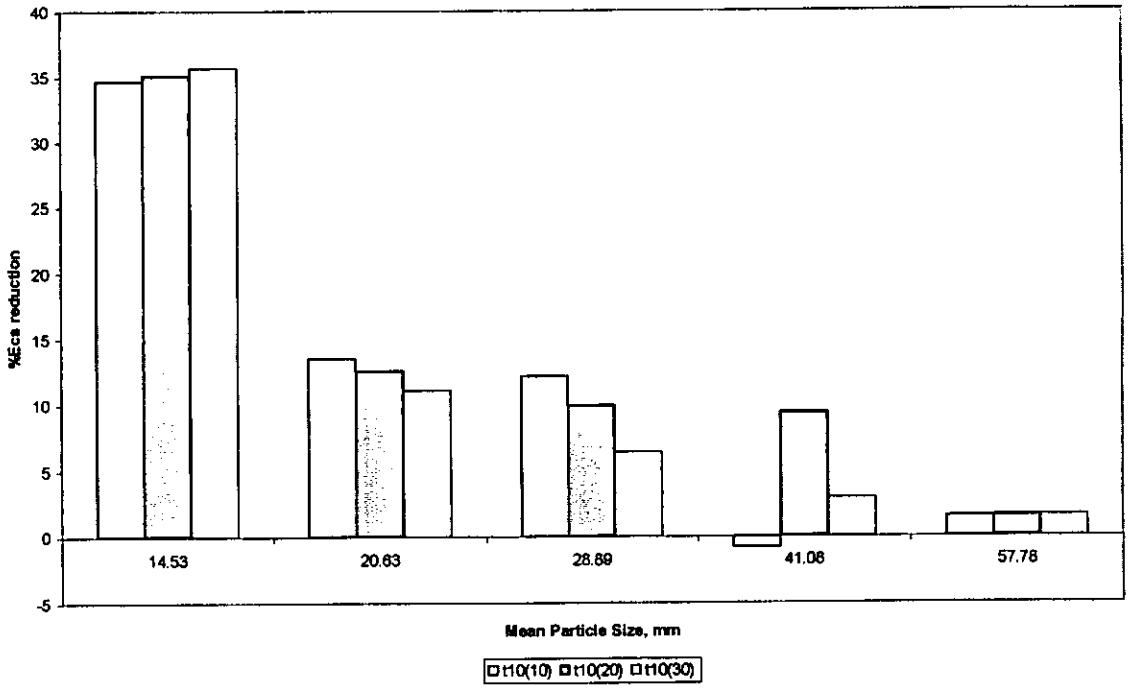

Figure 6.22. Effect of particle size on comparative crusher power data of Zinkgruvan treated samples and drop weight tested at full and 60%Ecs energy input.

6.4.5. Influence of Microwave Treatment on Breakage Rate

The grinding process can be treated as a rate process. The kinetics of a grinding process can be studied with batch grinding tests on mono-size samples. The typical procedure involves batch grinding the material within a certain size fraction, from which the breakage rate of that size fraction is determined, together with the breakage function of the material. The breakage function is essentially a size distribution resulting from breakage, usually expressed in matrix form. The results of the test are

interpreted in terms of the population balance model usually by estimating the values of the selection and breakage functions in the model.

6.4.5.1. Sample preparation

A bulk representative sample from the Zinkgruvan operation was received. The first stage in treatment was to jaw crush the ore sample to give ore particles of 100% passing 19mm. The test material was then closely sized using a $\sqrt[3]{2}$ sieve progression from 19mm down to 3.35mm. Riffling was then used to gain a 2 kg sub-sample for test-work on each mono-size fraction. Each mono-size fraction was kept separate and riffled in half. One sub-sample was microwave treated on a single mode cavity, at 10 kW for 0.2 seconds and the other was kept for comparison.

6.4.5.2. Batch grinding test procedure

The mill used for the test was cylindrical in shape with smooth interior surfaces; the joints between the barrel and the end plates were filled in to maintain the integrity of the sample. The mill had the following internal dimensions: D=30.48cm L=30.48cm. The mill was rotated at a constant speed of 70 r.p.m. The ball charge consisted of 279 steel balls with total weight of 19.82kg, the same as described in section 5.4.5.4.

A 500-gramme sample of dry ore was placed in the mill, which was run for 35 revolutions at a fixed speed of 70 r.p.m. After grinding period, the mill contents were removed, the ball charge screened out; this was returned to the mill. The product was then screened, using the lower size screen of each mono-size fraction. The undersize was weighted and the mass recorded. Thereafter the undersize and oversize were returned to the mill and the procedure repeated for periods of 35 revolutions till an equivalent to 5 minutes grinding cycles obtained.

6.4.5.3. Results and Discussion

The recorded masses of oversize retained for each batch-grinding test carried out for Zinkgruvan ore are summarized on the Table A3.5 in the appendices. The data was then plotted as the natural logarithm of mass retained against grinding time. The slopes of the curves for the treated and untreated mono-size fractions were determined. As only comparative data were required for the analysis the results were then reported as percentage change of rate of breakage of untreated versus the mean particle size for each mono-size fraction. The results are summarized on Table 6.5 and shown in Figure 6.23.

Table 6.5 Summarized results of the microwave effect on ore breakage rate.

Mean particle size, mm	Breakage rate (s^{-1})		% Change of breakage rate
	Untreated	Microwave treated	
4.025	0.0155	0.0197	27
5.72	0.0136	0.0162	19
8.1	0.0122	0.0150	23
11.5	0.0083	0.0117	40
14.5	0.0052	0.0107	106
16.1	0.0079	0.0136	72
17.5	0.0086	0.0152	76

Table 6.5 shows the comparative data of breakage rate between Zinkgruvan untreated and microwave treated at 10kW microwave power in a single mode cavity for 0.2 seconds exposure time. It can be seen that breakage rate of this ore decreases with the increase of particle size for the prevailing conditions of the test (ball mill charge). On this ore the particle size also has been found that microwave radiation has more significant effect. Figure 6.23 illustrates graphically the relationship between percentage change of breakage rate versus mean particle size between the treated and untreated samples. It has been found that microwave radiation has a significant effect

on the breakage rate of particles within range –19mm+9.5mm. These results match clearly with the findings from drop weight test crusher power data that showed that particles with mean particle size below 20.63mm have high percentage reduction of Ecs as illustrated in Figures 6.20 and 6.22.

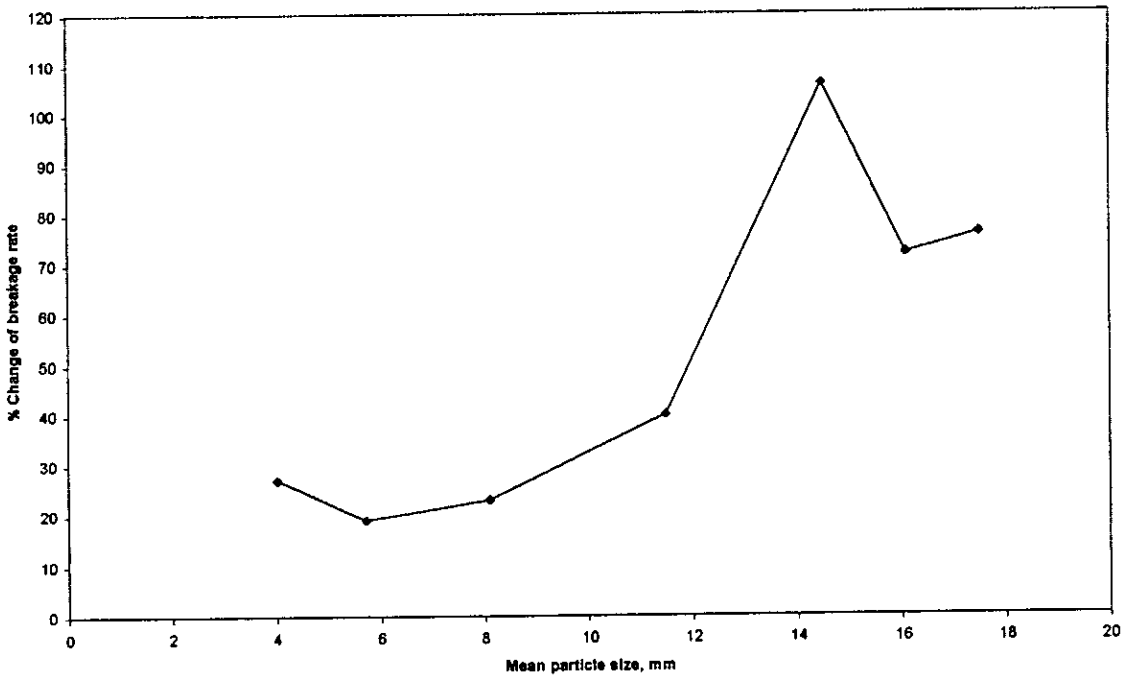

Figure 6.23. Effect of microwave treatment on breakage rate of Zinkgruvan ore.

The results illustrated in Figure A3.1 shows that breakage rate decreases with increase of particle size and at a certain point it become somehow constant. This suggests that as the particle size increases they are less likely to be broken during any typical impact in the mill, which is in contradiction with the literature. According to King (2001), the specific rate of breakage increases with particle size, which reflects the decreasing strength of the particles as the size increases. This is attributed to the greater density of micro-flaws in the interior of larger particles and to the greater likelihood that a particular large particle will contain a flaw that will initiate fracture under the prevailing stress conditions in the mill. However, the decrease in particle strength does not lead to an indefinite increase in the specific rate of breakage. King (2001) also

suggested that as the particle size becomes significant compared to the smallest grinding media, the prevailing stress levels in the mill are insufficient to cause fracture and the specific rate of breakage passes through a maximum and decreases with further increase in particle size. This is not what has been found in the present research. The results show that a minimum breakage rate is achieved at the mean particle size of 14.5mm. It is interesting to note that large particles show a greater difference in breakage rate between microwave treated and untreated samples. This can be explained by the fact that microwaves have more probability to create more micro-cracks on large particles than the smaller ones because of the surface area. Large particles have small surface area and therefore less heat dissipation. This results on high temperature gradient between minerals with consequence on high thermal stresses being developed.

6.4.6. Influence of Microwave Treatment on Bond Work Index

6.4.6.1. Sample Preparation

A bulk representative sub-sample was taken from the bulk sample received from Zinkgruvan mine. A jaw crusher was then used to obtain a 100% passing 19mm. Screening was then used to gain a sub-sample for test-work. Approximately 20kg of the 100% passing 3.35mm was obtained as required by the Bond test procedure. The sample was then riffled to produce two sub-samples of approximately 10 kg each. The test material was then closely sized using a $\sqrt[3]{2}$ sieve progression from 3.35 mm down to -38μm. Each fraction was kept separate and the overall size distribution calculated. One sub-sample was microwave treated on a single mode cavity at 10kW for 0.2 seconds exposure time.

6.4.6.2. Bond Work Index Test Procedure

The Bond work index test procedure has already been described in Section 5.4.6 of Chapter 5. A 1000ml graduated measuring cylinder was packed with ore to the 700cm^3 mark. It was then shaken until compact and the mass determined. This "unit volume" of 700cm^3 was selected as the volume of ore always present in the mill during closed circuit grinding. The ball mill dimension and charge were the same as described in section 5.4.5.4. The weight was noted at the beginning of each grinding cycle. The mill was run for 50 revolutions. After completion, the product of the last three cycles were thoroughly mixed and riffled to produce an approximate 150 g sample for size analysis. The closing sieve size used for test was 180 μm.

6.4.6.3. Results and Discussion

The result of size analysis of the feed material is shown in Figure A3.10 and F_{80} (size particle for which cumulative percentage of material passing is 80%) was found to be 2000 mm. The mass of unit volume was 1661.2g. The working index test was conducted at closing sieve of 180μm particle size. From the size analysis (Figure A3.10 in Appendices), the percentage of material less than 180μm was determined.

The results of the recorded data during grinding test for non-treated and microwave treated samples are illustrated in Tables A3.14 and A3.15 in Appendices. From the plots in Figures A3.10, A3.11 and A3.12 of the size distribution the F_{80} (initial feed) and P_{80} (final product for the untreated and microwave treated samples) were determined and from the Table A3.14 and A3.15 the grindability of untreated and microwave samples. Then the equation 5.18 was applied.

$$Wi = \frac{4.45}{P_1^{0.22} G^{0.8} (P^{-0.5} - F^{-0.5})} \tag{5.18}$$

For the untreated sample:

$$Wi = \frac{4.45}{180^{0.22} 3.4^{0.8} (150^{-0.5} - 2000^{-0.5})} = 8.37 kWh/t$$

For the microwave treated sample:

$$Wi = \frac{4.45}{180^{0.22} 3.86^{0.8} (150^{-0.5} - 2000^{-0.5})} = 7.56 kWk/t$$

The present result shows a decrease of Bond work index of 10%, which proves the trend that have been observed on breakage rate characterization. Therefore, application of microwave treatment, for this particular single mode cavity and power level, at the grinding circuit does not bring any benefit to the process economic compared with the application at the crushing stage. Occurrence of partial melting of the sample has been observed during microwave of smaller particles, which is another disadvantage to the down stream process, since this should be avoided.

6.5. Effect of Microwave Treatment on Mineral Liberation

6.5.1. Sample Preparation

A representative sample was produced from samples previously prepared for drop weight tests. Two samples, each with randomly selected 100 particles, were made from the monosize fraction 22.4x19mm. One sample was microwave treated on a single mode cavity, 15kW for 0.2 seconds and the other was kept for comparison. Thereafter, single particle breakage using drop weight tester was carried on. An equivalent of 2.5 kWh/t was the energy level used for breakage. Then, the samples were screened using 1.0 mm sieve size and the undersize sent for QEM*SEM analysis.

6.5.2. Procedure

Upon their receipt at the laboratory, a representative sub-samples from each of the samples was obtained by riffling for chemical assay of the head sample. The remaining were screened into four size fractions +500μm, +150/-500μm, +38/-150μm, and –38 μm. Individual size fractions were submitted for chemical assay, with copper, iron, lead and zinc were determined by an Inductively Coupled Plasma Mass Spectrometry (ICP). The tests were carried out by Rio Tinto Technology, Melbourne, Australia.

The four fractions were also submitted for quantitative mineralogical characterization. Representative samples were mounted in chlorinated epoxy resin, polished and carbon coated for analysis by QEM*SEM. In QEM*SEM analysis, three category particle type were defined as described on the Table 6.6 below:

Table 6.6. Particle types.

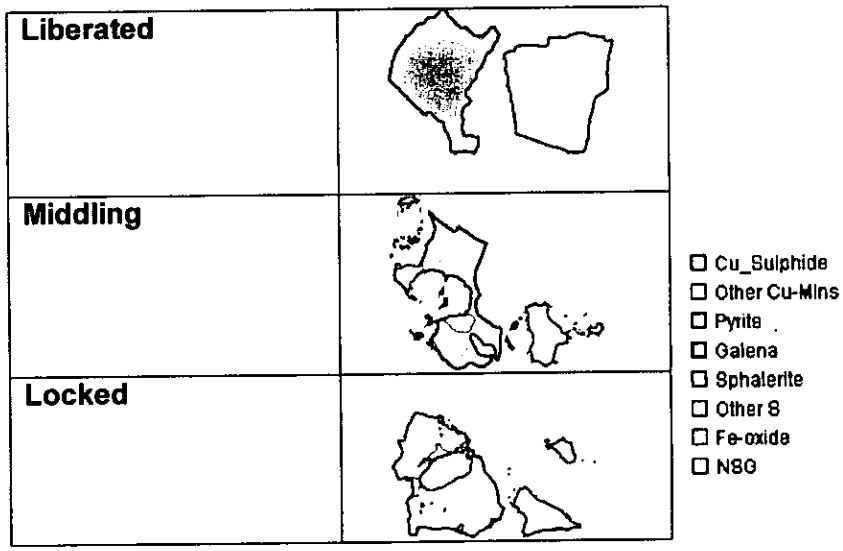

Grain counting was also used, describing the outline of each particle, the phases present, and degree of liberation and nature of locking calculated. The results are presented in tabular format on a size-by-size basis and their relative proportions provided, as illustrated in the Appendices on Tables A3.8 and A3.9.

6.5.3 Results and Discussion

The results of the effect of microwave treatment on the liberation characteristics of Zinkgruvan ore are illustrated in Figures 6.24. Figure 6.24 illustrates the QEM*SEM results of the liberation characteristics of galena in Zinkgruvan ore for untreated and microwave treated samples. The results show that in the +500μm fraction galena occurs mostly in the middling and locked fractions. The findings are in accordance with the mineralogy of the ore where galena is described to occur as subordinated mineral of sphalerite with grain varying from 20μm up to 200μm. It is therefore unlikely that galena may be liberated on this size fraction. However, in the size fractions -500μm + 38μm there is quite a significant amount of liberated galena. A thorough analysis of the microwave treated sample and untreated on the fine fractions, the results suggest that microwave treatment does have an effect on the mineral liberation.

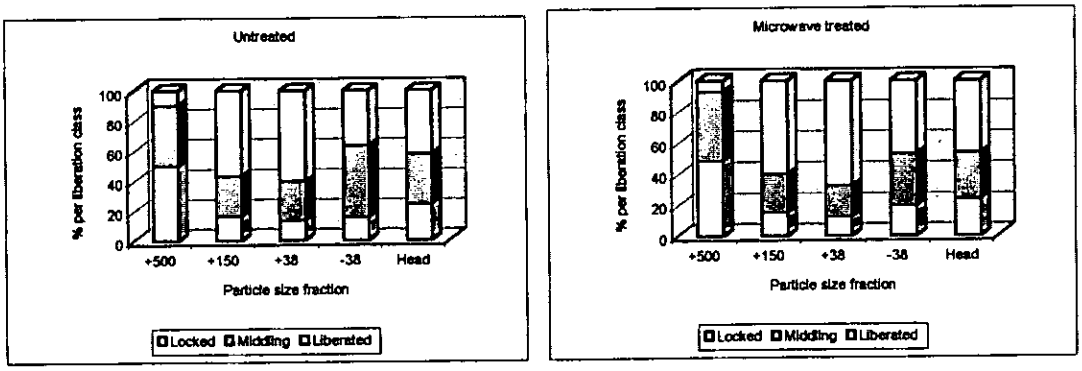

Figure 6.24. Galena liberation.

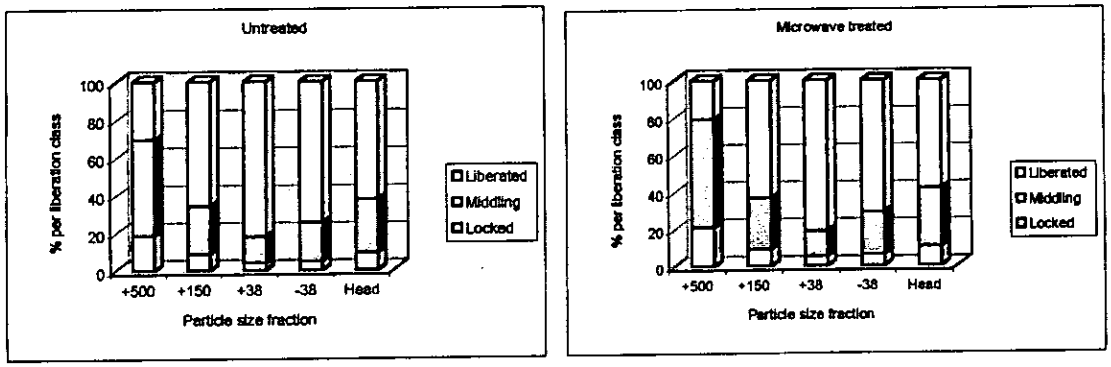

Figure 6.25. Sphalerite liberation.

As illustrated in Figures 6.25, microwave treatment does not have a significant impact on the liberation characteristics of galena and sphalerite. Galena in the +500 μm fraction occurs mostly in the middling and locked fractions, generally as composites with sphalerite and non-sulphide gangue (see Table 6.6).

6.6. Conclusions

An investigation into the effect of microwave radiation on the mineralogy, comminution processes and mineral liberation of Zinkgruvan ore has been carried out. The mineralogy of Zinkgruvan has been found dominated by the presence of a significant sphalerite granular aggregates that are intimately intergrown with galena and transparent gangue minerals. The sphalerite and galena may also occur finely disseminated throughout the gangue along grain boundaries and fractures region. These modes of occurrence have been found to significantly affect the interaction of the ore with microwave radiation. Dielectric properties of the major minerals and gangue (galena, sphalerite and feldspar) have significant difference at high temperatures. The exponential trend exhibited by sphalerite makes it difficult to treat this ore on high power densities due to the thermal effect on the loss factor.

The effect of microwave treatment on the Zinkgruvan ore strength has been investigated. The investigation consisted on the comparative study of the ore strength

using uniaxial compressive strength and point load tests. The comparative study was carried out on multimode and single mode microwave treated and untreated samples. The point load test results clearly show significant energy reductions on the microwave treated samples of up to 70% of the original point load index for the untreated sample. Such reductions have been obtained for a microwave exposure time of 0.5 seconds and 5 seconds for single mode and multimode cavities respectively. The importance of the electric field has also been demonstrated and it has been shown that significant reductions in ore strength can be achieved with short cavity residence times.

The effect of microwave treatment on the comminution and grindability of the Zinkgruvan ore has also been investigated. The microwaves have particularly a significant effect within range –22.4+9.5mm, with maximum effect observed on 14.5mm mean particle size on both drop weight and breakage rate tests. The effect of power density has also been shown to be significant, on test carried out on multimode and single mode cavities. Because of low power density developed within multimode cavities it was possible to treat the ore at 15kW microwave power, however the same power could not be achieved in single mode cavity. Nevertheless, due to high power density developed in single mode, similar effect was achieved at 10kW microwave power and short exposure times.

Microwaves, however, do not have significant effect on the mineral liberation of this particular ore and this could be mainly due to the dissemination of mineral phases. For this kind of ore, much high power density would be required at very short exposure time to produce a significant effect on the mineral liberation.

CHAPTER SEVEN
CONCLUSIONS AND FURTHER WORK

7.1. Conclusions

Comminution is an essential process in most mining operations to liberate the valuable minerals for subsequent beneficiation and concentration. It is the most energy intensive step in the process and the least efficient. Suggested methods to improve the efficiency of the process have included either fundamental changes in the technology or incremental improvements. Throughout the last century various authors have investigated the phenomena of thermally assisted liberation (T.A.L) as a fundamental technology to improve the efficiency of the process. Most, if not all have concluded that the process benefits of T.A.L whilst extremely attractive, are highly energy intensive and are therefore of limited commercial value. It was not until the end of the 1980's that microwave energy was first suggested as an energy source to achieve the benefits of T.A.L without the penalty of bulk heating solids.

Microwave assisted liberation is a technology that can provide the mineral processor with a new, powerful and significantly different tool to process complex ores that may not be amenable to current technology. First controlled and used during the Second World War in radar systems, the usefulness of microwaves in the heating of materials was first recognized in 1946. A large investment has been made over years in the development of microwave processing systems for a wide range of product applications. In general microwave systems consist of a microwave source, an applicator to deliver the power to the sample, and systems to control the heating. The most common applicators are multimode (e.g., home ovens), where numerous modes are excited simultaneously, and single-mode, where one resonant mode is excited.

Multimode applicators are known to have poor heating uniformity, low power density and usually designed for general purpose. While in single mode applicators, heating is more uniform, higher power density are created, however often they are product specific and in operation can be very sensitive to changes in products properties, geometry and position.

The initial workers in microwave-assisted liberation used multimode applicators. They concluded that while the amount of energy required to produce the benefits of T.A.L could be reduced considerably by the use of microwave energy, the energy input was still large and reductions in work index alone would not improve process economics. It was suggested, however, that improvements in grade of concentrate and recovery of useful mineral coupled with significant increases in grindability would make the prospect of microwave treatment extremely attractive.

A recent study considered the effect of microwave treatment on different ore mineralogy. It also investigated the effect of power level and exposure time on strength changes. It concluded that whilst long exposure times were necessary to create an effect such exposure times induced heat transfer by conduction between the different mineral phases thus reducing the temperature difference, the main factor for differential thermal expansion. Quite often, if good absorbers were present in the ore matrix, long exposure times could lead to partial melting that was proven to be detrimental to downstream processing. This study also concluded that ore mineralogy has a significant role regarding the effect of microwave treatment upon ore grindability. It was observed that a coarse grained and consistent mineralogy its more amenable for microwave effect on grindability than a fine grained and discrete mineralogy, albeit for samples treated in multimode cavities.

It has also been shown that use of numerical modelling technique can be an important research tool for a theoretical investigation of microwave-assisted comminution. Researchers, using numerical modelling, showed that using high power densities, similar to those achievable in single mode cavities could increase heating rate to the point where large stresses could be achieved without significant conduction heat transfer. However, the lack of basic data on dielectric properties of minerals constituted a severe hindrance for understanding of the problem.

The present research has focused on the understanding the interaction of microwave with minerals and ores. The effects of temperature, frequency and density upon dielectric properties of important mineral groups found on major ores were determined. It has also considered the effects of microwave treatment upon two mineralogically different ores: lead/zinc sulphide ore and a copper bearing carbonatite. A detailed measurement of dielectric properties was conducted using a TM_{0n0} cylindrical cavity capable of resonating at 0.615, 1.413 and 2.216 GHz frequencies. The measurement of five sulphide minerals (chalcocite, chalcopyrite, galena, pyrite and sphalerite) showed that real permitivity or dielectric constant and loss factor vary with temperature and density. The penetration depth however varied with frequency. The variation of the dielectric constant and loss factor with temperature was found to be mainly due to phase transformation during heating process. The investigation has found that galena and sphalerite have low loss factor at low temperature, suggesting therefore a poor heat dissipation of the stored microwave energy. However, a detailed analysis of data suggests that galena has significantly high loss tangent, the factor determining how well a material absorb electromagnetic energy and dissipates it as heat. This explains why galena has been reported to heat readily while sphalerite does

not heat at low temperature. Both minerals are good absorber of microwave radiation at high temperature.

The study also showed that by determining the dielectric constant for at least two packing densities, it is possible to use the linear relationship between dielectric constant and packing density to extrapolate the dielectric constant of the solid. This study found that dielectric properties of oxides do not vary with temperature, however they vary with density. Oxides are generally stable with temperature and were found to be fairly good absorbers. A detailed literature survey suggests that magnetite is a good absorber of microwave radiation, therefore should exhibit high value of loss factor. However, the present study has found low values for the loss factor of magnetite. A possible explanation for the discrepancy of the results from the literature and the present findings is that perturbation technique for the measurement of dielectric properties is not suitable for high loss materials. Dielectric properties of silicates have also been determined. The detailed measurement showed that silicates in general are low loss minerals with values of loss factor below 0.2.

Microwave assisted liberation of ores was also investigated. This included a copper carbonatite ore from the Palabora deposit in South Africa and a massive lead/zinc sulphide from the Zinkgruvan deposit in Sweden. The copper carbonatite ore was found to exhibit a consistent mineralogy of discrete grains of good absorbers of microwave radiation in a transparent gangue matrix. However, the lead/zinc sulphide consisted of small particles of galena (good absorber of microwaves) and sphalerite (good absorber at high temperature), finely disseminated in discrete elements of transparent gangue and quite often, discrete grains of gangue were also found disseminated in aggregates of Sphalerite. Different behaviour of the two ores upon microwave treatment was expected.

Microwave treatment was found to have a significant effect on the strength of both ores. Ore samples were microwave treated in a low and high electric field strengths microwave cavities. Significant reductions in ore strength were achieved using high electric field strength single mode microwave cavities for short exposure times. After microwave treatment visible fractures were observed and samples could be broken by hand. Reductions of up to 40% in calculated crusher power data and up to 70% in ore grindability were obtained for the copper carbonatite ore. While for the lead/zinc sulphide ore reductions of up to 35% in calculated crusher power data and over 70% in breakage rate were achieved. For both ores it has been found that grindability is intimately related to particle size, for this cavity.

Quantitative evaluation of the microwave effect on mineral liberation has also been carried out. It was found that mineral liberation of copper sulphides in the copper carbonatite ore was significantly increased by microwave treatment. More significant is that it occurred at coarse particle sizes, 500μm. Microwave treatment was found not to have a significant effect on the liberation of lead/zinc sulphides in the Zinkgruvan ore. However, this should be treated with caution since high stressing rates were applied on the comminution of samples for QEM*SEM studies. Methods of comminution that use high stressing have been found to mask the effect of preferential breakage on grain boundaries of particles that exhibit significant and visible microfractures. It has been reported that reduction of ore strength by microwave treatment is due to induced fractures at grain boundaries and this will require less energy for breakage.

7.2. Further Work

The influence of microwave treatment upon the processing of two complex ores has been discussed within this thesis and was also included measurement of dielectric properties of minerals. Dielectric properties measurements have been carried out and results discussed. It has been found however that resonant cylindrical cavity is not suitable for accurate measurement of high loss materials. It is therefore recommended that the technique be further investigated to improve measurement on high loss material and results should be compared with measurements using other techniques such as coaxial line.

Quantification of mineral liberation has also been discussed, however the use of high stressing comminution methods have been found to mask the micro-fractures induced by microwave treatment. A combination of laboratory/pilot scale experimental work using different comminution equipment such as cone crusher and rod mill is therefore recommended and mineral liberation compared. The work should also include the use of steady state simulation models to demonstrate the influence of the microwave pre-treatment on comminution and liberation efficiencies.

REFERENCES

Aird, R. (1998). Personal Communication, Palabora Mining Company.

Al-Harehsheh, M., Kingman, S.W. (2003). "Microwave Assisted Hydrometallurgical Extraction of Metals - A Review." Hydrometallurgy in print.

Andres, U., Jiresting, J., and Timoshkin (1999). "Liberation of minerals by high voltage electrical pulses." Powder Technology 104: 37-49.

Arai, M., Cross, T.E., and Binner, J.G.P. (1992). Microwave Complex Permitivity Measurement – Using a Surface Probe Technique –Effect of Surface Roughness on Measured Permitivity. Unpublished report of investigation. University of Nottingham.

Arai, M. (1995). High Temperature Dielectric Properties Measurements of Engineering Ceramics. Report of Investigation, University of Nottingham.

Arai, M., Binner, J G p., Carr, G E., and Cross, T E (1993). "High Temperature Dielectric Property Measurements of Engineering Ceramics." Mater. Res. Soc. Proc. 269: 483-493.

Asensio, I., and Sabatier, G., (1958). "Analyse thermique differentielle de quelques mineraux sulfures et arsenies de fer nickel et cobalt." Bull. Soc. Franc. Min. Crist. 81: 12.

Austin, L. (2002). "A treatment of impact breakage of particles." Powder Technology In press.

Austin, L. G., and Luckie, P.T (1971). "Methods for determination of breakage distribution parameters." Powder Technology 5: 45-52.

Austin, L. G., and Weller, K.R. (1982). Simulation and scale-up of wet ball milling. XIV Int. Miner. processing Congr., Toronto, 1-8.

Austin, L. G., and Brame, K. (1983). "A comparison of the Bond method for sizing wet tumbling mills with a size-mass balance simulation model." Powder Technology 34: 261-274.

Awachie, S. E. A. (1983). Development of Crusher Models Using Laboratory Breakage Data. PhD Thesis, University of Queensland (JKMRC).

Bailey, S. W., Cameron, E.N., Spedden, H.R., and Weege, R.J. (1956). "The alteration of ilmenites in beach sands." Economic Geology 51: 263.

Banini, G. A., Morrell, S., and Bourgeois F.S. (2000). "Quantitative measurement of surface breakage of industrial ores." Private communication.

Banini, G. A., and Bourgeois F.S. (2002). "A portable load cell for in-situ ore impact breakage testing." Int. J. Miner. processing 65: 31-54.

Batt, J., Binner, JGP., Cross, TE., Greenacre, N.R., Hamlyn, M G., Hutcheon, R.M., Sutton, W.H., and Weil, C.M. (1995). "A Parallel Measurement Programme in High Temperature Dielectric Property Measurements: An Update." Ceramics Transactions 59: 243-250.

Bearman, R. A., Briggs, C.A., and Kojovic, T. (1997). "The Application of Rock Mechanics Parameters to the Prediction of Comminution Behaviour." Minerals Engineering 10(3): 255-264.

Bearman, R. A. (1999). "The use of the point load test for the rapid estimation of Mode I fracture toghness." Int. j. Rock Mechanics and Mining Sciences 36: 257-263.

Beeson, R. (1990). "Broken Hill type lead-zinc deposits- an overview of their occurrence and geological setting." Trans Inst Min Metall 99: B163-B175.

Bengtsson, V. C. (2000). Lithogeological Characteristics of a Profile Across the Nygruvan Orebody, Zinkgruvan, South-Central Sweden, http://www.gvc.gu.se/biblio/B.serin/B234.pdf. 2003.

Blake, C. (2001). Mineralogical Characterisation of Zinkgruvan ore, Rio Tinto Technological Development, Ltd.

Bond, F. C. (1952). "The third theory of comminution." Minerals Engineering 4: 484.

Bond, F. C. (1961). "Crushing and Grinding Calculations-Part I." British Chemical Engineering 6(6): 378-385.

Bond, F. C. (1961). "Crushing and Grinding Calculations - Part II." British Chemical Engineering 6(8): 543-548.

Bradshaw, S. (2002). Design of Microwave Cavities. Private Communication.

Brady, B. H. G., & Brown, E.T. (1993). Rock Mechanics for Underground Mining, Chapman & Hall.

Broch, E., and Franklin J.A. (1972). "The Point Load Strength Test." Int. j. Rock Mechanics and Mining Sciences 9: 669-697.

Broch, E. S. (1971). Point Load Testing of Rocks. London, Imperial College of Science and Technology.

Buchner, R., Barthel, J., and stauber, J. (1999). "The dielectric relaxation of water between O C and 35 C." Chem. Phys. Lett. 306: 57-63.

Bykov, Y. V., Rybakov, KI., and Semenov, VE (2001). "High Temperature microwave processing of materials." J. Appl. Phys. 34: 55-75.

Chan, T. V., Chow, T. (2000). "Understanding Microwave Heating Cavities." London: Archtech. House.

Chatterjee, I., and Misra, M. (1991). "Electromagnetic and Thermal Modeling of Mirowave Drying of Fine Coal." Minerals and Metallurgical Processing: 110-114.

Chen, T., Dutrizac, JE., Haque, KE, Wyslouzil, W. and Kashyap, S. (1984). "The Relative Transparency of Minerals to Microwave Radiation." Can. Metall. Quartely 23(1): 349-351.

Church, R., Webb, WE., and Salsman, JB. (1994). Dielectric Properties of Low-Loss Minerals, USBM-RI 9194.

Clark, S. P. (1966). "Handbook of Physical Constants." The Geographical Society of America.

Deer, H., & Zussman (1962). Rock forming minerals, Longman group Ltd.

Deer, H., & Zussman (1966). An Introduction to the Rock Forming, Longman group Ltd.

Diernat, F., and Duffaut, P. (1966). Essais sur echantillons de forme irreguliere. Proc. 1st Congr. Int. Soc. Rock Mechanics, Lisbon.

Duffaut, P. (1968). "Effect d'echelle dans l'ecrasement de blocs de forme irreguliere." Revue de L'Industrie Minerale.

Duffaut, P., and Maury, V. (1970). Etudes photoelastiques sur l'essai Protodyakonov. 2nd Congr. Int. Soc. Rock Mechanics, Belgrade.

Dukino, R. D., Swain, M.V., and Loo, C.E. (2000). "A simple contact and fracture mechanics approach to tumble drum breakage." Int. J. Miner. processing 59: 175-183.

Evertsson, C. M., and Bearman R.A. (1997). "Investigation of Interparticle Breakage as Applied to Cone Crusher." Minerals Engineering 10(2): 199-214.

Fairs, G. L. (1954). "A method of predicting the performance of commercial mills in the fine grinding of brittle materials." Trans Inst Min Metall 63: 211-240.

Fletcher, R. (1995). Investigation into Microwave Heating of Uranium Dioxide. Electrical Engineering, University of Nottingham.

Florek, I., Labun, J., Murova, I., and Lovas, M (1996). The Measurement of Complex Electric Permitivity of Fine Grained Minerals at Microwave Frequencies. Int. Microwave Power Symposium, Boston, USA.

Frandich, R., Beraman, RA, Boland J and Lim, W (1997). "Mineral Liberation by Particle Bed Breakage." Minerals Engineering 10(2): 175-187.

Gaal, G., & Gorbatschev, R., (1987). "An Outline of the Precambrian Evolution of the Baltic Shield." Precambrian research 35: 15-52.

Gallawa, J. C. (1989). What are Microwaves?, http:/www.gallawa.com/microtech/mwave.html. 2003.

Gay, S. L. (1999). "Numerical verification of a non-preferential breakage liberation model." Int. J. Miner. processing 57: 125-134.

Goodier, J. (1933). "Compression of rectangular blocks." J Applied Mech, Trans Am Soc Mech Engrs 55: 39-44.

Greenacre, N. R. (1996). "Measurement of the High Temperature Dielectric Properties of Ceramics at Microwave Frequencies." PhD Thesis University of Nottingham.

Gross, J. (1938). "Crushing and grinding." US Bureau of Mines Bulletin 402: 1-48.

Hahne, R., Palsson, BI., Samskog, P.O. (2003). "Ore characterisation for-and simulation of primary autogenous grinding." Minerals Engineering 16: 13-19.

Haque, K. E. (1987). Microwave irradiation pre-treatment of refractory gold concentrate. International Symposium on Gold Metallurgy, Winnipeg, Canada.

Haque, K. E. (1999). "Microwave energy for mineral treatment processes - a brief review." Int. J. Miner. processing 57: 1-24.

Harrison, P. C. (1997). A fundamental study of the heating effect of 2.45 GHz microwave radiation of minerals. Birmingham, University of Birmingham.

Hedstrom, P., Simeonov, A., & Malmstrom, L. (1989). "The Zinkgruvan ore deposit, South central Sweden: A proximal Zn-Pb-Ag deposit in distal volcanic facies." Economic Geology 84: 1232-1261.

Herbst, J. A., and Fuerstenau, D.W. (1968). "The zero order production of fines in comminution and its implications in simulation." Trans SME/AIME 241: 531-549.

Herbst, J. A., and Fuerstenau, D.W. (1980). "Scale-up procedure for continuos grinding mill design using population balance models." Int. J. Miner. processing 7: 1-31.

Holderfield, S. P., and Salsman, J.B. (1992). "Observed Trends in the Dielectric Properties of Minerals at Elevated Temperatures." Mater. Res. Soc. Proc. 269: 589-594.

Hondros, G. (1959). "The evaluation of Poisson's ratio and the modulus of materials of a low tensile resistance." Aus J Applied Science 10: 243-268.

Hopkinson, B. (1914). "A method for measuring the pressure produced in the detonation of bullets." Philos Trans R Soc Ser A(213): 375-457.

Huston, S. (1993). Water, http:/www.bris.ac.uk/Depts/Chemistry/MOTM/water/water.html. 2002.

Hutcheon, R. M., de Jong, M S., Adams, PG., Lucuta, PG, McGregor, J E., and Bahan, L (1992). "RF and Microwave Dielectric Measurements to 1400 C and Dielectric Loss Mechanisms." Mater. Res. Soc. Proc. 269: 541-551.

Iskander, M. F. (1991). "Computer Modeling and Numerical Techniques for Quantifying Microwave Interactions with Materials." Mater. Res. Soc. Proc. 189: 149-157.

Internal Report, Palabora Mining Company, 1987.

Jacob, J., Chia, L.H.L., and Boey, F.Y.C. (1995). "Review: Thermal and non-thermal interaction of microwave radiation with materials." Journal of Material Science 30: 5321-5327.

Jacobs, I. S. (1982). "Tracking pyrite sulfur in the microwave desulfurization of coal." J. Appl. Phys. 53(2): 2730-32.

Jaeger, J. C., and Cook, N.G.W. (1979). Fundamentals of Rock Mechanics. Methuen and Co. London.

Johan, B. N., Petra, L., & Petra, B. (2002). Garpenberg- An Old Concentrator at Peak Performance, http://www.mining-technology.com/projects/zinkgruvan/. 2003.

Karkhanavala, M. D., and Momin, A.C., (1959). "The alteration of ilmenite." Economic Geology 54: 1095.

Kelly, R. M., and Rowson, N.A. (1995). "Microwave reduction of oxidised ilmenite concentrate." Minerals Engineering 8(11): 1427-1438.

King, R. P. (2001). Modeling & Simulation of Mineral Processing Systems, BH.

Kingman, S. W., Rowson, N.A. & Blackburn, S. (1997). Applications of Microwave Radiation to Enhance Performance of Mineral Separation Processes. Innovation in Physical Separation of Minerals. IMM.

Kingman, S. W., & Rowson, N.A. (1998). "Microwave treatment of minerals - a review." Minerals Engineering 11(11): 1081-1087.

Kingman, S. W., Corfield, G.M., & Rowson, N.A. (1999). "Effects of Microwave Radiation upon the Mineralogy and Magnetic Processing of a Massive Norwegian Ilmenite Ore." Magnetic and Mineral Separation 9: 131-148.

kingman, S. W. (1999). The effect of microwave radiation upon the comminution and beneficiation of minerals. PhD Thesis, The University of Birmingham.

Kingman, S. W., Vorster, W., & Rowson, N.A. (2000). "The influence of mineralogy on microwave assisted grinding." Minerals Engineering 13(3): 313-327.

Kingman, S. W., & Rowson, N.A. (2000). "The Effect of Microwave Radiation on the Magnetic Properties of Minerals." J Microwave Power and EE 35(3): 144-150.

Kingman, S. W., Jackson, K., Cumbane, A.J., Bradshaw, S.W., Greenwood, R. & Rowson, N.A. (2003). "An Investigation into the Influence of Microwave Treatment on Mineral Ore Comminution."

Kingman, S. W., Jackson, K., Cumbane, A.J., Bradshaw, S.W., Greenwood, R. & Rowson, N.A. (2003). Towards Economic Microwave Assisted Comminution, University of Nottingham.

Klein, O., Donovan, S., and Dressel, M (1993). "Microwave Cavity Perturbation Technique: Part I - Principles." Int. J. of Infrared and Millimeter Waves 14(12): 2423-2457.

Klein, O., Donovan, S., and Dressel, M (1993). "Microwave Cavity Perturbation Technique: Part III -Applications." Int. J. of Infrared and Millimeter Waves 14(12): 2489-2502.

Klein, O., Donovan, S., and Dressel, M (1993). "Microwave Cavity Perturbation technique: Part II - Experimental Scheme." Int. J. of Infrared and Millimeter Waves 14(12): 2459-2487.

Koukkala, V. T., and Vuoristo, T. (2002). Hopkinson Pressure Bar Experiment, http://www.ccm.udel.edu/reports-pubs/spring02-reviews/. 2003.

Kraszewski, A. (1977). "Prediction of the dielectric properties of two phase mixtures." J Microwave Power 12(3): 215-222.

Laplante, A. R., McIvor, R.E., and Finch, J.A. (1988). "Error Analysis for Bond Work Index Determinations part1: Accuracy and Reproducibility." Minerals Engineering 1(2): 113-125.

Large, D. J., MacQuaker, J., Vaughan, D.J., Sawlowicz, Z. and Gize, A.P. (1995). "Evidence for Low-Temperature Alteration of Sulfides in the Kupferschiefer Copper Deposits of Southwestern Poland." Economic Geology 90: 2143-2155.

Lepp, H. (1957). "Stages in the oxidation of magnetite." Amer. Min. 42: 679.

Levy, C. (1958). "Analyse thermique des minerais sulphures." Bull. Soc. Franc. Min. Crist. 81: 29.

Marland, S., Merchant, A., & Rowson, NA (2001). "Dielectric properties of coal." Fuel 80(13):1839-1849.

Mason, B. (1943). "Mineralogical aspects of the system FeO-Fe2O3-MnO-Mn2O3." Geol. For. Forh. Stockholm 65: 97.

McGill, S. L., Walkiewicz, J.W., and Smyres, G.A. (1988). "The effect of power level on the heating rate of selected chemical and minerals." Mater. Res. Soc. Proc. 124: 247-252.

McLaughlin, R. J. W. (1957). "The differential thermal investigations of clays." Min. Soc. 14.

Meredith, R. (1998). Engineers Handbook of Industrial Microwave Heating, Peter Peregrinus Ltd.

Metaxas, A. C., & Meredith, R.J. (1983). Industrial Microwave Heating, Peter Peregrinus Ltd.

Middlemiss, S., and King, RP (1994). Investigation of the micro-fracture characteristics of geological materials by indentation techniques. SME/AIME Anual Meeting.

Middlemiss, S., and King, RP (1996). "Microscale fracture measurements with application of comminution." Int. J. Miner. processing 44-45: 43-58.

Morrell, S., and Morrison, R.D. (1989). Ore charge, ball load and material flow effects on an energy based SAG mill model. Proceedings advances in

Autogenous and SAG Technology, University of British Columbia, Vancouver.

Mosher, J., and Tague CB (2001). "Conduct and Precision of Bond Grindability Testing." Minerals Engineering 14(10): 1187-1197.

Napier-Munn, T. E., Ed. (1996). Mineral Comminution Circuits. Their Operation and Optimisation. Mining and Mineral Processing 2. Australia, University of Queensland.

Narayanan, S. (1985). Development of a laboratory single particle particle breakage technique and its application to ball mill modeling and scale up. PhD Thesis, University of Quensland (JKMRC).

Narayanan, S., Whiten, WJ (1988). "Determination of comminution characteristics from single particle breakage tests and its application to ball mill scale-up." Trans Inst Min Metall 97: c115-c124.

Nelson, S. O. (1983). "Observations on the Density Dependence of Dielectric Properties of Particulate Materials." Journal of Microwave Power 18(2): 143-152.

Nelson, S. O. (1988). "Estimating the Permittivity of Solids from Measurements on Granular or Pulverized Materials." Mater. Res. Soc. Proc. 124: 149-154.

Nelson, S. O., and Trabelsi, S. (2003). "Free-space measurement of dielectric properties of cereal grain and oilseed at microwave frequencies." Meas. Sci. Technol. 14: 589-600.

Oespchuck, J. M. (1984). "Microwave Theory and Techniques." IEEE Trans. Microwave Theory Tech 32(9): 1200-1224.

Parr, J. M., & Plimer, I.R. (1993). Models for Broken Hill type Lead-Zinc-Silver Deposits. Geological Association of Canada. Special Paper 40: 253-288.

Pauw, O. G., and Mare, M.S. (1988). "The determination of optimun breakage routes for an ore." Powder Technology 54: 3-13.

Piret, E. L. (1953). "Fundamental aspects of grinding." Chem. Eng. Prog. 49: 56-63.

Plimer, I. R. (1988). "Broken Hill, Australia and Bergslagen, Sweden." Geologie en Mijnbouw 67: 265-278.

Pocock, J. (1995). An Investigation into Reclamation of Silica Sand from Foundry Greensands. Internal Report, University of Birmingham.

Protodyakonov, M. M. (1960). New Methods of Determining Mechanical Properties of Rock. Inter. Conf. on Strata Control, Paris.

Protodyakonov, M. M. (1962). Methods of Studying the Strength of Rocks used in USSR. Int. Symp. on Mining Research, University of Missouri, Pergamon Press.

Rio Tinto Annual Report, 1992

Rio Tinto Annual Report, May 2003

Rowson, N. A., and Rice, N.M. (1990). "Magnetic enhancement of Pyrite by caustic microwave treatment." Minerals Engineering 3(3-4): 355-361.

Rowson, N. A., and Rice, N.M. (1990). "Desulphurisation of coal using low power microwave energy." Minerals Engineering 3(3-4): 363-368.

Salsman, J. B. (1991). "Technique for Measuring the Dielectric Properties of Minerals as a Function of Temperature and Density at Microwave Heating Frequencies." Mater. Res. Soc. Proc. 189: 509-515.

Salsman, J. B. (1992). "Measurement of Dielectric Properties in the Frequency Range of 300 MHz to 3 GHz as a Function of Temperature and Density." Ceramics Transactions 59: 203-215.

Salsman, J. B., Williamson, R.I., Tolley, W.K. and Rice, D.A. (1996). "Short-Pulse Microwave Treatment of Disseminated Sulfide Ores." Minerals Engineering 9(1): 43-54.

Schmidt, E. R., and Vermaas, F.H.S. (1955). "Differential thermal analysis and cell dimensions of some natural magnetites." Amer. Min. 40: 422.

Schonert, K. (1972). "Role of fracture physics in understanding comminution phenomena." Trans SME/AIME 252: 21-26.

Sentence, W., 1998. Personal Communication, Palabora Mining Company.

Stephens, M. B., Wahlgren, C., Weijermars, R. & Cruden, A.R. (1996). "Left-lateral transpressive deformation and its tectonic implications, Sveconorwegian orogen, Baltic Shield, southwestern Sweden." Precambrian research 79: 261-279.

Stolen, S., and Gronvold, F. (1990). "Thermodynamics of Copper Sulfides." J. Chem. Thermodynamics 22: 1035-1057.

Tavares, L. M., and King R.P. (1998). "Single particle fracture under impact loading." Int. J. Miner. processing 54: 1-28.

Tavares, L. M., and King R.P. (2002). "Modeling of particle fracture by repeated impacts using continuum damage mechanics." Powder Technology 123: 138-146.

Tinga, W. R. (1992). "Rapid High Temperature Measurement of Microwave Dielectric Properties." Mater. Res. Soc. Proc. 269: 503-515.

Tinga, W. R., and Xi, W. (1993). "Design of a New High Temperature Dielectrometer System." J Microwave Power and EE 28(2): 93-103.

Tinga, W. R., and Tian, B.Q. (1993). "Single Frequency Relative Q Measurements Using Perturbation Theory." IEEE Trans. Microwave Theory Tech 41(11): 1922-1927.

Tinga, W. R. (1994). "Microwave System Design and Dielectric Property Measurements." Mater. Res. Soc. Proc. 347: 1-14.

Tinto, R. (2003). Rio Tinto Anual Report.

Valery, W. (1997). A model for dynamic and steady-state simulation of autogenous and SAG mills. PhD Thesis, University of Queensland (JKMRC).

Varlamoff, N. (1948). "Materiaux pour l'etude du mineral jaune d'etain: occurrence geologie et origine du mineral." Ann. Soc. Geol. Belgique 72: 289.

Veasey, T., Fitzgibbon KE. (1990). "Thermally Assisted Liberation of Minerals - A Review." Minerals Engineering 3(1/2): 181-185.

Viswanathan, M. (1990). "Investigations on the Effect of Microwave Pre-treatment on Comminution." International Coal Preparation Congress: 151-155.

Vorster, W., Kingman, SW and Rowson, NA (2000). Applications of Microwave Radiation for the Procesing of Minerals. SAIChE, South Africa.

Walkiewicz, J., Kazonich, G., & McGill SL., (1988). "Microwave Heating Characteristics of Selected Minerals and Compounds." Minerals and Metallurgical Processing 5(1): 39-42.

Walkiewicz JW., C., A.E, McGill SL., (1991). "Microwave Assisted Grinding." IEEE Trans. on Industry Applications 27(2): 239-242.

Wang, Y., Forssberg, E., and Svensson, M. (2001). Microwave assisted comminution and liberation of minerals. Mineral Processing on the Verge of the 21st Century, Rotterdan.

Weichert, R., and Herbst, J. (1986). An ultra fast load cell for measuring particle breakage. World Congress Particle Technology: Part II. Comminution.

Whiten, W. J. (1974). "A matrix theory of comminution machines." Chem. Eng. Sci. 29: 588-599.

Whiten, W. J. (1976). "Ball mill simulation using small calculators." Proceedings of AusIMM 258: 47-53.

Whittaker, G. (1994). Microwave Heating Mechanisms, http:/homepages.ed.ac.uk/ah05/ch1a.html. 2003.

Whittaker, G. (1997). A Basic Introduction to Microwave Chemistry, http://homepages.ed.ac.uk/ah05/. 2003.

Whittles, D. N., Kingman, S.W., & Reddish, D.J. (2003). "Application of numerical modeling for prediction of power density on microwave assisted breakage." Int. J. Miner. processing 68: 71-91.

Wightman, E. (2002). QEM*SEM Analysis of Microwave Samples, Rio Tinto Technical Services Development Group.

Woodcock, J. T. (1989). Possibilities for using microwave energy in the extraction of gold. First Australian Symposium on Microwave Power, 139-153.

Worner, H. K. (1990). Microwave irradiation of composites. US Patent No. 4076607.

Zavitsanos, P. D., and Bleiler, K.W. (1978). Coal desulphurisation. US Patent No. 4076607.

Zavitsanos, P. D., Bleiler, K.W., and Golden, J.A. (1979). Coal desulphurisation using alkali metal or alkali earth compounds and electromagnetic energy. US Patent No. 4152120.

ARTICLE IN PRESS

ELSEVIER

Available online at www.sciencedirect.com
SCIENCE DIRECT®

Int. J. Miner. Process. xx (2003) xxx–xxx

INTERNATIONAL JOURNAL OF MINERAL PROCESSING

www.elsevier.com/locate/ijminpro

Recent developments in microwave-assisted comminution

S.W. Kingman[a,*], K. Jackson[a], A. Cumbane[a], S.M. Bradshaw[b], N.A. Rowson[c], R. Greenwood[c]

[a] *School of Chemical Environmental and Mining Engineering, University of Nottingham, University Road, Nottingham, NG7 2RD, UK*
[b] *Department of Chemical Engineering, University of Stellenbosch, Stellenbosch, South Africa*
[c] *School of Chemical Engineering, University of Birmingham, Birmingham, B15 2TT, UK*

Received 12 May 2003; received in revised form 10 September 2003; accepted 10 September 2003

Abstract

The influence of high electric field strength microwave energy on copper carbonatite ore has been elucidated. It has been shown that very short exposures times can lead to significant reductions in ore strength as determined by point load tests. Comparative drop weight tests were carried out to determine any potential change in required comminution energy for microwave-treated material. It was shown that reductions in required comminution energy of over 30% could be achieved for microwave energy inputs of less than 1 kW h t^{-1}. Comparative specific rate of breakage grinding studies showed that significant increases in grindability could also be achieved after short microwave exposure times, changes being related to particle size. QEM*SEM liberation studies showed that the amount of locked and middling copper sulphides was reduced from 69.2% to 31.8% in the +500 μm size fraction. Conclusions are made regarding the potential future development of this technology.

© 2003 Elsevier B.V. All rights reserved.

Keywords: energy requirements; grindability; impact energy; mineral liberation

1. Introduction

The mineral resource and environmental industries are major employers and represent a significant proportion of gross domestic product for many countries worldwide. World consumption of minerals is increasing, a trend likely to continue if the substantial and rising expectations of countries in the Pacific Rim, Central and South America, and Africa are to be met. The sustainable development and use of raw resources requires new, better and more efficient processes. The recent UK Government Technology Foresight document, from the Natural Resources and Environment Panel (1999), stated that new developments were required to improve and adapt existing unit processes. In particular, improvements in rock breaking and mineral liberation techniques and reductions in energy requirements for metal production processes were required.

Various approaches have been taken in an attempt to improve the efficiency of comminution processes. These have included steady state comminution circuit modelling and the development of novel comminution

* Corresponding author. Tel.: +44-115-951-4081; fax: +44-115-951-4115.
E-mail address: sam.kingman@nottingham.ac.uk (S.W. Kingman).

0301-7516/$ - see front matter © 2003 Elsevier B.V. All rights reserved.
doi:10.1016/j.minpro.2003.09.006

ARTICLE IN PRESS

devices such as the high pressure grinding rolls by Schönert (1988). Whilst both of these techniques have offered improvements, the improvements have been incremental. The ability to alter the properties of the ore to reduce strength and improve liberation is ultimately the only way that step changes in the efficiency of comminution processes will be made. One such way of changing the fundamental properties of the ore has been microwave pre-treatment. Pioneering work was reported by Walkiewicz et al. (1988, 1991). Other workers in the field include Tavares and King (1995). Although promising reductions in grindability or ore strength were obtained, the economics of the process were considered unfavourable at the time. More recent work confirmed that microwave radiation is extremely effective in inducing fracture in mineral specimens. Kingman et al. (1999) exposed massive Norwegian ilmenite ores to microwave radiation for varying times and showed reductions in Work Index of up to 90%. The influence of the microwave treatment on downstream magnetic separation was also quantified and increased recovery of ilmenite was demonstrated for microwave-treated samples in comparison to untreated samples. It was concluded that short, high-power treatments were most effective because over-exposure of the sample led to reductions in downstream processing efficiency. Kingman and Rowson (2000) extended this work to investigate the reasons for possible increases in recovery of valuable mineral after microwave treatment. It was shown that increased recovery was due not only to increases in liberation but also to enhancement of the magnetic properties of the material. Kingman et al. (2000a) also carried out a qualitative study of the influence of mineralogy on the response of ores to microwave radiation. It was concluded that samples with a mixture of 'good heaters' and 'medium heaters' in a lattice of 'poor heaters' with a coarse grain size gave greatest reduction in work index after microwave treatment. Poorest response could be expected from ores containing highly disseminated, fine-grained minerals. A further conclusion from the work was that whilst the technical benefits were attractive, the economics were poor, with significant microwave energy inputs being used to give the reductions in comminution energy.

The influence of microwave treatment on flowsheet design has also been investigated by Kingman et al. (1999). Rod mill feed from a South African copper plant was subjected to microwave treatment at various power levels for various time-periods. The comparative Bond Work Index determined for each sample was used to investigate the performance and design of the actual grinding circuit for the ore in question. Using flowsheet-modelling software, it was shown that reducing the Work Index meant that a conventional system, e.g., an open-circuit rod mill followed by a closed-circuit ball mill, could be replaced by a single, open-circuit, rod mill. It was appreciated that this might not be the best operational procedure but was carried out as an indication of the possible influence of microwave treatment on flowsheet design. However, the conclusion drawn from the work was that, again, the technical benefits were attractive but the economics were poor, as the reduction in work index was achieved at high microwave power input. This effectively implies a high microwave energy cost that could not be justified based on the work index reduction. In order to improve the efficiency of microwave-assisted comminution to the point where it is potentially economically viable, improved understanding of the physics of microwave heating is required. The majority of the early test work involving microwave treatment of ores was carried out in multimode cavities. This is by far the most widely used type of microwave applicator, used in almost all domestic ovens and a large number of industrial units. The major benefit of this type of cavity is its mechanical simplicity and versatility. A basic, multimode cavity consists of a metal box, at least several wavelengths long in two dimensions. In simple terms, when the microwaves are launched into the box, they form a complex pattern of areas of high and low electric field strength, otherwise known as modes. In most materials, the electric field rather than the magnetic field is responsible for heating and it has been shown that the power density (or volumetric absorption of microwave energy) is proportional to the square of the strength of the electric field. Due to the complex distribution of the areas of high field strength, ensuring uniform high power density within a sample and achieving rapid heating rates is very difficult. This helps explain why previous work has reported poor economics as extended residence times have been required to induce the desired effects in the treated ore samples.

ARTICLE IN PRESS

The influence of power density on change in ore strength is also of great importance and has recently been investigated by Whittles et al. (2003). These workers carried out a series of comparative, two-dimensional finite-difference simulations to examine the thermo-mechanical response of ores to microwave treatment. The simulations were carried out on a simulated ore of microwave-responsive 1-mm^2 grains of pyrite within a microwave-transparent calcite matrix. After the simulation of heating and thermal stress generation at various power densities over a range of exposure times, uniaxial compressive strength tests were simulated. The results clearly showed that high power densities or electric field strengths were vital to rapid stress generation within the ore matrix.

Simulation of samples treated at a power density of 1×10^9 W m^{-3} showed a theoretical reduction in strength from 125 to 80 MPa in 30 s microwave exposure. However, simulations of samples treated at a power density of 1×1011 W m^{-3} showed a theoretical reduction in strength from 125 to 60 MPa in 0.05 s. This reduction in time is suggested as being a result of reduced thermal conduction through the sample and greater thermal gradients across the grain boundaries of the adsorbing and non-adsorbing phases within the model. It is also important to note that the greater strength reduction was achieved using only 1/6th of the energy. This has important implications for the economic viability of the process.

The production of high-strength electric fields and, hence power densities, in a multimode cavity is difficult. Therefore, it is necessary to move to a different type of cavity. A single mode cavity comprises a metallic enclosure into which a microwave signal of the correct electromagnetic field polarisation will undergo multiple reflections. The superposition of the reflected and incident waves gives rise to a standing wave pattern that is very well defined in space. The precise knowledge of electromagnetic field configurations enables the ore to be placed in the position of maximum electric-field strength allowing maximum heating-rates to be achieved at all times. In general, the heating zone in single mode cavities is small, which means that very high power density can easily be achieved.

In the early evolution of microwave heating, such cavities saw little industrial use. This was mainly because they lacked the versatility offered by multimode cavities and are typically best suited to heating filamentous materials. However, they can offer extremely rapid heating rates and the ability to heat materials that appear transparent to microwaves in multimode cavities using similar input power levels.

The aim of the work described in this paper was to investigate the comminution behaviour of ore treated at high microwave power but for short residence times. Initial characterisation of comminution behaviour of the treated ore was done in terms of ore crushing parameter, grindability and QEM*SEM liberation data.

2. Experimental

2.1. Materials

The ore used for this investigation was a South African copper carbonatite utilised in previous studies (Kingman, 1999). Representative portions of the sample were analysed by qualitative, backscattered SEM to determine the major gangue and ore minerals and their relative abundances. This analysis revealed that the sample consisted of various proportions of calcite ($CaCO_3$), dolomite ($CaMg(CO_3)_2$), apatite ($Ca_5(PO_4)_3(F,Cl,OH)$), olivine ($Mg_3Si_2O_5(OH)_4$), phlogophite ($KMg_3AlSiO_{10}(F,OH)_2$), serpentine ($Mg3Si_2O_5(OH)_4$), pyroxene and plagioclase feldspar. Carbonate minerals were found to be particularly abundant and consisted generally of calcite and dolomite. Magnetite was found to be abundant within this sample (approx. 20%). It occurred as discrete, liberated grains (often >300 μm) and to a lesser extent as intergrowths with transparent gangue. EDAX examination of the magnetite confirmed that it contained predominately of Fe and O with Mg and Ti being present in smaller amounts. The principal copper-bearing sulphide minerals were found to include cubanite ($CuFe_2S_3$), chalcopyrite ($CuFeS_2$), bornite (Cu_5FeS_4) and chalcocite (Cu_2S).

2.2. Microwave treatment

Samples were irradiated in a variable power (3–15 kW), microwave heater manufactured by Sairem of France. A schematic of the apparatus is shown in Fig. 1. Essentially the apparatus consists of a power supply

ARTICLE IN PRESS

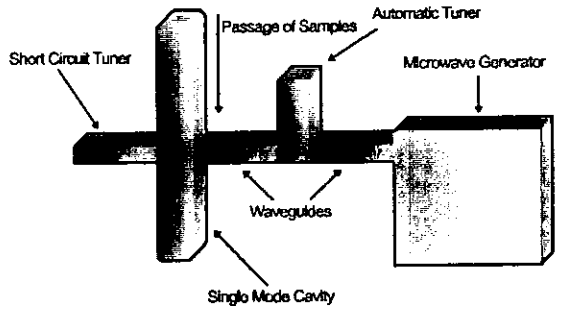

Fig. 1. Schematic of microwave apparatus.

and water-cooled 2.45 GHz magnetron for generation of the microwave energy, a single mode TE_{10n} applicator and a short-circuit tuner to produce the standing wave. The applicator consisted of 82-mm ID tube mounted in the broad face of WR430 waveguide and extended 125 mm on either side of the waveguide. The apparatus also included an automatic E-H tuner to match the impedance of the generator to the impedance of the applicator, ensuring a minimum amount of reflected power. Samples were exposed in the cavity for varying time-periods and at different power levels as seen in Table 1.

To achieve very short exposure times, the residence time was controlled by using a pneumatic piston in which the speed of the return stroke could be controlled. A schematic of the apparatus is shown in Fig. 2. Samples were placed in 75-mm ID cylindrical glass tubes, which were then passed vertically down through the single mode cavity to give the appropriate cavity residence time. In all tests, there was approximately 1 kg of material within the microwave-heating zone, the actual mass being dependent on particle size.

Table 1
Matrix for point load tests

Particle size (mm)	Applied power level (kW)	Exposure time (s)
−53+45	untreated	N/A
−53+45	5	0.1, 0.5, 1
−53+45	10	0.1, 0.5, 1
−53+45	15	0.1, 0.5, 1
−37+31	untreated	N/A
−37+31	5	0.1, 0.5, 1
−37+31	10	0.1, 0.5, 1
−37+31	15	0.1, 0.5, 1

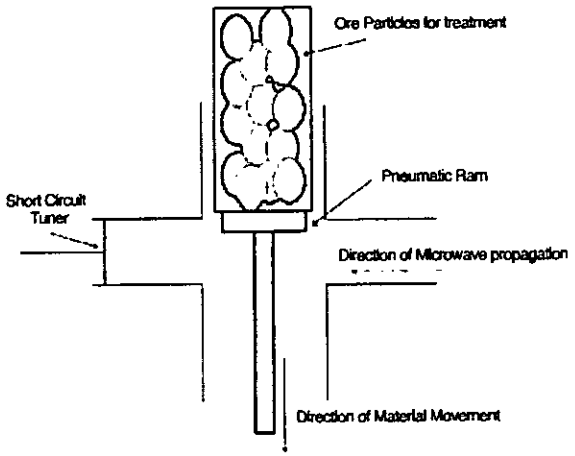

Fig. 2. Cross section of ore presentation system.

2.3. Point load testing

Point load tests were developed to give a quick but reproducible method of determining uniaxial compressive strength of samples without the need for large amounts of sample preparation. The test has recently been adapted by Bearman et al. (1997) for prediction of comminution behaviour in rocks. The point load test has the advantage of requiring no sample preparation so that a statistically sound test sample can be rapidly processed and an assessment made of the strength.

The test is very simple, a particle is measured and placed between a pair of specially shaped, hardened-steel tips. Force is then applied between the tips and the maximum force sustained by the particle is recorded. A schematic of the test principle is shown in Fig. 3. An approximation to the uniaxial compressive strength, known as $I_s(50)$ can then be calculated (Broch and Franklin, 1972). Several empirical equations have been developed to convert the test data to $I_s(50)$ and then to an approximation of compressive strength (Hoek and Brown, 1980). As only comparative data were required, only the $I_s(50)$ value was used and the equation used in this work is given below:

$$I_s(50) = \left[\frac{\left(\frac{\text{Depth}}{50}\right)^{0.45} \times \text{Force}}{\left(\frac{4 \times \text{Width} \times \text{Depth}}{\pi}\right)}\right] \quad (1)$$

ARTICLE IN PRESS

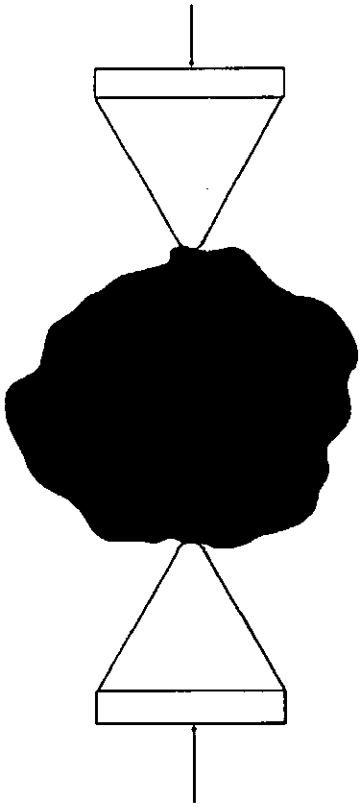

Fig. 3. Principle of operation of point load apparatus.

Samples of ore were subjected to point load tests, both as untreated material and after each type of treatment, the matrix of tests being shown in Table 1. For each test, 10 pieces of ore were treated and the $I_s(50)$ value for each sample calculated. The value reported is the median of the 10 tests, also given for completeness is the mean standard deviation and range.

2.4. Drop weight testing

Whilst changes in point load index are useful for comparative purposes, they are difficult to interpret in terms of changes in process efficiency. A standard test has been developed by the Julius Kruttschnitt Mineral Research Centre (JKMRC), University of Queensland, Australia (Napier-Munn et al., 1996). It characterises ores in terms of constants known as "impact breakage parameters".

In the drop weight test, a known mass falls through a given height onto a single particle providing an event that allows characterisation of the ore under impact breakage. Although the test is physically simple, it is supported by detailed data analysis. Although the drop weight test has advantages over the point load test in terms of statistical reliability and the potential use of the data from the analysis, it has a number of disadvantages, particularly the length of time taken to carry out a test. For each drop weight test, 15 samples were tested in 5 size fractions at 3 levels of energy input. Details of the recommended size fractions, number of particles and energy levels are given in Table 2. After each test has been completed, the resulting fragments are collected and sieved to give a product size distribution. The measured size distribution is then used to determine breakage functions for the material.

The analytical procedure is based on the assumption that product size distributions are a function of input energy or specific comminution energy (Ecs kW h t^{-1}). To model the breakage process the JKMRC developed a method of relating energy to geometric size reduction. The basic principle of the method is as follows. If a single particle is broken, the size distribution of the daughter particles may be considered as a $\sqrt{2}$ series and a cumulative size distribution graph plotted. The graph is then replotted after dividing the x-axis by the original particle size. A series of marker points are then used to describe the size distribution. These are defined as a percentage passing t, a fraction of the original particle size. Thus, t_2 is the percentage passing half of the original size, etc. The value of t_{10}, i.e., the amount passing 10% the original mean size, is used as a characteristic of size reduction and may be considered a fineness index. To make use of this technique, the marker points t_2, t_4, t_{25}, t_{50} and t_{75} are stored in matrix form against t_{10}. This information is then used to calculate the values of A and b, which are

Table 2 t2.1
Nominal energy input particle size combinations for JKMRC drop weight tests t2.2

Particle size range (mm)	Number of particles	Energy 1 (kW h t^{-1})	Energy 2 (kW h t^{-1})	Energy 3 (kW h t^{-1})	t2.3
63 × 53	10	0.2	0.125	0.05	t2.4
45 × 37.5	15	0.5	0.125	0.05	t2.5
31.5 × 26.5	30	1.25	0.5	0.125	t2.6
22.4 × 19	30	1.25	0.5	0.125	t2.7
16 × 13.2	30	1.25	0.5	0.125	t2.8

ARTICLE IN PRESS

defined as the ore impact breakage parameters. A and b are related to ECS and t_{10} by the following Eq. (2):

$$t_{10} = A[1 - e^{(-b \cdot ECS)}] \quad (2)$$

The drop weight test provides effective characterisation of an ore for crushing. It should be remembered that chipping and abrasion occur in tumbling mills and that additional tests would be required to obtain a comprehensive assessment of the benefits of microwave treatment. The impact parameter $A \times b$ has been correlated, although not well, to the Bond Work Index using Eq. (3) (Napier-Munn et al., 1996):

$$A \times b = -3.5WI + 117 \quad (3)$$

To enable comparison, drop weight tests were carried out both on untreated material and on material treated at 15 kW for 0.2 s. From the results, breakage parameters specific comminution energy were calculated. The energy levels used in this investigation were half those recommended in the standard method as it was found that if the recommended energy levels were used no discrimination between treated and untreated material was produced despite the appearance of significant visible fracture in the microwave-treated samples.

2.5. Grindability testing

To understand the grindability behaviour of the material, 2×500 g samples of the following size fractions were produced: $-19+16$, $-16+13.2$, $-13.2+9.6$, $-9.6+6.7$, $-6.7+4.75$ and $-4.75+3.35$ mm. One sample was left untreated and the other was exposed to microwave energy in the single mode cavity for 0.2 s at 15 kW. The samples were then ground for increasing lengths of time (1–5 min) in a 12-in. Bico Braun ball mill with a standard Bond mill charge at a speed at 70 rpm. The mass left in the original fraction after a specific time being determined by sieving. The data were evaluated using a standard population balance method (Austin et al., 1984; Wang and Forrsberg, 2000). The breakage function was evaluated by plotting the natural logarithm of mass remaining in a specific size fraction as a function of cumulative grinding time.

2.6. Liberation tests

Samples of treated and untreated material (15 kW, 2.45 GHz, 0.2 s) produced in drop weight tests were screened into four size fractions viz. $+500$ μm, $+150/-500$ μm, $+38/-150$ m and -38 μm. Representative sub-splits of the samples were mounted in chlorinated epoxy resin, polished and carbon coated for analysis by QEM*SEM (Napier-Munn et al., 1996). In each size fraction results were reported in terms of % locked, middling and liberated where these were defined as <30% liberated, 30–80% liberated and >80% liberated, respectively. Liberation characteristics were determined for copper sulphides only.

3. Results and discussion

3.1. Point load tests

Fig. 4 shows the change in $I_s(50)$ as a function of microwave exposure time for material in the size range $-53+45$ mm. It can be clearly seen that microwave treatment has a significant effect on the strength of the ore, with exposures as short as 0.1 s giving reductions in $I_s(50)$ of approximately 40%. Table 3 shows the full data set for the experiment. It can be seen that the results for microwave-treated material show a larger standard deviation than the untreated. Examination of the upper and lower limits revels why this is the case. Indeed, for most of the microwave-treated material, the strength of at least one (or often more) particles was close to zero. Naturally, this gives rise to the large standard deviation for treated samples because the untreated samples all had reasonable strength.

Previous work (Kingman, 1999) has shown reduction in ore strength to be related to microwave power level. This is also shown here with significant reductions in strength noted for 10 and 15 kW but not for 5 kW. It is apparent that a critical power density exists above which the damage is significant. For this ore within this cavity, this is shown to be produced by at least 10 kW. After the initial drop in strength, little benefit is gained by increased exposure time. This was suggested by Whittles et al. (2003) in their paper.

For all exposure times, 5 kW gives the smallest reduction in strength. However, in all cases, these

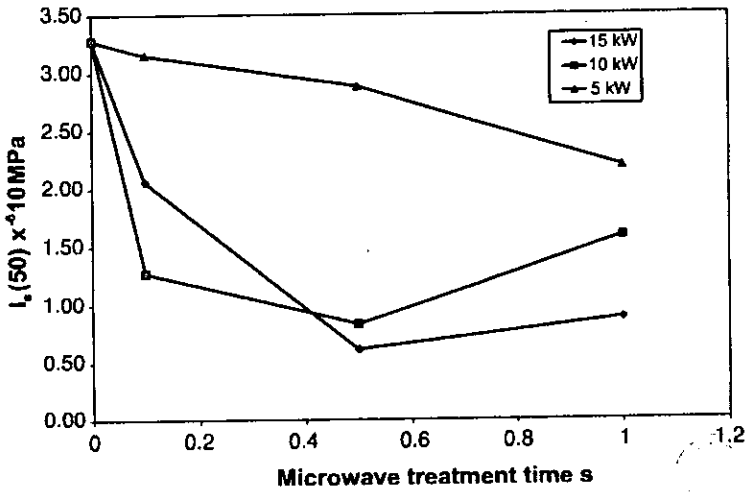

Fig. 4. $I_s(50)$ as a function of microwave exposure time for material −53+45 mm.

results are highly significant, as previous work showed that at least 10 and often 180 s were required to achieve small reductions in strength. In this study, significant reductions in strength are demonstrated for an exposure time of 0.1 s, up to 1800 times less than that previously used.

Fig. 5 shows a similar plot for −37+31 mm material. It can be clearly seen that significant reductions in strength can be achieved in short exposure times of less than 0.1 s. The plot is broadly similar to that shown in Fig. 4 with the complete data for this size fraction is shown in Table 4.

Table 3
$I_s(50)$ as a function of microwave exposure time for material −53+45 mm showing statistical measures

Treatment	Time	$I_s(50) \times 10^{-6}$ MPa				
		Mean	Standard deviation	Median	Upper limit	Lower limit
Untreated	–	3.32	0.88	3.28	4.67	1.95
15 kW	0.1	2.06	1.73	2.06	5.47	0.53
	0.5	0.93	1.02	0.62	3.18	0.06
	1.0	1.29	1.06	0.88	3.26	0.06
10 kW	0.1	1.82	1.30	1.28	3.83	0.16
	0.5	1.86	1.74	0.83	4.89	0.06
	1.0	1.98	1.48	1.59	4.36	0.07
5 kW	0.1	1.82	1.30	3.16	4.64	1.36
	0.5	2.34	1.07	2.89	3.44	0.06
	1.0	2.29	1.07	2.19	4.13	0.74

3.2. Drop weight tests

Drop weight tests were carried out on microwave- and non-microwave-treated samples using the energy levels shown in Table 2. After completion of the tests, the appearance function and breakage parameters were calculated. Before breakage in the drop weight tester the microwave-treated sample exhibited significant amounts of visible fractures and many pieces could be crumbled by hand. The untreated sample, by contrast, was wholly competent.

Table 5 shows the breakage parameters for the treated and untreated material. The value of A is the theoretical maximum value of t_{10}, whilst $A \times b$ is the slope of a plot of Ecs versus t_{10} at Ecs = 0. For most hard rocks (for a reasonable range of b values), there is a limiting value for A, the maximum value that t_{10} can achieve as Ecs is increased. This value is approx. $A = 50$. Note, for crusher breakage, t_{10} is typically 10–20% (Napier-Munn et al., 1996). The impact breakage parameter b is actually an indicator of the amenability of the ore to size reduction by impact. It can be seen that the value of b is significantly higher for the microwave treated material, suggesting a much softer ore.

Figs. 6 and 7show the effect of specific comminution energy on the breakage index t_{10} for different size classes. It can be clearly seen that the microwave-treated ore shows reduced values of Ecs over almost

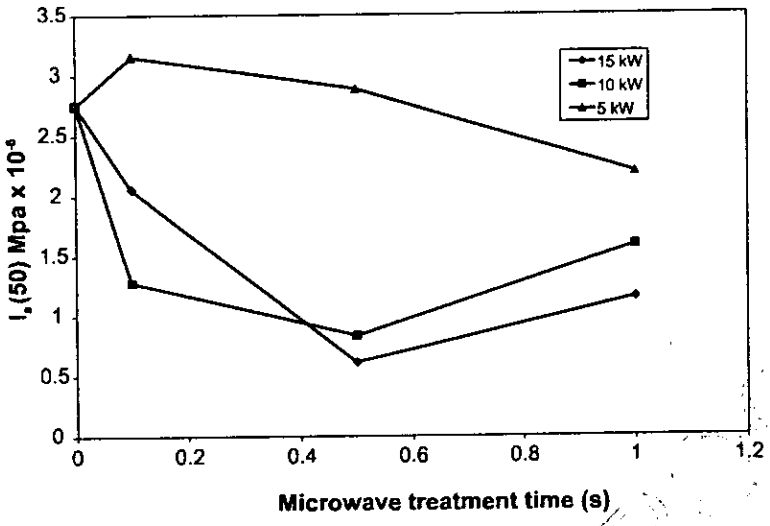

Fig. 5. $I_s(50)$ as a function of microwave exposure time for material −37+31 mm.

the entire range of t_{10} values, indicating that the material is softer because of microwave treatment. This is particularly true for the larger particle sizes indeed for the smallest size fractions the data is similar. The role of particle size in microwave assisted comminution is discussed later in this paper.

3.3. Grinding tests

Fig. 8 shows a plot of the specific rate of breakage versus particle size for treated and untreated material. It can be seen that the difference in specific rate of breakage decreases with particle size. The largest particle size fraction (−19+16 mm) is most influenced with over 70% difference between the non-treated and treated samples. For the smallest size fraction (−4.75+3.35 mm), the percentage change is 11%, whilst not as much as the larger fractions is still significant. The reason for the reduction with particle size is almost certainly related to the mineralogy or texture of the samples. The major microwave adsorbing phase within the material is magnetite. The magnetite is observed to occur in large aggregates sometimes greater than 10 mm in size. In order for differential expansion as a result of microwave heating to occur the heated phase must be entirely surrounded by transparent material. As the particle size decreases, the amount of magnetite, which is not totally surrounded by transparent gangue, will increase and thus the percentage change in specific rate of breakage will drop. It is likely therefore that more greater changes in specific rate of breakage could be achieved in ores, which have a finer texture.

It can also be seen that the specific rate of breakage in the larger size fractions is low. This is expected for

Table 4
$I_s(50)$ as a function of microwave exposure time for material −37+31 mm showing statistical measures

Treatment	Time	$I_s(50)$ MPa $\times 10^{-6}$				
		Mean	Standard deviation	Median	Upper limit	Lower limit
Untreated	–	2.88	1.06	2.75	4.38	1.05
15 kW	0.1	1.67	1.31	1.30	3.44	0.10
	0.5	1.52	1.43	1.08	4.22	0.07
	1.0	1.30	1.10	1.15	3.44	0.07
10 kW	0.1	1.50	0.91	1.37	3.01	0.10
	0.5	1.59	0.91	0.89	4.95	0.10
	1.0	1.35	0.45	1.28	2.11	1.00
5 kW	0.1	2.28	0.81	2.36	3.47	1.15
	0.5	0.75	0.60	0.71	1.24	0.10
	1.0	1.87	0.78	1.54	2.89	1.07

Table 5
Breakage parameters for treated and non-treated ore

Treatment	A	b	$A \times b$
15 kW 0.2 s	52.5	2.35	123.4
NON	54.3	1.61	87.4

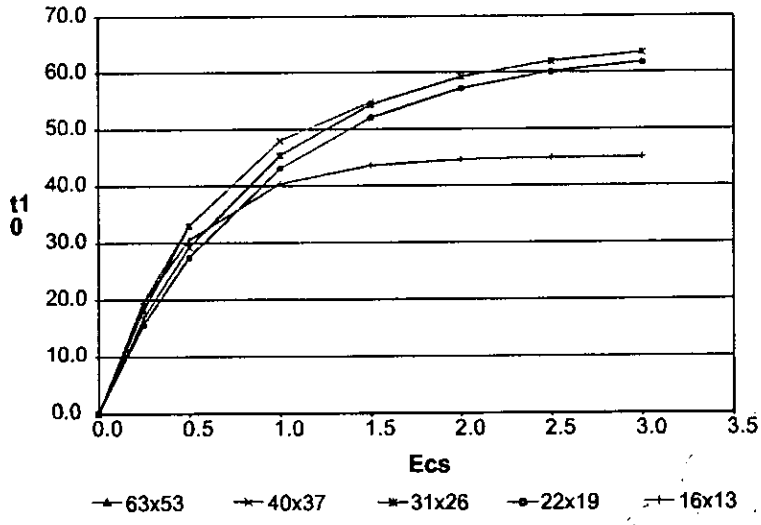

Fig. 6. Plot of t_{10} versus Ecs for different sized untreated ore.

laboratory mills and has previously been noted (King, 2001).

3.4. QEM*SEM liberation results

Results of the QEM*SEM study for copper sulphide minerals are shown in Fig. 9a and b. It can be seen that microwave treatment has had the most significant influence on the +500 μm fraction. The amount of liberated material in this fraction has increased from 31.8% in the untreated fraction to 69.2% in the treated fraction. The amounts of liberated, middlings and locked copper sulphides in the other size fractions remain relatively similar. The significant increase in liberation of the copper sulphide mineral in the coarse size fraction is potentially important as could increase the effective liberation size of the copper sulphide within the ore. This would have the effect of reducing grinding energy consumption as the required grind size would be coarser and it also would also potentially increase the total recovery as less material would be overground and lost to slimes. Fig. 10 shows typical images obtained from the QEM*SEM analysis, they

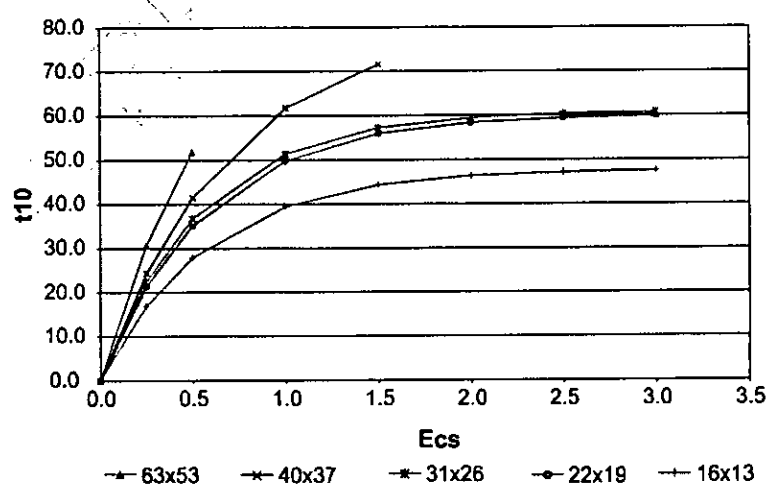

Fig. 7. Plot of t_{10} versus Ecs for different sized treated ore.

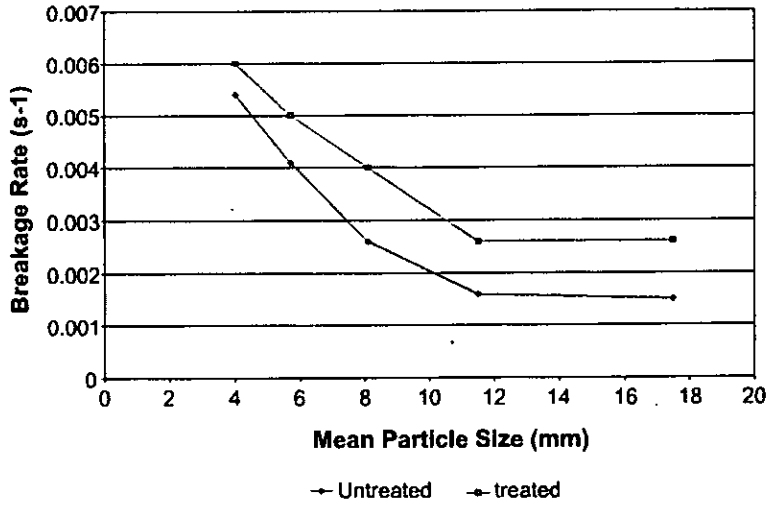

Fig. 8. Plot of specific rate of breakage versus mean particle size for treated and untreated samples.

indicate the nature of the classification, i.e., locked, middlings and liberated.

3.5. Explanation of mechanism of strength reduction

The impressive strength reductions achieved in the present work with very short, high power microwave exposure can be explained by considering the temperature gradients produced across grain boundaries. If a very high microwave power density is generated within a microwave absorbing phase for a short residence time, then significant temperature gradients would be expected to develop between the absorbing and non-absorbing phases, leading to large thermal stresses. On the other hand, if the ore were heated slowly at low power, as was carried out in previous work, thermal conduction would reduce the size of the thermal gradients across the grain boundaries between the absorbing and non-absorbing phases. In turn, this would lead to small thermal stresses and less weakening of the ore. Recent thermo-elastic simulations by Whittles et al. (2003) showed that this is true. High power densities (10^{11} W m^{-3}) maintained for short times (0.1 s) produced thermal gradients that in turn gave rise to significant thermo-mechanical stresses. These could reduce the material strength significantly. Lower power densities (10^{9} W m^{-3}) achieved lower strength reductions at total energy inputs almost an order of magnitude larger.

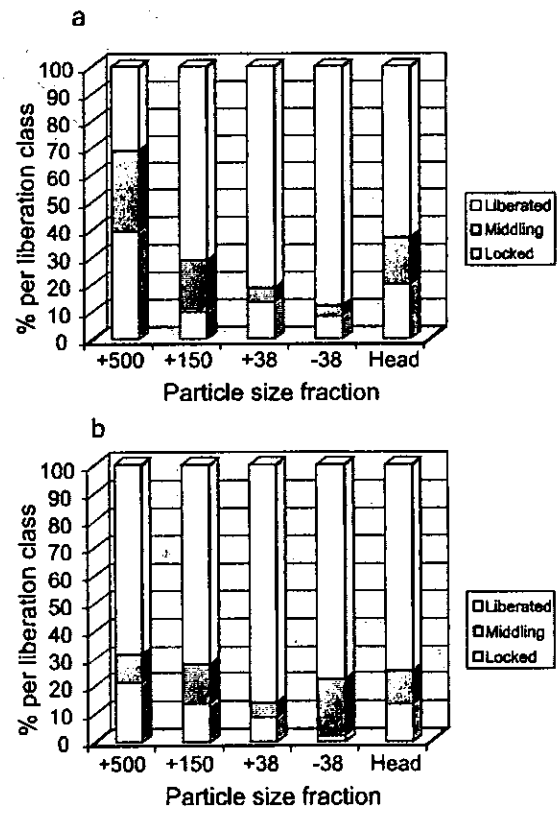

Fig. 9. (a) Liberation spectrum for copper sulphide minerals for untreated copper ore. (b) Liberation spectrum for copper sulphide minerals for ore treated 15 kW 0.1 s.

ARTICLE IN PRESS

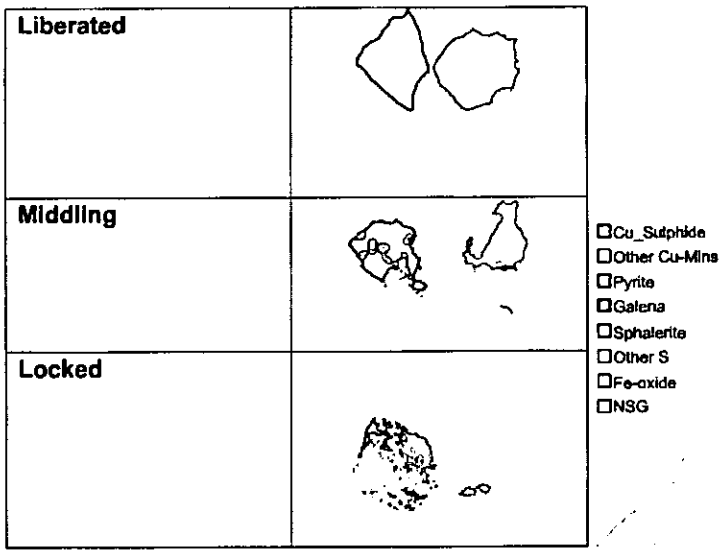

Fig. 10. Examples of copper ore liberation characteristics, i.e., liberated, locked and middlings.

3.6. Industrial significance

As stated earlier, the major disadvantage of previous work on microwave assisted comminution has been the amount of energy required to achieve the desired effects compared with the potential savings. Energy balances presented in previous work (Kingman et al., 2000a,b) showed that, for ore similar to that used in this test programme, a microwave energy input of over 43 kW h t^{-1} was required to achieve a reduction in work index of over 70% from 14 to 4 kW h t^{-1}.

In the present work, a 30% reduction in impact breakage parameters has been achieved at much lower microwave energy input. For material treated at 15 kW for 0.2 s, assuming 1 kg in cavity, it can be shown that the microwave energy input was:

$$\text{Energy} = 15 \times \left(\frac{0.2}{3600}\right) \times \frac{1000}{1} = 0.83 \text{ kW h } t^{-1}$$

The result of increasing the electric field strength (or power density) is clear; significant strength reduction or reductions in grinding resistance can be achieved at low microwave energy inputs. Furthermore, these values suggest that scale-up is potentially feasible in terms of energy added to the process.

Reductions in specific comminution energy of 30% coupled with significant improvements in ore grindability are attractive in themselves; however, it must be remembered that the benefit of a softer ore is not only in the reduced crushing energy, but also in reduced mill size (or greater throughput for the same size mill) and also the very significant reduction in the circulating load (Kingman, 1999). It should also be remembered that potentially the most important potential benefit of microwave assisted comminution is increased liberation at larger sizes. This was clearly demonstrated by the QEM*SEM liberation data, in which the liberation in the +500 μm fraction was doubled. Other benefits of microwave-assisted comminution include:

- Reduced plant size for set throughput
- Potentially reduced wear costs per tonne
- Lower water consumption (less mills required)
- Smaller downstream recovery circuits (liberation at higher sizes)

The TE_{10n} (electric field orientation transverse to the direction of propagation of the microwaves) cavity used for this test programme was 'an off the shelf' model designed for general heating applications. No attempt was made to optimise the cavity design with regard to the particle size distribution of the feed material or the dielectric properties of the material. This process will undoubtedly lead to higher power

ARTICLE IN PRESS

densities and lower residence time. This is of particular importance, as it will enable the input microwave power to be kept to a minimum and the throughput to be maximised. This will be vital if plant implementation is to be achieved.

In the same way optimised cavity design and electric field strength should enable similar if not better results to be obtained with ore of different mineralogy. This study was completed on a material with a relatively coarse liberation size whose major microwave heated phase (magnetite) was also relatively large. It would obviously be desirable to achieve similar results with much finer grained ores. This work has shown that the degree of failure is related to microwave power densities giving rise to thermally induced stresses and strains. It is highly likely therefore that if ores of finer mineralogy are to be treated then higher power densities would be required than those used in this work. This is because faster heating rates are required to produce the same level of stress in a smaller particle than a large one.

It is well known within the microwave-engineering field that staged development is vital for successful development. The next stage of this work will therefore be to develop a continuous pilot scale processing system that will process up to 1 t/h of ore. The facility will be designed to handle several specific ore types, which will allow some degree of optimisation in the presentation of the microwave energy to the ore. This test facility will also allow determination of the above benefits at reasonable scale.

4. Conclusions

For the first time, significant changes in ore breakage and liberation characteristics have been demonstrated at microwave powers inputs that potentially may be economic.

The influence of microwave radiation of high electric field strength has been quantified. It has been shown that significant reductions in strength can be achieved in very short microwave exposure times. There was some suggestion from the experimental data that the reduction in strength up to a certain level is related to applied power level. However, there appears to be a certain power level at which little more breakage can be induced.

Drop weight tests were carried out and the influence of microwave pre-treatment quantified. It was shown that reductions in required breakage energy of over 30% could be achieved for modest microwave energy inputs of less than 1 kW h t^{-1}. Further work is suggested at the tonne-per-hour level to allow more scale up data to be produced and a more detailed economic analysis to be carried out.

Grindability tests have shown that significant reductions in specific rate of brewage of over 40% can be obtained in a ball mill. These reductions, however, were shown to be intimately related to particle size.

QEM*SEM data showed that the liberation of copper sulphide minerals in the +500 μm size fraction increased by over 100% in the microwave treated material.

References

Anon, 1999. Technology Foresight—Natural Resources and Environment, Office of Science and Technology, London, UK.

Austin, L.G., Klimpel, R.R., Luckie, P.T., 1984. Process Engineering of Size Reduction: Ball Milling SME, New York. ISBN 0-89520-421-5.

Bearman, R.A., Briggs, C.A., Kojovic, T., 1997. The application of rock mechanics parameters to the prediction of comminution behaviour. Min. Eng. 10 (3), 255–264.

Broch, E., Franklin, J.A., 1972. The point load strength test. Int. J. Rock Mech. Min. Sci. 9, 669–697.

Hoek, E., Brown, E.T., 1980. Underground Excavations in Rock The Inst. Min. and Metall., London.

King, R.P., 2001. Modelling and Simulation of Mineral Processing Systems, Butterworth Heinemann.

Kingman, S.W., 1999. The Influence of Microwave Radiation on the Comminution and Beneficiation of Minerals. PhD thesis, University of Birmingham, UK.

Kingman, S.W., Rowson, N.A., 2000. The effect of microwave radiation on the magnetic properties of minerals. J. Microw. Power Electromagn. Energy 35 (2), 141–150.

Kingman, S.W., Corfield, G., Rowson, N.A., 1999. Effect of microwave radiation on the mineralogy and magnetic processing of ilmenite. Magn. Electr. Sep. 9, 131–148.

Kingman, S.W., Vorster, W., Rowson, N.A., 2000a. The influence of mineralogy on microwave assisted grinding. Min. Eng. 13 (3), 313–327.

Kingman, S.W., Vorster, W., Rowson, N.A., 2000b. The effect of microwave radiation on the processing of palabora copper ore. Trans. S. Afr. Inst. Min. Metall., 197–204 (May/June).

Napier-Munn, T.J., Morell, S., Morrison, R.D., Kojovic, T., 1996. Mineral Comminution Circuits. Their Operation and Optimisation. JKMRC Monograph Series in Mining and Mineral Processing, vol. 2. University of Queensland, Australia.

ARTICLE IN PRESS

Schönert, K., 1988. A first survey of grinding with high-compression roller mills. Int. J. Miner. Process. 22, 401–412.

Tavares, L.M., King, R.P., 1995. Microscale investigation of thermally assisted comminution. Proceedings XIX International Mineral Processing Congress, San Francisco, vol. 1, pp. 203–208.

Walkiewicz, J.W., Kazonich, G., McGill, S.L., 1988. Microwave heating characteristics of selected minerals and compounds. Miner. Metall. Process. 5 (1), 39–42.

Walkiewicz, J.W., Lindroth, D.P., McGill, S.L., 1991. Microwave assisted grinding. IEEE Trans. Ind. Appl. 27 (2), 239–242.

Wang, Y., Forrsberg, E., , 2000. Microwave assisted comminution and liberation of minerals. In: Ozbayoglu, E., et al. (Ed.), Mineral Processing on the Verge of the 21st Century. Balkema, Rotterdam. ISBN 905809 1724.

Whittles, D., Kingman, S.W., Reddish, D., 2003. The influence of power density on microwave assisted breakage. Int. J. Miner. Process. 68, 71–91.

An Investigation into the Influence of Microwave Treatment on Mineral Ore Comminution

S.W. Kingman[1], K. Jackson[1], A. Cumbane[1], S.M. Bradshaw[2], N.A. Rowson[3] and R. Greenwood[3]

[1]School of Chemical Environmental and Mining Engineering, University of Nottingham, Nottingham, NG7 2RD, United Kingdom [2]Department of Chemical Engineering, University of Stellenbosch, Stellenbosch, South Africa; [3]School of Chemical Engineering, University of Birmingham, Birmingham, B15 2TT, United Kingdom.

Abstract

The influence of microwave pre-treatment on mineral ore breakage has been investigated. Samples of Swedish lead-zinc ore were microwave pre-treated prior to strength testing and any change in strength with microwave exposure time determined. Comparisons of change in strength were made between microwave treated and untreated material. Using a multimode microwave cavity it was found that strength could be reduced by up to 70% in 0.5 s when using 15 kW of microwave power. Similar strength reductions were achieved at applied power levels of 5 and 10 kW only after 10 s of treatment. Drop weight tests were used to quantify the change in strength in terms of reduction in required comminution energy. Reductions of up to 40% were achieved for particles of mean size 14.53 mm. Preliminary tests in a single mode microwave cavity gave strength reductions of 50% at 10 kW of microwave power with a residence time of 0.1 s, indicating that high electric field strength, and hence power density, is important in the failure of ore.

Introduction

A relatively recent review (Veasey and Fitzgibbon, 1990) considered the economic and technical potential for the application of heat treatment to improve the efficiency of mineral ore comminution processes. Despite attractive technical benefits, it was suggested that the economic analysis for most applications was poor i.e. more energy was added than was saved by reductions in comminution energy. However, the authors did suggest that microwave heating might offer an economic way of applying energy to samples.

Interest in the application of microwave radiation to minerals started in the mid 1980's (Chen et al., 1984) when results were reported concerning the heating of 40 mineral types individually with microwave energy. The results showed that most minerals could be divided into two groups: (1) those for which little or no heat was generated, and the mineral properties remained essentially unchanged, and (2) those for which considerable heat was generated and the minerals were either thermally stable or decomposed/reacted rapidly into a different product. The test results also indicated that most silicates, carbonates and sulphates reported to group 1 whilst most sulphides, metal oxides, sulphosalts and arsenides reported to group 2. This work was extended some years later by the US Bureau of Mines (Walkiwicz et al., 1988) who reported test results of microwave heating of a number of minerals and reagent grade chemicals with similar results being produced to the earlier study. Several recent studies have investigated the application of low power microwave radiation to mineral ores. Massive Norwegian ilmenite ores exposed to microwave radiation for varying times showed reductions in Bond Work Index of up to 90%. (Kingman et al., 1998). The recovery of ilmenite using magnetic separation was improved for microwave-treated samples in comparison with untreated samples. It was concluded that microwaves were best applied for short times at high power because over-exposure of the sample led to reductions in downstream processing efficiency (Kingman et al., 1999). This work was extended to investigate the reasons for possible increases in recovery of valuable mineral after microwave treatment (Kingman and Rowson, 2000a). It was shown that increased recovery was due not only to increases in liberation but also to enhancement of the magnetic properties of the material. Qualitative work has also been carried out on the influence of mineralogy on the response of ores to microwave radiation (Kingman et al., 2000b). Ores with a coarse grain size gave the best response. The poorest response could be expected from ores containing highly disseminated, fine-grained minerals.

Almost all the above test work was carried out at low applied power levels (<2.6kW) in multipurpose microwave applicators. The purpose of the current investigation is to assess quantitatively the

influence of higher applied microwave power levels, impedance matching and microwave applicator type on the required comminution energy for a given size reduction.

Experimental

The material used for this investigation was a lead-zinc ore obtained from a mine in Sweden. Representative samples of ore were supplied from the mine site. Upon receipt the samples were air dried and crushed to 100% passing 63mm. The ore was then characterised.

Ore Characterisation

Mineralogy

A mineralogical investigation was carried out to determine the principle ore and gangue minerals contained within the sample. Two representative samples were prepared for analysis. They were prepared using a diamond saw, with polished sections being produced from each sample. The sections were systematically examined using conventional reflected light microscopy techniques. The individual opaque phases were identified on the basis of their optical properties. A number of reflected light photomicrographs were also captured using a Buehler Omnimet *'Enterprise'* image analysis system. A selected number of the polished sections were systematically examined using qualitative scanning electron microscopy techniques. This was done to provide additional information on the compositions of individual phases and also served to confirm their identities. A number of false colour, computer enhanced backscattered electron images were also prepared to illustrate important mineralogical features of the ore.

Microwave Treatment

Microwaves were generated using a 3-15 kW variable power generator operating at 2.45 GHz. This was connected to an E-H plane automatic tuner and this in turn was connected to a resonant

applicator as shown in Figure 2. The bulk of the tests were carried out in a multimode applicator. Comparative tests to ascertain the influence of electric field were also carried out in a single mode applicator. The generator, E-H tuner and applicators were manufactured and supplied by Sairem Ltd, France. The automatic E-H tuner was employed to match the impedance of the generator (and waveguide) to that of the applicator and its load, thus ensuring maximum absorbance of microwave energy by the load.

For the multimode tests, the samples were placed in a 5 litre capacity glass beaker and the generator set to the required forward power level. The sample was placed onto a rotating turntable within the cavity, the door closed and the generator started. Ten specimens in the single size-range -31 +27mm were used per test and samples were treated at applied power levels of 5, 10 and 15kW for 1, 5 and 10 seconds respectively. For all tests, an attempt was made to keep the mass of sample (1kg) in the cavity consistent and the position of the load identical.

For the single mode cavity tests, a TE_{10n} cavity was used(Metaxas and Meredith, 1983). This consisted of an 82 mm dia. tube mounted in the broadside of WR 430 waveguide. The sample residence-time in the cavity was controlled using a pneumatic system, as shown in Figure 3. The generator and tuning system were identical to those used for the multimode tests. The mass of sample was kept at 1kg.

Strength Testing

The Point Load test (Broch and Franklin, 1972) was used to determine the strength of the ore samples. The test has two principle advantages, firstly it can be used with irregular particles smaller than cored specimens required for determination of unconfined compressive strength and more importantly, the test samples require no preparative treatment. Thus, tests can be carried out more rapidly, giving the requisite statistical validity in a reasonable time.

For testing the sample is placed between two shaped tips and a compressive force applied. From the dimensions of the particle and the force applied, an index value, known as Is_{50}, is calculated from equation 2. The index is known as Is_{50} since it is intended to correlate to tests performed on 50 mm-diameter cores. The relationship is empirical and several have been developed by different authors The formula used in this work was:

$$Is_{50} = \left[\frac{\left(\frac{Depth}{50} \right)^{0.45} \times Force}{\left(\frac{4 \times Width \times Depth}{\pi} \right)} \right] \quad (2)$$

Where all dimensions are in millimetres and the force is in Newtons. Is_{50} has been shown to be approximately $1/14^{th}$ of the uniaxial compressive strength (Hoek and Brown 1980) but, as only comparative data were required, the Is_{50} value itself is reported in this work. Ten specimens in the single size-range -31 +27mm were used per test condition and the Is_{50} values were averaged to report a single value of Is_{50} per test condition.

Breakage Testing

The Point Load test measures only the ultimate strength of the particle so that the associated energy requirement for failure cannot easily be deduced. However, the Drop Weight Test (Napier Munn et al., 1996) developed at the Julius Krutschnitt Mineral Research Centre (JKMRC) in Brisbane Australia, allows determination of the amount of comminution energy required to produce a certain degree of breakage within a sample of a certain size.

In a test, samples of material are crushed as individual particles at a combination of energy inputs and size fractions. The nominal energies suggested by the JKMRC cover a range from 0.1 $kWht^{-1}$ to 2.5 $kWht^{-1}$. The combination of size fractions and energy inputs is shown in Table 1. After each test has been completed, the resulting fragments are collected and sieved to give a product size

distribution. The size distributions are then used to determine breakage functions for the material and thus allow calculation of the required comminution energy to induce a certain degree of breakage. The size distribution is defined as a percentage passing t, a fraction of the original particle size. Thus, t_2 is the percentage passing half of the original size etc. The characteristic size t_{10} is used as a fineness index. The values of A and b, which are defined as the material breakage parameters, are related to Ecs and t_{10} by the following equation (2):

$$t_{10} = A[1 - e^{(-b.ECS)}] \qquad 2$$

The fitting procedure generally yields a value of about 50 for A, while b is indicative of the softness of the ore, a larger value indicating a softer ore.

To determine the influence of microwave treatment on the breakage behaviour of the material, two drop-weight tests were carried out. The first was on untreated, "as received" material, utilising the energies detailed in Table 1. The second was carried out on a sample of ore that had been microwave-treated in the multimode cavity for 1 second at 15kW. The samples were treated using a procedure identical to that earlier. For the treated sample, the comminution energy input (Ecs) was reduced by 40% for all breakage events in an attempt to produce similar breakage characteristics for the microwave treated material as for the untreated sample. These data were then used to provide an estimate of the potential comminution energy savings that may be achieved by microwave treatment.

Results and Discussion

Mineralogy

Previous research (Kingman et al., 2000) has demonstrated a close relationship between the effectiveness of microwave treatment and the mineralogy of the ore. It was shown that of particular importance was the degree of dissemination of the adsorbing minerals within the host rock and also

the size of the adsorbing species. The purpose of the mineralogical investigation was therefore to investigate these factors, qualitatively for the ore in question.

The transparent gangue mineralogy of this sample was found to vary. Discrete, transparent, gangue-rich bands were clearly evident and were found to be typically rich in biotite and K-feldspar. Within the sphalerite- and galena-rich portions of the ore, the transparent gangue minerals were found to occur as rounded and sub-rounded aggregates that consist predominantly of quartz and K-feldspar. The major lead mineral present was found to be galena, which often occurred along the fractures within the transparent gangue. The grain size of the transparent gangue minerals was found to be highly variable. Generally, however, the transparent gangue minerals were medium grained in size, with the bulk of the gangue minerals exhibiting a grain size of between 50 and 150μm in size. Sphalerite was found to be the dominant zinc mineral within the sample and generally it occurred as granular aggregates that were intimately intergrown with galena and the transparent gangue minerals. The relative distribution of sphalerite in the sample was highly variable and in some cases was locally abundant, occurring within discrete sphalerite-rich bands that may exceed several millimetres in width. However, generally the sphalerite grains ranged in size from an effective lower limit of 10μm to the largest grains that exceed 100μm in size. The bulk of the sphalerite however exhibited a more restricted grain size of between 20 and 75μm. Typical images, obtained from the mineralogical analysis, are shown in Figure 1a and 1b.

Point Load Strength Testing

Figure 4 shows a plot of the percentage change in strength versus microwave exposure time for samples treated in the multimode microwave cavity. It can be seen that the microwave treatment has had a significant effect on the strength of the ore samples particularly at the highest power. For samples treated at 15kW, less than 40% of the original strength remains after only 1 second of

exposure. In comparison, samples treated for the same time at both 10 and 5kW show little change in strength. This would suggest that microwave induced failure is related to the applied power level. For samples treated at 5 and 10kW a significant decrease in strength occurs only after prolonged heating of the sample. For instance, samples treated at 5kW have 70% of their original strength remaining after 5 seconds exposure and samples treated at 10kW for the same time have just under 50% of their original strength left. There is some evidence from the data that it is possible to induce only a certain amount of thermal damage for a certain applied power level. Samples treated at 15kW exhibit significant reductions in strength after only 1 second of treatment but show little further decrease in strength with an increase in exposure time.

Drop Weight Test

Table 2 shows the calculated values of specific comminution energy for different degrees of breakage for different particle sizes for the untreated material. The calculations are carried out by fixing the value of t_{10} in equation 2, using the appropriate breakage parameters A, b, and then calculating the value of Ecs. The breakage parameters used for the calculation of the data in Table 2 were calculated by using the specific energy inputs detailed in Table 1. These are as in the recommended test method. (Napier Munn et al., 1996). The values of the impact breakage parameters for untreated ore were A=70.6 and b=1.53.

Table 3 shows the calculated specific comminution energy for different degrees of breakage for different particle sizes for material that was microwave-treated for 1 second at 15kW. The data were calculated by using a similar method to that above. However, the breakage parameters were determined by using breakage events with energy inputs of only 60% of those above. The value of 60% was used after consideration of the change in strength shown by the point load tests. Had both test samples been the same, the normal effect of using 60% of the original energy values would be a

much coarser product and, hence, giving lower values of the breakage parameters A and b. However, even with the reduced input energy it was found that the values of the impact breakage parameters were A=61.2 and b=2.19. It is particularly significant that parameter b, indicating the softness of the ore, is greatly reduced in comparison with the untreated material. .

A comparison of Table 2 and 3 however, shows almost identical values of Ecs for the larger size fractions (41.08 and 57.78 mm) but significantly smaller values for the treated material in the smaller factions. For example, to produce a t_{10} of 10% particles with an average size of 14.53 mm would require a comminution energy input of 0.1kWh/t for the untreated and 0.06kWh/t for the treated. For a t_{10} of 20%, the untreated material would require 0.21kWh/t and the microwave treated material would require 0.12kWh/t.

These results are significant as they show that similar breakage behaviour can be achieved for the microwave treated material as for the untreated material but with only 60% of the comminution energy input.

The results obtained in the multimode applicator have shown that microwave treatment can have a significant influence on the amount of energy required for breakage. It has also been shown the effectiveness of the treatment is related to the power level of the applied radiation. A recent paper (Whittles et al., 2003) has shown that failure in microwave treated samples is a function of electric field strength. Numerical simulations of rapidly-heating pyrite within a microwave transparent matrix were used to show that failure is a result of temperature gradients across grain boundaries and that the higher the value of the temperature gradient the more rapid the failure. It was also suggested that failure was caused by responsive mineral phases heating very rapidly in a microwave transparent matrix, this rapid heating would then cause expansion within the microwave transparent matrix. It was then shown that as the matrix did not heat it confined the expansion of the heating particle and

actually made it go into compression. The rapid initial expansion, however, led to stretching of the matrix tangentially to the direction of initial expansion and thus failure.

Figure 1 shows the nature of the ore. It can be seen that the ore is made up of microwave absorbent phases (galena and sphalerite) within an essentially transparent matrix of gangue. After microwave treatment, a significant degree of strength reduction would be expected as the heated phases expand within the restraining transparent matrix and this has been demonstrated. The suggestion of Whittles et al. (2003) that the degree of failure is related to electric field strength has also been corroborated as the change in strength produced after treatment at 15kW for 1 second was much greater than that produced by material treated at 5kW or 10kW. To investigate this further, more tests were carried out using a single mode microwave cavity.

The power density (or volumetric absorption of microwave energy) is known to be proportional to the square of the electric field strength within the material (Metaxas and Meredith, 1983). This suggests that if the electric field within a mineral can be increased this may give rise to more rapid heating rates and a reduction in the required residence time within the microwave cavity. One method of producing such fields is by using single mode microwave applicators. A single mode cavity is a metallic enclosure in which the superposition of the reflected and incident microwaves gives rise to a standing wave pattern that is very well defined in space and usually localised in a small volume. The precise knowledge of electromagnetic field configurations enables the dielectric material to be placed in the position of maximum electric field strength, allowing maximum-heating rates to be achieved at all times.

Tests were carried out to determine if increasing the electric field strength by using a single mode applicator would cause more rapid failure or failure at lower power than in the multimode applicator. Tests were carried out at 5, 7.5 and 10kW and samples were treated for 0.1, 0.5 and 1 seconds

respectively. No test was carried out at 15kW due to sample melting. As for the tests carried out in the multimode cavity, 10 tests were carried out for each treatment condition and the average is reported. The sample residence-time in the cavity was controlled using a pneumatic system, as shown in Figure 3. The generator and tuning system was identical to that used for the multimode tests.

Figure 5 shows a plot of percentage of original strength versus microwave exposure time. It can be seen that treatment in the single mode cavity has had a significant influence on the strength of the ore. As previously stated, samples were not exposed to 15kW as the residence time could not be reduced to a level to avoid extremely rapid melting of the rock matrix. As an example, if samples treated at 10kW are compared, (Figures 4 and 5) it can be seen that 5 seconds of treatment was required to give a reduction in strength of 50% in the multimode cavity but only 0.5 seconds was required for the same reduction in the single mode cavity. The maximum strength reduction observed in Figure 5 is slightly lower than that shown in Figure 4. This provides more evidence of the importance of power density in the overall mechanism of failure. Samples treated at 15kW in the single mode cavity were found to melt completely and retain none of their original structure. A shorter residence time was therefore required; in this study this could not be achieved in a controlled manner with the experimental apparatus used. However, if it were possible to halve the residence time to 0.05 seconds, significant decreases in strength would still be expected. If the microwave power were to be increased to well above 15kW, the residence time could be reduced even further.

It is clear, therefore, that power density or electric field strength does have a significant influence on the change in strength observed in exposed samples. This has important ramifications for the industrial development of the technology. The review discussed earlier in this paper (Veasey and Fitzgibbon, 1990) stated that, although the benefits of thermally assisted comminution were technically attractive, the economic were often poor. This study has shown that significant reductions

in the required comminution energy may be achieved for low microwave energy inputs

The microwave energy requirement for samples treated in the single-mode cavity can be compared to those in the multimode cavity. Assuming a 1kg load in each case:

Multi-mode cavity (10W for 5s) = $$10\left(\frac{\left(\frac{5}{3600}\right)}{\left(\frac{1}{1000}\right)}\right) = 13.88 kWh/t \quad (3)$$

Single-mode cavity (10kW for 0.5s) = $$10\left(\frac{\left(\frac{0.5}{3600}\right)}{\left(\frac{1}{1000}\right)}\right) = 1.38 kWh/t \quad (4)$$

If the power level were to be increased to 15kW and the residence time reduced to 0.05 seconds, as suggested above, this would mean only 0.21 kWh/t of microwave energy would be used. Typically, an ore may require a total of up to 20kWh/t for the size reduction process or more if very fine grinding is required. Therefore, microwave energy inputs of this magnitude may be attractive economically.

It should be stressed that the single-mode cavity used was not optimised. With further cavity development, higher powers and even shorter exposure times would become feasible and the microwave energy requirement reduced even further.

Conclusions

The change in strength of samples exposed to microwaves in multimode cavities has been shown to be related to applied microwave power level. By using comparative drop weight tests it has also been shown that reductions in required comminution energy of at least 40% can be achieved for material microwaved treated for 1 second at 15kW. The importance of electric field strength has also been demonstrated and it has been shown that significant reductions in ore strength can be

achieved with cavity residence times of less than 0.5 seconds. It is suggested that by utilising high electric field strength and very short cavity residence times that the microwave assisted comminution of this ore may be economic

References

Broch E. and Franklin J.A. (1972) The Point Load Strength Test. International Journal of Rock Mechanics and Mining Sciences., Vol.9, 669 to 697

Chen TT, Dutrizac JE, Haque KE, Wyslouzil W Kashyap S., (1984), The Relative Transparency of Minerals to Microwave Radiation. Can. Metall. Quart. 23, 1, 349-351

Hoek E and Brown ET, Underground Excavations in Rock, 1980, The Inst. Min. and Metall., London.

Kingman SW, Rowson NA, Blackburn S, 1998.Chapter 24, Applications of Microwave Radiation to Enhance Performance of Mineral Separation Processes, Innovation in Physical Separation Technologies, Inst. Min. Metall. ISBN 1870706358.

Kingman SW Corfield G Rowson NA (1999a). Effect of Microwave Radiation on the Mineralogy and Magnetic Processing of Ilmenite, Magnetic and Electrical Separation Vol. 9, pp131-148

Kingman SW Rowson NA (2000a)The Effect of Microwave Radiation on the Magnetic Properties of Minerals. Journal of Microwave Power and Electromagnetic Energy, Vol.35, No2 pp141-150.

Kingman SW Vorster W Rowson NA (2000b). The Influence of Mineralogy on Microwave Assisted Grinding. Minerals Engineering., Vol.13, No.3, pp313-327.

Metaxas, A.C., Meredith, R.J. (1983). Industrial Microwave Heating, Peter Peregrinus Ltd, London

Napier-Munn TJ Ed., 1996,.Mineral Comminution Circuits. Their Operation and Optimisation. JKMRC Monograph Series in Mining and Mineral Processing 2, University of Queensland, Australia.

Veasey TJ and Fitzgibbon KE. (1990). Thermally Assisted Liberation of Minerals – A Review. Minerals Engineering,. Vol.3, No.1/2, pp181-185

Walkiwicz JW, Kazonich G, McGill SL. (1988). Microwave Heating Characteristics of Selected Minerals and Compounds., Minerals and Metallurgical Processing Vol.5, No.1, 39-42

Whittles, D.N, Kingman, S.W., Reddish, D.J. (2003). Application of Numerical Modelling for Prediction of the Influence of Power Density on Microwave Assisted Breakage, International Journal of Mineral Processing, Vol.64 No.1-4 pp 71-91.

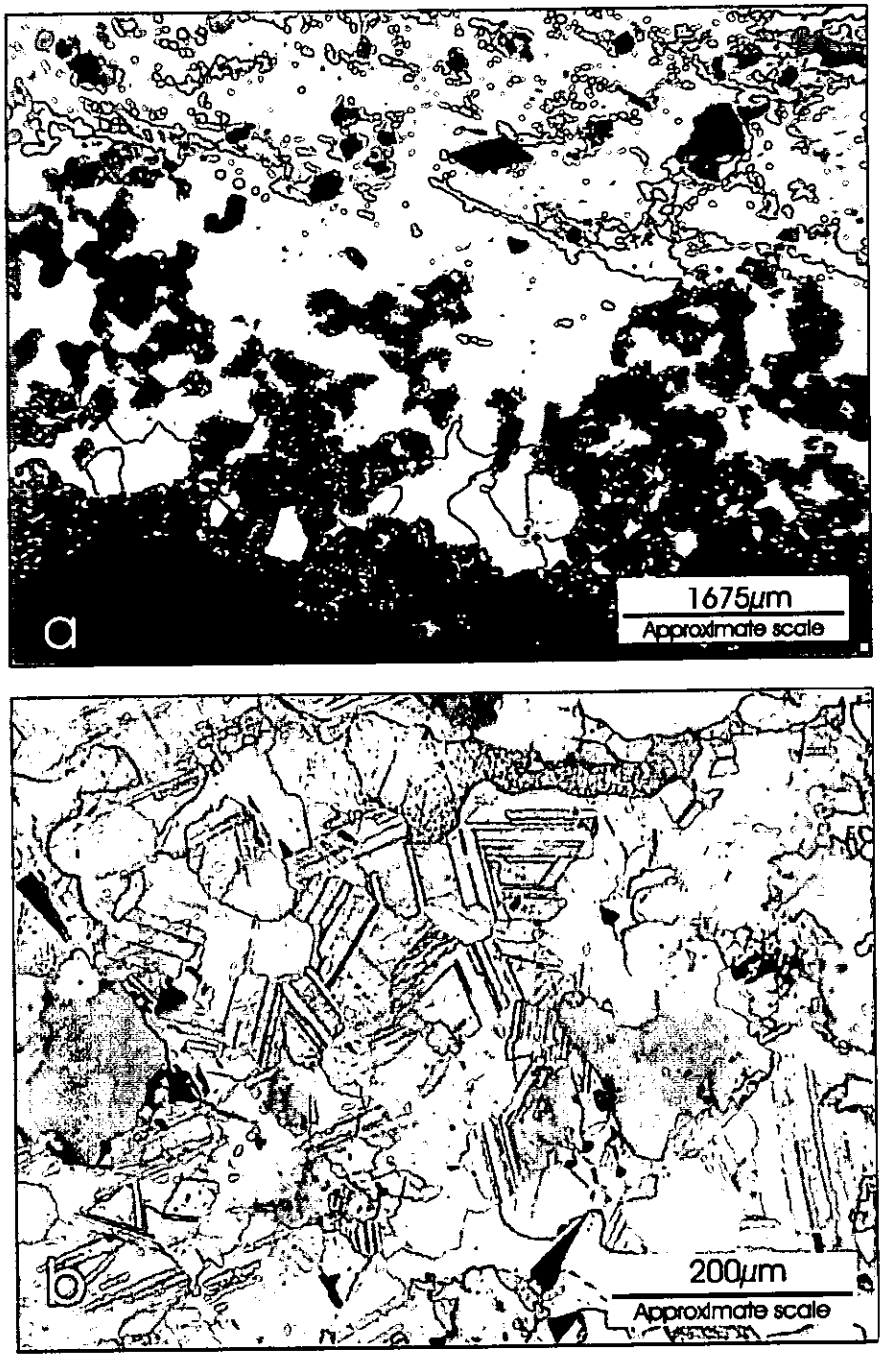

Figure 1

A monochrome backscattered scanning electron microscope image illustrating the preferred orientation of film-like galena aggregates (white) within a sphalerite-rich band (medium grey). The transparent gangue (dark grey shades) is locally abundant, occurring as discrete gangue-rich layers (lower portion of image). These bands are typically biotite-rich and commonly exhibit a preferred orientation. Galena may be locally abundant. (**b**) A colour reflected light photomicrograph illustrating the granular and twinned nature of the sphalerite aggregates (light and dark brown shades) as enhanced by structure etching. Galena (silver-blue shades) is present along the margins of the sphalerite grains. Transparent gangue (dark grey shades) is also present.

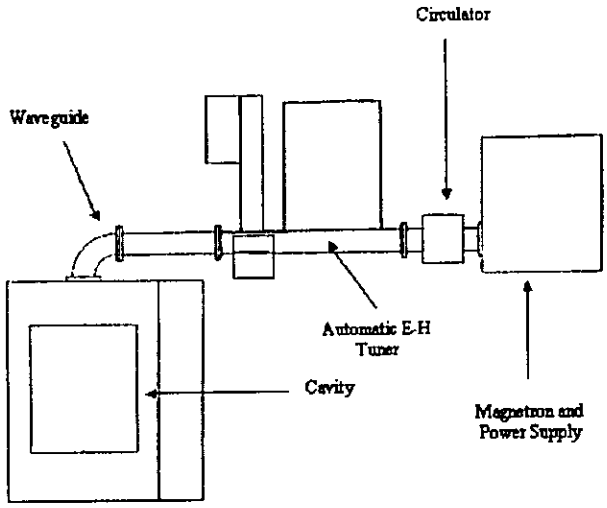

Figure 2: Diagram of Microwave Generator System (Multimode Cavity Fitted)

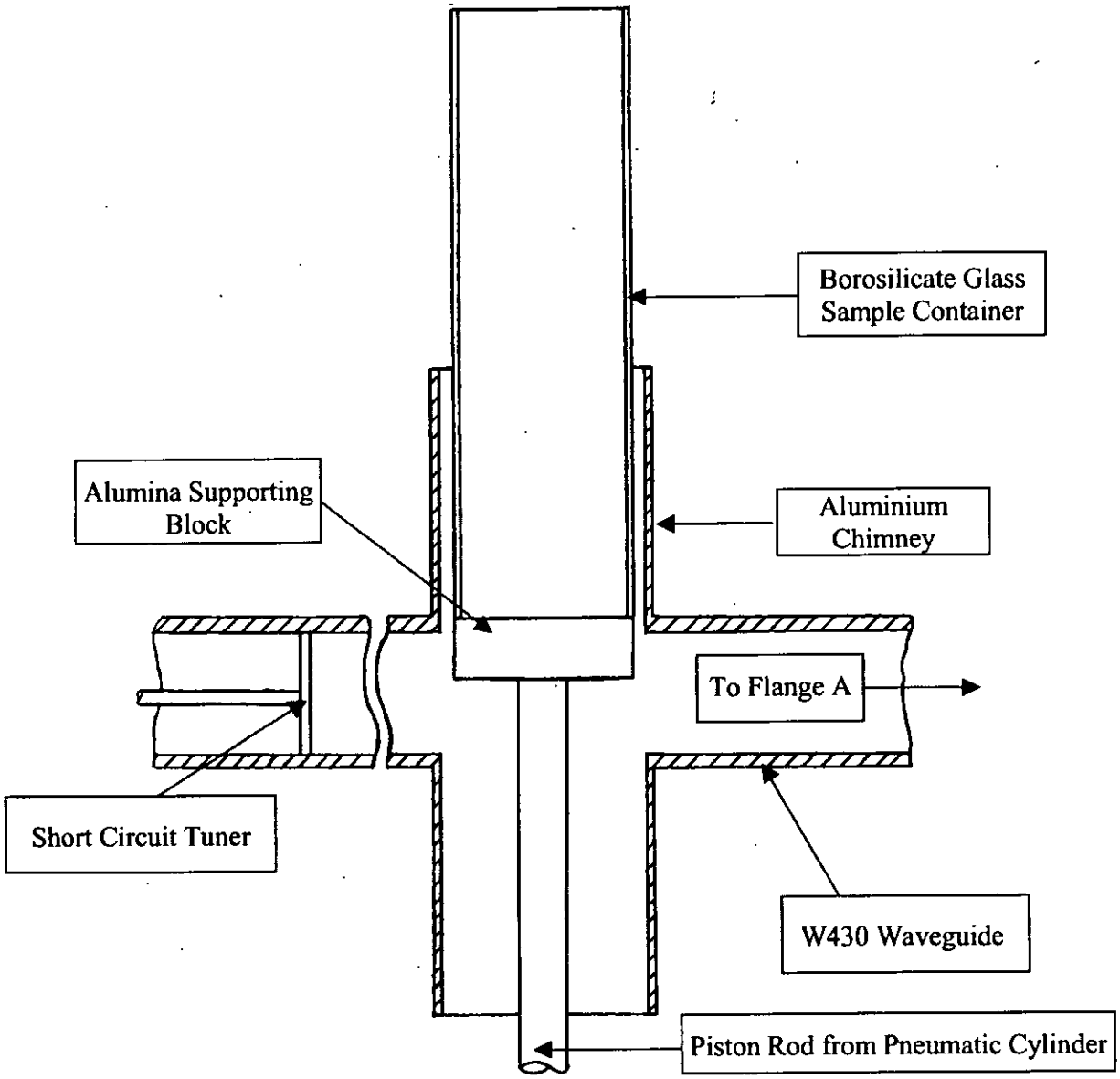

Figure 3: Sketch of Arrangement for Tests in Single Mode Cavity

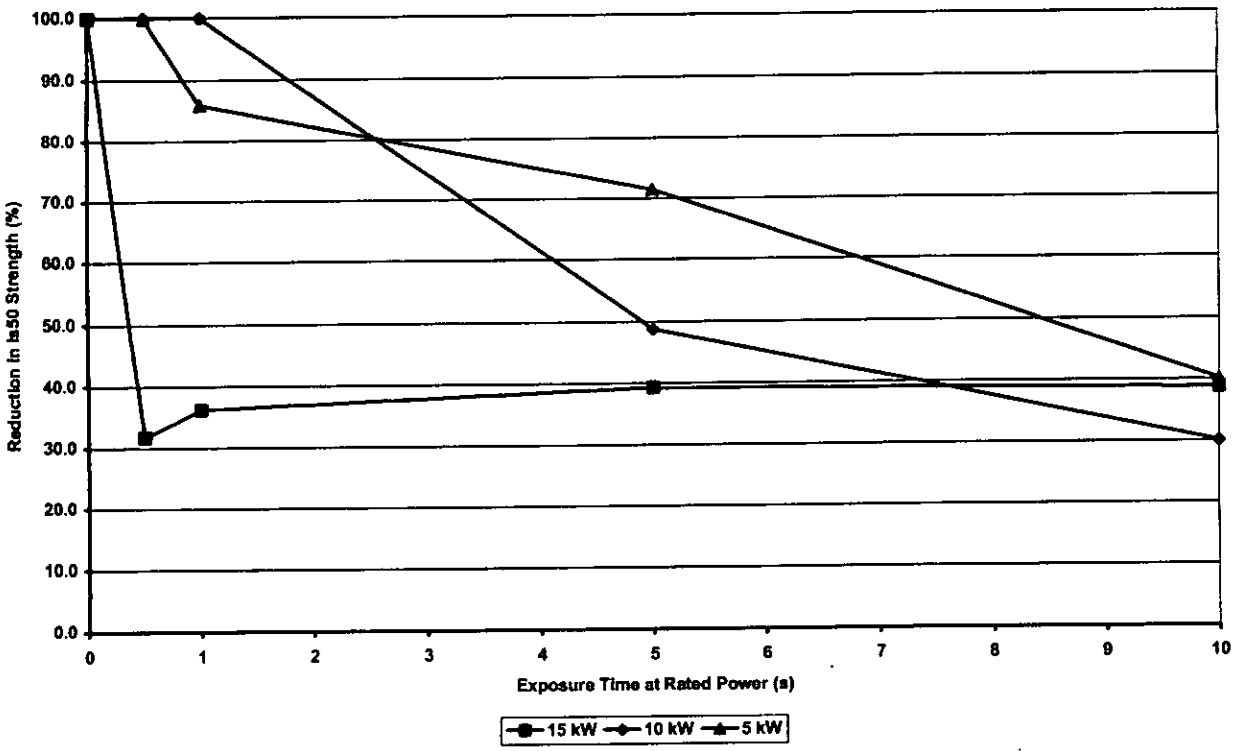

Figure 4: Point Load Test Results for Multimode Cavity

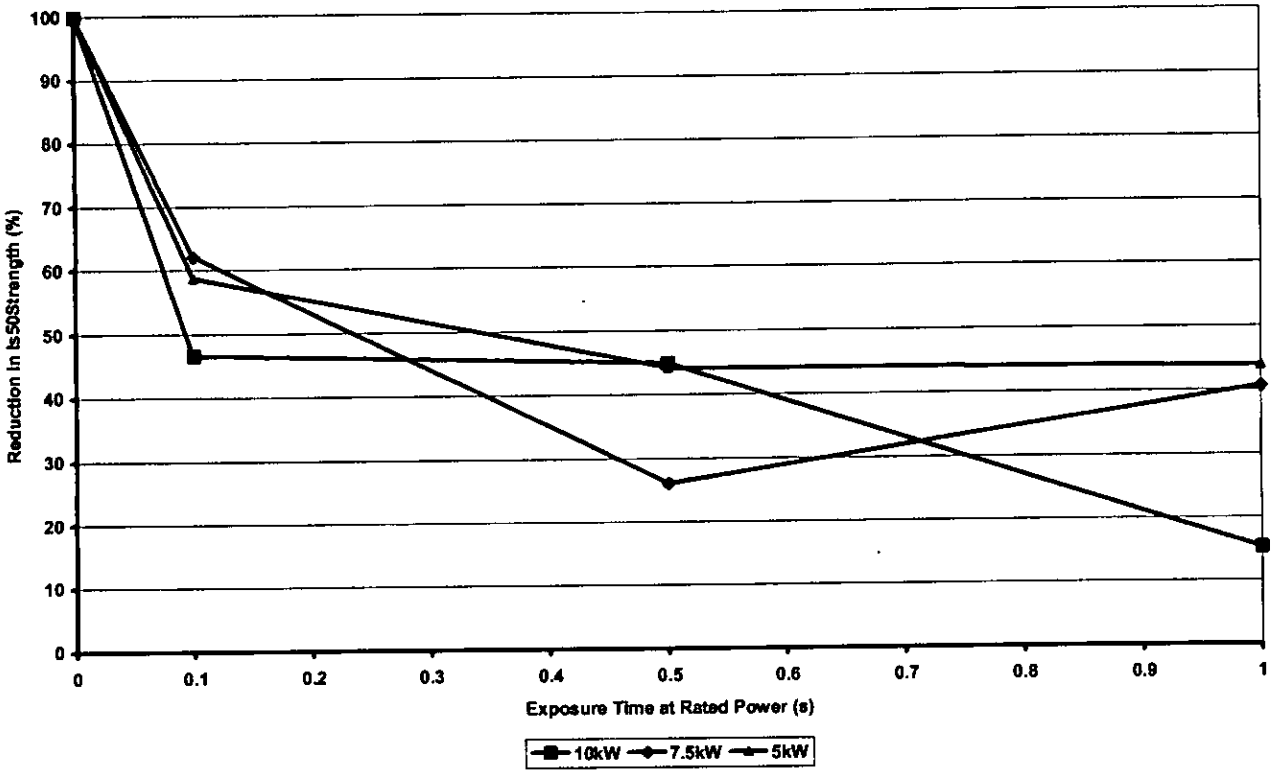

Figure 5: Point Load Test Results for Single-mode Cavity

Particle Size Range (mm)	Number of Particles	Energy 1 ($kWht^{-1}$)	Energy 2 ($kWht^{-1}$)	Energy 3 ($kWht^{-1}$)
63 x 53	10	0.4	0.25	0.1
45 x 37.5	15	1.0	0.25	0.1
31.5 x 26.5	30	2.5	1.0	0.25
22.4 x 19	30	2.5	1.0	0.25
16 x 13.2	30	2.5	1.0	0.25

Table 1. Drop Weight Test Energy Input/Sample Size Combinations

	Mean Size (mm)				
	14.53	20.63	28.89	41.08	57.78
T_x	Ecs (kWh/t)				
10	0.10	0.10	0.12	0.10	0.09
20	0.21	0.23	0.26	0.22	0.19
30	0.35	0.38	0.43	0.37	0.31

Table 2. Calculated Power Data for Non Treated Material Broken with Energy Input as in Table 1

	Mean Size (mm)				
	14.53	20.63	28.89	41.08	57.78
T_x	Ecs (kWh/t)				
10	0.06	0.07	0.10	0.11	0.10
20	0.12	0.17	0.21	0.21	0.20
30	0.21	0.29	0.37	0.37	0.33

Table 3. Calculated Power Data for Non Treated Material Broken with Energy Input of 40% Table 1

Dielectric Properties of Sulphide Minerals

A.J. Cumbane[+], *N.J. Miles*[+], *E. Lester*[+], *S.W. Kingman*[+] *and S.M. Bradshaw*[*]

[+]*School of Chemical, Environmental and Mining Engineering, University of Nottingham, Nottingham, NG7 2RD UK*

[*]*School of Chemical Engineering, University of Stellenbosch, Stellenbosch, South Africa*

Abstract

A good estimate of the microwave absorption properties of a material is vital for accurate cavity design from electro-magnetic numerical simulations. A measurement system, comprising a circular cylindrical TM_{0n0} cavity and based on a perturbation technique, has been used for the determination of dielectric properties of five powdered sulphide minerals, which were measured at frequencies of 615MHz, 1410 MHz and 2210 MHz. The complex permittivity was measured from ambient temperature to 650 °C. The dielectric properties of galena and sphalerite exhibit little variation with temperature up to 500 °C. The dielectric properties of pyrite, chalcocite and chalcopyrite, show significant variation with temperature. These are related to composition and phase transformations during heating and were demonstrated by thermo-gravimetric analysis. It was found that the relationship between dielectric constant and powder density was well described by an expression of the form $\sqrt{\varepsilon'} = m\rho + 1$.

1. Introduction

Microwave heating is becoming an increasingly attractive, alternative method of improving the efficiency of the comminution process and, thus, mineral liberation. It has been demonstrated that such improvement is the result of differential heating that can induce stresses sufficient to cause fractures in ores (Whittles et al., 2003). Kingman et al. 2002, 2003 have shown that significant strength reductions can be achieved by exposing mineral ores to high density microwave power for short times. Under these conditions, the process can be operated at economically viable energy consumption.

Early work on dielectric heating of mineral sulphides gave qualitative data the heating rates in microwave ovens (Chen et al. 1984 and Walkiewicz et al. 1988) and their frequency dependency. The contribution made by Chen et al., although qualitative in nature, was the first attempt to assess the heating rates of different minerals within a dielectric field. Thereafter, Walkiewicz et al. 1988 published a more detailed, quantitative study of the microwave heating characteristics of various minerals and chemical compounds. Chemical grade minerals were treated in a 1 kW, 2.45GHz microwave heater and the resulting temperatures and associated exposure times reported. These studies indicated that in general sulphide minerals are good absorbers of microwave energy.

McGill et al. (1988) discussed the effect of power level on mineral heating rate. Minerals similar to those utilised in the studies by Walkiewicz et al. 1988 were powdered and exposed to various microwave power levels ranging from 500 to 2000W. It was observed that an increase in power led to an increase in heating rate of some lossy minerals.

The recent work of Whittles et al. (2003) used a two-dimensional model of a pyrite calcite ore in order to determine the effect of microwave power dissipation on thermal stress development. This model serves as an archetype for many ores that contain disseminated mineral species that are good absorbers of microwave energy in a microwave-transparent host rock. It was found that high power density (10^{11} W m^{-3}) in the absorbing phase sustained for less than 1 sec led to 50% strength reduction under simulated uniaxial compression.

In order to design microwave applicators to achieve the power densities suggested by the thermal stress study good knowledge of the dielectric properties of the different mineral phases is vital. Salsman, 1991, 1992 reported the use of a coaxial probe system used in a furnace to heat powdered mineral samples. The complex permittivity of chalcocite and chalcopyrite were reported at frequencies from 0.3 - 3 GHz and from 25 to 325 °C. Holderfield and Salsman, 1992 reported the dielectric constant for a number of minerals at temperatures up to 325 °C.

A lack of fundamental data concerning the interaction between microwave energy and a wide range of minerals seriously hinders implementation of the technology. Better

predictions of the behaviour of complex minerals will also improve cavity design by giving cavity designers a better idea of the power loss densities required to achieve a particular heating rate.

The aims of this paper are threefold. First, complex permittivity data are reported for a number of industrially important sulphide minerals within the ISM frequency range and over a range of temperatures. Second, thermo-gravimetric analysis help elucidate the reason for the variation in permittivity with temperature. Finally, the usefulness of correlations for the variation of permittivity with density was examined.

1.1 Measurement of dielectric properties

The two main methods of measurement of complex permittivity relevant at the ISM frequencies are transmission line methods and cavity perturbation methods. Both of these methods have been adapted for use at high temperature. Transmission line methods, typically using open-ended coaxial probes, have the advantage of providing broadband measurement but are limited in temperature to about 500 °C (Tinga, 1992). The data presented by Salsman, 1991, 1992 and Holderfield and Salsman, 1992 on various minerals used a coaxial probe method. Cavity perturbation methods have also been widely used, and are well suited to measurement of small, low loss samples. This method does not require samples with smooth surfaces, which is an advantage when dealing with mineral samples and when eliminates surface mismatch problem that can arise in transmission lines methods due to thermal expansion. A parallel measurement program run in the early 1990s compared data from different techniques for alumina at temperatures up to 1400 °C (Batt et al., 1995). It was found that agreement on the dielectric constant up to $\varepsilon' \sim 40$ was good (±10%). However, there were differences of ± 50% in the values of ε''. Free space measurement methods have also been used but are less suitable than the other methods at the ISM frequencies of interest, as the sample size needs to be inconveniently large.

The cavity perturbation method used in this work is well understood. The measurement of the resonant frequency and quality factor before and after sample insertion allows the calculation of the real and imaginary part of the complex permittivity of the sample, using the perturbation equations (1) and (2).

$$\varepsilon' = 1 + 2 * J_1^2(X_{on}) * \frac{V_c}{V_s} * \frac{f_0 - f_s}{f_0} \qquad (1)$$

$$\varepsilon'' = J_1^2(X_{on}) * \frac{V_c}{V_s} * (\frac{1}{Q_s} - \frac{1}{Q_o}) \quad (2)$$

Where:

ε' is the dielectric constant or real permittivity,

ε'' is the loss factor or imaginary permittivity,

V_c is the volume of the cavity (mm^3),

V_s is the volume of the sample (mm^3),

f_o is the resonant frequency of empty cavity (Hz),

f_s is the resonant frequency of cavity and sample (Hz),

Q_s is the quality factor of cavity and sample,

Q_o is the quality factor of empty cavity,

J_1 is the first order Bessel function and

X_{on} is the n^{th} root of J_0

1.2 Nature of sulphide minerals

Sulphides are complex minerals in both their chemistry and origin. They are usually deposited from aqueous solutions in fracture zones of the Earth's crust, located in or near large, deep igneous bodies known as batholiths. Great effort has been made to understand their origins and properties because they are amongst the most valuable of all economic minerals, giving rise to many of the base metals commonly used today.

A sulphide is, essentially, an oxygen-free compound of sulphur and one or more metals. In its simplest form, the sulphide structure can be regarded as spherical packing of sulphur atoms with the smaller, metal atoms in the interstitial spaces. Their association is, in varying degrees, a mixture of metallic, ionic and covalent bonds.

Most sulphides have a metallic appearance, with a strong colour and metallic lustre. The majority are opaque, have high densities and many are brittle, which easily distinguishes them from the native metals. Few are resistant to atmospheric weathering and usually convert to secondary ore minerals.

Pyrite (FeS_2) is the most abundant of sulphide minerals. It occurs in a wide variety of geological conditions but, in many cases, its mode of origin is uncertain (Deer et al

1962). It may be found in large masses or in veins of hydrothermal origin and as a primary or secondary mineral in both igneous and sedimentary rocks. Large masses of pyrite may also be found in contact with metamorphic ore deposits, often in association with other sulphides, some of which have been formed by the replacement of iron by other metals.

Differential thermal analysis of pyrite has been carried out by a number of investigators. A large exothermic peak corresponding to oxidation of the mineral within the range 450°C to 650°C, with individual components at 510 and 550°C has been observed.

Chalcopyrite ($CuFeS_2$) is an important copper-bearing ore mineral. It is found, together with other sulphides, among primary ores of magmatic origin. Chalcopyrite is oxidized to sulphates of iron and copper on exposure to air and water or with slight heating. When heated in air, chalcopyrite shows an exothermic peak due to oxidation centred on about 500°C (Deer et al, 1962). It has been suggested when chalcopyrite is heated development of a lamellar intergrowth of bornite occurs, followed by the conversion of chalcopyrite to pyrrhotite and a solid solution of bornite with chalcocite.

Sphalerite (ZnS) in its pure form is a colourless compound but almost all specimens found in nature are coloured through the presence of iron and other elements (Deer et al, 1962). Sphalerite is the most common of the zinc bearing minerals and its occurrence, often in vein deposits associated with galena, is widespread. The less common form of ZnS, wurtzite, is stable only at high temperatures. On heating in air, sphalerite is oxidized to zinc sulphate but, if much iron is present, ferric and ferrous sulphates are also formed and zinc ferrites are formed at temperatures above 1000°C. The differential thermal analysis pattern of sphalerite shows a large exothermic peak, corresponding to oxidation, at about 1000°C that masks any peak that may occur through the sphalerite-wurtzite transition at about 1020°C.

Galena (PbS) is the most widely distributed of the sulphide minerals and the most important of the lead minerals. It occurs most frequently together with sphalerite, and such lead-zinc ores often contain recoverable amounts of copper, silver, antimony and bismuth. The main types of occurrence of lead-zinc sulphides include deposits of low, intermediate and high temperature origin. Thus, galena of high temperature origin is

found in veins and replacements in pegmatites, calcico-silicate rocks, limestones and other sediments. In addition to various sulphides, commonly associated minerals include barites, fluorite, quartz and calcite (Deer et al, 1962). On heating in air galena is oxidized to lead sulphate and it melts at 1115°C.

2. Experimental procedure

1. The experimental system, shown in Figure 1, comprised four main components: right circular cylindrical cavity of diameter 373 mm and height 37.3 mm. The cavity resonates in the TM_{0n0} mode with the first 3 modes being at 0.615, 1.413 and 2.216 GHz.
2. A carbolite tube furnace capable of operating at temperatures up to 1800°C was mounted above the cavity. A sample holder and piston mechanism allows the sample to be moved rapidly from the furnace to the cavity.
3. A Hewlett Packard 8753C vector network analyser capable of operating between the frequency range 300 kHz to 6 GHz
4. A computer, customised with a program to control the operation of the system.

A compressed pellet of mineral sample, encased within a quartz tube was raised into the microwave resonant cavity. Measurement of the frequency shift and quality factor was made at three selected resonant frequencies, i.e. 0.615, 1.413 and 2.216 GHz. The quartz tube was mounted on a computer operated robotic arm, used to raise and lower the sample between the cavity and the furnace so that the temperature of the specimen could be varied. Further detail is given in Arai et al., 1993.

Selected mineral specimens,of galena, chalcopyroite, sphalerite, pyrite and chalcocite, supplied by Gregory Bottley & Lloyd, London, were used for measurement of the dielectric properties and purity of the samples was confirmed using X-ray diffraction. Sample preparation consisted of crushing and grinding the minerals to -200μm, using a cone crusher and a Raymond laboratory hammer mill respectively. A 4-mm diameter quartz tube was first filled with a small and compressed amount of silica fibre as a sample holder. The sample was then poured into the tube and shaken to settle to an approximate height of 8-10mm. The weight of the sample was then determined to four significant figures. The sample holder was placed in the furnace and the temperature increased at a rate of 1°C per minute. It was then maintained at

the chosen level for 5 minutes to stabilise the temperature within the sample pellet before each measurement was taken. Measurement time was approximately 15 s, thus it is hoped that heat loss from the sample during this time is small. All experiments were carried out within an air atmosphere and measurements were taken between 25°C and 600°C at 25°C intervals.

Thermo-gravimetric analysis

Thermo-gravimetric analysis (TGA) allows phase or chemical changes of samples during heating to be inferred by continuous monitoring of weight changes. The samples were heated in a Perkin Elmer Pyris 1 Thermo-gravimetric Analyser. Approximately 50-100mg of each sample was heated from ambient to 650°C at a rate of 20°C per minute. The sample was then held at 650°C for a further 20 minutes. The experiment was first carried out using air and then using nitrogen to observe the effect of an inert atmosphere. The gas flow rate was 30cc/min in each case.

3. Results

To check the operation of the equipment, measurement on a 4-mm diameter solid quartz rod was carried out. The measured value of dielectric constant was in agreement with published data. In addition, results of the measurement of dielectric constant and loss factor of quartz carried out at three different densities are shown in Figures 2 and 3. A variation of dielectric constant with density was found.

The temperature dependence of dielectric constant and loss factor of sulphides at a frequency of 615 MHz are shown in Figures 4 and 5 respectively. It has been found, as shown in Figure 4, that the dielectric constants of pyrite and chalcopyrite have similar trends over the range of temperature used. Both are constant between 50 and 375°C and then increase from 375 to 475°C, after which they remain constant. The loss factors of chalcopyrite and pyrite also show similar trends. They are constant up to 350°C. Thereafter the loss factor exhibits a peak at the temperatures of 400°C and 450°C for chalcopyrite and pyrite respectively.

Chalcocite exhibits similar trends but the positive slope occurs in the temperature range 200-350°C. The loss factor shows two peaks at temperatures of around 150°C and around 250°C. The other sulphide minerals, galena and sphalerite, are thermally stable up to 425°C. The dielectric constant and loss factor for these minerals are

constant over this temperature range. Above this temperature, both galena and sphalerite show a positive slope. Similar trends in variation of dielectric constant and loss factor with temperature at frequencies of 1.41 GHz and 2.216 GHz are shown in Figures 6 to 9.

The results of thermo-gravimetric analysis of sulphide minerals carried out in air and nitrogen atmospheres are shown in Figures 10 and 11. It has been found that galena and sphalerite are stable minerals over the temperature range of the experiment and, regardless of the heating conditions during differential thermal analysis, the minerals are stable at temperatures up to 500°C, as shown in Figures 10 and 11. Pyrite, chalcocite and chalcopyrite show a variation in sample mass during heating. In fact, it can be seen that these effects are a function of the localised atmosphere. When heating in air, an increase in mass is observed for chalcocite and chalcopyrite while pyrite shows a reduction, as shown in Figure 10. When heating in a nitrogen atmosphere, however, a small loss of weight is observed in all three minerals, with chalcopyrite reporting a loss of up to 10% (Figure 11).

4. Discussion

The dielectric properties of materials are temperature and bulk density dependent, the nature of the dependence being a function of the dielectric relaxation processes operating under the particular test conditions and the applied frequency.

4.1 Modelling effect of density

Mineral ores are heterogeneous mixtures of multiple mineral phases and, under typical processing conditions, are often present in powder form following comminution. Prediction of mixture properties from pure mineral data, or the variation of complex permittivity with density from a single datum is a valuable tool. There exist a considerable number of dielectric mixture formulae. Tinga et al., 1973, summarize many of these.

Nelson (1988) has investigated relationships to allow prediction of the complex permittivity of granular or pulverized materials at different bulk density. It was found that dielectric proprieties could be expressed in terms of a powder-air mixture by the following empirical relationships:

$$\varepsilon'^{1/k} = a\rho + 1 \qquad (6)$$

$$\sqrt{\varepsilon''+e} = c_1\rho + c_0 \qquad (7)$$

Where

1. k can take the value 2 or 3 depending on the material
2. a, c_0, c_1 and e are constants for a specific material at a given frequency and
3. ρ is the density of the powder-air mixture.

These relationships are valid only for a powder-air mixture, where ε' = 1 and ε'' = 0 at zero density.

In his research, Nelson used data from some earlier studies on the density dependence of the dielectric properties of particulate materials to see how well they might support the relationships. The data included measurements taken on pulverized coal, goethite and hard red winter wheat at frequencies of 150 MHz and 11.7 GHz at a temperature of 20 °C. Nelson used equations (6) and (7) to determine the solid permittivity by extrapolation. It was found that in general a value of k = 3 gave the best results and better agreement with other mixture formulae, especially the Looyenga formula. This is perhaps not surprising considering the $1/3^{rd}$ exponent in that expression. Nelson also found that k = 2 also yielded a good fit to his experimental data.

An attempt to use a similar approach with the obtained data in the present research has been made. Experimental data points using measurements of the dielectric constant of quartz at four bulk densities were plotted against the bulk density using k=2 or 3 in equation 6.

The results are shown in Figures 12 and 13, where straight lines were obtained by least squares curve fitting with the (1, 0) point included. More detailed information about the coefficients of empirical equations is given in Table 3. This was obtained by linear regression analysis to establish the intercept A_0 and slope A_1, relating dielectric constant and bulk density of quartz at a range of temperature and frequency.

Standard deviation analysis for the developed models was carried out and the results are given in Table 4. It has been found from the correlation coefficients that the k=2 relationship gives a better fit than k=3.

4.2 Effect of Bulk Density On The Dielectric Properties Of Sulphides

The effect of bulk density on the dielectric properties of sulphide minerals has been investigated using the method described above. A summary of linear relationships between bulk density and dielectric constant at a temperature of 25°C is given in Table 5.

An attempt to use equation 7 on the relationship between loss factor and density for sulphides was made, however it was not successful. A possible explanation is the fact that perturbation technique becomes less accurate for the evaluation of loss factor for lossy materials. As reported in Batt et al., 1995 discrepancies in the value for loss factor using different measuring techniques could be up to 50% at high temperature. With such an error it is likely that values may be scattered and so difficult to obtain linear relationship.

4.3 Effect Of Frequency On The Dielectric Properties

With the exception of some extremely low-loss materials, the dielectric properties of most materials vary with the frequency of the applied electric field. An important factor contributing to the frequency dependence of the dielectric properties of most materials is the polarization arising from the orientation of molecules having permanent dipole moments with the imposed electric field.

From the results shown in Figures 4 to 9, it can be observed that dielectric properties of sulphide minerals vary with frequency. To better illustrate the dependence of dielectric properties on frequency an analysis has been carried out for pyrite and the results are shown in Figure 14. The results show little variation in the relationship between dielectric constant and loss factor with frequency.

4.4. Effect Of Temperature

Several authors have reported the effect of temperature on the composition and mineral phases of sulphides. Such an effect of temperature on the dielectric properties can be observed in the results shown in Figures 4 to 9. Furthermore, the thermo-gravimetric analysis curve results in Figures 10 and 11 show general trends of material weight loss during heating. To further investigate the critical points where such changes occur a derivative function known as differential thermal analysis is required. The results of differential thermal analysis for the sulphide minerals are shown in Figures 15 and 16 for experiments carried out on air and nitrogen atmosphere respectively.

It has been found from heating in air that the critical temperature for weight change in chalcocite is 350°C, below which it is stable. An increase in weight is observed between this temperature and 500°C, which could be related to the oxidation of chalcocite. Results from heating chalcocite in a nitrogen atmosphere show a decrease in weight at temperatures above 350°C.

The dielectric property results, however, show an increase of dielectric constant at temperatures between 200°C and 350°C. In addition, the results for loss factor show two regions of high microwave absorption, i.e. between 100°C and 275°C and above 400°C that could be related to complex phase transformation within the mineral. In addition, in published data of dielectric properties of chalcocite by Salsman (1991), variation of dielectric constant with temperature shows different trend. It shows a peak at temperature around 100°C and then decreases up to 300°C. A further paper by Holderfield and Salsman (1992) on the dielectric constant of chalcocite shows not only a different trend but, great difference on the order of magnitude of the values presented. No attempt to compare the two reports was made by the authors.

Despite these results, there should be some complex phase transformation occurring during heating that cannot be explained by the weight variation for this particular mineral. It has long been reported for copper/sulphur compounds that the region from Cu_2S to $Cu_{1.75}S$ shows a wide variety of phases and phase transitions of a complex nature (Gronvold et al. 1987). Such a number of phases and phase transformations must have an effect on the dielectric properties but they cannot be detected through differential thermal analysis.

In contrast to chalcocite, the dielectric properties of pyrite, galena, sphalerite and chalcopyrite are consistent with the thermo gravimetric results. For example, the results for pyrite show that the mineral is quite stable up to 350°C and above this temperature a loss of weight is observed. It is interesting to note that loss of weight occurs regardless of the heating conditions in air or nitrogen atmospheres. The present finding could suggest that, during phase transition from pyrite to pyrrhotite, free sulphur is formed, which is further liberated as sulphur dioxide or sulphur fumes depending on the prevailing heating conditions.

Although chalcopyrite exhibits similar trends to pyrite for dielectric constant and loss factor, it shows a different thermo-gravimetric curve pattern. The thermo-gravimetric

curve of chalcopyrite (Figure 15) shows that the mineral is stable up to 350°C. Between 350°C and 400°C there is a phase transition similar to the process occurring during the phase transition of pyrite to pyrrhotite. This finding is consistent with results of loss factor for chalcopyrite where a maximum value is observed at the temperature of 400°C (Figures 3, 5 and 7). Furthermore, the results suggest that the increase in loss factor observed for pyrite and chalcopyrite in this temperature range is due to the presence of a similar mineral phase with high absorption of microwave radiation. Above the temperature of 400°C, chalcopyrite undergoes an oxidation process that results in a stable mineral phase that eventually decomposes and sulphur dioxide is liberated at temperature above 500°C. The liberation of free sulphur at temperature above 500°C was observed on TGA results of chalcopyrite during heating in a nitrogen atmosphere (Figure 16).

The results of thermo-gravimetric analysis of galena and sphalerite show that both minerals are thermally stable at temperatures up to 500°C but above this temperature, small variations have been observed. It has also been found that galena and sphalerite, when cold, are less receptive to microwave radiation than the other sulphides. Only at temperatures above 400°C do they become receptive to microwave radiation (Figures 4 to 9).

Overall, the present findings are consistent with differential thermal analysis data on sulphide minerals reported by a number of investigators. These findings suggest that, during heating in an oxidising environment, pyrite is converted in pyrrhotite with the liberation of sulphur fumes and chalcocite and chalcopyrite are converted into Cu or Cu-Fe sulphates. The present results are fully in accordance with observations reported by Chen et al in 1984, who carried out microwave heating experiments on minerals and observed the heating response and product examination. It was reported that pyrite and chalcopyrite heats readily when exposed to microwaves, with emission of fumes. The product examination revealed the presence of pyrrhotite and sulphur fumes when heating pyrite and Cu-Fe sulphides and sulphur fumes for chalcopyrite product.

5. Conclusions

A knowledge of dielectric properties, particularly loss factor, is important for an accurate prediction of power loss density, which has been shown to be dependent on

the internal electric field strength, frequency of the microwave radiation and the dielectric loss factor of the materials. With the knowledge of the power loss density, it is possible to model the selective microwave heating of minerals and, thus, the thermal stresses that can be induced in real ores.

Bulk density effects on dielectric properties have been observed and the relationships developed by Nelson (1988) have been found to be valid for quartz but his square root model produces a smaller error than the cube root model. The linearity of square roots and cube roots of dielectric constant of quartz with bulk density are consistent with published dielectric mixture formulae that specify the additivity of the dielectric constants of the constituents of the mixture.

The linearity of the k=2 and k=3 relationships for dielectric constant with bulk density provide a means of estimating the dielectric constant of the air and any given material at any bulk density, including solid material, by utilizing a measurement of dielectric constant for the material at any known density and the $\rho = 0$, $\varepsilon' = 1$ intercept.

The dielectric properties of a number of sulphide minerals have been measured, including chalcocite, chalcopyrite, pyrite, sphalerite and galena. Galena and sphalerite have been found to be thermally stable at temperatures up to 500°C and their dielectric properties exhibit little variation with temperature. The dielectric properties of pyrite, chalcocite and chalcopyrite, however show a significant variation with temperature. The changes observed are compositional and related to phase transformations during heating.

6. Acknowledgements

The authors would like to thank the University of Nottingham and Rio Tinto Technical Services Ltd for sponsoring the present research.

7. References

1. Arai, M., Binner, J.G.P., Carr, G.E. and Cross, T.E. 1993. High temperature dielectric property measurements of engineering ceramics. Ceramics Transactions, 36, pp483-492.

2. Batt, J., Binner, JGP, Cross, TE, Greenacre, NR, Hamlyn, MG, Hutcheon, RM, Sutton, WH and Weil, CM, 1995. A parallel measurement programme in High temperature dielectric property measurements: an update. Ceramics Transactions, 59, pp243-250.

3. Greenacre, N. 1996. Measurement of the High Temperature Dielectric Properties of Ceramics at Microwave Frequencies, PhD Thesis, University of Nottingham.

4. Nelson, S.O. 1988. Estimating the permitivity of solids from measurements on granular or pulverized materials. Materials Research Society Symposium Proceedings, vol. 124, pp149-154.

5. Salsman, J. 1991. Technique for measuring the dielectric properties of minerals as a function of temperature and density at microwave heating frequencies, Materials Research Society Symposium Proceedings, vol. 189, pp509-515.

6. Salsman, J. 1992. Measurement of dielectric properties in the frequency range of 300 MHz to 3 GHz as a function of temperature and density. Ceramics Transactions, vol. 59, pp203-214.

7. Holderfield, S.P. and Salsman, J. 1992. Observed trends in the dielectric properties of minerals at elevated temperatures. Materials Research Society Symposium Proceedings, vol. 269, pp589-594.

8. McGill, S.L., Walkiewicz, J.W., 1988. The effect of power level on microwave heating of selected chemicals and minerals. In Sutton, W.H. et al (Eds), Mat. Res. Soc. Symp. Proc. Reno, NV, M4.6, vol. 124.

9. Church R.H., Webb, W.E. and Salsman, J.B. 1993. Dielectric properties of low-loss minerals, USBOM Report of Investigations 9194.

10. Walkiewicz J.W., Kazonich G. and McGill S.L. 1988. Microwave heating characteristics of selected minerals and compounds, Minerals and Metallurgical Processing. Pp39-42.

11. Tinga, W.R. 1992. Rapid high temperature measurement of microwave dielectric properties. Mat. Res. Soc. Symp. Proc., vol 269, pp505-516.

12. Tinga, W.R., Vos, WAG and Blossey, DF, 1973. Generalized approach to multiphase dielectric mixture theory, J. Appl. Phys., 44(9), 3897-3902.

13. Walkiewicz, J.W., Clark, A.E. and McGill S.L. 1991. Microwave Assisted Liberation; IEEE Transactions on Industry Applications, vol. 27, no2.

14. Chen, T., Dutrizac, J.E., Haque, K.E., Wyslouzil, W. and Kashyap, S. 1984. The relative transparecency of minerals to microwave radiation, Canadian Metallurgical quaterly, vol 23, pp. 349-351.

15. Kingman S.W., Jackson, K., Cumbane, A.J., Bradshaw, S.M., Rowson, N.A. and Greenwood, R. 2003. Recent developments in microwave assisted comminution, submitted to Int. J. Min. Proc., May 2003.

16. Kingman S.W., Jackson, K., Cumbane, A.J., Bradshaw, S.M., Rowson, N.A. and Greenwood, R. 2003. An investigation into the influence of microwave treatment on mineral ore comminution, submitted to Powder Technology, May 2003.

17. Whittles, D., Reddish, D. and Kingman; S.W. 2003. Application of numerical modeling for prediction of the influence of power density on microwave assisted breakage. Int. J. Miner. Process. 68, 71-91.

18. Deer, W.A., Howie, R.A. and Zussman, J. 1966. An introduction to rock-forming minerals, pp445-461.

19. Deer, W.A., Howie, R.A. and Zussman, J. 1962; Rock-forming minerals, volume 5, pp128-180.

20. Gronvold, F., Stolen, S., Westrum, E. and Galeas, C. 1987. Thermodynamics of copper sulphides III. Heat capacities and thermodynamic properties of $Cu_{1.75}S$, $Cu_{1.80}S$ and $Cu_{1.85}S$ from 5 to about 700 K, Journal of Chemical Thermodynamics, vol. 19, pp 1305 – 1324.

Table 1.

Microwave heating at frequency of 2.45GHz (after Chen et al, 1984)

Mineral	Power (W)	Heating response	Product examination
Arsenopyrite	80	Heat, some sparking	S and As fumes
Chalcopyrite	15	Heats readily with emission of sulphur fumes	Pyrite and Cu-Fe-sulphide
Galena	30	Heats readily with much arcing	Sintered mass of Galena
Pyrite	30	Heats readily, emission of sulphur fumes.	Pyrrhotite with S fumes
Sphalerite (high Fe content)	100	Difficult to heat when cold	Converted to Wurtzite
Sphalerite (low Fe content)	>100	Does not heat	No change, sphalerite

Table 2.

Effect of Microwave heating on the Temperature of Natural Minerals (after Walkiewicz et al, 1988)

Mineral	Chemical composition	Temperature, C	Time, min
Chalcocite	Cu_2S	746	7
Chalcopyrite	$CuFeS_2$	920	1
Galena	PbS	956	7
Pyrite	FeS_2	1019	6.75
Sphalerite	ZnS	88	7
Pyrrhotite	FeS_{2-x}	886	1.75

Table 3.

Coefficients of empirical equations relating the dielectric constant (ε') and density (ρ) of quartz.

Regression model	Temperature, °C	Measurement frequency, MHz					
		615		1410		2210	
Coefficient		A_0	A_1	A_0	A_1	A_0	A_1
$\sqrt{\varepsilon'} = A_0 + A_1\rho$	100	0.9786	0.3271	0.9648	0.331	0.978	0.327
	200	0.981	0.327	0.968	0.331	0.981	0.327
	300	0.983	0.327	0.971	0.331	0.983	0.327
$(\varepsilon')^{1/3} = A_0 + A_1\rho$	100	0.997	0.194	0.989	0.196	0.997	0.194
	200	0.998	0.194	0.987	0.196	0.995	0.194
	300	1.001	0.194	0.991	0.196	0.998	0.194

Table 4.

Standard deviation for experimental and calculated dielectric constant based on k=2 and k=3 models.

Density	Experimental	Calculated, k=2 model	Deviation, %	Calculated, k=3 model	Deviation, %
0	1.00	1.05	4.84	1.20	20.32
0.934	4.57	4.11	-10.05	3.88	-14.92
1.3	5.49	5.85	6.53	5.56	1.12
1.337	5.96	6.05	1.51	5.75	-3.51
2.648	15.00	14.95	-0.38	15.71	4.72
Standard deviation, %			5.82		11.59

Table 5.

Coefficients of empirical equations relating the dielectric constant ($\sqrt{\varepsilon'}$) and density (ρ) of sulphides.

Regression model	Mineral	Measurement frequency, MHz					
		615		1410		2210	
Coefficient		A_0	A_1	A_0	A_1	A_0	A_1
$\sqrt{\varepsilon_r'} = A_0 + A_1\rho$	Chalcocite	1.007	0.8016	0.9985	0.767	1.000	0.7738
	Chalcopyrite	0.9885	0.7514	0.9912	0.735	0.992	0.7414
	Galena	0.9968	0.5229	0.9978	0.5302	0.993	0.5301
	Pyrite	0.998	0.3799	0.9975	0.5729	0.998	0.5753
	Sphalerite	1.001	0.379	1.001	0.386	1.001	0.4027

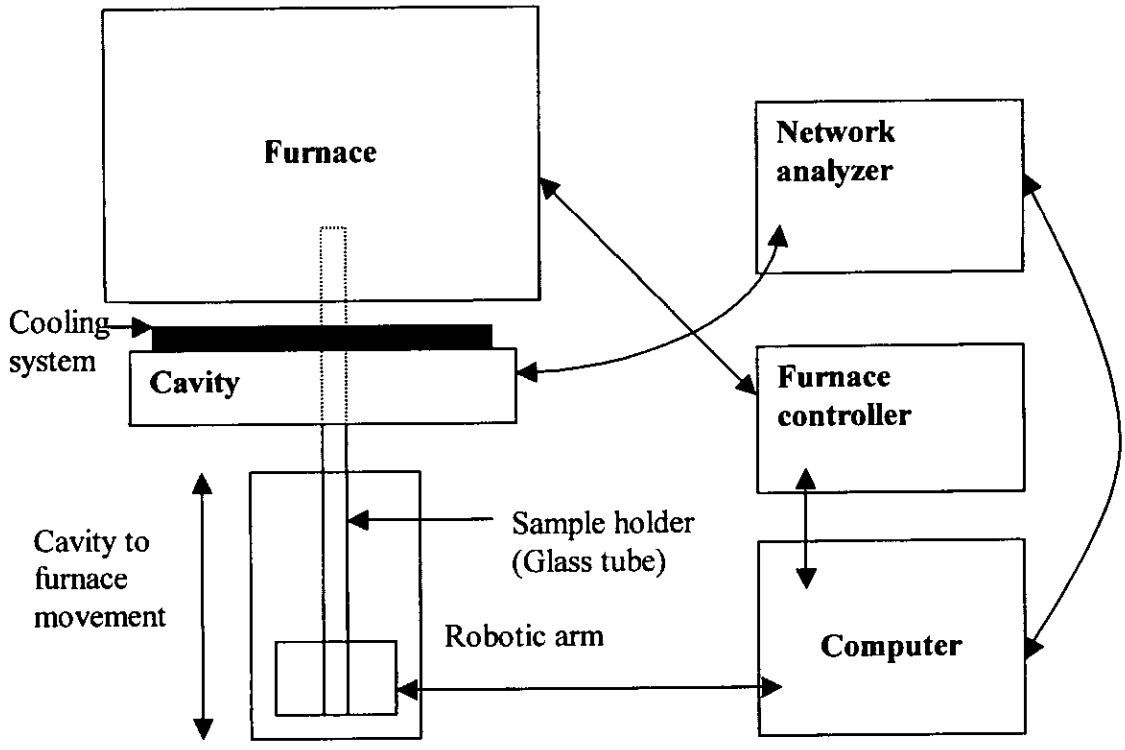

Figure 1. Diagrammatic representation of the measurement system (after Greenacre, 1996).

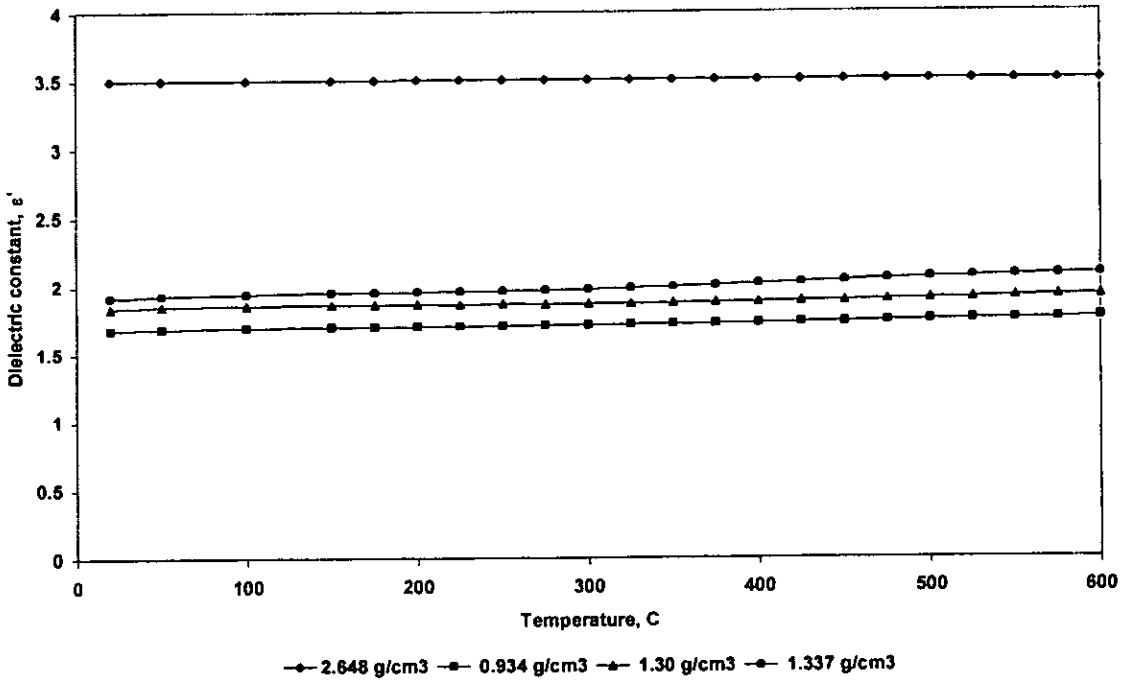

Figure 2. The dependence of dielectric constant of quartz with temperature measured at different packing densities.

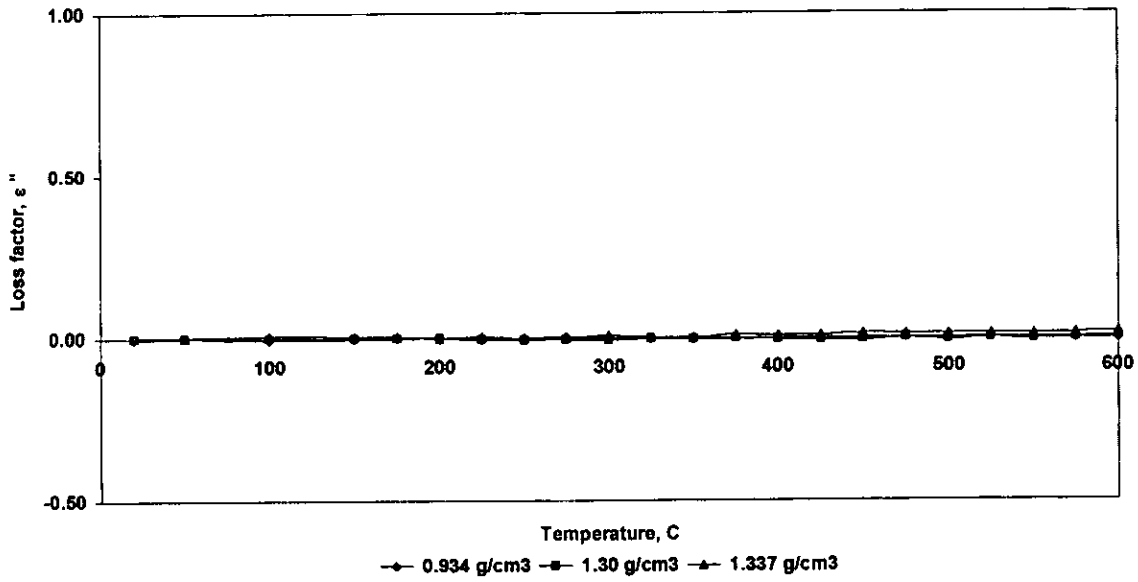

Figure 3. The dependence of loss factor of quartz with temperature measured at different packing densities.

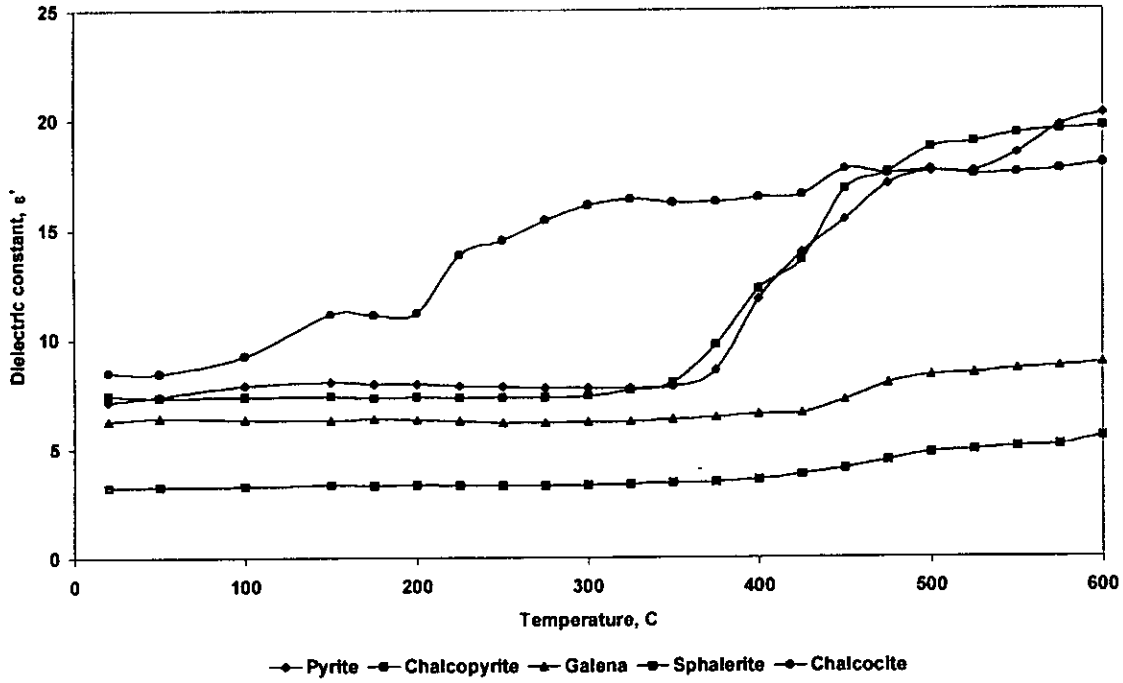

Figure 4. The dependence of dielectric constant of sulphide minerals with temperature measured at the frequency of 615 MHz.

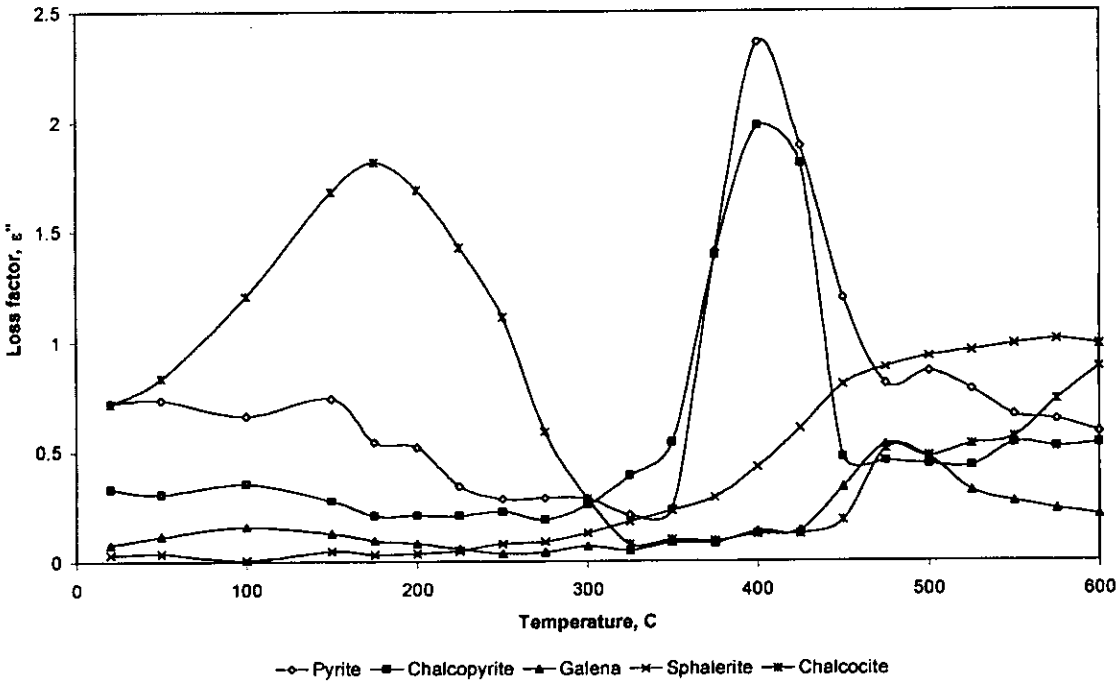

Figure 5. The dependence of loss factor of sulphide minerals with temperature measured at the frequency of 615 MHz.

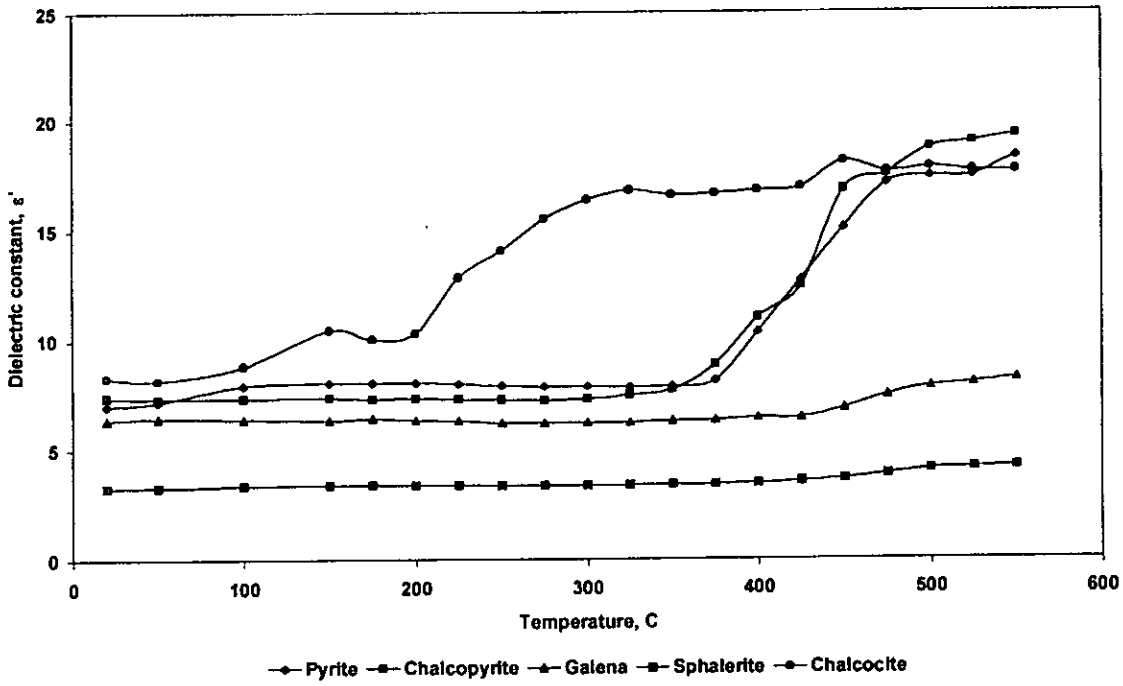

Figure 6. The dependence of dielectric constant of sulphide minerals with temperature measured at the frequency of 1.41 GHz.

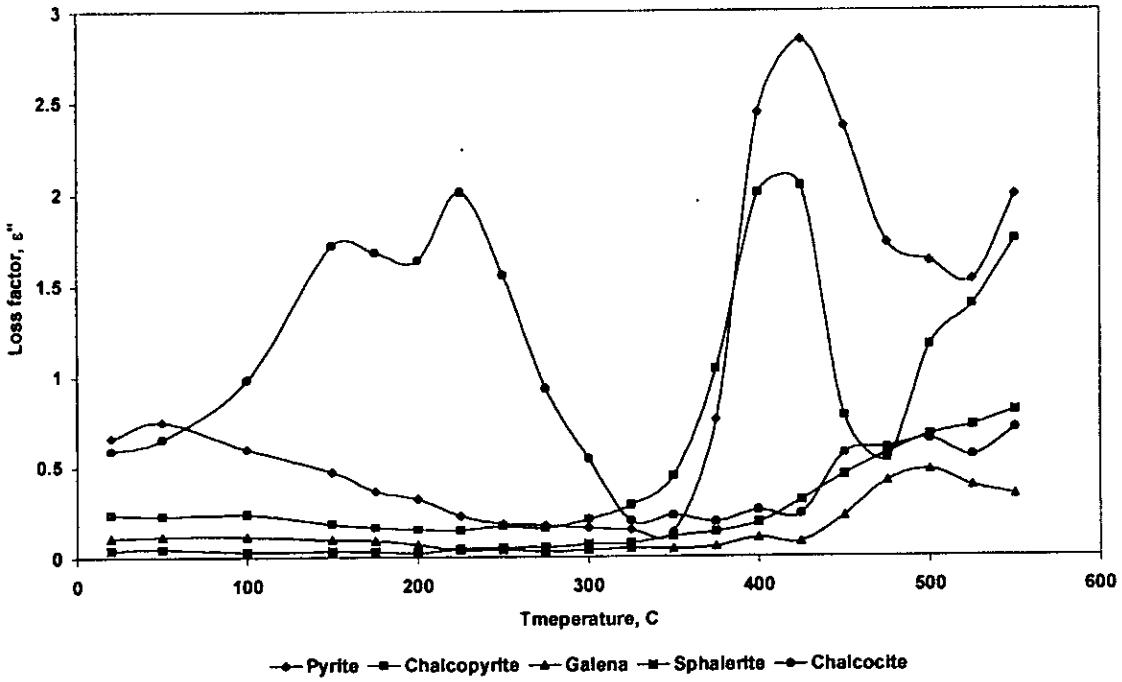

Figure 7. The dependence of loss factor of sulphide minerals with temperature measured at the frequency of 1.41 GHz.

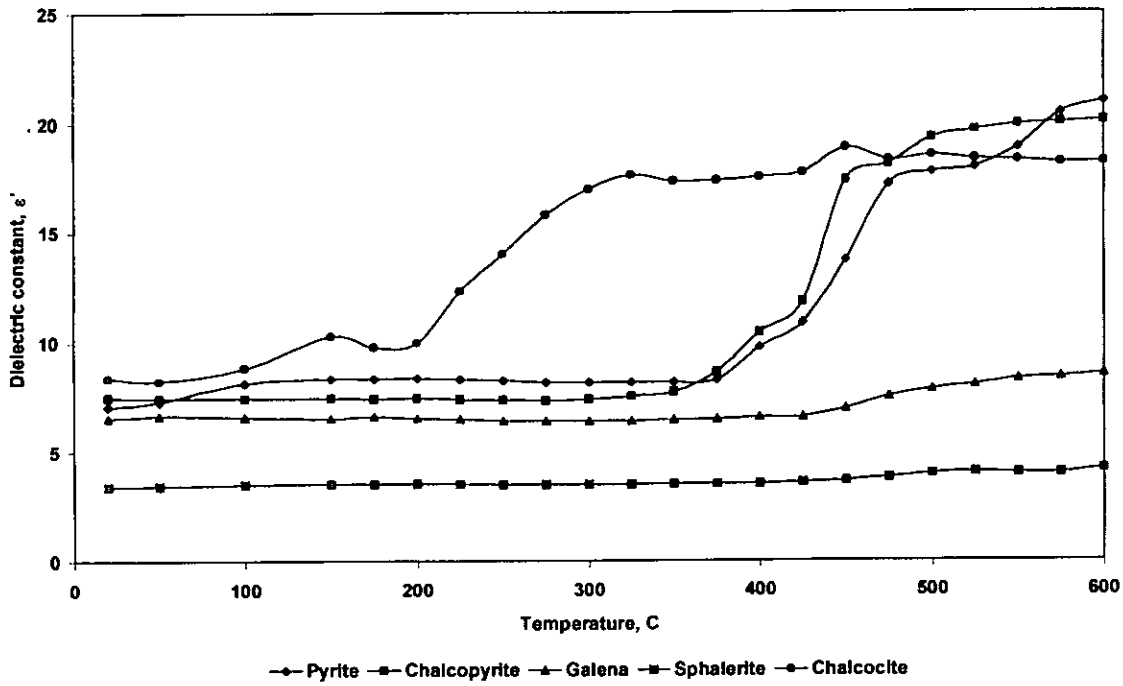

Figure 8. The dependence of dielectric constant of sulphide minerals with temperature measured at the frequency of 2.216 GHz.

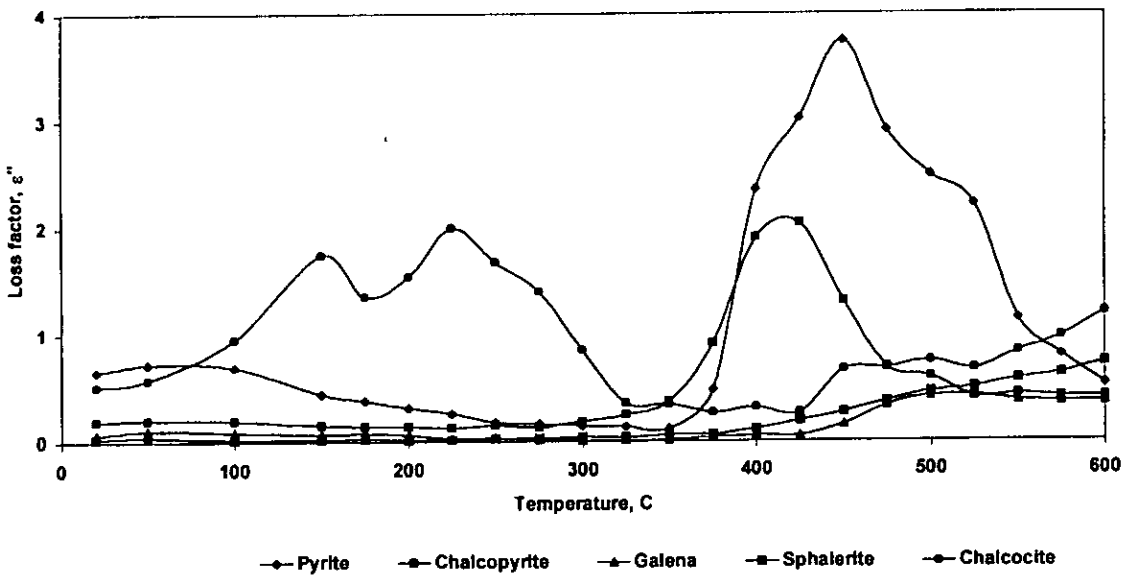

Figure 9. The dependence of loss factor of sulphide minerals with temperature measured at the frequency of 2.216 GHz.

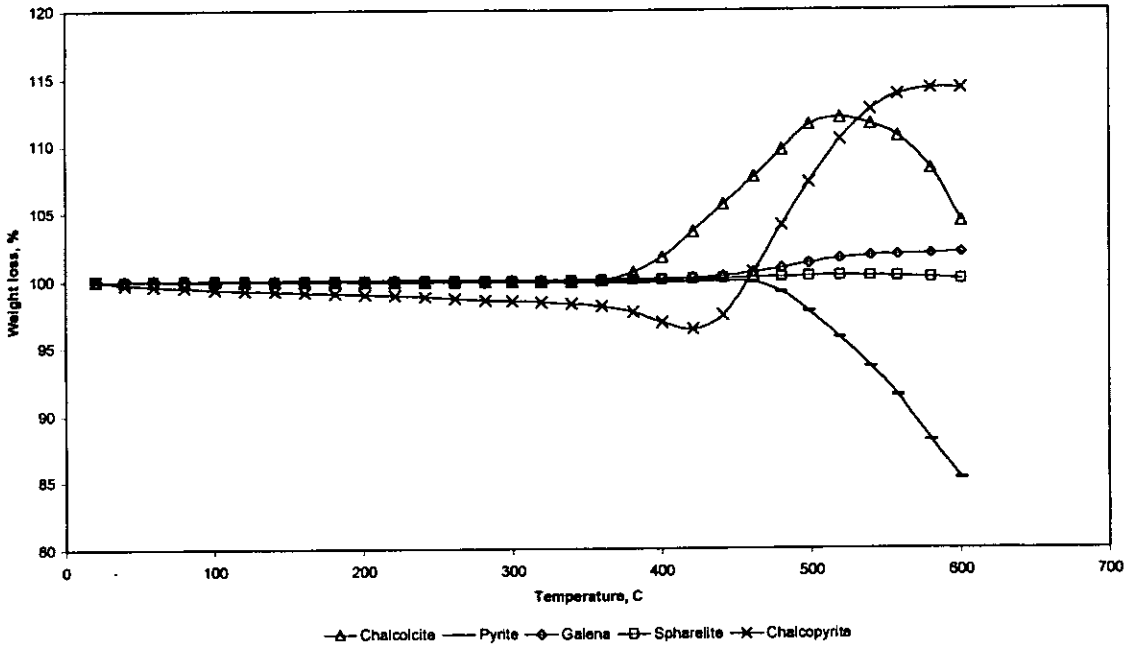

Figure 10. Thermo-gravimetric analysis of sulphides in air.

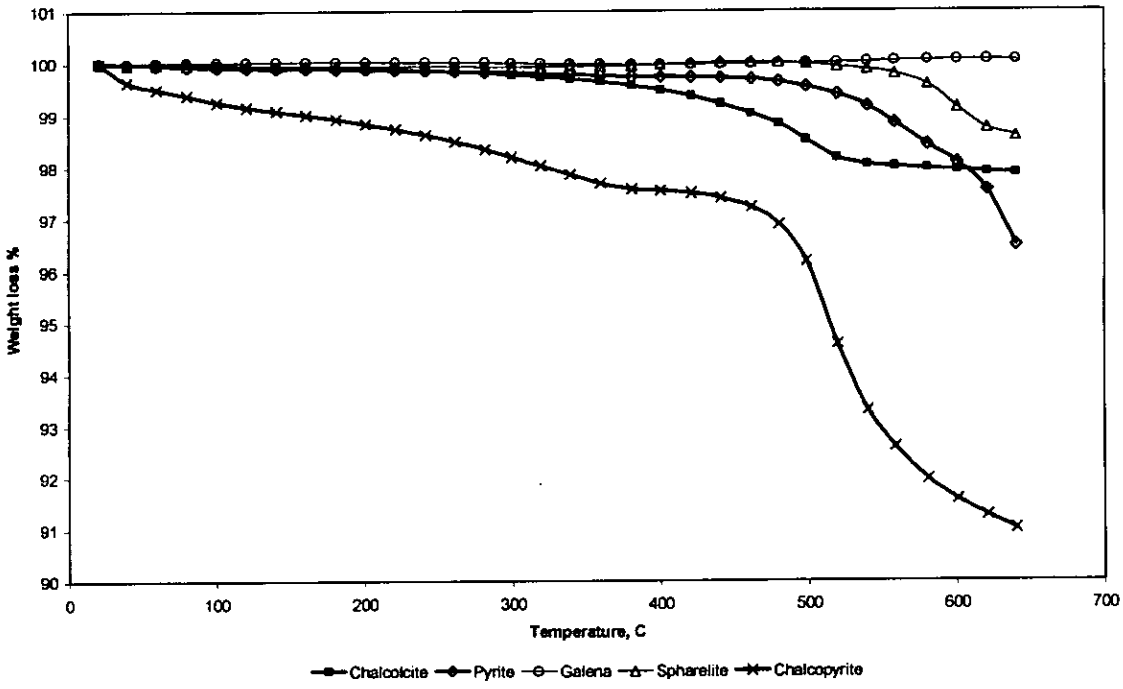

Figure 11. Thermo-gravimetric analysis of sulphides in nitrogen atmosphere.

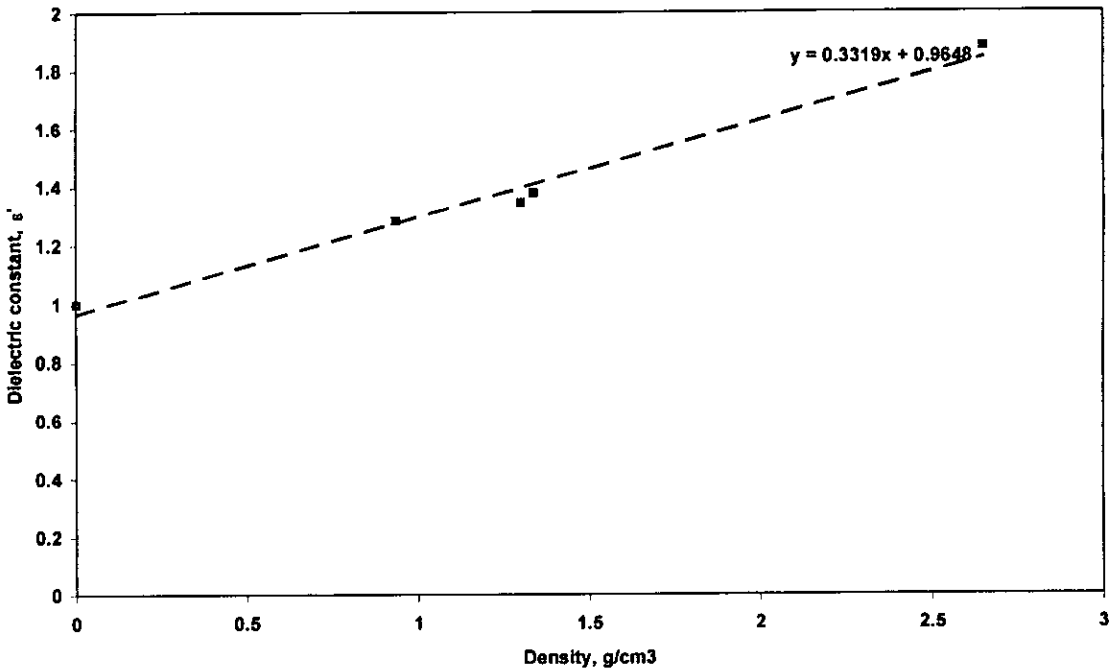

Figure 12. Relationship between density and dielectric constant of quartz for k=2.

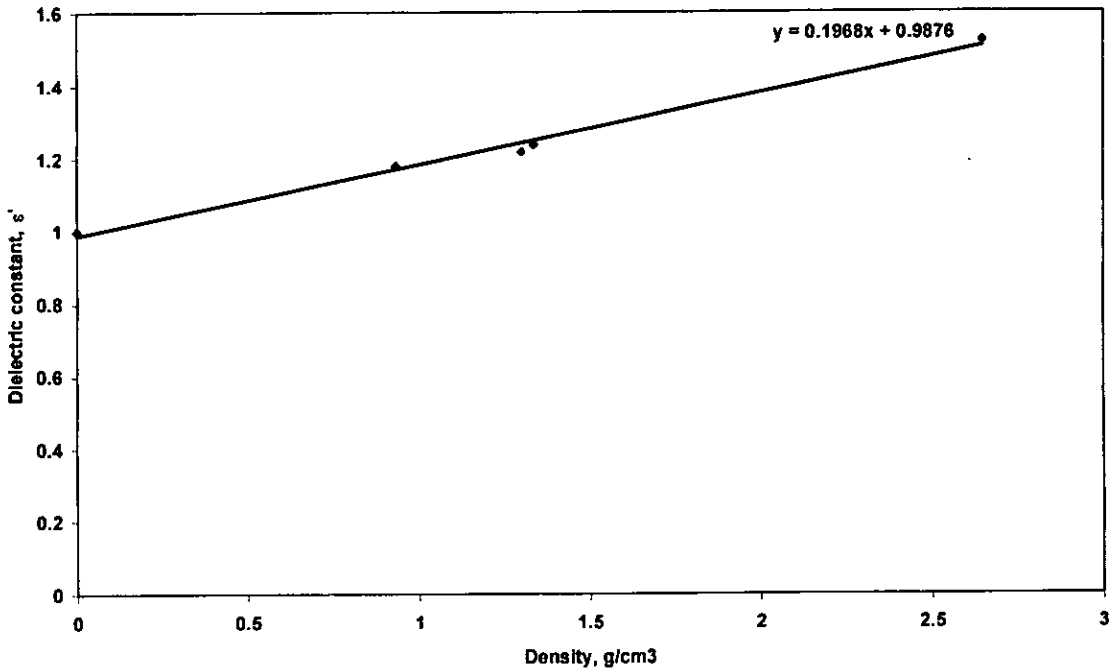

Figure 13. Relationship between density and dielectric constant of quartz for k=3

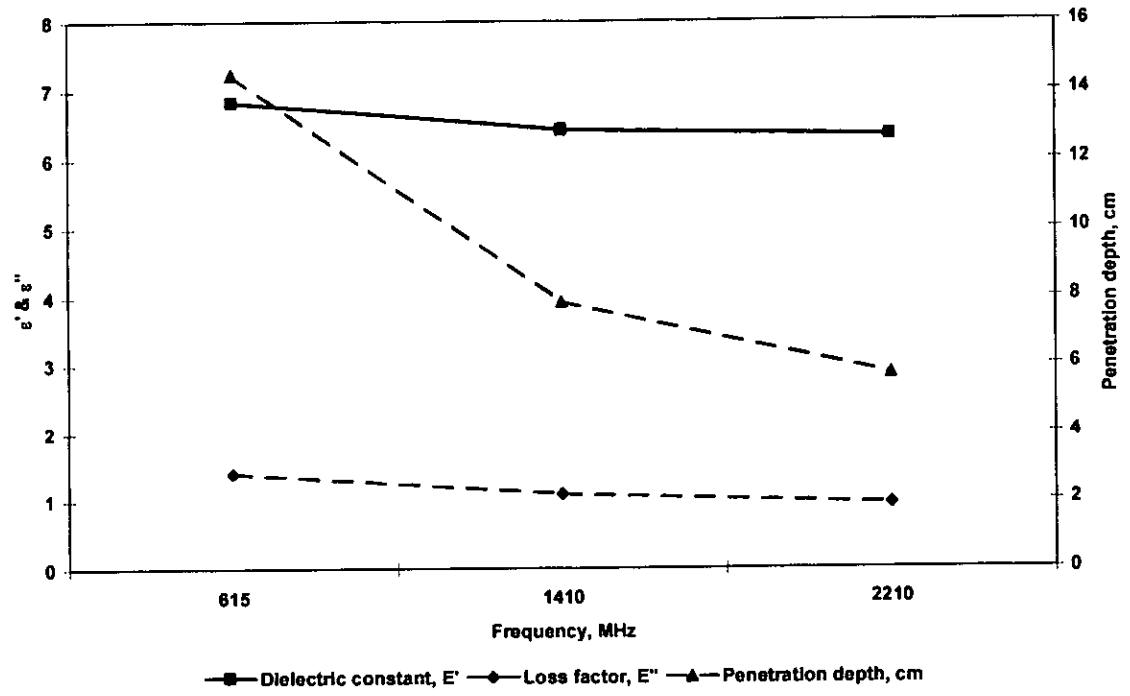

Figure 14. Effect of frequency on the dielectric properties of pyrite measured at 25°C.

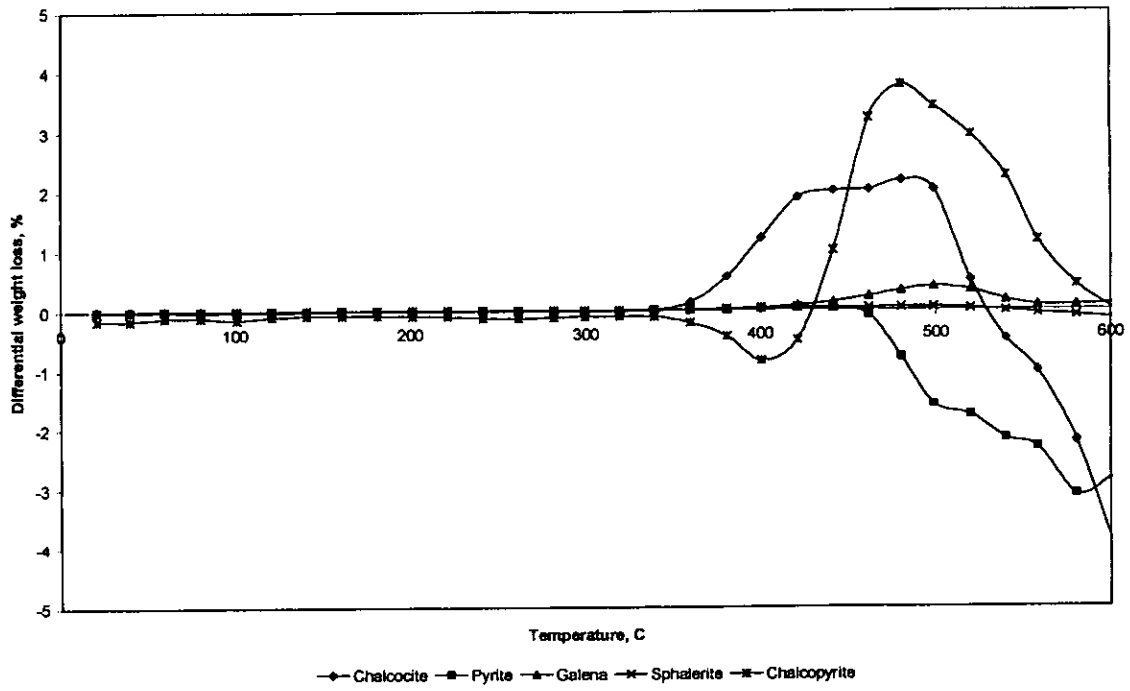

Figure 15. Differential thermal analysis of sulphide minerals in air.

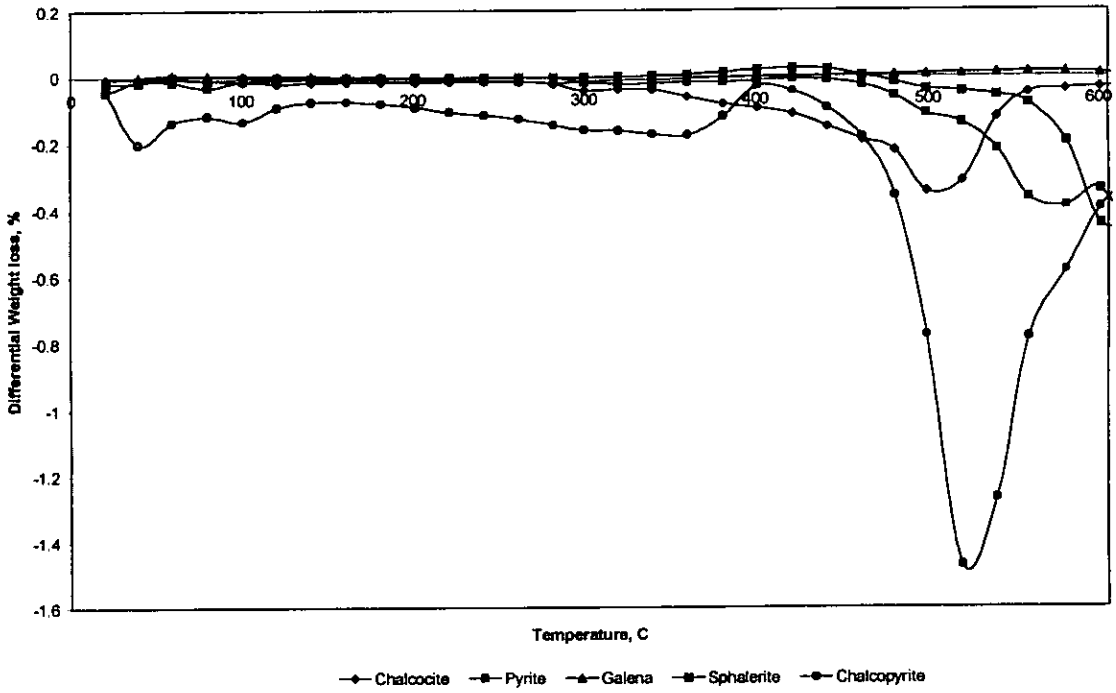

Figure 16. Differential thermo-gravimetric analysis of sulphide minerals under inert conditions.

LIST OF APPENDICES

1. Dielectric Properties Results

2. Palabora Microwave Assisted Comminution Data

3. Zinkgruvan Microwave Assisted Comminution Data

APPENDIX 1
DIELECTRIC PROPERTY DATA

1.1 XRD results

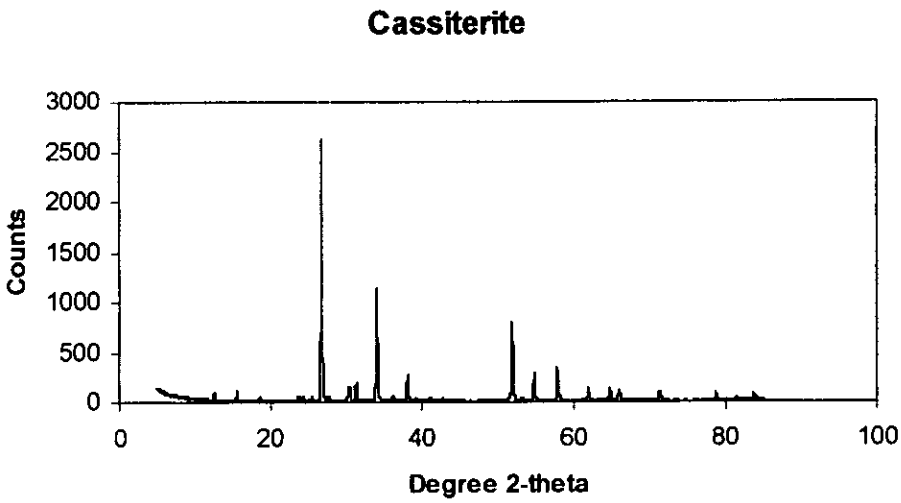

Figure A.1.1 X-ray diffraction of cassiterite

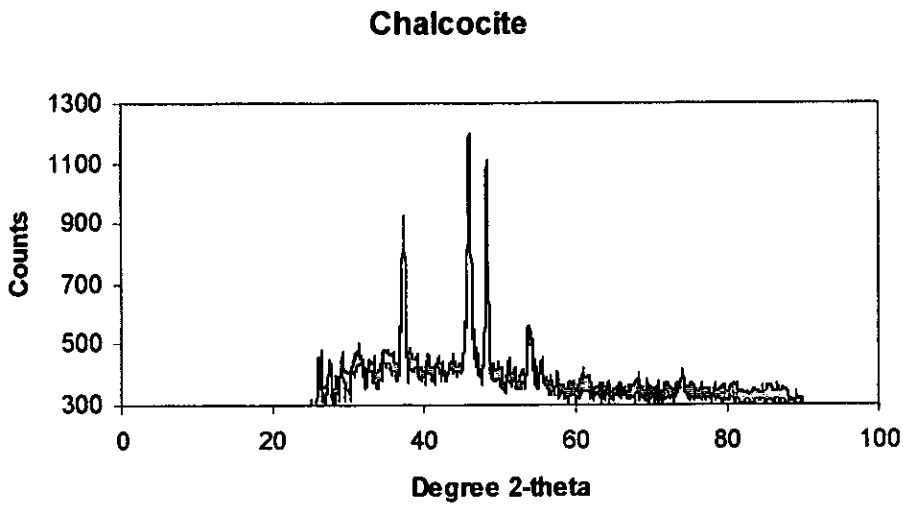

Figure A.1.2 X-ray diffraction of chalcocite

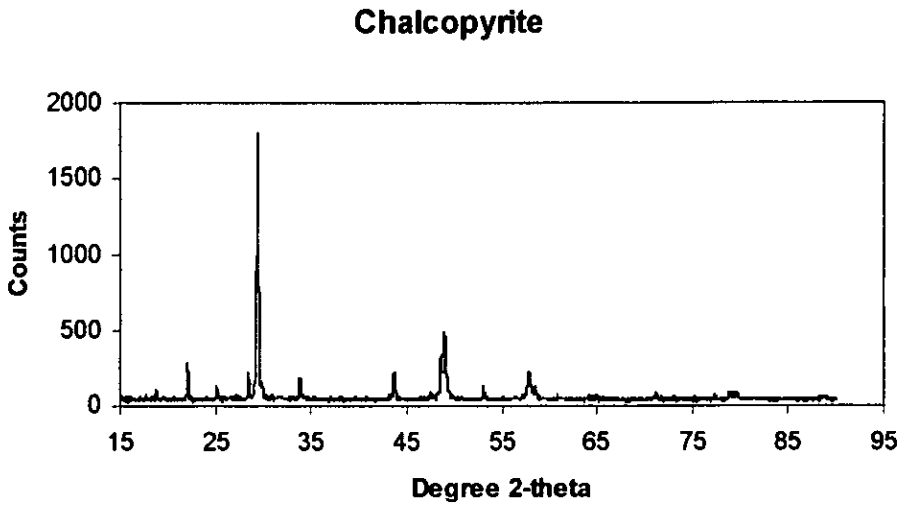

Figure A.1.3 X-ray diffraction of chalcopyrite

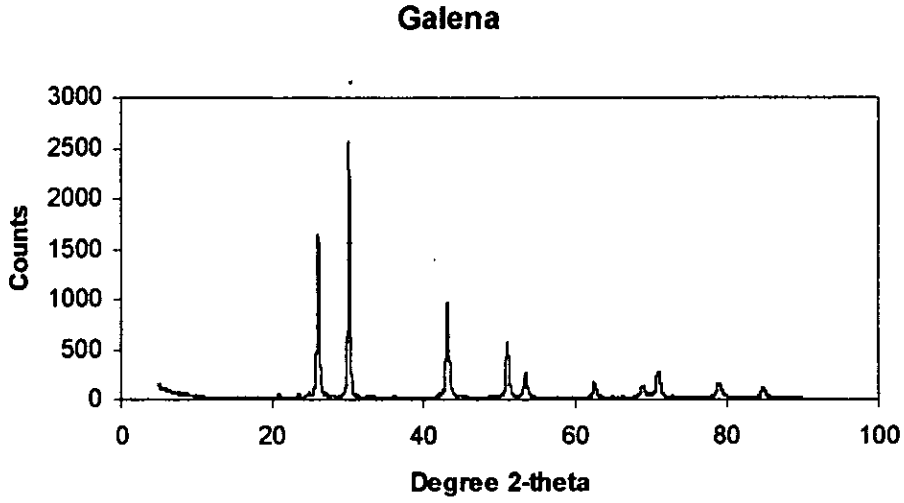

Figure A.1.4 X-ray diffraction of galena

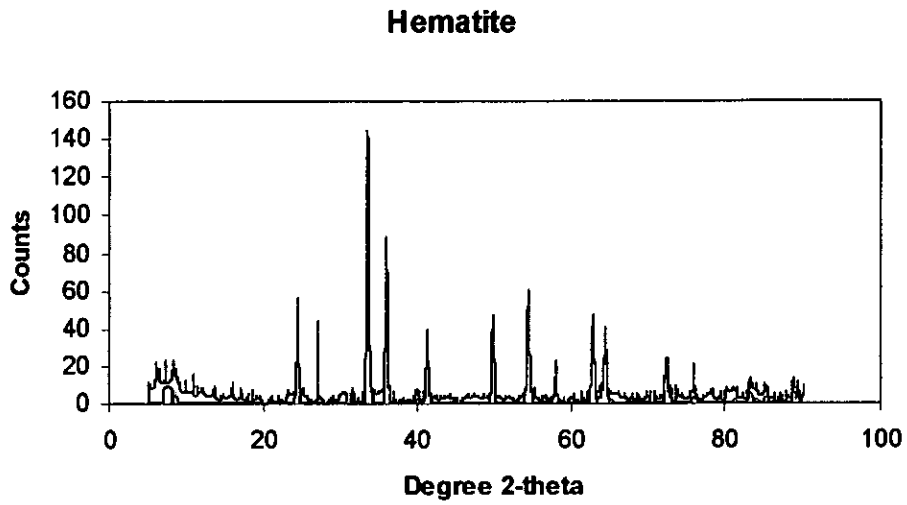

Figure A.1.5 X-ray diffraction of hematite

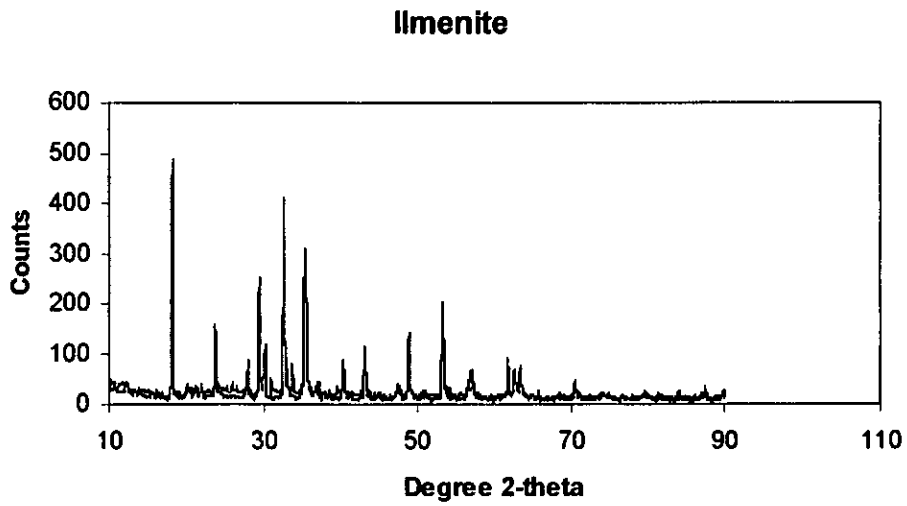

Figure A.1.6 X-ray diffraction of ilmenite

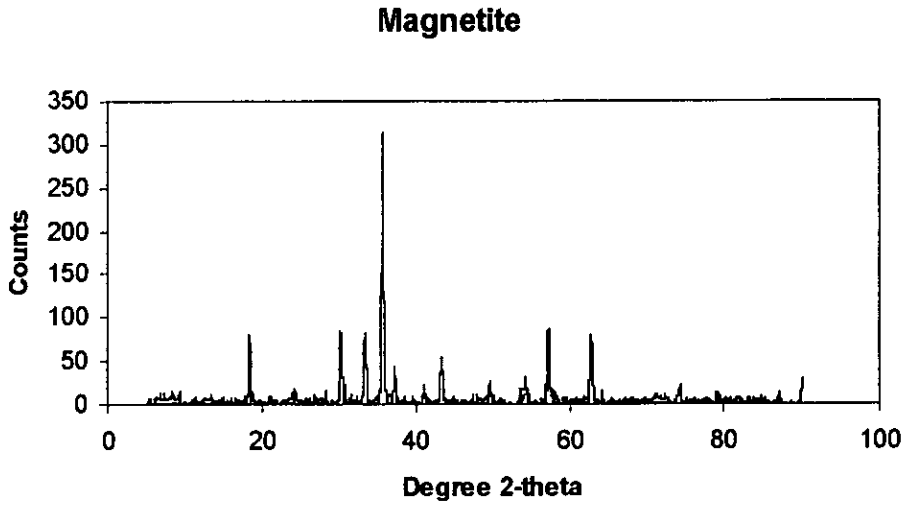

Figure A.1.7 X-ray diffraction of magnetite

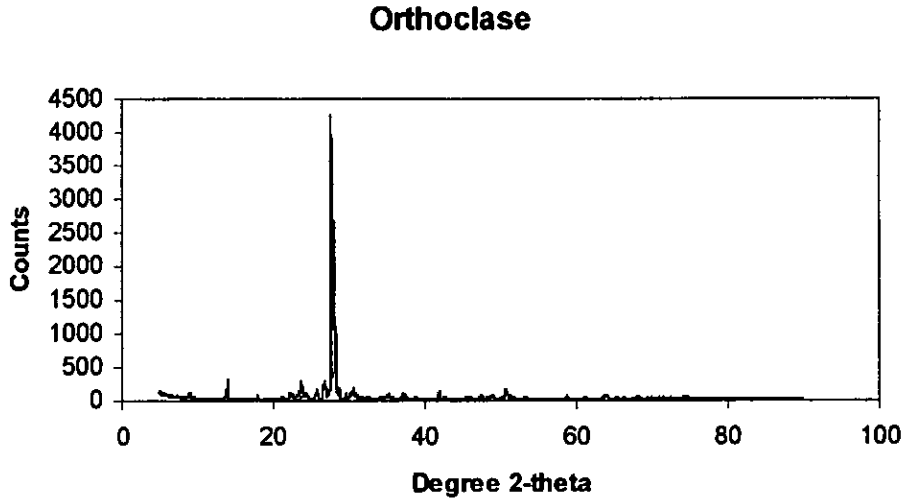

Figure A.1.8 X-ray diffraction of orthoclase

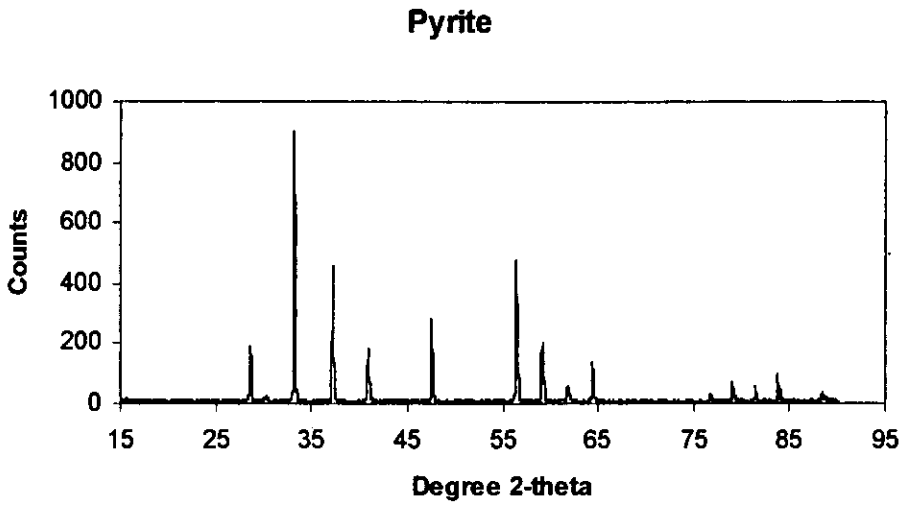

Figure A.1.9 X-ray diffraction of pyrite

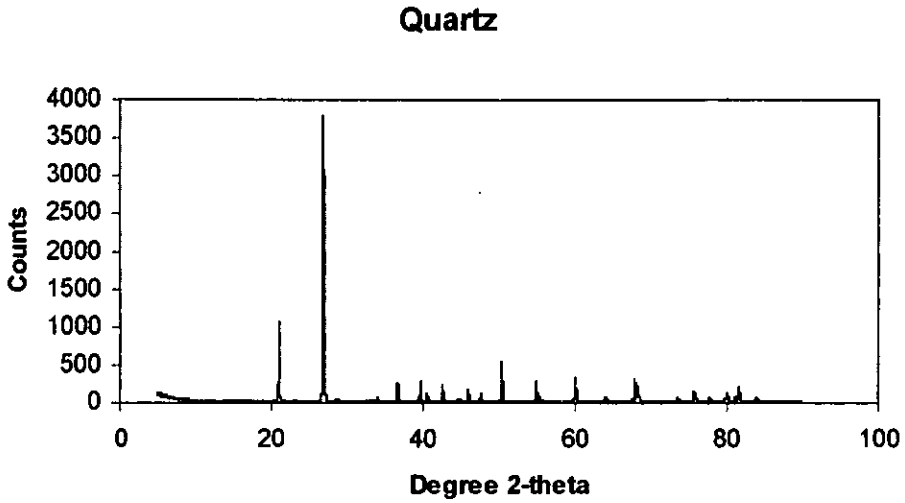

Figure A.1.10 X-ray diffraction of quartz

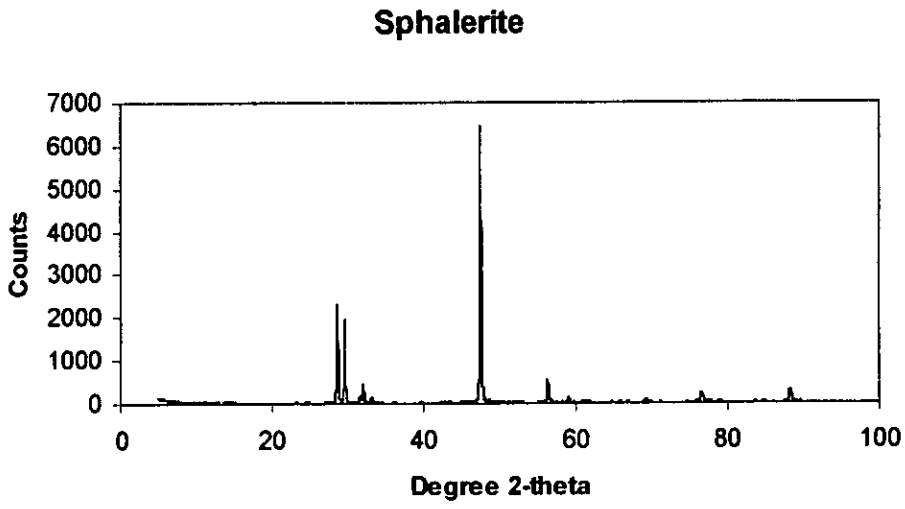

Figure A.1.11 X-ray diffraction of sphalerite

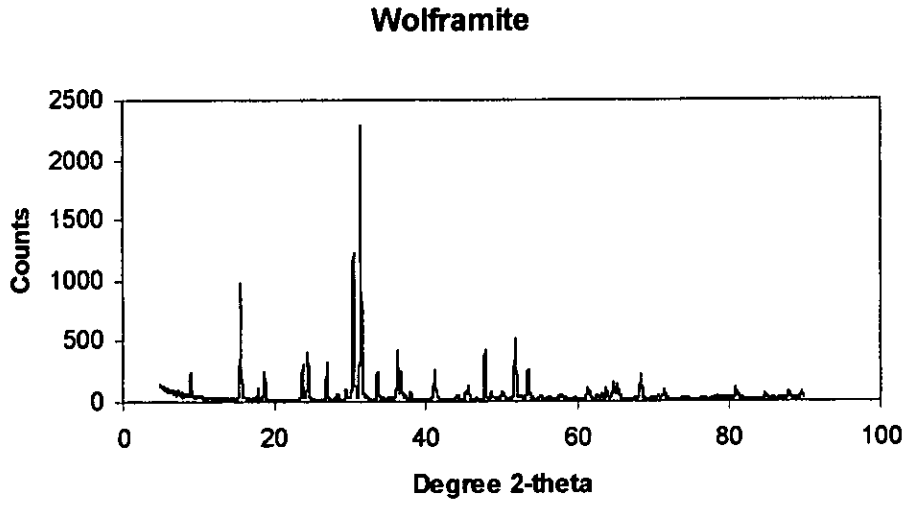

Figure A.1.12 X-ray diffraction of wolframite

1.2 Dielectric properties of minerals

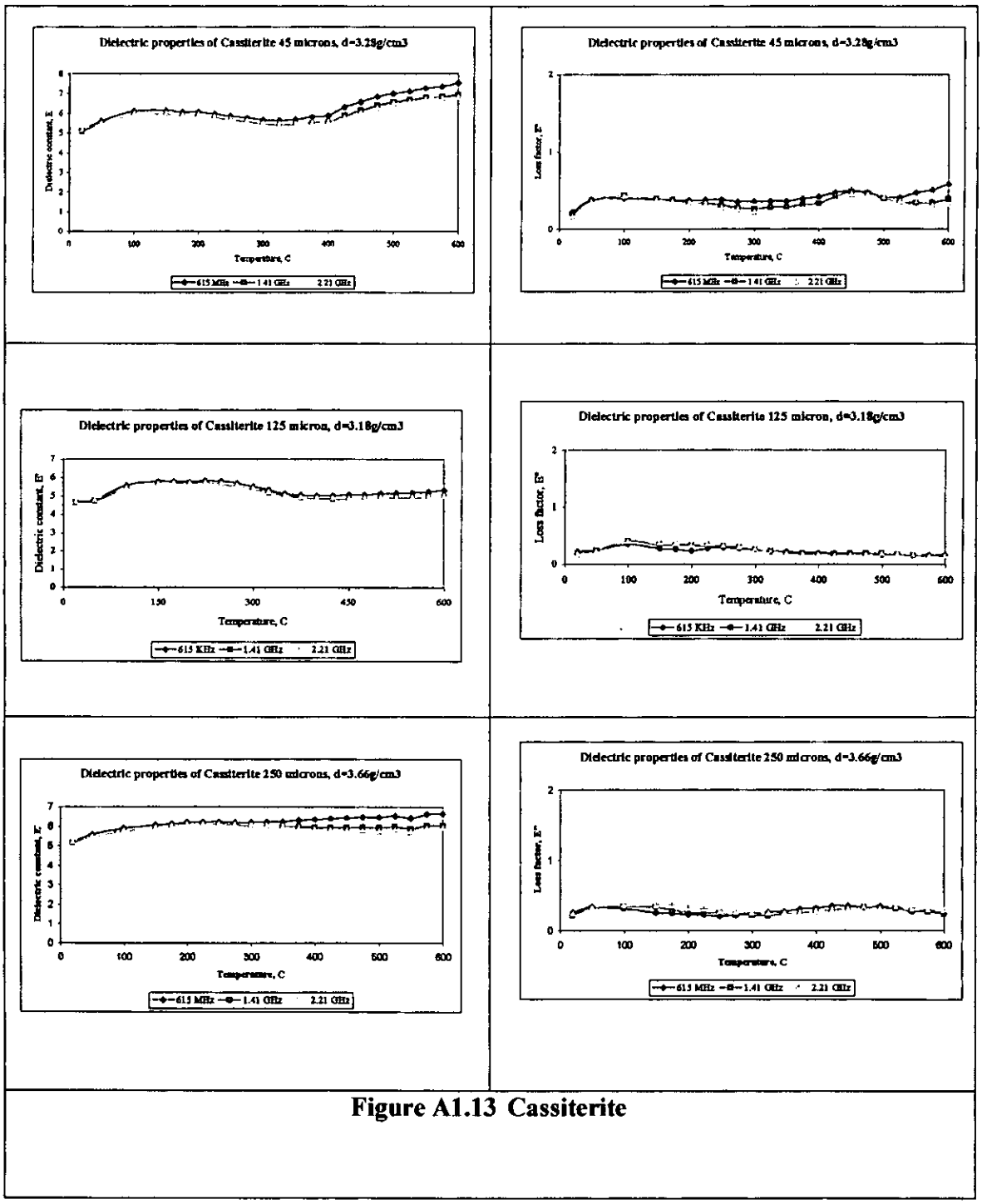

Figure A1.13 Cassiterite

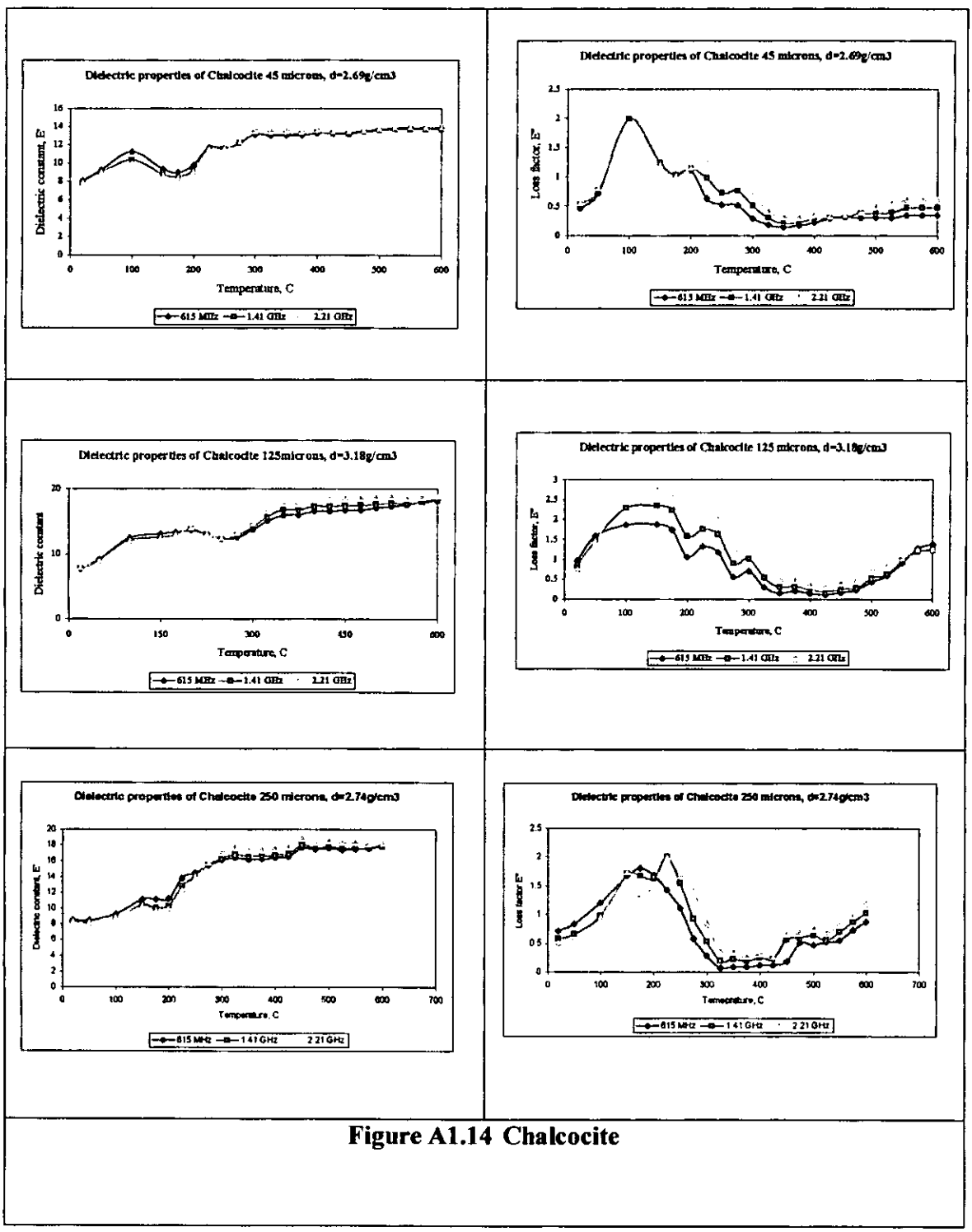

Figure A1.14 Chalcocite

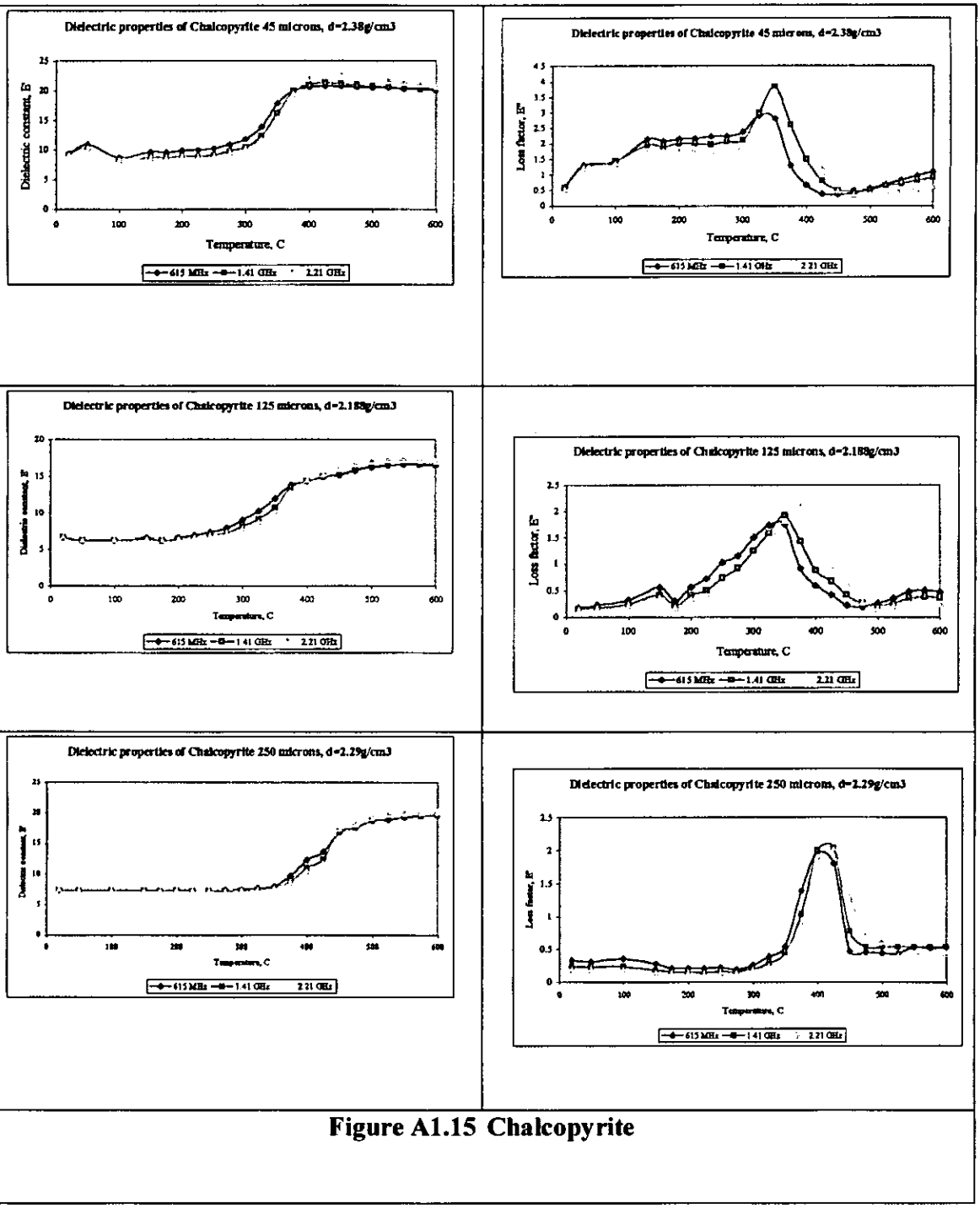

Figure A1.15 Chalcopyrite

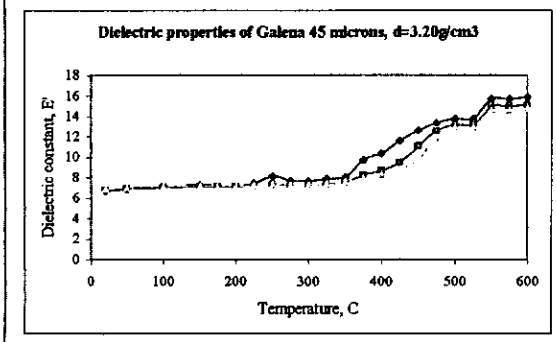

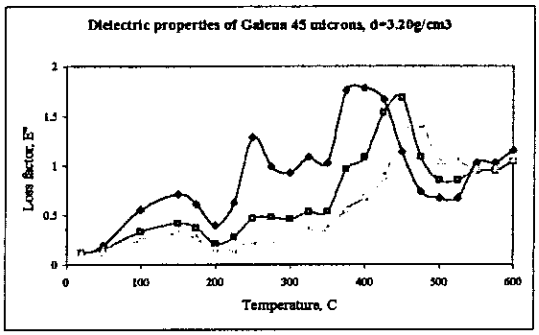

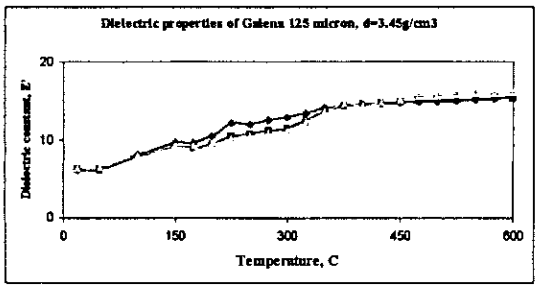

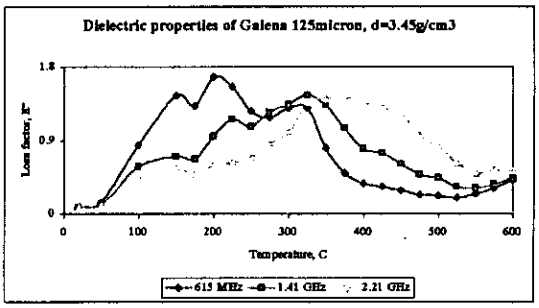

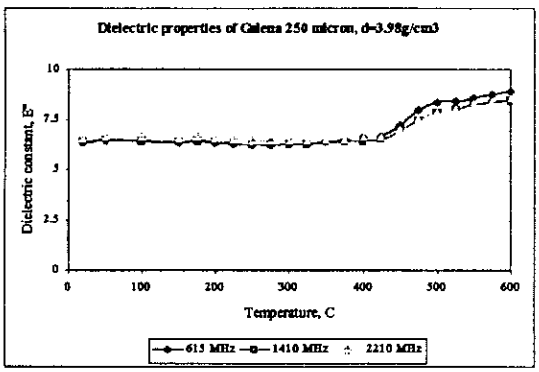

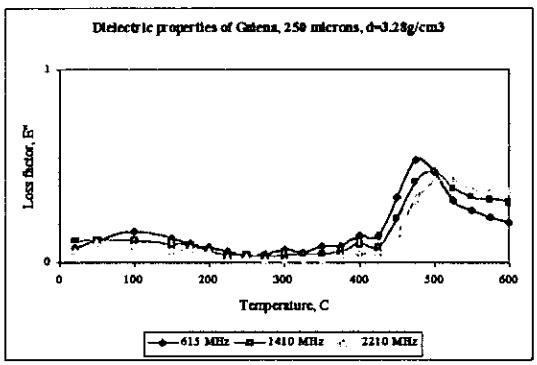

Figure A1.16 Galena

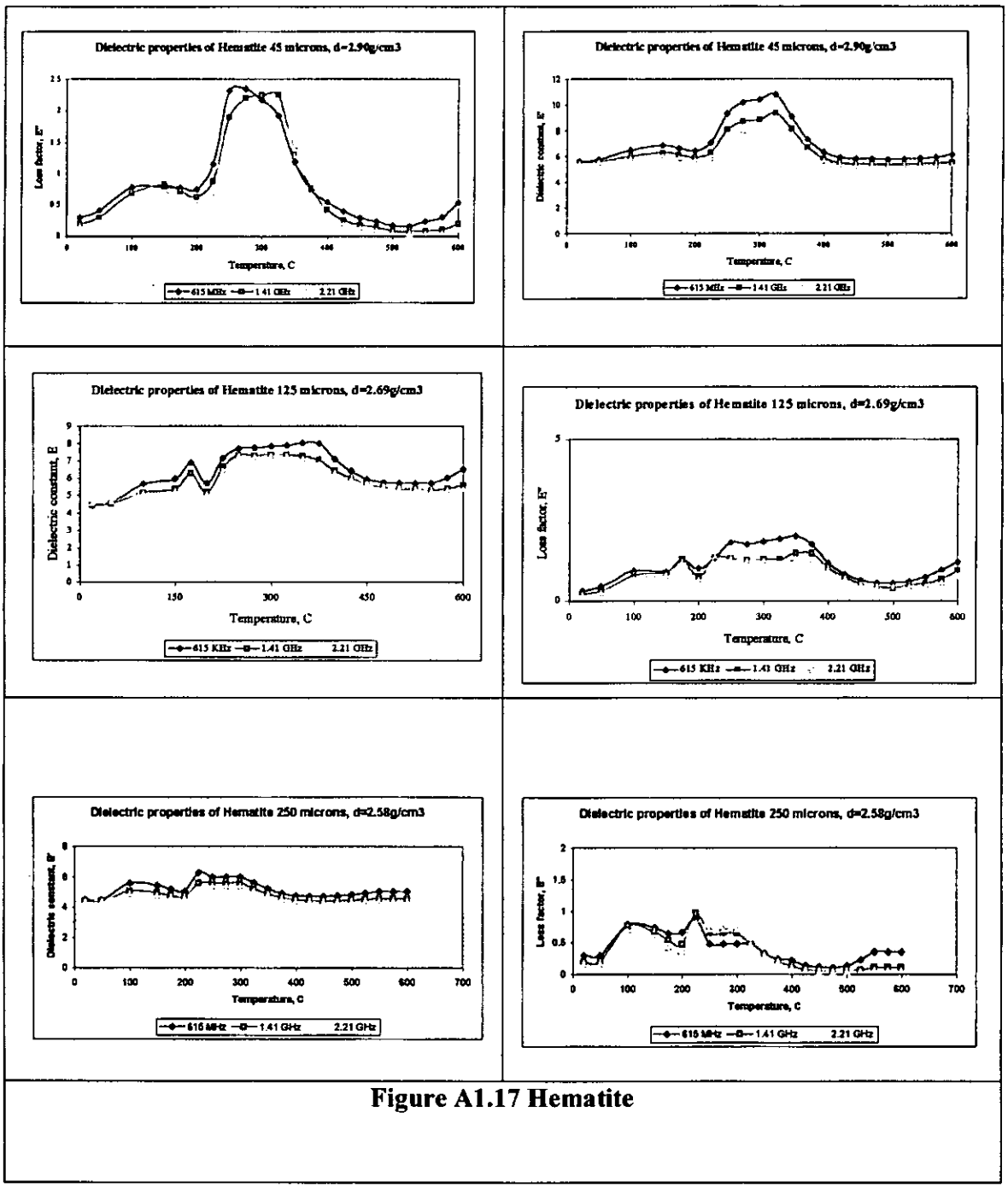

Figure A1.17 Hematite

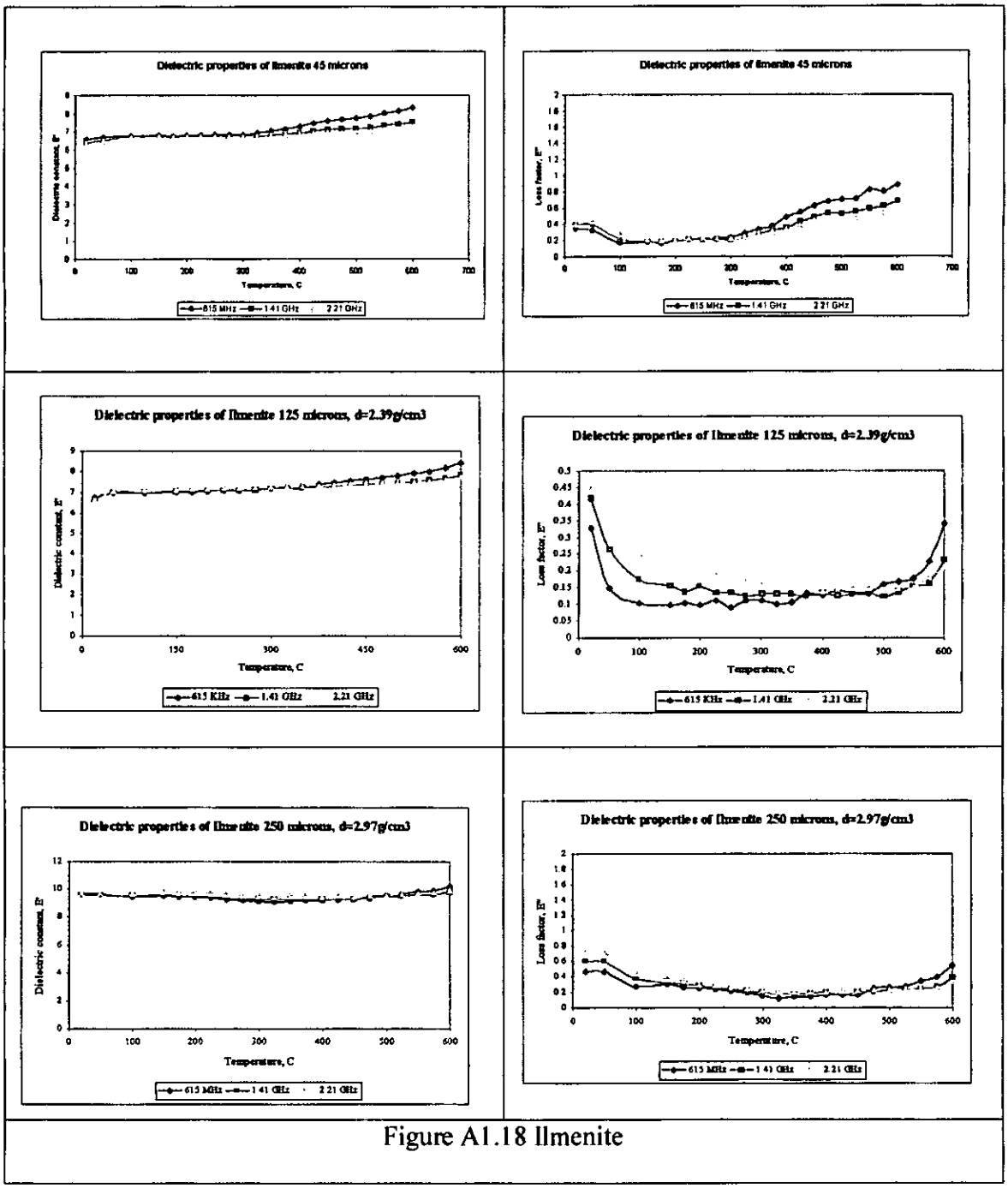

Figure A1.18 Ilmenite

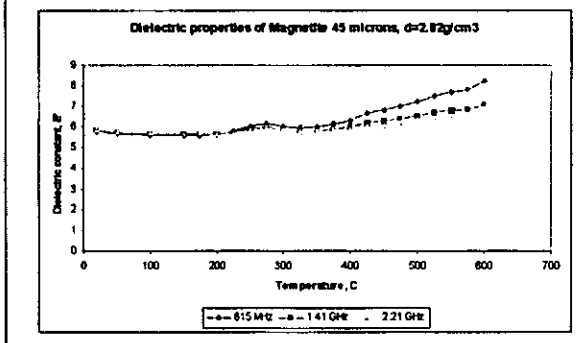

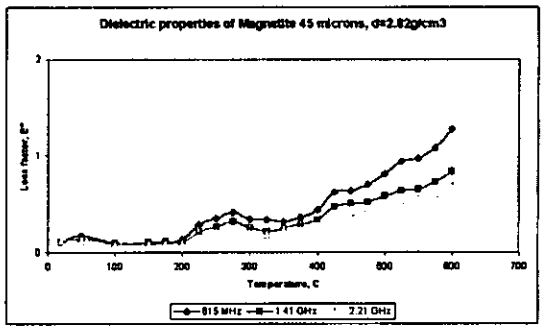

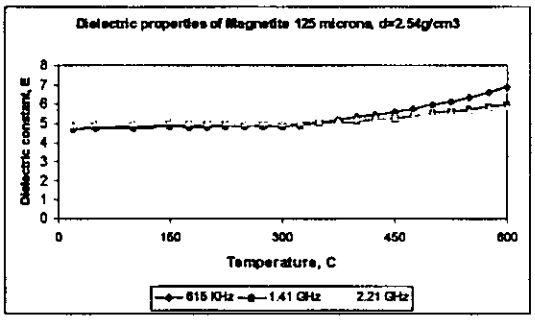

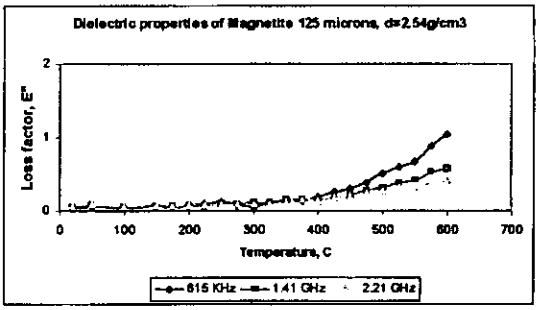

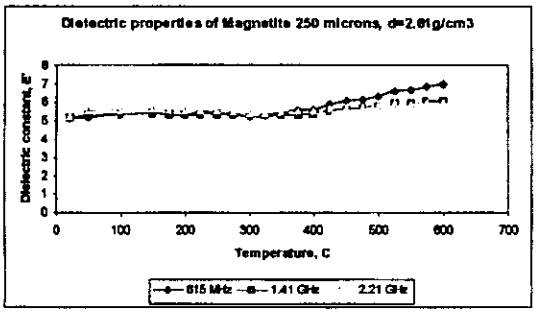

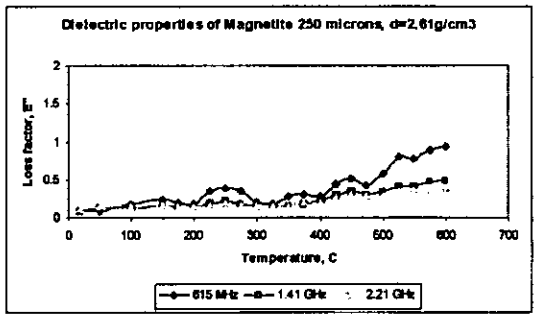

Figure A1.19 Magnetite

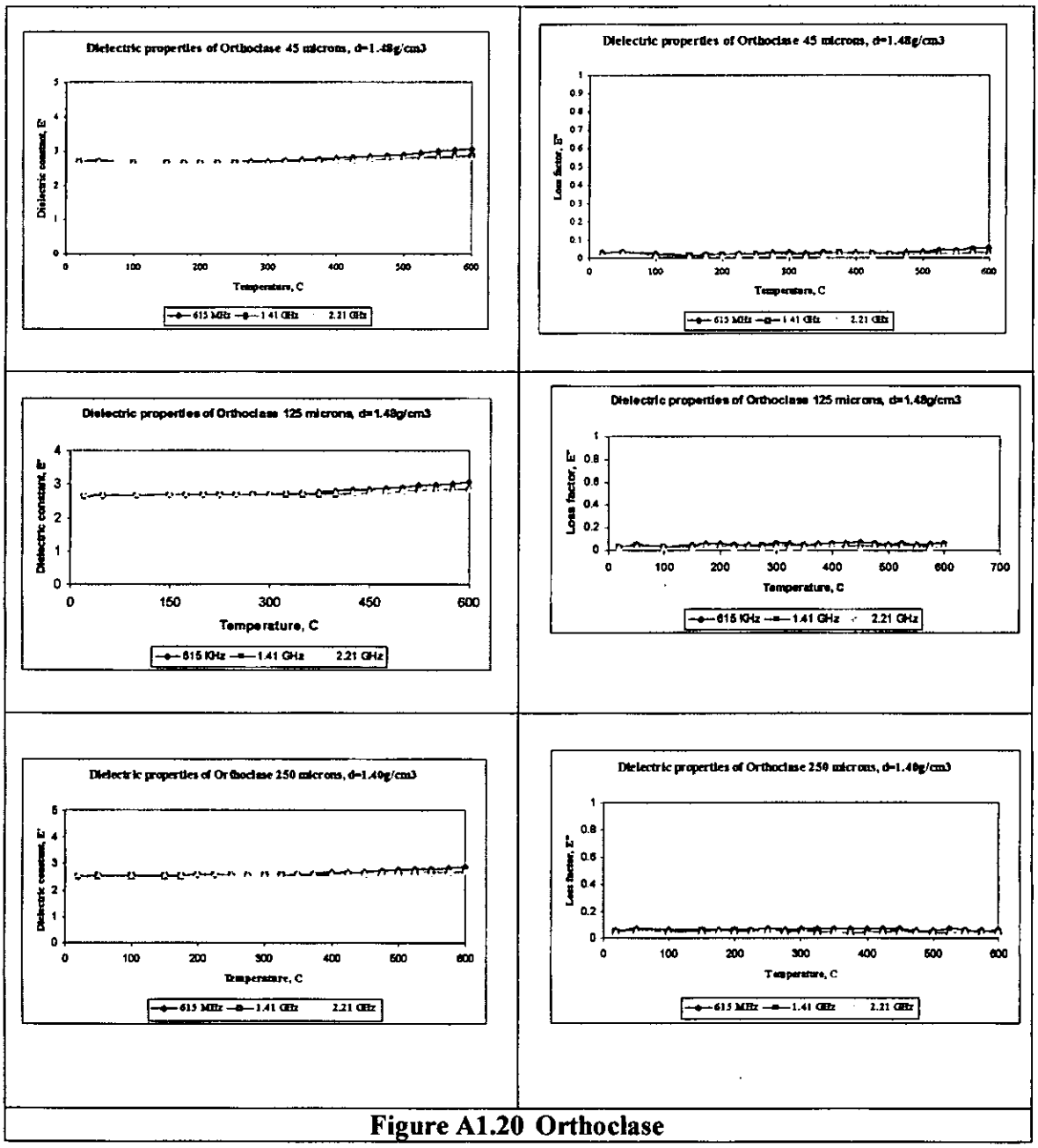

Figure A1.20 Orthoclase

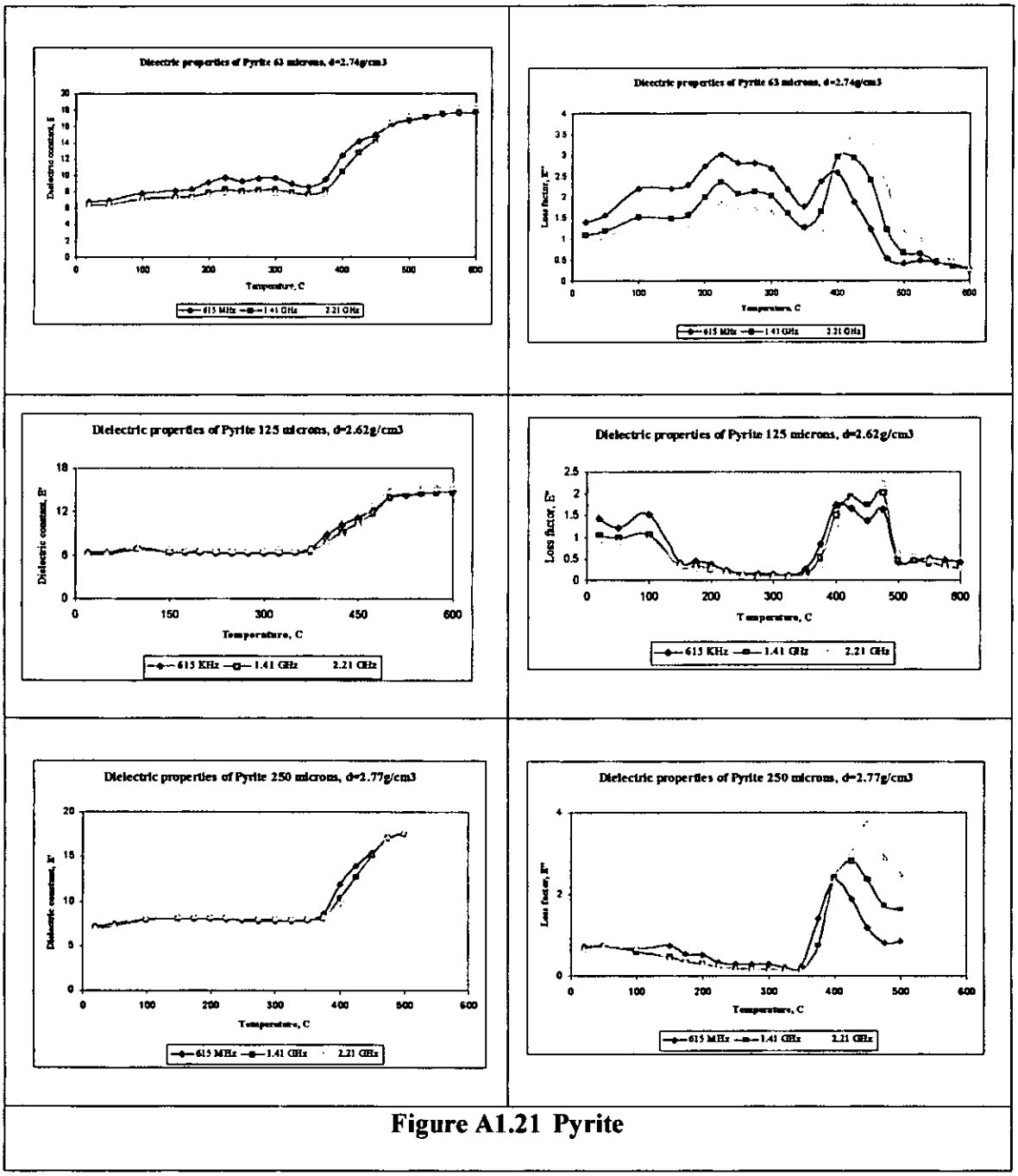

Figure A1.21 Pyrite

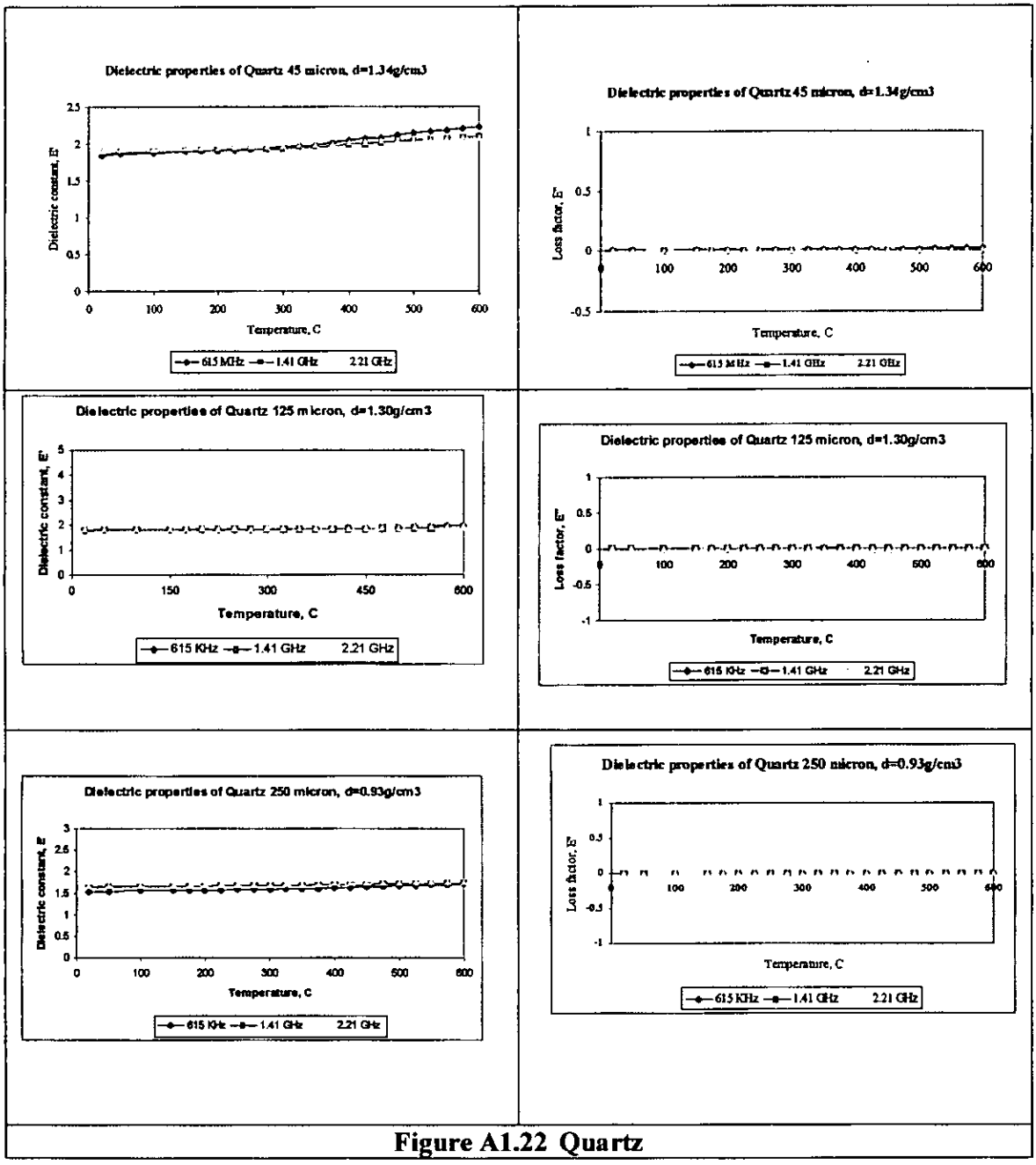

Figure A1.22 Quartz

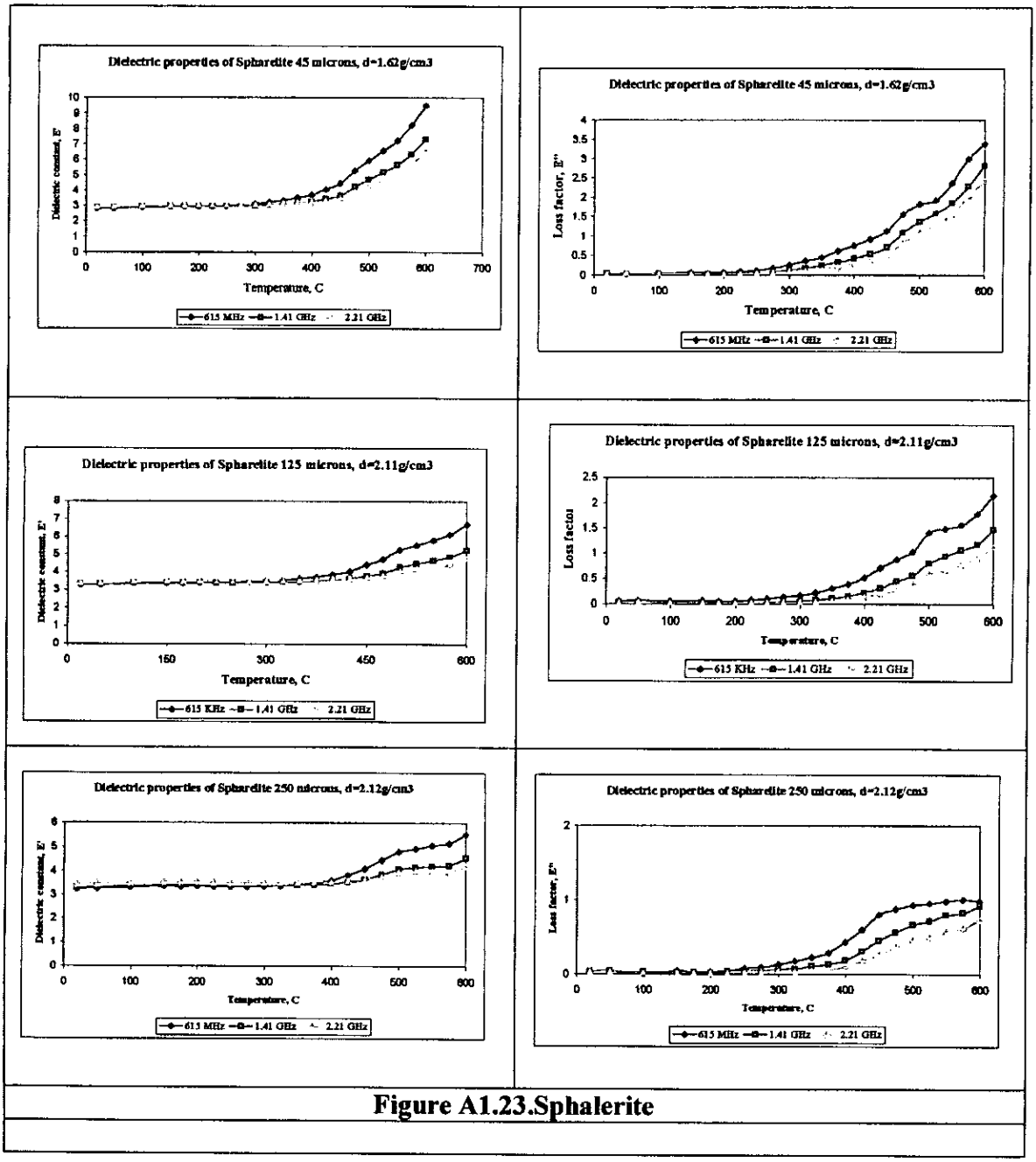

Figure A1.23.Sphalerite

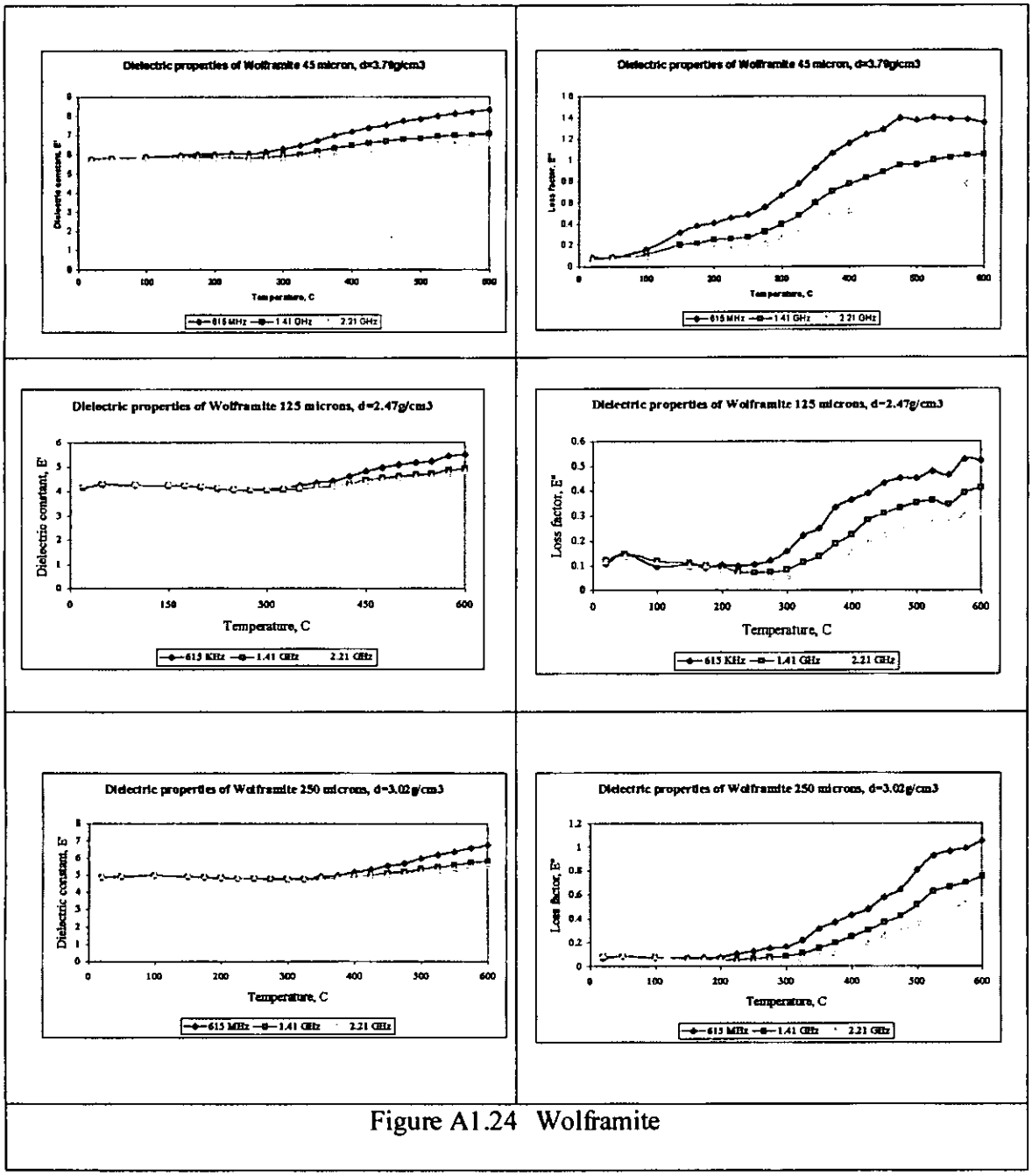

Figure A1.24 Wolframite

APPENDIX 2
PALABORA MICROWAVE ASSISTED COMMINUTION

2.1 Point Load Test Data

Table A2.1. Point Load Index results

Microwave Power, kW	Exposure Time, s	Is(50), MPa		
		Mean	Median	Range
Particle size, 37x31 mm				
Untreated	-	2.88±1.06	2.75	1.04 – 4.01
Single mode treatment				
15	0.1	1.67±1.30	1.30	0.10 – 3.90
	0.5	1.52±1.43	1.12	0.12 – 4.21
	1	1.30±1.10	1.14	0.07 – 3.44
10	0.1	1.40±0.90	1.37	0.10 – 3.01
	0.5	1.59±1.68	0.89	0.10 – 4.95
	1	1.38±0.45	1.29	1.00 – 8.20
5	0.1	2.28±0.81	2.44	0.14 – 5.07
	0.5	1.74±0.59	0.71	0.10 – 1.87
	1	1.87±0.78	2.18	1.06 – 8.70
Multimode treatment				
15	1	1.50±0.8	0.86	0.60 – 2.40
	5	1.00±1.20	0.30	0.03 – 2.43
	10	1.00±0.90	0.67	0.14 – 2.41
10	1	3.40±2.90	3.30	0.40 – 6.60
	5	1.60±1.40	0.66	0.45 – 2.71
	10	2.30±2.30	1.14	0.30 – 5.11
5	1	4.60±2.10	5.73	2.12 – 6.60
	5	3.20±3.60	2.30	0.17 – 9.13
	10	2.30±2.30	1.02	0.85 – 4.86
Particle size, 53x45 mm				
Untreated	-	3.31±0.88	3.28	1.95 – 4.70
Single mode treatment				
15	0.1	1.57±1.72	2.06	0.50 – 5.50
	0.5	0.93±1.02	0.61	0.06 – 3.20
	1	1.29±1.08	1.27	0.06 – 2.50
10	0.1	1.98±1.48	1.60	0.06 – 4.40
	0.5	1.86±1.74	0.83	0.06 – 4.90
	1	1.82±1.30	1.28	0.16 – 3.80
5	0.1	3.09±1.09	3.15	1.36 – 4.60
	0.5	2.34±1.08	2.88	0.06 – 3.44
	1	2.29±1.06	2.19	0.74 – 4.12

2.2 Drop Weight Test Data

Table A2.2. Palabora untreated, full energy

JKTech Drop Weight Test Parameters for Crushers and FAG/SAG Mills									
Tested at University of Nottingham									
Client:							**Test Date:**		
Sample Source:		Palabora					**Tester:**	KJ/AC	
Sample Name:		Palabora Untreated, full energy				**Job No:**			
Base Data		t_{10}	E_{is}	t_{10}	E_{is}		t_{10}	E_{is}	
		39.4	0.40	23.8	0.25		17.5	0.10	
		59.3	1.01	20.0	0.25		12.1	0.10	
		59.5	2.50	52.0	1.00		25.8	0.25	
		66.6	2.50	50.9	1.00		22.1	0.25	
		64.7	2.47	43.1	1.00		19.2	0.25	
SAG/FAG MILL PARAMETERS									
A:	63.2		**b:** 1.83		**A*b:**	115.7		**Ta:**	0.64
CRUSHER PARAMETERS									
CRUSHER APPEARANCE FUNCTION DATA									
t_{10}	t_{75}		t_{50}	t_{25}		t_4		t_2	
10	2.6		3.4	5.2		21.4		51.4	
20	5.4		7.0	10.7		43.4		82.1	
30	8.7		11.0	16.5		63.8		97.2	
POWER DATA									
	Mean Size (mm)								
	14.53		20.63	28.89		41.08		57.78	
t_{10}	**Ecs (kWh/t)**								
10	0.15		0.11	0.08		0.11		0.07	
20	0.32		0.24	0.19		0.19		0.16	
30	0.54		0.40	0.32		0.32		0.28	
DENSITY DATA									
Mean	3.11		**Std Dev** 0.44		**Max**	4.23		**Min**	2.55

Table A2.3. Palabora untreated, 50% energy input

JKTech Drop Weight Test Parameters for Crushers and FAG/SAG Mills									
Tested at University of Nottingham									
Client:						**Test Date:**			
Sample Source:		Palabora					**Tester:**	KJ/AC	
Sample Name:		Palabora Untreated, 50% energy				**Job No:**			
Base Data		t_{10}	E_{ls}	t_{10}	E_{ls}		t_{10}	E_{ls}	
		15.1	0.20	9.2	0.12		2.9	0.05	
		33.0	0.50	10.4	0.12		5.3	0.05	
		50.6	1.25	28.7	0.50		10.0	0.13	
		48.3	1.25	27.0	0.50		8.9	0.12	
		41.7	1.24	32.6	0.50		8.0	0.12	
SAG/FAG MILL PARAMETERS									
A:	54.3		**b:**	1.61		**A*b:**	87.4		**Ta:**	0.64
CRUSHER PARAMETERS									
CRUSHER APPEARANCE FUNCTION DATA									
t_{10}	t_{75}		t_{50}	t_{25}		t_4		t_2	
10	3.0		3.7	5.4		22.8		53.6	
20	5.9		7.5	11.0		43.2		83.0	
30	9.1		11.5	16.9		61.1		95.8	
POWER DATA									
	Mean Size (mm)								
	14.53		20.63	28.89		41.08		57.78	
t_{10}	**Ecs (kWh/t)**								
10	0.11		0.15	0.14		0.11		0.11	
20	0.26		0.34	0.31		0.25		0.25	
30	0.48		0.57	0.52		0.43		0.43	
DENSITY DATA									
Mean	3.11		**Std Dev**	0.44		**Max**	4.23		**Min**	2.55

Table A2.4. Palabora, Multimode treated 15kW, 1 s, full energy

JKTech Drop Weight Test Parameters for Crushers and FAG/SAG Mills									
Tested at University of Nottingham									
Client:						**Test Date:**			
Sample Source:		Palabora					**Tester:**	KJ/AC	
Sample Name:		Palabora 15kW for 1s, full energy				**Job No:**			
Base Data		t_{10}	E_{ls}	t_{10}	E_{ls}		t_{10}	E_{ls}	
		40.4	0.40	31.4	0.25		12.1	0.10	
		55.6	1.01	26.2	0.25		14.5	0.10	
		61.2	2.51	52.6	1.00		27.5	0.25	
		62.0	2.49	49.5	1.00		24.7	0.25	
		55.2	2.51	41.5	1.00		23.1	0.25	
SAG/FAG MILL PARAMETERS									
A:	57.4		**b:** 2.45		**A*b:**	140.6		**Ta:**	1.04
CRUSHER PARAMETERS									
CRUSHER APPEARANCE FUNCTION DATA									
t_{10}	t_{75}		t_{50}	t_{25}		t_4		t_2	
10	2.7		3.3	5.2		24.5		54.8	
20	5.1		6.5	10.3		46.1		84.7	
30	7.7		10.2	15.8		64.2		97.0	
POWER DATA									
	Mean Size (mm)								
	14.53		20.63	28.89		41.08		57.78	
t_{10}	**Ecs (kWh/t)**								
10	0.11		0.10	0.08		0.08		0.07	
20	0.26		0.21	0.18		0.17		0.15	
30	0.45		0.36	0.30		0.29		0.26	
DENSITY DATA									
Mean	3.11		**Std Dev** 0.44		**Max**	4.23		**Min**	2.55

Table A2.5. Palabora multimode treated at 15kW, 1 s, drop weight tested at 50% energy input

JKTech Drop Weight Test Parameters for Crushers and FAG/SAG Mills									
Tested at University of Nottingham									
Client:						**Test Date:**			
Sample Source:		Palabora					**Tester:**	KJ/AC	
Sample Name:		Palabora 15kW 1s 50% energy				**Job No:**			
Base Data		t_{10}	E_{ls}	t_{10}	E_{ls}		t_{10}	E_{ls}	
		23.0	0.20	16.3	0.17		7.5	0.05	
		45.6	0.70	14.6	0.13		5.8	0.05	
		50.3	1.25	38.1	0.50		14.0	0.13	
		53.6	1.25	36.4	0.50		13.3	0.12	
		51.8	1.24	41.4	0.50		15.9	0.12	
SAG/FAG MILL PARAMETERS									
A:	54.5		**b:** 2.48		**A*b:**	135.2		**Ta:**	1.04
CRUSHER PARAMETERS									
CRUSHER APPEARANCE FUNCTION DATA									
t_{10}	t_{75}		t_{50}	t_{25}		t_4		t_2	
10	2.5		3.3	5.1		23.7		55.1	
20	4.9		6.5	10.3		45.3		84.4	
30	7.8		10.1	15.9		63.8		96.1	
POWER DATA									
	Mean Size (mm)								
	14.53		20.63	28.89		41.08		57.78	
t_{10}	**Ecs (kWh/t)**								
10	0.07		0.09	0.08		0.08		0.08	
20	0.16		0.21	0.19		0.19		0.19	
30	0.28		0.36	0.33		0.32		0.32	
DENSITY DATA									
Mean	3.11		**Std Dev** 0.44		**Max**	4.23		**Min**	2.55

Table A2.6. Palabora, single mode treated, 15kW, 0.2 s, drop weight tested at 50% energy input.

JKTech Drop Weight Test Parameters for Crushers and FAG/SAG Mills									
Tested at University of Nottingham									
Client:		Palabora					**Test Date:**	30-May-02	
Sample Source:		Single Mode					**Tester:**	KJ	
Sample Name:		15kW 0.2s				**Job No:**			
Base Data		t_{10}	E_{is}	t_{10}	E_{is}		t_{10}	E_{is}	
		26.2	0.20	15.2	0.12		6.5	0.05	
		41.6	0.50	12.7	0.13		6.8	0.05	
		55.1	1.25	35.7	0.50		14.1	0.13	
		53.8	1.24	33.1	0.50		15.0	0.12	
		42.8	1.24	26.1	0.50		12.2	0.13	
SAG/FAG MILL PARAMETERS									
A:	52.5		**b:** 2.35		**A*b:**	123.4		**Ta:**	0.97
CRUSHER PARAMETERS									
CRUSHER APPEARANCE FUNCTION DATA									
t_{10}	t_{75}		t_{50}	t_{25}		t_4		t_2	
10	2.4		3.2	5.1		23.2		52.5	
20	5.4		7.0	10.9		42.7		80.5	
30	8.9		11.3	17.2		59.2		92.1	
POWER DATA									
	Mean Size (mm)								
	14.53		20.63	28.89		41.08		57.78	
t_{10}	**Ecs (kWh/t)**								
10	0.1343		0.1039	0.0973		0.0917		0.0723	
20	0.3102		0.2309	0.2160		0.1973		0.1531	
30	0.5661		0.3946	0.3680		0.3218		0.2448	
DENSITY DATA									
Mean	3.11		**Std Dev** 0.44		**Max**	4.23		**Min**	2.55

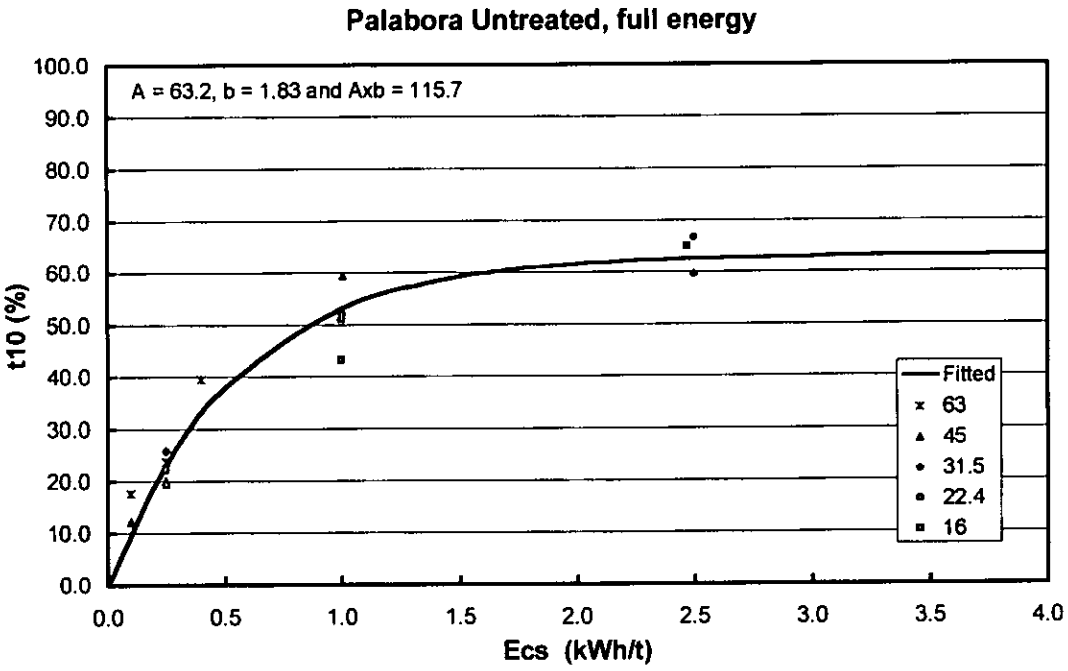

Figure A2.1

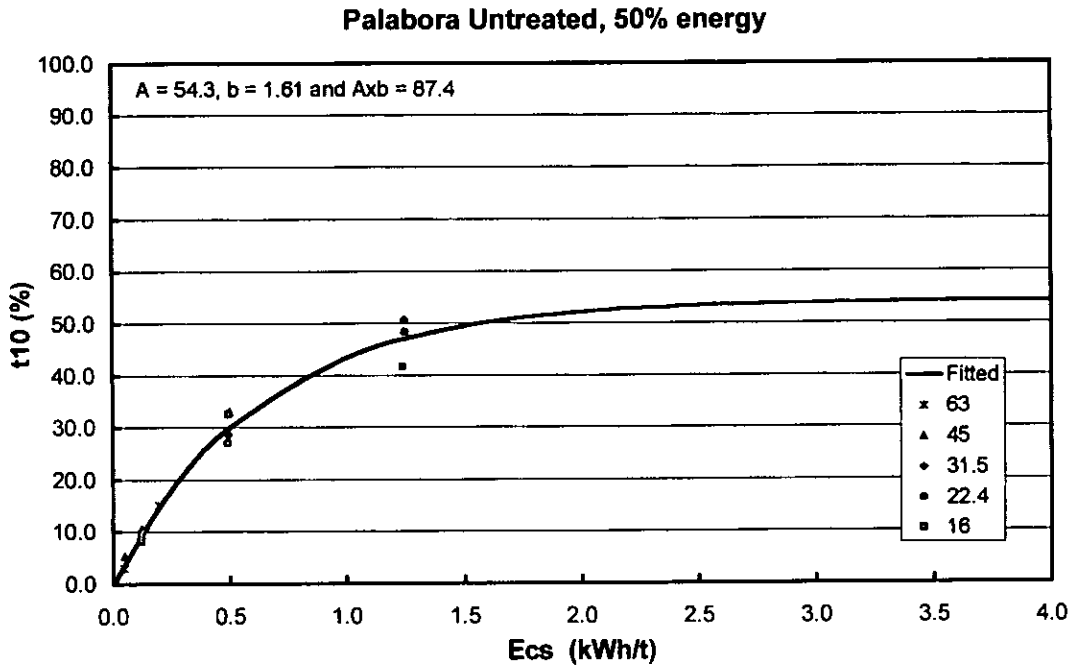

Figure A2.2

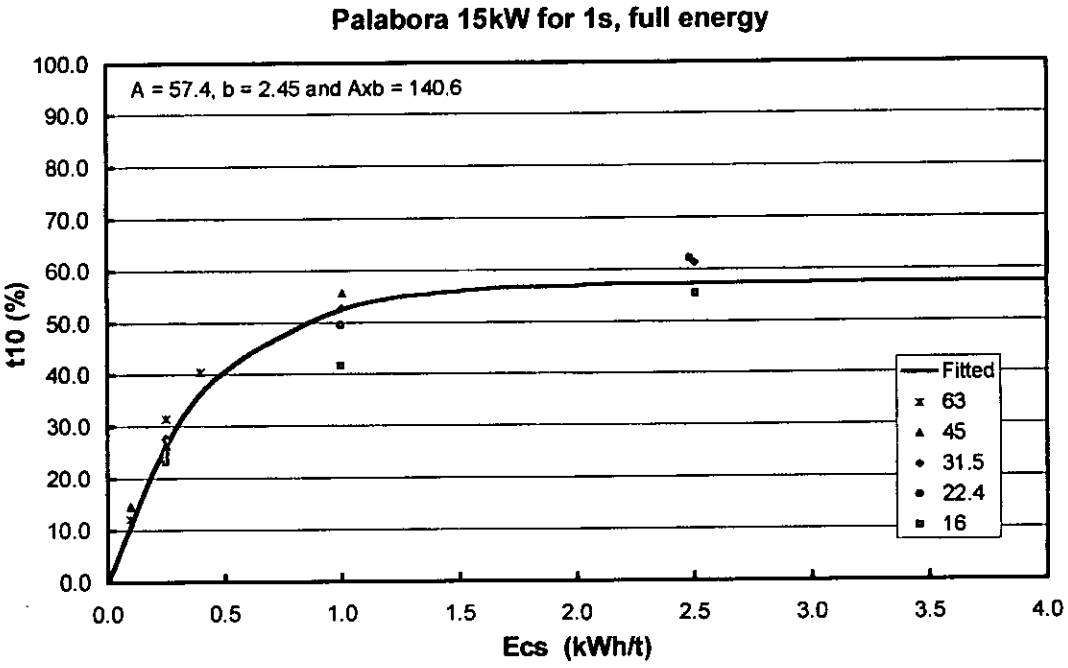

Figure A2.3. Multimode treated

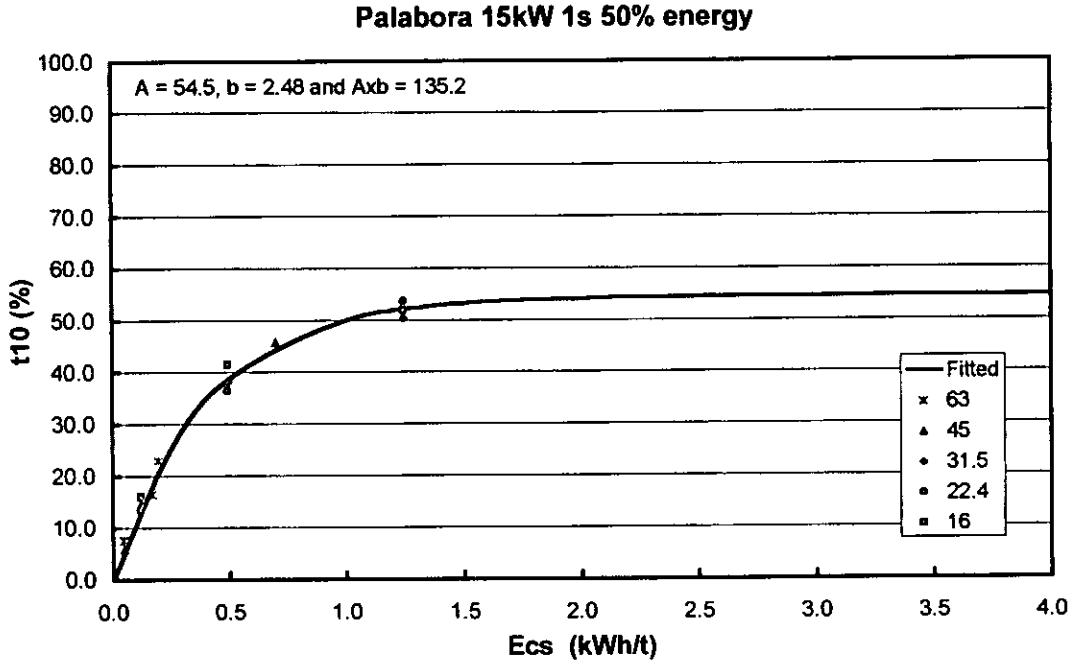

Figure A2.4. Multimode treated

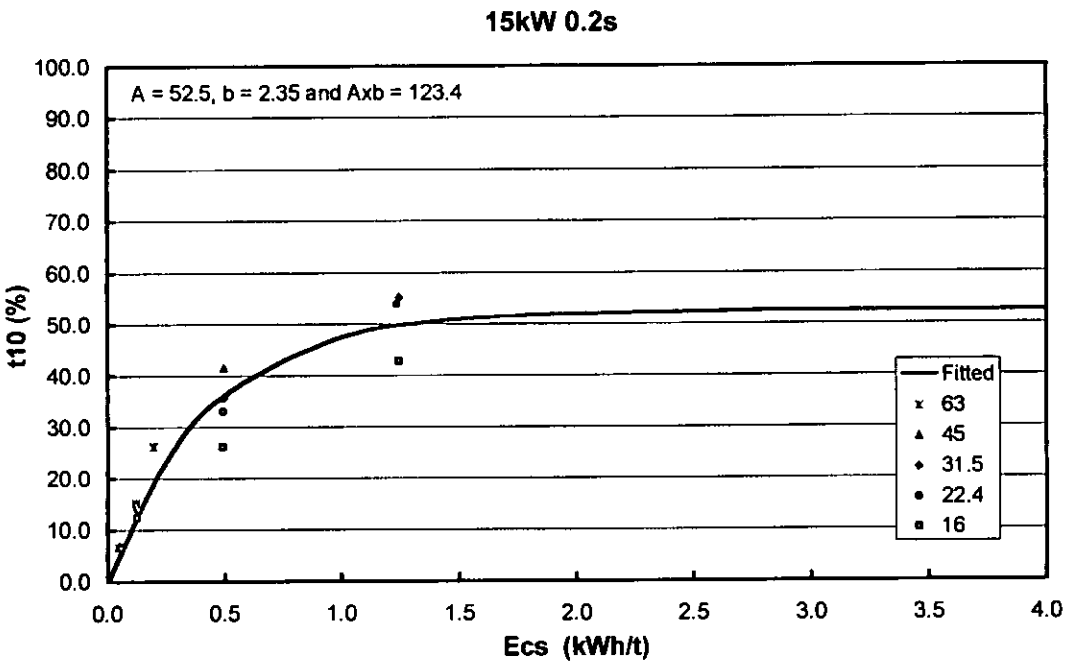

Figure A2.5. Single mode treated

2.3 Grindability Test Data

Table A2.7 Summary of the masses of oversize retained

Size range, mm	Sample description	Grinding time, s					
		30	60	120	180	240	300
-19+16 mm	Treated	306.1	266.8	248.2	220.1	200	184.3
	Untreated	455.8	401.5	365	329.5	316.8	316
-13.2+9.5 mm	Treated	393.9	346.7	302.2	268.5	231.1	216.3
	Untreated	436.6	417.4	368.9	340.8	319.2	299.4
-9.5+6.7 mm	Treated	342	291	231.2	190.5	158	132.5
	Untreated	401.3	348.2	303.2	274.5	237.7	211.2
-6.7+4.75 mm	Treated	341	255.6	195.2	149.9	115.6	105.2
	Untreated	352.4	299.7	232	176.3	155.7	138.8
-4.75+3.35 mm	Treated	265.4	193.8	145.7	106.1	82.6	66.9
	Untreated	309.3	228.2	177.5	132	103.2	83.2

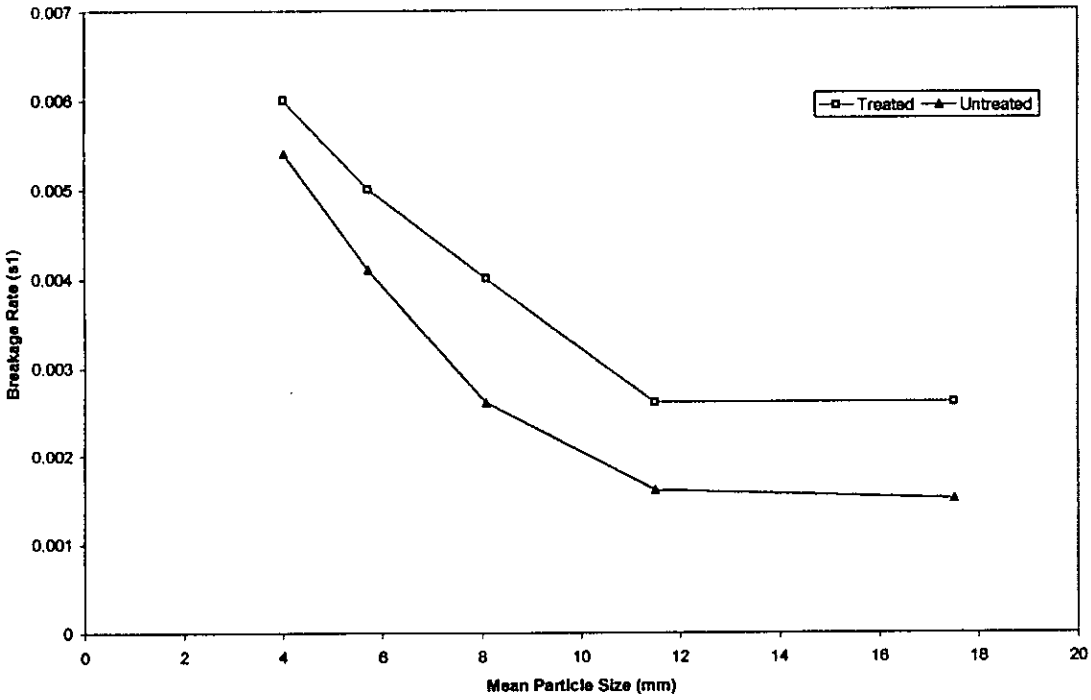

Figure A2.6. Effect of microwave treatment on breakage rate versus mean particle size relationship.

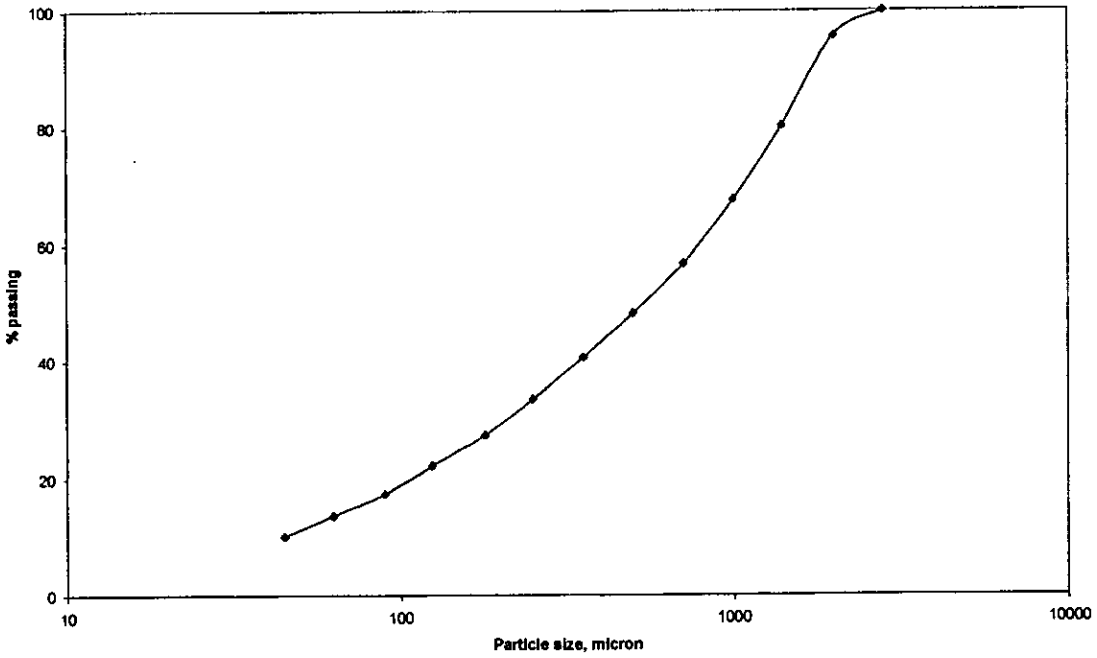

Figure A2.7. Size analysis of the initial feed for standard Bond work index test, Palabora untreated sample.

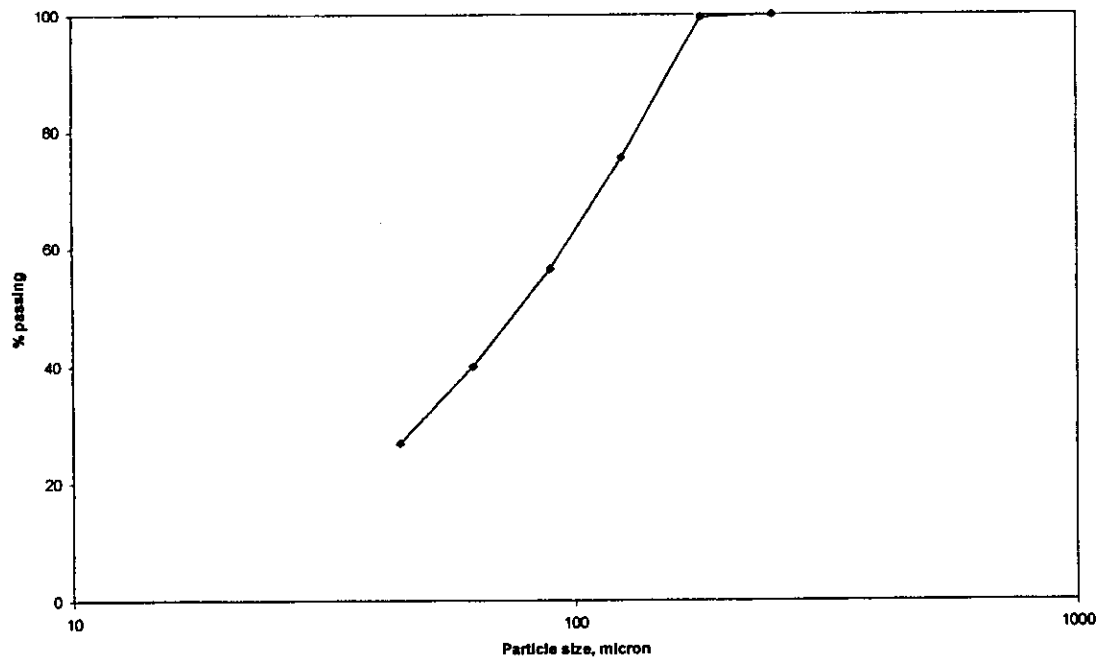

Figure A2.8. Size analysis of the product for standard Bond work index test, Palabora untreated sample.

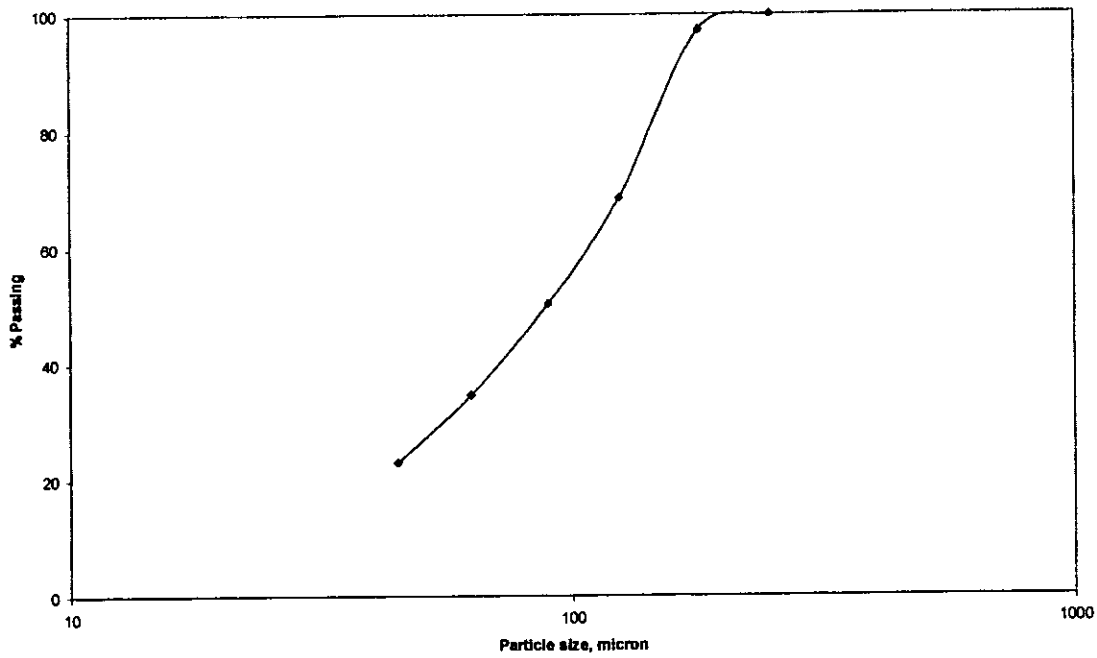

Figure A2.9. Size analysis of the product for standard Bond work index test, Palabora microwave treated sample.

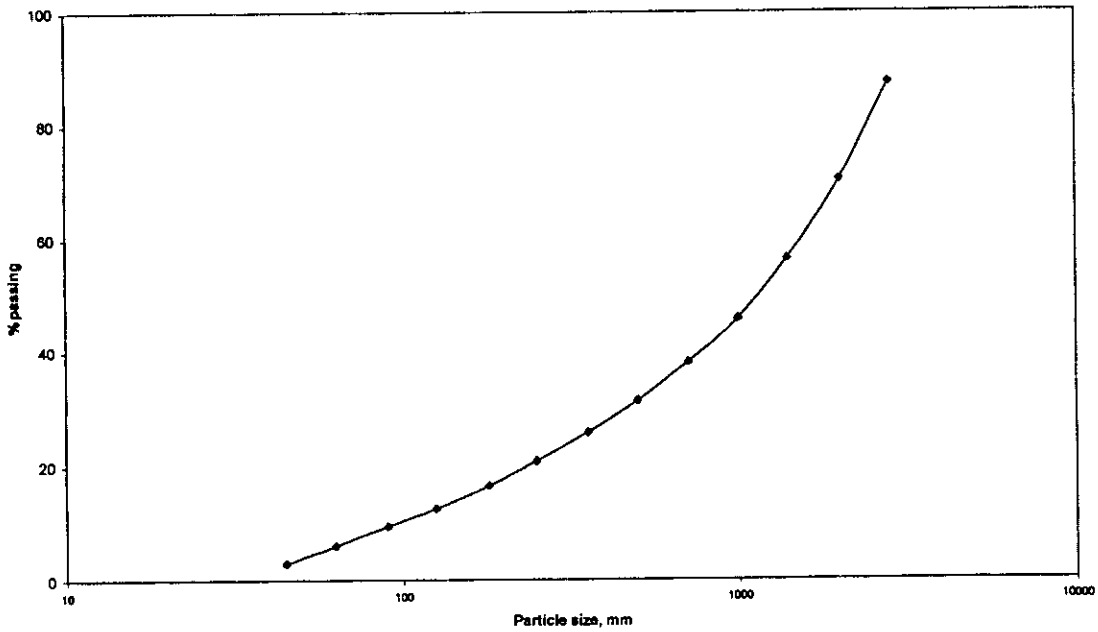

Figure A2.10. Size analysis of Palabora sample, microwave treated and jaw crushed.

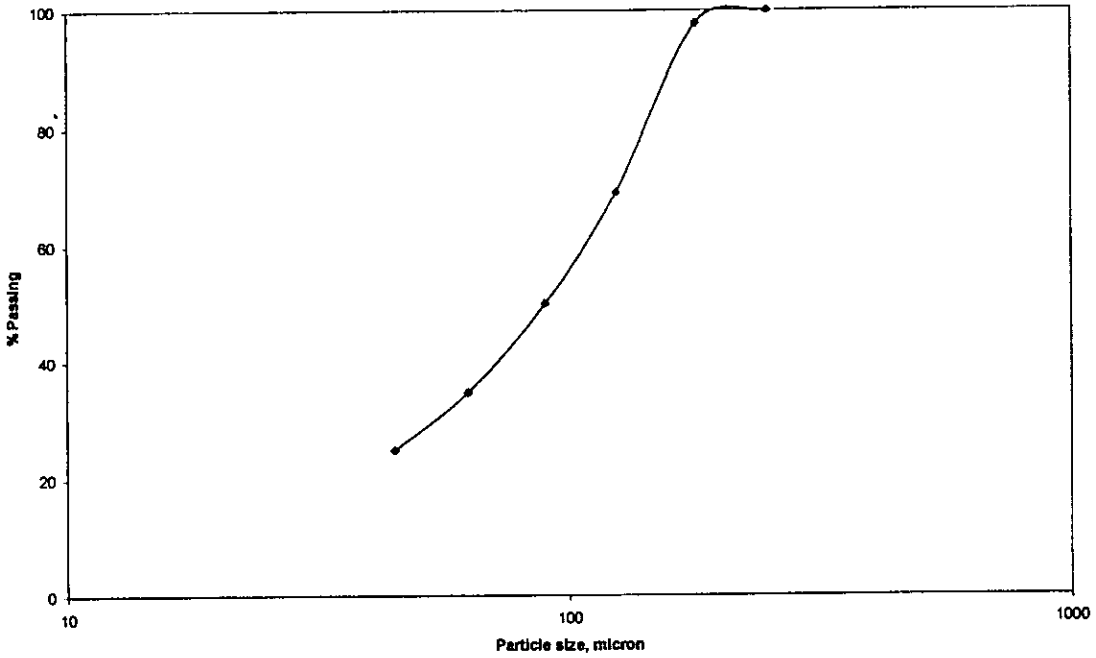

Figure A2.11. Size analysis of the final product of Palabora ore, microwave treated and jaw crushed, bond work index test

Table A2.8 Palabora untreated Bond Work Index data

Percentage below 180μm in Feed:					27.6
Weight of unit volume:					1455.2g
Weight of product required for 250% circulating load:					475.48g
Period	No. of revolutions	-180μm in product (g)	-180μm in feed (g)	-180μm produced (g)	Grindability (G), g/rev
1	50	471	407	63.35	1.27
2	226	560	130	430	1.90
3	138	411.9	154.56	257.34	1.87
4	162	420	113.6	306.31	1.89
5	159	411	115.92	295	1.86
6	163	409.5	113.4	296	1.81
7	167	414.6	113	301.6	1.80
8	167	418.1	114.4	303.6	1.81

Table A2.9 Palabora microwave treated Bond Work Index data

Percentage below 180μm in Feed:					27.6%
Weight of unit volume:					1455.2g
Weight of product required for 250% circulating load:					416.1g
Period	No. of revolutions	-180μm in product (g)	-180μm in feed (g)	-180μm produced (g)	Grindability (G), g/rev
1	50	465	401.6	63.4	1.268
2	220	589.5	128.3	461.2	2.096
3	125	411.9	162.7	249.2	2.13
4	152	420	113.7	306.2	2.01
5	149	414.1	116	298	2.00
6	151	417.1	114	302	2.00

Table A2.10 Palabora microwave treated, Jaw crushed Bond Work Index data

Percentage below 180μm in Feed:					20.8%
Weight of unit volume:					1452.2g
Weight of product required for 250% circulating load:					415.27g
Period	No. of revolutions	-180μm in product (g)	-180μm in feed (g)	-180μm produced (g)	Grindability (G), g/rev
1	50	366	293.6	72.4	1.44
2	238	575	73.2	501.8	2.10
3	143	437.6	115	322.6	2.26
4	145	410.8	87.52	323.2	2.23
5	149	416.3	82.16	332.8	2.23
6	149	411.4	83.26	328.1	2.20

2.4. Palabora Mineral Liberation data

Table A2.11. Modal Abundance and Chemical Assays

	PalaboraA						PalaboraB					
	+500	+150	+38	-38	Head	Norm.	+500	+150	+38	-38	Head	Norm.
PSD	32.22	31.06	21.37	15.35	100.00		31.91	31.46	21.86	14.77	100.00	
Chemical assay												
Cu	0.58	0.64	0.78	0.76	0.67		0.91	0.90	1.00	0.89	0.92	
Fe	11.40	11.00	8.54	5.77	9.53		11.40	10.70	8.55	5.59	9.70	
Pb												
Zn												
QS Assay												
Cu	1.09	1.74	0.77	0.66	1.12		1.54	1.40	1.02	1.85	1.43	
Fe	22.16	28.97	10.15	7.93	18.47		18.38	30.18	11.15	5.33	18.58	
Pb												
Zn												
Cu Sulphide	2.35	4.02	2.08	1.78	2.72	1.93	4.22	3.29	2.68	5.22	3.74	2.66
Pyrite	0.64	0.58	0.11	1.20	0.60	0.71	0.02	0.02	0.04	0.00	0.02	0.02
Galena	0.00	0.00	0.00	0.06	0.01	0.01	0.00	0.00	0.01	0.02	0.00	0.01
Sphalerite	0.00	0.00	0.01	0.02	0.01	0.01	0.07	0.00	0.00	0.00	0.02	0.03
Other S	0.00	0.03	0.00	0.00	0.01	0.01	0.02	0.01	0.04	0.00	0.02	0.02
Fe-oxide	30.13	39.26	13.13	9.59	26.18	13.61	24.29	41.69	14.68	5.12	24.83	13.86
NSG	61.49	50.74	78.49	83.51	65.16	77.41	67.44	51.23	79.20	84.91	67.49	78.88
Other	5.38	5.37	6.16	3.84	5.31	6.31	3.93	3.76	3.35	4.73	3.87	4.52
					100.00	100.00					100.00	100.00

Table A2.12. Liberation Data

	PalaboraA					PalaboraB				
Cu Sulphide	+500	+150	+38	-38	Head	+500	+150	+38	-38	Head
Locked[1]	39.40	10.20	13.60	8.50	20.07	21.40	13.70	8.70	2.10	13.35
Middling[2]	29.80	18.80	5.30	3.90	17.17	10.40	14.40	5.40	20.60	12.07
Liberated[3]	30.80	71.00	81.10	87.60	62.75	68.20	71.90	85.90	77.30	74.58
	100	100	100	100	100	100	100	100	100	100

	PalaboraA					PalaboraB				
Fe-oxide	+500	+150	+38	-38	Head	+500	+150	+38	-38	Head
Locked	2.00	1.40	5.20	3.40	2.71	2.70	0.80	2.30	6.50	2.58
Middling	8.80	9.60	9.80	16.90	10.51	23.40	8.20	11.70	27.60	16.68
Liberated	89.20	89.00	85.00	79.70	86.78	73.90	91.00	86.00	65.90	80.74
	100	100	100	100	100	100	100	100	100	100

APPENDIX 3
ZINKGRUVAN MICROWAVE ASSISTED COMMINUTION

3.1 Point Load Test Data

Table A3.1 Summarized results of the effect of microwave treatment on point load index

Microwave power, kW	Exposure time, s	Is(50), MPa		
		Mean	Median	Range
Untreated	-	6.0±1.8	5.7	3.76 – 8.23
Single mode treatment				
10	0.1	3.06±1.56	2.52	1.30 – 5.02
	0.5	2.36±2.19	1.44	0.60 – 6.03
	1	0.96±0.61	1.09	0.20 – 1.60
7.5	0.1	3.27±1.35	2.92	2.00 – 5.53
	0.5	2.13±1.17	2.15	0.78 – 8.05
	1	1.37±1.55	0.63	0.41 – 4.10
5	0.1	3.09±1.06	2.91	1.92 – 4.50
	0.5	2.32±0.50	1.52	0.91 – 6.20
	1	2.30±0.57	2.33	1.54 – 3.09
Multimode treatment				
15	1	3.1±1.8	2.24	1.18 – 5.09
	5	2.4±1.4	2.04	0.97 – 4.40
	10	2.3±1.1	2.28	0.70 – 3.60
10	1	5.1±3.7	3.03	3.02 – 9.35
	5	2.7±0.9	3.26	1.70 – 3.50
	10	1.8±0.8	1.96	0.59 – 2.80
5	1	9.1±1.8	8.91	7.08 – 11.23
	5	7.7±2.6	7.40	4.80 – 11.14
	10	4.1±2.7	3.55	0.90 – 7.90

3.2 Drop weight test data

Table A3.2 Drop weight test for Untreated sample

JKTech Drop Weight Test Parameters for Crushers and FAG/SAG Mills

Tested at University of Nottingham

Client:								**Test Date:**			
Sample Source:								**Tester:**			
Sample Name:	Zinkgruvan untreated, full energy							**Job No:**			
Base Data		t_{10}	E_{is}		t_{10}	E_{is}		t_{10}	E_{is}		
		37.1	0.40		25.2	0.25		10.5	0.10		
		54.3	1.01		23.2	0.25		7.9	0.10		
		71.9	2.51		50.7	1.00		21.9	0.25		
		70.2	2.50		52.7	0.99		23.9	0.25		
		68.2	2.48		55.8	0.98		23.4	0.25		
SAG/FAG MILL PARAMETERS											
A:	70.5		**b:**	1.54		**A*b:**	108.6		**Ta:**	0.93	
CRUSHER PARAMETERS											
CRUSHER APPEARANCE FUNCTION DATA											
t_{10}	t_{75}		t_{50}		t_{25}		t_4		t_2		
10	3.2		3.9		5.5		23.9		53.2		
20	6.5		7.9		11.2		44.8		84.5		
30	10.0		12.1		17.0		62.7		99.1		
POWER DATA											
	Mean Size (mm)										
	14.53		20.63		28.89		41.08		57.78		
t_{10}	**Ecs (kWh/t)**										
10	0.09		0.10		0.12		0.10		0.09		
20	0.21		0.22		0.26		0.22		0.19		
30	0.35		0.37		0.42		0.37		0.31		
DENSITY DATA											
Mean	3.52		**Std Dev**	0.54		**Max**	5.57		**Min**	2.78	

Table A3.3. Microwave treated sample drop weight tested at standard energy input

JKTech Drop Weight Test Parameters for Crushers and FAG/SAG Mills										
Tested at University of Nottingham										
Client:							**Test Date:**			
Sample Source:	Zinkgruvan 15kW for 1s Series 2						**Tester:**	KJ/AC		
Sample Name:	Zinkgruvan 15kW for 1s, full energy				**Job No:**					
Base Data		t_{10}	E_{is}		t_{10}	E_{is}		t_{10}	E_{is}	
		35.3	0.39		23.5	0.25		8.4	0.10	
		54.7	1.01		21.4	0.25		9.0	0.10	
		70.1	2.51		52.7	1.01		22.7	0.25	
		65.7	2.50		49.8	1.01		29.1	0.25	
		64.2	2.52		47.2	1.00		29.7	0.25	
SAG/FAG MILL PARAMETERS										
A:	65.6		**b:**	1.74		**A*b:**	114.1		**Ta:**	0.80
CRUSHER PARAMETERS										
CRUSHER APPEARANCE FUNCTION DATA										
t_{10}	t_{75}		t_{50}		t_{25}		t_4		t_2	
10	3.2		3.8		5.4		24.2		52.0	
20	6.4		7.8		11.0		44.7		82.0	
30	10.0		12.2		17.0		61.8		95.7	
POWER DATA										
	Mean Size (mm)									
	14.53		20.63		28.89		41.08		57.78	
t_{10}	**Ecs (kWh/t)**									
10	0.09		0.09		0.11		0.11		0.10	
20	0.19		0.19		0.24		0.23		0.21	
30	0.32		0.32		0.39		0.39		0.33	
DENSITY DATA										
Mean	3.38		**Std Dev**	0.47		**Max**	3.97		**Min**	1.87

Table A3.4. Microwave treated sample drop weight tested at 60% of the standard input energy

JKTech Drop Weight Test Parameters for Crushers and FAG/SAG Mills										
Tested at University of Nottingham										
Client:							**Test Date:**		January/February 2002	
Sample Source:	Zinkgruvan							**Tester:**	AC	
Sample Name:	Zinkgruvan Multimode 15kW 1s, 60% energy						**Job No:**			
Base Data	t_{10}	E_{is}		t_{10}	E_{is}		t_{10}	E_{is}		
	24.2	0.24		13.3	0.15		6.7	0.06		
	43.4	0.60		11.1	0.15		10.6	0.06		
	56.3	1.50		37.4	0.60		19.3	0.15		
	57.4	1.50		44.3	0.60		19.6	0.15		
	63.7	1.50		52.3	0.60		24.5	0.15		
SAG/FAG MILL PARAMETERS										
A:	61.2		**b:**	2.19		**A*b:**	134.0		**Ta:**	0.80
CRUSHER PARAMETERS										
CRUSHER APPEARANCE FUNCTION DATA										
t_{10}	t_{75}		t_{50}		t_{25}		t_4		t_2	
10	3.2		4.0		5.7		23.0		52.6	
20	6.9		8.4		11.7		42.6		81.6	
30	11.1		13.4		18.2		59.1		94.1	
POWER DATA										
	Mean Size (mm)									
	14.53		20.63		28.89		41.08		57.78	
t_{10}	**Ecs (kWh/t)**									
10	0.06		0.07		0.10		0.11		0.10	
20	0.12		0.17		0.21		0.21		0.20	
30	0.21		0.29		0.37		0.37		0.33	
DENSITY DATA										
Mean	3.38		**Std Dev**	0.47		**Max**	3.97		**Min**	1.87

3.3 Grindability test data

Table A3.5 Results of the effect of microwave treatment on ore grindability

Size range, mm	Sample description	Grinding time, s					
		30	60	120	180	240	300
-19+16 mm	Treated	317.1	267.2	209.8	194.6	177.5	167
	Untreated	385.8	326.2	290	273.3	258.5	222.8
-16+13.2	Treated	281	220.7	181.1	165.5	163.7	154.4
	Untreated	400.1	365.3	323.8	302.9	295.3	281.9
-13.2+9.5 mm	Treated	352.3	289.1	264.1	227	204.7	186.8
	Untreated	389.8	340.5	306.1	271.1	236.7	225.9
-9.5+6.7 mm	Treated	319	265	203.5	183.3	131.4	120
	Untreated	347	291.6	248.6	209.5	177	155
-6.7+4.75 mm	Treated	307	218.8	150.8	114.3	101.3	81.1
	Untreated	332.6	270.3	196.7	162	150	117.2
-4.75+3.35 mm	Treated	277	202.4	138.2	104.4	83.9	69.7
	Untreated	313.8	237.4	176.1	135.6	110.2	94

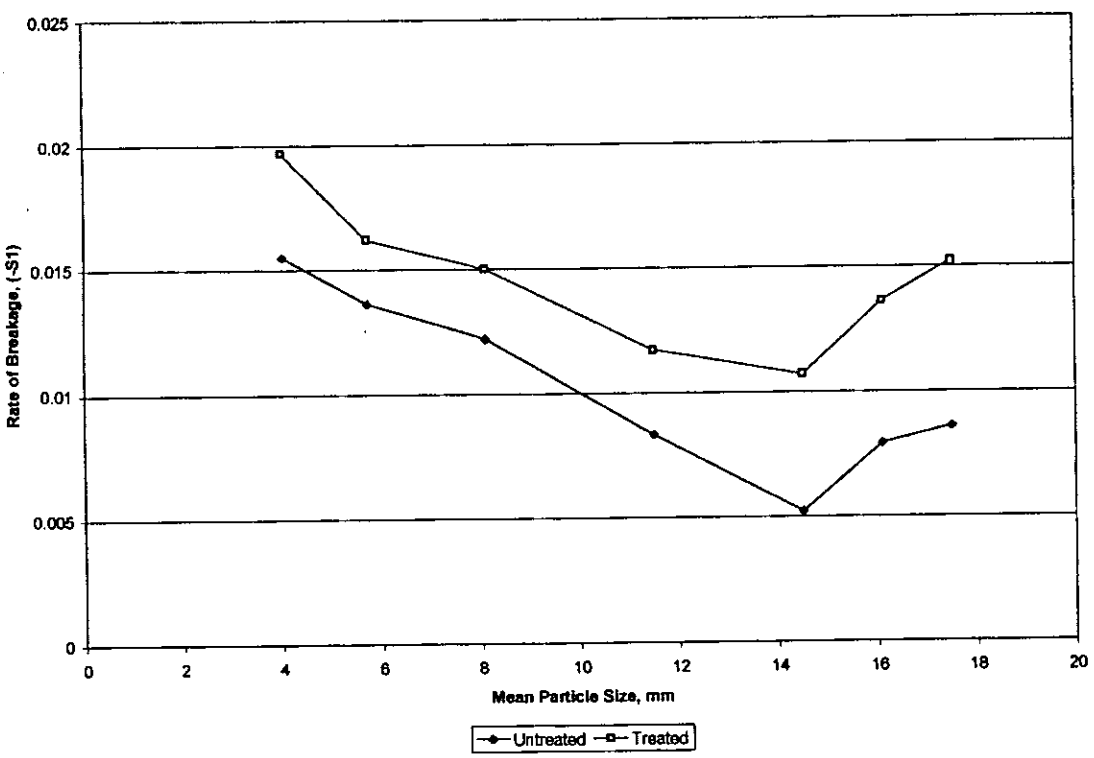

Figure A3.1. Effect of microwave treatment on breakage rate of Zinkgruvan ore.

3.4 Bond Work Index Test data

Table A3.6 Results of standard Bond Work index test for Zinkgruvan untreated sample.

Percentage less than 180μm in Feed:					37.3%
Weight of unity volume:					1661.2g
Weight of product required for 250% circulating load:					475.48g
Period	No. of revs	-180μm in product (g)	-180μm in feed (g)	-180μm produced (g)	Grindability (G), g/rev
1	50	696.6	277.25	419.35	8.387
2	43	444	116.26	327.74	7.621
3	53	384.5	74.10	310.4	5.852
4	70	405.5	65.36	340.14	4.85
5	84	438.2	68.9	414.8	4.99
6	80	480.2	74.6	405.6	5.07
7	78	475.6	81.6	394	3.81
8	60	400	175.9	224.7	3.745
9	88	469	148	321	3.64
10	83	461	173	288.2	3.47
11	88	469.4	170.5	298.9	3.40
12	89	480.3	173.7	306.6	3.44

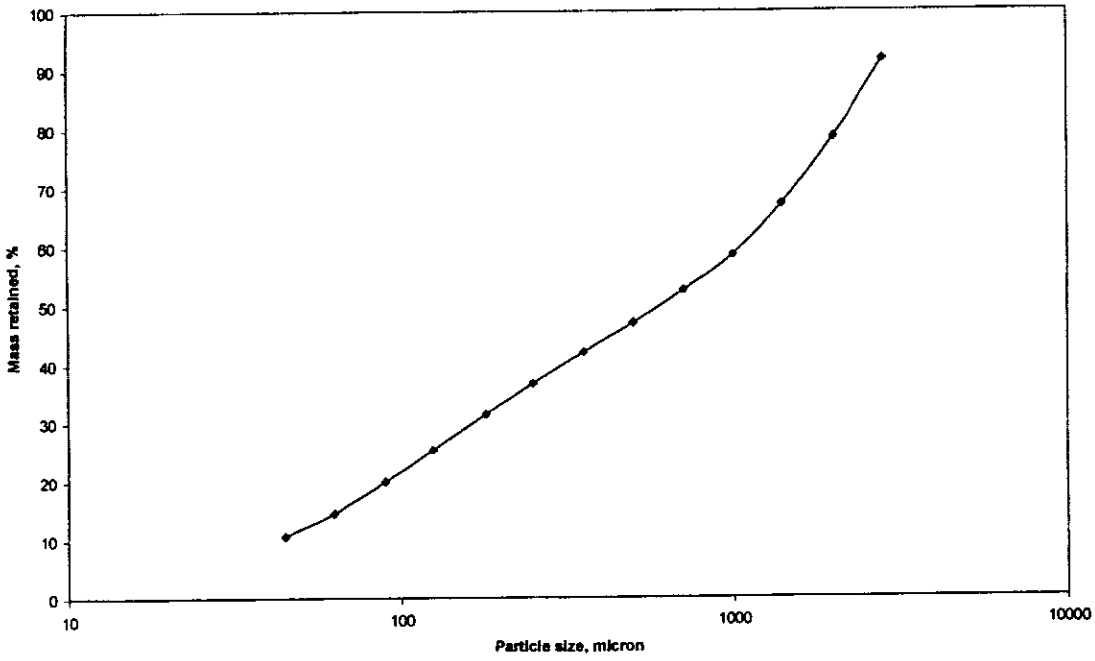

Figure A3.2. Size analysis of the initial feed for standard Bond work index test, Zinkgruvan untreated sample.

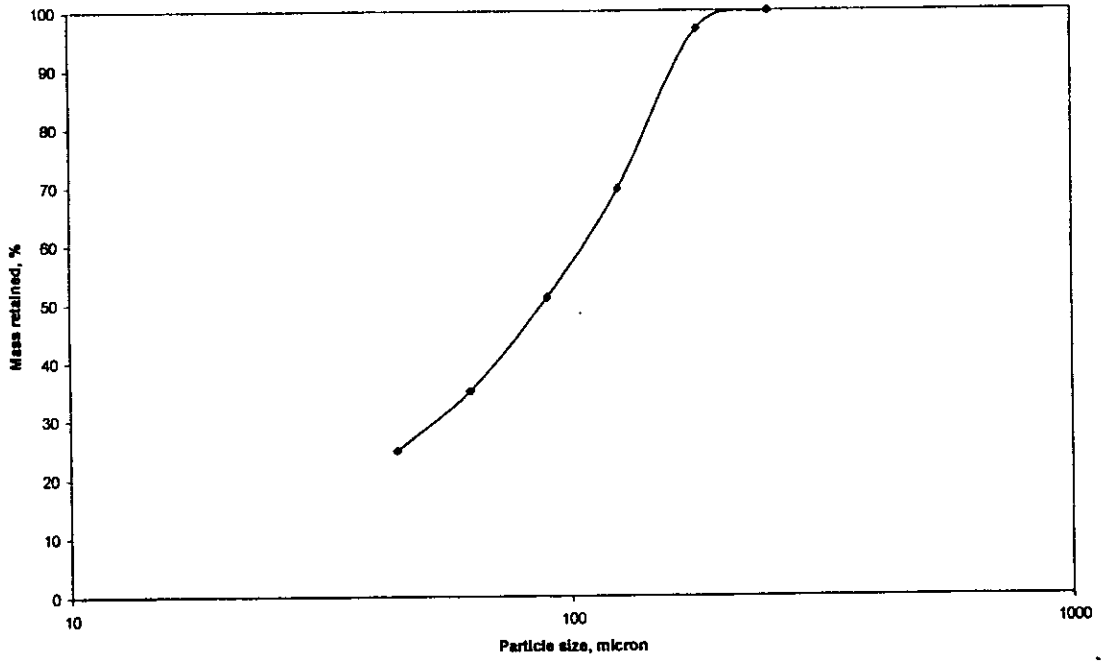

Figure A3.3 Size analysis of the final product of standard Bond work index test for Zinkgruvan untreated sample.

Table A3.7 Results of standard Bond Work index test for Zinkgruvan microwave treated sample.

Percentage less than 180μm in Feed:					37.3%
Weight of unity volume:					1661.2g
Weight of product required for 250% circulating load:					475.48g
Period	No. of revs	-180μm in product (g)	-180μm in feed (g)	-180μm produced (g)	Grindability (G), g/rev
1	50	637.9	614.6	23.3	0.466
2	513	1394.4	236	1158	2.25
3	25	534	418	116	4.64
4	60	429.5	197	232.5	3.87
5	82	485.7	158.9	326.8	3.98
6	74	453.7	179.7	278	3.76
7	81	462	169.3	292	3.61
8	84	454	170.9	283.7	3.37

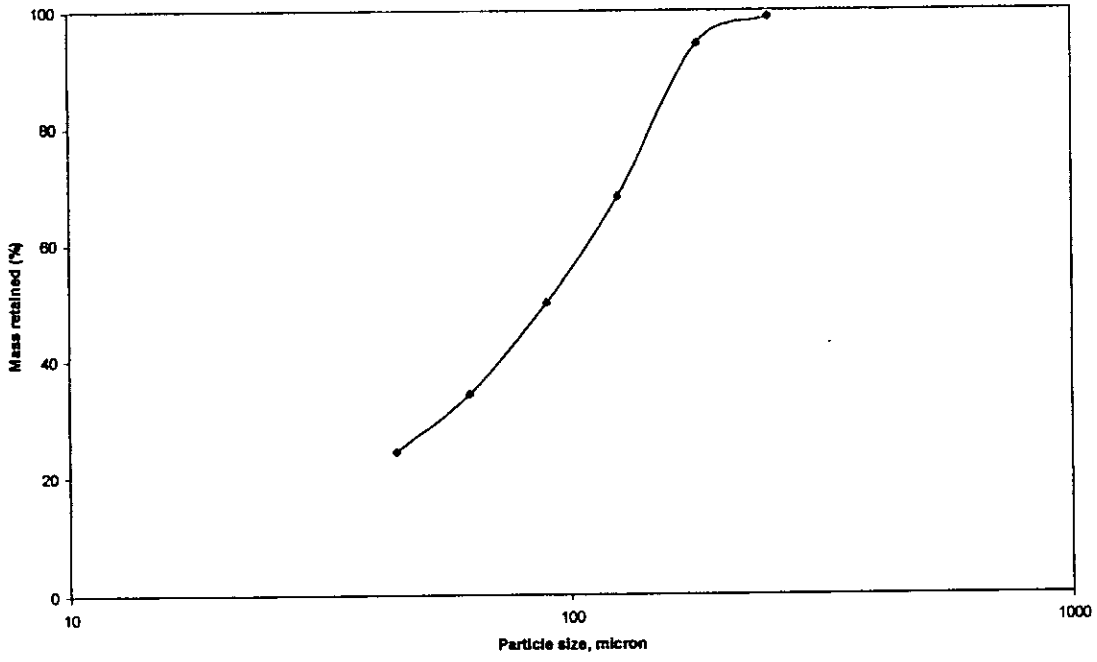

Figure A3.4 Size analysis of the final product of standard Bond work index test for Zinkgruvan microwave treated sample.

3.5 Zinkgruvan Mineral Liberation Data

Table A3.8 Modal Abundance And Chemical Assays

	ZinkgruvanA					ZinkgruvanB				
	+500	+150	+38	-38	Head	+500	+150	+38	-38	Head
PSD	25.94	29.72	26.75	17.59	100.00	25.65	30.68	26.71	16.96	100.00
Chemical assay										
Cu										
Fe	3.73	4.18	4.58	4.05	4.15	3.42	3.91	4.83	3.86	4.02
Pb	8.59	10.70	12.90	16.60	11.78	8.93	11.30	14.60	16.85	12.52
Zn	18.10	20.90	24.30	26.90	22.14	19.50	22.10	27.20	27.45	23.70
QS Assay										
Cu										
Fe	0.81	0.85	0.65	0.79	0.77	0.64	0.49	1.09	0.27	0.65
Pb	13.70	29.05	24.39	39.29	25.62	13.31	33.26	24.11	38.72	26.63
Zn	22.98	25.85	26.96	24.80	25.22	24.44	24.69	26.92	23.74	25.06
Cu Sulphide	0.01	0.01	0.01	0.04	0.01	0.01	0.01	0.02	0.00	0.01
Pyrite	0.65	1.16	0.60	1.12	0.87	0.55	0.47	1.63	0.20	0.75
Galena	15.82	33.53	28.18	45.39	29.59	15.38	38.41	27.85	44.75	30.76
Sphalerite	34.25	38.57	40.15	36.96	37.59	36.44	36.80	40.15	35.41	37.37
Other S	0.00	0.03	0.00	0.00	0.01	0.00	0.00	0.00	0.00	0.00
Fe-oxide	0.00	0.00	0.02	0.00	0.01	0.00	0.04	0.08	0.00	0.03
NSG	48.72	26.39	30.57	15.87	31.45	46.80	23.96	29.60	19.23	30.52
Other	0.55	0.33	0.46	0.63	0.47	0.82	0.31	0.67	0.41	0.55
					100.00					100.00
	NOTE: For Zinkgruven QS Fe assay is low (Fe in sphalerite is not accounted for)									

Table A3.9 Liberation Data

	ZinkgruvanA					ZinkgruvanB				
Galena	+500	+150	+38	-38	Head	+500	+150	+38	-38	Head
Locked	49.90	16.20	13.20	15.50	24.02	48.40	15.20	12.50	19.60	23.74
Middling	40.10	26.40	25.90	47.80	33.59	44.60	24.50	19.40	33.20	29.77
Liberated	10.00	57.40	60.90	36.70	42.40	7.00	60.30	68.10	47.20	46.49
	100	100	100	100	100	100	100	100	100	100

	ZinkgruvanA					ZinkgruvanB				
Sphalerite	+500	+150	+38	-38	Head	+500	+150	+38	-38	Head
Locked	18.70	8.50	4.20	4.80	9.35	21.10	9.10	5.40	6.30	10.71
Middling	50.80	25.50	13.80	20.50	28.05	58.40	28.00	13.60	23.10	31.12
Liberated	30.50	66.00	82.00	74.70	62.60	20.50	62.90	81.00	70.60	58.17
	100	100	100	100	100	100	100	100	100	100